



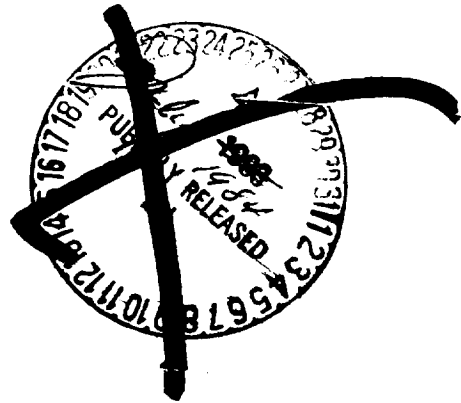
ENERGY EFFICIENT ENGINE
HIGH-PRESSURE TURBINE DETAILED DESIGN REPORT



by:

Robert D. Thulin, David C. Howe
and Irwin D. Singer

UNITED TECHNOLOGIES CORPORATION
Pratt & Whitney Aircraft Group
Commercial Products Division

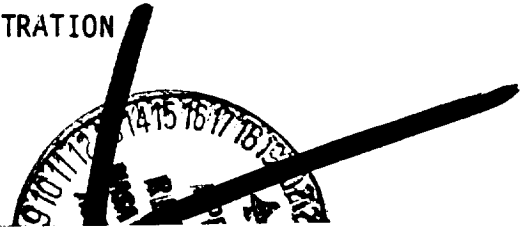


Prepared for:

NATIONAL AERONAUTICS AND SPACE ADMINISTRATION

Lewis Research Center
Cleveland, OH 44135

Contract NAS3-20646

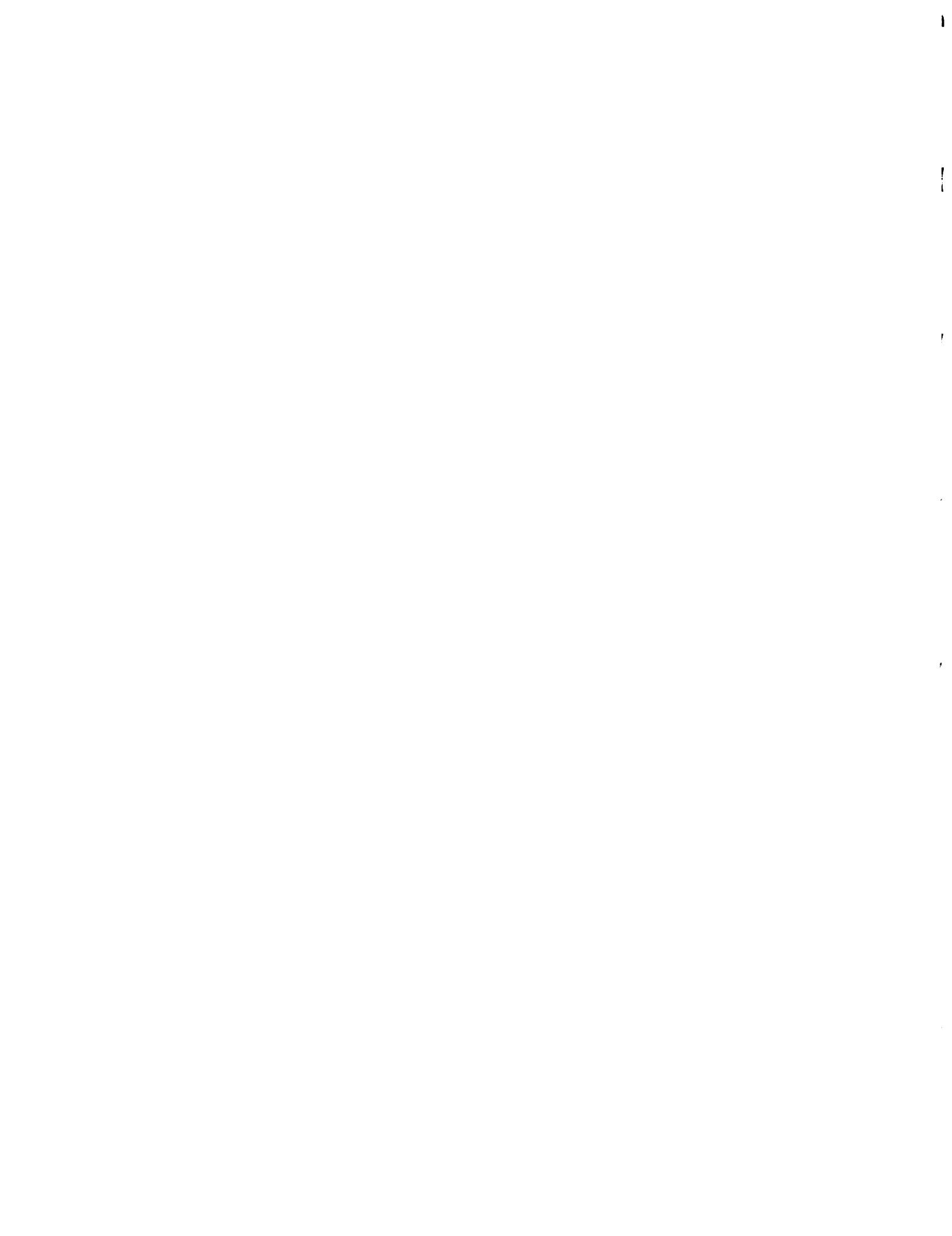


(NASA-CR-165608) ENERGY EFFICIENT ENGINE
HIGH-PRESSURE TURBINE DETAILED DESIGN REPORT
(Pratt and Whitney Aircraft Group) 164 p
HC A08/MF A01 CSCL 21E

N84-28788

Unclas
G3/07 19723

1. REPORT NO. NASA CR-165608	2. GOVERNMENT AGENCY	3. RECIPIENT'S CATALOG NO.	
4. TITLE AND SUBTITLE Energy Efficient Engine -- High-Pressure Turbine Detailed Design Report		5. REPORT DATE January 1982	6. PERFORMING ORG. CODE
7. AUTHOR(S) Mr. Robert D. Thulin, Mr. David C. Howe and Mr. Irwin D. Singer		8. PERFORMING ORG. REPT. NO. PWA-5594-171	
9. PERFORMING ORG. NAME AND ADDRESS UNITED TECHNOLOGIES CORPORATION Pratt & Whitney Aircraft Group Commercial Products Division		10. WORK UNIT NO.	11. CONTRACT OR GRANT NO. NAS3-20646
12. SPONSORING AGENCY NAME AND ADDRESS National Aeronautics and Space Administration Lewis Research Center 21000 Brookpark Road, Cleveland, Ohio 44135		13. TYPE REPT./PERIOD COVERED Contractor Report	
15. SUPPLEMENTARY NOTES Project Manager Carl C. Ciepluch, NASA-Lewis Research Center		14. SPONSORING AGENCY CODE	
16. ABSTRACT The Energy Efficient Engine high-pressure turbine is a single stage system based on technology advancements in the areas of aerodynamics, structures and materials to achieve high performance, low operating economics and durability commensurate with commercial service requirements. Low loss performance features combined with a low through-flow velocity approach results in a predicted efficiency of 88.8 for a flight propulsion system. Turbine airfoil durability goals are achieved through the use of advanced high-strength and high-temperature capability single crystal materials and effective cooling management. Overall, this design reflects a considerable extension in turbine technology that is applicable to future, energy efficient gas-turbine engines.			
17. KEY WORDS (SUGGESTED BY AUTHOR(S)) Single Crystal Material Airfoils Single Stage Turbine Energy Efficient Engine Low Through Flow Velocity			
19. SECURITY CLASS THIS (REPT) Unclassified	20. SECURITY CLASS THIS (PAGE) Unclassified	21. NO. PGS	22. PRICE *



FOREWORD

The Energy Efficient Engine Component Development and Integration Program is being conducted under parallel National Aeronautics and Space Administration contracts to the Pratt & Whitney Aircraft Group, Commercial Products Division and the General Electric Company. The overall project is under the direction of Mr. Carl C. Ciepluch. Mr. John W. Schafer is the NASA Assistant Project Manager for the Pratt & Whitney Aircraft effort under Contract NAS3-20646, and Mr. M. Vanco is the NASA Project Engineer responsible for the portion of the program described in this report. Mr. William B. Gardner is the Pratt & Whitney Aircraft Program Manager for the Energy Efficient Engine Program. This report was prepared by Mr. R. Thulin, Mr. D. Howe, and Mr. I. Singer of Pratt & Whitney Aircraft.



TABLE OF CONTENTS

	Page
SECTION 1.0 SUMMARY	1
SECTION 2.0 INTRODUCTION	2
SECTION 3.0 DESIGN OVERVIEW	4
3.1 Design Goals and Challenges	4
3.2 High-Pressure Turbine General Description	5
3.3 Design Performance Data	7
SECTION 4.0 HIGH-PRESSURE TURBINE AERODYNAMIC DESIGN	9
4.1 Overview	9
4.2 Component Aerodynamic Design	10
4.2.1 Flowpath Definition	10
4.2.2 Airfoil Definition	11
4.2.3 High-Pressure and Low-Pressure Turbine Matching	19
4.2.4 Aerodynamic Efficiency Status	19
4.2.5 Supporting Technology Programs	19
4.2.5.1 Uncooled Rig Technology Program	20
4.2.5.2 Supersonic Cascade Program	22
4.2.5.3 Leakage Program	25
SECTION 5.0 AIRFOIL DURABILITY	30
5.1 Overview	30
5.2 Turbine Vanes	30
5.2.1 Vane Cooling Management System	31
5.2.2 Vane Materials	34
5.2.3 Turbine Vane Durability Assessment	38
5.3 Turbine Blades	38
5.3.1 Blade Cooling Management System	38
5.3.2 Blade Materials	42
5.3.3 Turbine Blade Durability Assessment	45
SECTION 6.0 SECONDARY AIRFLOW SYSTEM	48
6.1 Overview	48
6.2 Secondary Flow Summary	48
6.3 Secondary Flow System Design Features	51
6.4 Thermal Analysis	54
SECTION 7.0 COMPONENT MECHANICAL DESIGN	59
7.1 Overview	59
7.2 Turbine Rotor Assembly	59
7.2.1 General Description	59
7.2.2 Blades	63
7.2.2.1 Mechanical Design Features	63
7.2.2.2 Airfoil Vibration Analysis	68
7.2.3 Blade Attachment	76
7.2.3.1 Mechanical Design Features	76
7.2.3.2 Structural Analysis	76

TABLE OF CONTENTS (Continued)

	Page
7.2.4 Disk	78
7.2.4.1 Mechanical Design Features	78
7.2.4.2 Structural Analysis	78
7.2.5 Sideplate and Vortex Plate	80
7.2.5.1 Mechanical Design Features	80
7.2.5.2 Structural Analysis	85
7.2.6 Air Seals	85
7.2.6.1 Mechanical Design Features	85
7.2.6.2 Structural Analysis	85
7.3 Vane and Inner Case	93
7.3.1 General Description	93
7.3.2 Vanes	93
7.3.2.1 Mechanical Design Features	93
7.3.2.2 Structural Analysis	96
7.3.3 Inner Support, Tangential on-Board Injection and High-Pressure Compressor Seal	96
7.3.3.1 Mechanical Design Features	96
7.3.3.2 Structural Analysis	97
7.4 Outer Case and Outer Airseal	100
7.4.1 Mechanical Design Features	100
7.4.2 Structural Analysis	104
7.5 Active Clearance Control System	104
7.5.1 General Description	106
7.5.2 Blade Tip Clearance Definition	107
7.6 Number 4 & 5 Bearing Compartment and Lubrication System	112
7.6.1 General Description	112
7.6.2 Bearing Mechanical Design Features	112
7.6.3 Seals	115
7.6.4 Lubrication System	115
7.7 Turbine System Weight Summary	117
 SECTION 8.0 HIGH-PRESSURE TURBINE COMPONENT TEST RIG DESIGN	 118
8.1 Introduction	118
8.2 General Description and Major Features	118
8.3 Mechanical Design	120
8.3.1 Rotating Hardware	120
8.3.2 Bearing and seals	121
8.3.3 Air Seals	122
8.3.4 Static Hardware	131
8.4 Secondary Flow System and Thrust Balance	131
8.5 Rig Instrumentation	132
8.5.1 Performance Instrumentation	135
8.5.2 Structural Integrity Instrumentation	135
8.6 Facility/Rig Adaptation	136
 SECTION 9.0 CONCLUDING REMARKS	 137
 APPENDIX A VANE AND BLADE AIRFOIL COORDINATES	 139
APPENDIX B LIST OF SYMBOLS	146
 REFERENCES	 148

LIST OF ILLUSTRATIONS

<u>Number</u>	<u>Title</u>	<u>Page</u>
2-1	Logic Diagram of High-Pressure Turbine Effort	3
3.2-1	Energy Efficient Engine High-Pressure Turbine Component	6
4.2.1-1	High-Pressure Turbine Flowpath Definition	10
4.2.2-1	Vane Assumed Profiles For Inlet Temperature and Pressure Loss	12
4.2.2-2	Vane Root Section Aerodynamic Contour and Pressure Distribution	13
4.2.2-3	Vane Mean Section Aerodynamic Contour and Pressure Distribution	13
4.2.2-4	Vane Tip Section Aerodynamic Contour and Pressure Distribution	14
4.2.2-5	Turbine Vane Stacking	14
4.2.2-6	Effect of Inlet Temperature and Vane Loss Profile on Blade Inlet Angle	15
4.2.2-7	Blade Root Section Aerodynamic Contour and Pressure Distribution	16
4.2.2-8	Blade One-Quarter Root Section Aerodynamic Contour and Pressure Distribution	16
4.2.2-9	Blade Mean Section Aerodynamic Contour and Pressure Distribution	17
4.2.2-10	Blade One-Quarter Tip Section Aerodynamic Contour and Pressure Distribution	17
4.2.2-11	Blade Tip Section Aerodynamic Contour and Pressure Distribution	18
4.2.2-12	Turbine Blade Stacking	18
4.2.5-1	Turbine Uncooled Rig Performance Trends Showing Benefits of Decreasing the C_x/U and Increasing the AN^2 Parameter	21
4.2.5-2	Efficiency Gains Associated with High Blade Reaction Levels	22
4.2.5-3	Spanwise Distribution of Total Pressure Loss for the Profiled Wall Cascade	23

LIST OF ILLUSTRATIONS (Continued)

<u>Number</u>	<u>Title</u>	<u>Page</u>
4.2.5-4	Predicted Vane Cooling Losses Compared to Test Results	23
4.2.5-5	Effect of Trailing Edge Ejection Flow on Blade Pressure Coefficient	24
4.2.5-6	Plane Cascade Base Blade, Mean Section Trailing Edge Cooling Air Ejection	24
4.2.5-7	Results of Blade-Disk Model Testing Showing Leakage in the Attachment Area Is Less Than Predicted	25
4.2.5-8	Sealing Effectiveness of Rear Sideplate Design	26
4.2.5-9	Results With and Without W-Seals in the Blade Platform Area	26
4.2.5-10	Promising Feather Seal Configurations Evaluated	27
4.2.5-11	Energy Efficient Engine High-Pressure Turbine Vane Inner Attachment Leakage Rig	28
4.2.5-12	Comparison of 0.025 to 0.050 cm (0.010 to 0.020 in) Thick Two-Piece Overlapping Feather Seals	29
4.2.5-13	Two-piece Overlapped Seals in Ground Versus Electro-discharge Machined Slots	29
5.2-1	Combustor Exit Profile Used for Turbine Vane Durability Assessment for Flight Propulsion System at Hot Day Sea Level Takeoff Operating Conditions	30
5.2.1-1	Turbine Vane Cooling Design	31
5.2.1-2	Turbine Vane Inner Platform Cooling Scheme	33
5.2.1-3	Turbine Vane Outer Platform Cooling Scheme	33
5.2.1-4	Turbine Vane Inner Platform Heat Transfer Coefficients	33
5.2.1-5	Turbine Vane Outer Platform Heat Transfer Coefficients	33
5.2.1-6	Suction Surface Film Effectiveness	35
5.2.1-7	Vane Thermal Analysis Results	35
5.2.1-8	Pressure Wall Film Temperatures	36

LIST OF ILLUSTRATIONS (Continued)

<u>Number</u>	<u>Title</u>	<u>Page</u>
5.2.1-9	Suction Wall Film Temperatures	36
5.2.1-10	Vane Surface Temperature Profile	37
5.2.1-11	Vane Surface Heat Transfer Coefficients Used to Determine Surface Temperature Profiles	37
5.2.3-1	Vane Limiting Strain Cycle	39
5.2.3-2	Predicted Strain	39
5.3-1	Turbine Vane Exit Profile for Flight Propulsion System at Hot Day Sea Level Takeoff Operating Conditions	40
5.3.1-1	Turbine Blade Cooling System	41
5.3.1-2	Blade Thermal Analysis Results (Midspan Location)	43
5.3.1-3	Surface Temperature Profile	44
5.3.1-4	Blade Surface Heat Transfer Coefficients Used to Determine Surface Temperature Profiles	44
5.3.3-1	Blade Limiting Strain Cycle	45
5.3.3-2	Predicted Strain	46
5.3.3-3	Blade Temperature Comparison with Creep Limits for Flight Propulsion System at Hot Day Sea Level Takeoff Operating Conditions	47
5.3.3-4	Effects of Wall Thickness Tolerance on Blade Life	47
6.2-1	High-Pressure Turbine Secondary Flow System Map	49
6.3-1	Secondary Flow System Design Features	52
6.3-2	Mini Tangential On-Board Injection System	52
6.3-3	Flow Characteristics of Blade Coolant Supply System	53
6.4-1	Detailed Turbine Model Used for Thermal Analysis	55
6.4-2	Typical Transient Response of Turbine Disk During Snap Acceleration/Deceleration	56

LIST OF ILLUSTRATIONS (Continued)

<u>Number</u>	<u>Title</u>	<u>Page</u>
6.4-3	Detailed Turbine Case and Outer Airseal Model Used in Thermal Analysis	57
6.4-4	Results of Temperature Analysis	58
7.1-1	High-Pressure Turbine Mechanical Configuration	60
7.2.1-1	High-Pressure Turbine Rotor Assembly	60
7.2.1-2	Energy Efficient Engine High Rotor Imbalance Response	61
7.2.1-3	Energy Efficient Engine High Rotor Critical Speeds and Mode Shapes (Percent Rotor Strain Energy)	62
7.2.2-1	Turbine Blade Mechanical Configuration	63
7.2.2-2	Radial Taper in Turbine Blade To Minimize Stress	65
7.2.2-3	Degree of Tilt in the High-Pressure Turbine Blade to Achieve the Desired Balance Between Gas Bending Load Stresses and Stresses Resulting from Centrifugal Loads	65
7.2.2-4	Uncoated Blade Wall Thickness and Internal Rib Design	66
7.2.2-5	Core Support Method	67
7.2.2-6	Blade Tip Squealer Geometry	67
7.2.2-7	Graphical Display of Turbine Blade Defined by the NASTRAN Analytical Technique	68
7.2.2-8	Single Crystal Major Axes Orientation	69
7.2.2-9	High-Pressure Turbine Resonance Diagram	70
7.2.2-10	Blade Vibration Characteristics in First Mode	70
7.2.2-11	Blade Vibration Characteristics in Second Mode	71
7.2.2-12	Blade Vibration Characteristics in Third Mode	71
7.2.2-13	Blade Vibration Characteristics in Fourth Mode	72
7.2.2-14	Blade Vibration Characteristics in Fifth Mode	72

LIST OF ILLUSTRATIONS (Continued)

<u>Number</u>	<u>Title</u>	<u>Page</u>
7.2.2-15	Crystallographic Orientation	73
7.2.2-16	Predicted Frequencies Versus Crystal Secondary Orientation Angle	74
7.2.2-17	Axial Shift in Crystal Orientation	74
7.2.2-18	Predicted Frequency with Modified Configuration	75
7.2.3-1	Blade Attachment Stress Results	77
7.2.4-1	High-Pressure Turbine Disk Design Features	79
7.2.4-2	Elliptical Cooling Air Supply Hole	79
7.2.4-3	Schematic Showing Disk and Blade Deflections Caused by First Coupled Mode Vibration	80
7.2.4-4	Boundary Conditions Used in Disk Structural Analysis	81
7.2.4-5	Flight Propulsion System Disk and Sideplate Calculated Minimum Low Cycle Fatigue Life Levels	82
7.2.5-1	Disk Sideplate and Vortex Plate Design	82
7.2.5-2	Typical Sideplate Loads	83
7.2.5-3	Blade and Sideplate Assembly Sequence	84
7.2.5-4	Anti-Torque Pin Details	84
7.2.6-1	Turbine Seal Designs	86
7.2.6-2	Rear Thrust Balance Seal	87
7.2.6-3	Thrust Balance Seal Rotor and Stator Resonance Diagram	88
7.2.6-4	Thrust Balance Seal Rotor and Stator Coincidence Diagram	88
7.2.6-5	Number 4 Bearing Buffer Seal Assembly	89
7.2.6-6	Number 4 Bearing Buffer Seal Rotor and Stator Resonance Diagram	90

LIST OF ILLUSTRATIONS (Continued)

<u>Number</u>	<u>Title</u>	<u>Page</u>
7.2.6-7	Number 4 Bearing Buffer Seal Rotor and Stator Coincidence Diagram	90
7.2.6-8	High-Pressure Compressor Discharge Seal Assembly	91
7.2.6-9	High-Pressure Compressor Discharge Seal Rotor and Stator Resonance Diagram	92
7.2.6-10	High-Pressure Compressor Discharge Seal Rotor and Stator Coincidence Diagram	92
7.3.1-1	High-Pressure Turbine Vane and Inner Case Mechanical Design	93
7.3.2-1	Turbine Vane Assembly	94
7.3.2-2	Design Approach to Vane Leakage Control	94
7.3.2-3	Uncoated Vane Minimum Wall Thickness Distribution	95
7.3.3-1	Turbine Inner Support, Tangential On-Board Injection System, and High-Pressure Compressor Seal Land Support System	96
7.3.3-2	Nozzle Configuration for the Primary Tangential On-Board Injection System	98
7.3.3-3	Nozzle Configuration for the Secondary or Mini Tangential On-Board Injection System	98
7.3.3-4	High-Pressure Compressor Discharge Seal Clearance Summary	99
7.3.3-5	Inner Vane Case Stress Summary	99
7.3.3-6	Case Structure Deflection Summary	100
7.4-1	High-Pressure Turbine Outer Case and Outer Airseal Assembly	101
7.4.1-1	Mechanical Design Features	101
7.4.1-2	Details of the Outer Airseal Shoe Design	103
7.4.1-3	Outer Case and Outer Airseal Materials Map	103

LIST OF ILLUSTRATIONS (Continued)

<u>Number</u>	<u>Title</u>	<u>Page</u>
7.4.2-1	Shell Analysis Model	104
7.4.2-2	Temperature Map	105
7.4.2-3	Stress Map	105
7.5.1-1	High-Pressure Turbine Active Clearance Control System	106
7.5.2-1	Typical Rotor and Case Growth History	107
7.5.2-2	Rotor and Case Response with Two Cooling Bleed Schedules	108
7.5.2-3	Effect of Mixed Bleed	109
7.5.2-4	Rotor and Case Response with Optimum Mixed Cooling Bleed Schedule	110
7.5.2-5	Resultant Blade Tip Clearances	111
7.6.1-1	Integrated Core/Low Spool Number 4 and 5 Bearing Compartment - Temperature and Pressure Distribution at Sea Level Takeoff -30C (+250F) Operating Conditions	112
7.6.1-2	Number 4 and 5 Bearing Compartment Bearing and Seal Arrangement	113
7.6.2-1	Number 4 and 5 Bearing Compartment - Locations of Maximum Stress and Deflection	114
7.6.3-1	Dry Face Seal Pressure, Temperature and Speed Experience	116
7.6.4.1	Oil Scupper Line for the Number 4 and 5 Bearing Compartment	117
8.2-1	High-Pressure Turbine Component Test Rig	119
8.3.1-1	High-Pressure Turbine Component Test Rig Critical Speed and Mode Shapes	120
8.3.3-1	High-Pressure Turbine Rig Thrust Piston Seal Resonance	123
8.3.3-2	High-Pressure Turbine Rig Thrust Piston Seal Coincidence	123
8.3.3-3	Front Compartment Front Airseal (Thrust Piston Seal)	124
8.3.3-4	High-Pressure Turbine Rig Front Bearing Rear Seal Resonance	125
8.3.3-5	High-Pressure Turbine Rig Front Bearing Rear Seal Coincidence	125

LIST OF ILLUSTRATIONS (Continued)

<u>Number</u>	<u>Title</u>	<u>Page</u>
8.3.3-6	Front Compartment Rear Airseal	126
8.3.3-7	High-Pressure Turbine Rig High-Pressure Compressor Discharge Seal Resonance	126
8.3.3-8	High-Pressure Turbine Rig High-Pressure Compressor Discharge Seal Resonance	127
8.3.3-9	High-Pressure Compressor Discharge Seal	127
8.3.3-10	High-Pressure Turbine Rig Thrust Balance Seal Resonance	128
8.3.3-11	High-Pressure Turbine Rig Thrust Balance Seal Coincidence	129
8.3.3-12	Thrust Balance Seal and Damper	129
8.3.3-13	High-Pressure Turbine Rig Number 4 Bearing Buffer Seal Resonance	130
8.3.3-14	High-Pressure Turbine Rig Number 4 Bearing Buffer Seal Coincidence	130
8.3.3-15	Number 4 Bearing Buffer Seal - Rig	131
8.3.4-1	Active Clearance Control Growth Summary	132
8.4-1	High-Pressure Turbine Component Test Rig Secondary Flows	133

LIST OF TABLES

<u>Table No.</u>	<u>Title</u>	<u>Page</u>
3.2-I	Advanced Technology Design Concepts	5
3.3-I	High-Pressure Turbine Predicted Performance at Aerodynamic Design Point	8
4.1-I	General Aerodynamic Parameters	9
4.2.2-I	Gas Triangles	12
4.2.3-I	High-Pressure Turbine Aerodynamics After Restaggering	19
4.2.4-I	High-Pressure Turbine Efficiency Estimate Based on Uncooled Rig Test Results Aerodynamic Design Point	20
4.2.5-I	Turbine Uncooled Rig Efficiency	22
5.2.2-I	Vane Materials and Coatings	38
5.2.3-I	Vane Life	40
5.3.2-I	Blade Materials	45
5.3.3-I	Blade Life	46
6.2-I	Secondary Flow Status Summary	50
7.2.2-I	High-Pressure Turbine Blade Stress Summary	63
7.2.3-I	Blade Attachment Stress Summary	77
7.2.4-I	Disk Life and Stress Summary	78
7.3.2-I	Vane Materials and Coatings	95
7.5.2-I	Flight Cycle For Clearance Analysis	108
7.5.2-II	High-Pressure Turbine Active Clearance Control System	109
7.5.2-III	High-Pressure Turbine Gapping Requirements	111
7.5.2-IV	High-Pressure Turbine Tip Clearance Results	111
7.6.3-I	Integrated Core/Low Spool Seal Operating Conditions	116

LIST OF TABLES (Cont'd)

<u>Table No.</u>	<u>Title</u>	<u>Page</u>
7.7-I	Preliminary Weight summary For Integrated Core/Low Spool High-Pressure Turbine Component	117
8.3-I	High-Pressure Turbine Component Rig Forced Response Results	121
8.3.2-I	Front Compartment Operating Conditions	121
8.3.2-II	Operating Conditions of the Rear Compartment Seals	122

SECTION 1.0 SUMMARY

The high-pressure turbine designed for the Energy Efficient Engine is a single stage configuration that utilizes technology advancements in the areas of aerodynamics, structures and materials to enhance efficiency, durability and performance retention. In addition, the single stage design offers a large savings in initial engine cost, weight, and maintenance cost because of the significant reduction in the number of components, especially expensive air-cooled airfoils.

On the basis of aerothermal-mechanical analyses as well as results from supporting technology programs, the high-pressure turbine meets the performance and durability goals for both the integrated core/low spool and the flight propulsion system. The predicted efficiency for the flight propulsion system is 88.8 percent, which exceeds the goal of 88.2 percent. For the integrated core/low spool, the expected test efficiency is 87.1 percent, which exceeds the goal of 86.7 percent. The turbine aerodynamic design utilizes low loss performance features with low through flow velocity to achieve this efficiency.

The turbine airfoils exceed the established durability/life requirements by the use of advanced materials and efficient cooling management. Both the vanes and blades are constructed with advanced high-temperature, high-strength single crystal alloys and coated with an improved oxidation resistant coating. For added thermal protection, vane platforms are coated with an advanced thermal barrier coating. Acceptable metal temperatures are maintained through the use of impingement, convection and film cooling techniques to minimize cooling without compromising durability. Total cooling requirements are 2.75 and 6.41 percent of core engine airflow for the blade and vane, respectively.

Turbine performance is enhanced by the advancements in sealing technology. Cooling air leakage is effectively reduced by the use of full ring, boltless sideplates as well as the extensive use of feather seals and W-seals. An active clearance control system maintains close blade tip clearances throughout the operating range. In this system, the blade tip seal is constructed of an abradable, ceramic material and the blade has an abrasive tip treatment. At design conditions, the calculated clearance of 0.032 cm (0.0126 in) surpasses the goal of 0.047 cm (0.0186 in).

The high-pressure turbine in the integrated core/low spool and envisioned for the future flight propulsion system is also the same design for the High-Pressure Turbine Component Test Rig. This rig will be used to assess turbine aerodynamic behavior and performance before the component is evaluated in the integrated core/low spool.

Overall, the high-pressure turbine design for the Energy Efficient Engine represents a considerable extension in the state-of-the-art of turbine technology. Much of this technology, especially the high temperature capability materials, will have wide application in derivative and future gas-turbine engines.

SECTION 2.0 INTRODUCTION

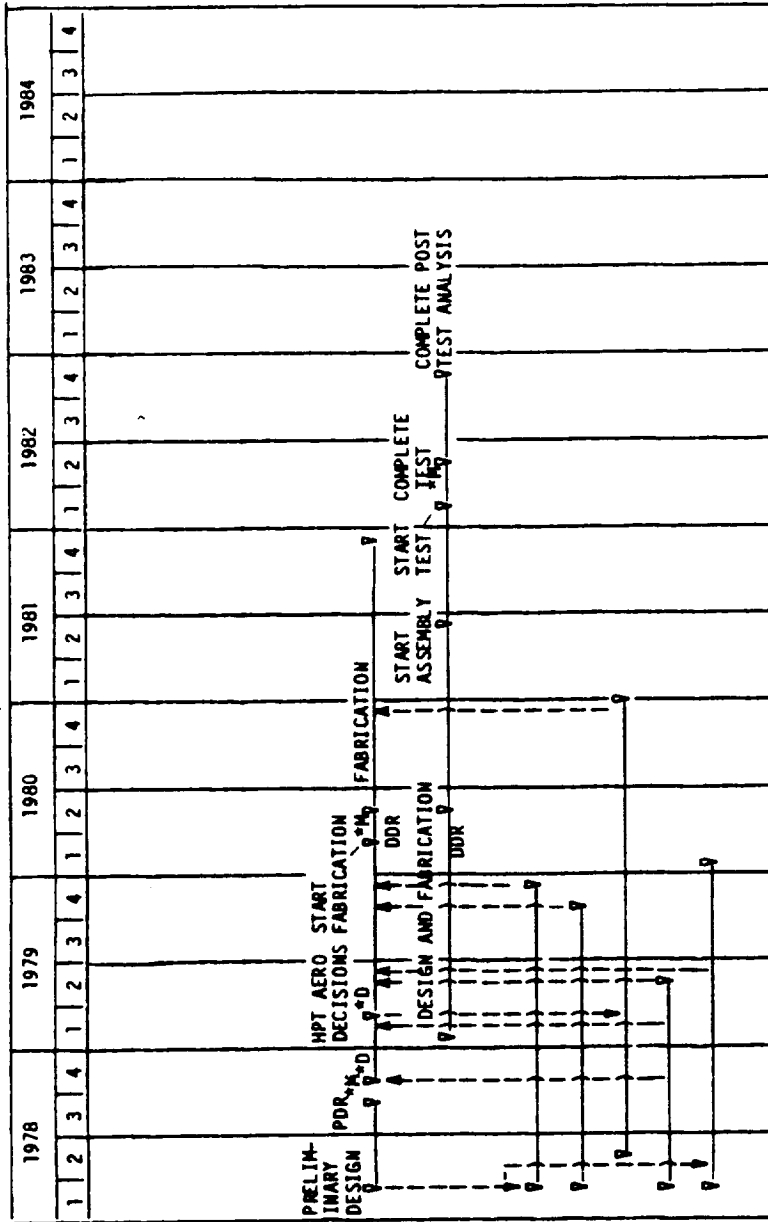
The Energy Efficient Engine Component and Development Program, sponsored by the National Aeronautics and Space Administration, is directed towards developing and demonstrating the technology to achieve greater fuel efficiency for future commercial gas-turbine engines. The overall program goals outlined for the program include a reduction in fuel consumption of at least 12 percent and a reduction in direct operating cost of at least 5 percent relative to the base Pratt & Whitney Aircraft JT9D-7A base engine. To demonstrate the technology to accomplish these goals, the Energy Efficient Engine Program is organized into four tasks which involve:

- Task 1 Flight Propulsion System Analysis, Design and Integration
- Task 2 Component Analysis, Design and Development
- Task 3 Core Design, Fabrication and Test
- Task 4 Integrated Core/Low Spool Design, Fabrication and Test

A major accomplishment under the Task 2 effort has been the design of an advanced high-pressure turbine system. Figure 2-1 presents a logic diagram of the high-pressure turbine design effort within the overall Energy Efficient Engine Program.

The high-pressure turbine component has been designed to meet the requirements for the flight propulsion system and the integrated core/low spool. In addition, the turbine design is the same for the High-Pressure Turbine Component Test Rig, which will be used to assess turbine aerodynamic performance before the component is tested in the integrated core/low spool. The design emphasizes the utilization of advancements in the areas of aerodynamics, materials/cooling management and structures to achieve aggressive performance and durability design goals.

This report presents a comprehensive description of the aerodynamic and thermal-mechanical design of the Energy Efficient Engine high-pressure turbine. A description of the high pressure turbine rig design is also presented.



COMPONENT ANALYSIS, DESIGN, AND FABRICATION

COOLED RIG PROGRAM

SUPPORTING TECHNOLOGY

LEAKAGE TESTS

SUPERSONIC CASCADE TESTS

COOLING MODEL TESTS

UNCOOLED RIG TESTS

FABRICATION DEVELOPMENT

*M DENOTES MAJOR MILESTONE

*D DENOTES KEY DECISION POINT

Figure 2-1 Logic Diagram of High-Pressure Turbine Effort

SECTION 3.0 DESIGN OVERVIEW

3.1 DESIGN GOALS AND CHALLENGES

The Energy Efficient Engine high-pressure turbine concept is a single stage configuration capable of high work extraction and high system efficiency. Performance and durability design goals established for the turbine component address the overall program goals as well as the requirements for a future commercial flight propulsion system.

The turbine efficiency goal for the flight propulsion system is 88.2 percent. This represents a considerable increase in efficiency compared to a current technology single-stage design. However, the expected test efficiency goal for the integrated core/low spool is lower -- 86.7 percent. This is based on the anticipation that leakage rates and part quality in the integrated core/low spool vehicle will be worse than for a fully developed flight propulsion system. In addition, restagger for compatibility with the increased annulus low-pressure turbine and rematching associated with other component performance losses further reduce efficiency.

Other key design goals include a specific work output of 448,000 J/kgm (192.96 Btu/lbm), an expansion ratio of 4.0, a combined turbine cooling/leakage flow rate of 11.2 percent of core engine flow, and a rim speed of 527 m/sec (1730 ft/sec).

In terms of component durability, the flight propulsion system design goals consist of a vane and blade life of 10,000 hours, and disk life of 20,000 hours. In addition, an airfoil coating life goal of 6000 hours was established.

The achievement of these performance and durability goals with a single stage turbine introduces certain design challenges. The two most prominent challenges center around maintaining acceptable blade stress with the high rim speed operation and minimizing system cooling flows and leakage losses. The following paragraphs outline how these challenges have been approached, and the specific design features that contribute to meeting the turbine performance and durability goals are described in the next section.

To achieve the efficiency goal, the single stage turbine must operate at a high ratio of wheel speed to specific work (high velocity ratio) and a low ratio of through flow to wheel speed (C_x/U). The aerodynamic parameters of velocity ratio and C_x/U can be translated into blade stress and blade attachment stress, which results in a high AN^2 (the product of annulus area and wheel speed squared). It is this structural concern that constrains attaining a high level of aerodynamic performance with a highly loaded, single stage turbine. In the design of the Energy Efficient Engine turbine, this challenge has been addressed by the application of high strength blade and disk alloys, along with increased blade taper.

The efficient management of cooling flow is essential since significant penalties in efficiency as well as increases in fuel burned result from the large percentage airflow required to cool the turbine components. From a performance standpoint, the goal is to minimize the amount of coolant, while maintaining acceptable metal temperatures to meet durability requirements. The turbine design addresses this challenge by utilizing advanced high temperature capability materials for the airfoils along with thermal barrier coatings and an efficient cooling management system. This combination reduces the cooling requirement by approximately 30 percent in comparison to current-technology commercial engines.

3.2 HIGH-PRESSURE TURBINE GENERAL DESCRIPTION

A cross sectional view of the high-pressure turbine for the Energy Efficient Engine is presented in Figure 3.2-1.

The parts of the engine comprising the high-pressure turbine are those discussed in this report and are shown in Figure 3.2-1. The design is based on modularity to facilitate accessibility and maintainability. Along with the high rim speed and large annulus area, the single stage design has numerous features to reduce cost, increase aerodynamic efficiency, improve cooling effectiveness, reduce cooling air leakage, and minimize performance deterioration. These various technology features are listed in Table 3.2-I.

TABLE 3.2-I

ADVANCED TECHNOLOGY DESIGN CONCEPTS

REDUCED COST CONCEPTS:

- Single-Stage Turbine
- Reduced Number of Airfoils

INCREASED AERODYNAMIC EFFICIENCY CONCEPTS:

- High AN²/High Rim Speed
- Contoured Vane End Walls
- Low Loss Airfoils
- Reduced Tip Loss Configuration and Active Clearance Control
- High Airfoil Loadings

REDUCED LEAKAGE CONCEPTS:

- Reduced Leakage Length
- Improved Gap Sealing
- Improved Rim Sealing
- W-Seals

REDUCED COOLANT FLOW CONCEPTS:

- Single-Stage Turbine
- Improved Airfoil Cooling Effectiveness
- Single Crystal Airfoil Materials
- Thermal Barrier Platform Coatings
- Efficient Coolant Supply System
- Low Windage

PERFORMANCE RETENTION CONCEPTS:

- Ceramic Outer Air Seal/ Abrasive Blade Tip

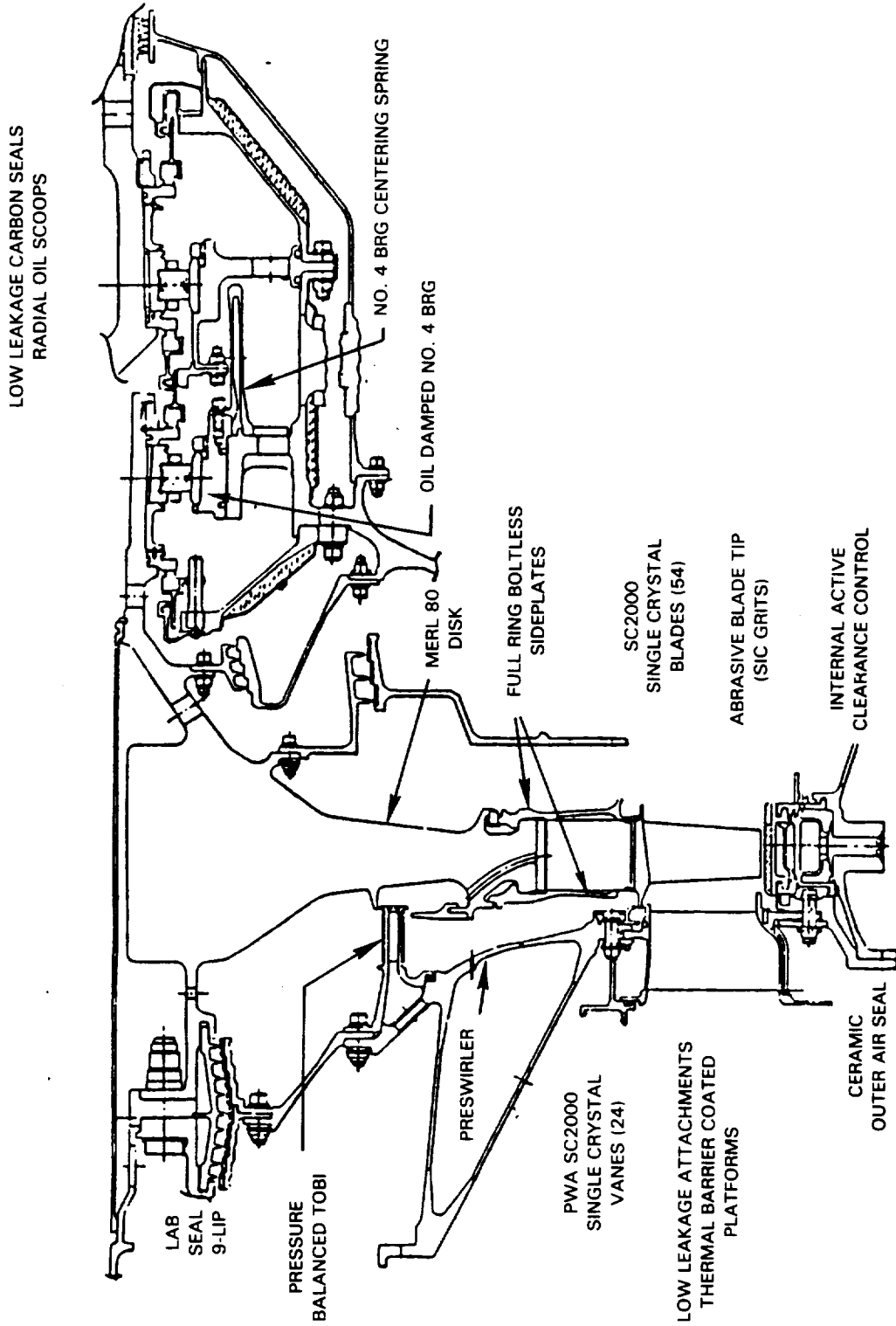


Figure 3.2-1 Energy Efficient Engine High-Pressure Turbine Component

The single stage configuration offers a potentially large savings in engine cost, weight and maintenance costs because of a significant reduction in the number of components, especially expensive air-cooled turbine airfoils. In comparison to the base engine two stage version, the single stage turbine has 43 percent fewer airfoils. Also, the overall number of turbine parts has been reduced by elimination of the second stage disk, seals, outer airseals and related components.

The capability to operate at higher blade loadings because of a reduction in airfoil number results in substantial performance gains. Other performance enhancement features include contoured vane endwalls and an active clearance control system to minimize operating clearances at cruise conditions.

A reduction in cooling flow with no compromise in durability is obtained primarily through the use of advanced high-temperature materials and efficient airfoil cooling methods. Both the vane and blade materials are single crystal alloys which offer superior creep strength properties, along with good resistance to thermal fatigue. In addition, the vane platforms are coated with a thermal barrier coating for additional temperature capability. The internal cooling system of the airfoils is efficiently designed to promote a high heat transfer rate with a minimum of coolant airflow.

A substantial reduction in leakage has been achieved by the use of advanced sealing techniques and the relatively fewer number of airfoils, which reduces leakage sources. Besides the ceramic seals in the active clearance control system, leakage is reduced in the blade attachment by the use of full-ring boltless sideplates and W-seals. Also, feather seals are employed in the vane inner and outer platforms to reduce leakage.

Turbine performance retention in the flight propulsion system will be enhanced by an advanced blade tip sealing system. The turbine blade incorporates an abrasive material tip treatment that is used in conjunction with an abradable ceramic outer airseal.

3.3 DESIGN PERFORMANCE DATA

The engine performance data used to design the high-pressure turbine are a combination of flight propulsion system predictions and integrated core/low spool expectations. This design approach was taken to maximize the performance of the high-pressure turbine during integrated core/low spool testing, while still demonstrating a component that is representative of the flight propulsion system. As a result, the design uses power and flow levels expected for the integrated core/low spool, while assuming predicted flight propulsion system levels for the aerodynamic losses. This approach results in a high-pressure turbine exit flow parameter that is incompatible with the design inlet flow parameter of the low-pressure turbine. This flow parameter discrepancy requires that the high-pressure turbine blade be restaggered for the integrated core/low spool test.

The design performance data for the high-pressure turbine is summarized in Table 3.3-I. This table also compares this design performance with similar data for the flight propulsion system and integrated core/low spool from which it was derived.

TABLE 3.3-I

HIGH-PRESSURE TURBINE PREDICTED PERFORMANCE AT AERODYNAMIC DESIGN POINT
(10,668 m (35000 ft), 0.8 Mach Number, Standard Day)

	<u>Component Design (Before Restagger)</u>	<u>Flight Propulsion System Prediction</u>	<u>Integrated Core/Low Spool Expectation</u>
N (RPM)	13233	13178	13233
Total W_c/a (% W_{ae})	16.84	15.95	16.84
HPT W_c/a (% W_{ae})	14.10	13.19	14.10
FP_{in} ($W \sqrt{T}/P$)	16.98	16.82	16.98
FP_{out} ($W \sqrt{T}/P$)	66.74	65.98	68.16
Pr	3.998	4.032	4.084
Δh (Btu/sec)	13384	13086	13409
Efficiency (%)	87.9*	88.8	87.1
Efficiency Goal (%)	--	88.2	86.7

*Based on flight propulsion system aerodynamic losses and integrated core/low spool cooling flows

SECTION 4.0
HIGH-PRESSURE TURBINE AERODYNAMIC DESIGN

4.1 OVERVIEW

The aerodynamic definition of the high-pressure turbine was based on a series of analyses to establish the flowpath, airfoil contours, solidity and matching characteristics that achieve the highest level of performance within the constraints of the basic mechanical definition. Moreover, the final design was influenced by results obtained from different supporting technology programs that were in progress concurrent with the design process. These programs served as design and diagnostic tools to address unique requirements of the component design. The different programs consisted of the Uncooled Rig Program, the Supersonic Cascade Rig Program and the Leakage Program. The contribution of these programs to the turbine aerodynamic design is summarized in Section 4.2.5.

As a result of these design analyses and supporting technology programs, the low throughflow velocity and high reaction aerodynamic approaches were selected as the basis for the component design. Also, the airfoil design philosophy of low uncovered turning, low exit wedge angle was maintained. The general parameters governing the aerodynamic design of the turbine component are listed in Table 4.1-I.

TABLE 4.1-I
GENERAL AERODYNAMIC PARAMETERS

STAGES	Design Point (Mn 0.8; 10,668 m (35000 ft))	Flight Propulsion System Sea Level Takeoff (Hot Day)
		1
PT _{IN} Pa (psia)	1,324,491 (192.1)	
CE _T K (°R)	1633 (2940)	1708 (3076)
RI _T K (°R)	1561 (2811)	1641 (2955)
N (RPM)	13232.	13866.
ΔH (Btu/sec)	13384.	
FP _{in} (W $\sqrt{T_T/P_T}$)	16.984	
W _{C/A} (%W _{ae})	14.10	
PR	4.0	
Reaction	43.0 percent	
Velocity Ratio	0.556	
NASA Work Factor ($\Delta h/u^2$)	1.62	
C _{x/U}	0.351	
AN ² (IN ² RPM ²)	4.06 x 10 ¹⁰	4.46 x 10 ¹⁰
U _{RI} m/sec (ft/sec)	481 (1580)	504 (1655)
Clearance cm (in)	0.0469 (0.0185)	
Efficiency (Design)	87.9 percent	

As described previously in Section 3.3, a mixture of cycle performance data from flight propulsion system predictions and the integrated core/low spool expectations was used in the design of this turbine. The design intent was to satisfy flight propulsion system requirements through application of the results gained from the supporting technology programs. As work progressed it became apparent that the high-pressure turbine in the integrated core/low spool design should be matched to the expected integrated core/low spool performance. The turbine design, therefore, uses the power and flow requirements of the integrated core/low spool while assuming the level of aerodynamic losses in the flight propulsion system. The high-pressure turbine exit flow parameter resulting from this approach does not match the integrated core/low spool low-pressure turbine flow parameter (Section 4.2.3). To achieve the desired low-pressure turbine inlet aerodynamic conditions in the integrated core/low spool, the high-pressure turbine blade was restaggered open 0.25 degree from its aerodynamic definition.

4.2 COMPONENT AERODYNAMIC DESIGN

4.2.1 Flowpath Definition

The flowpath for the high-pressure turbine component is presented in Figure 4.2.1-1, showing the turbine elevation and axial length. In the single stage configuration, there is a total of 24 vanes and 54 blades.

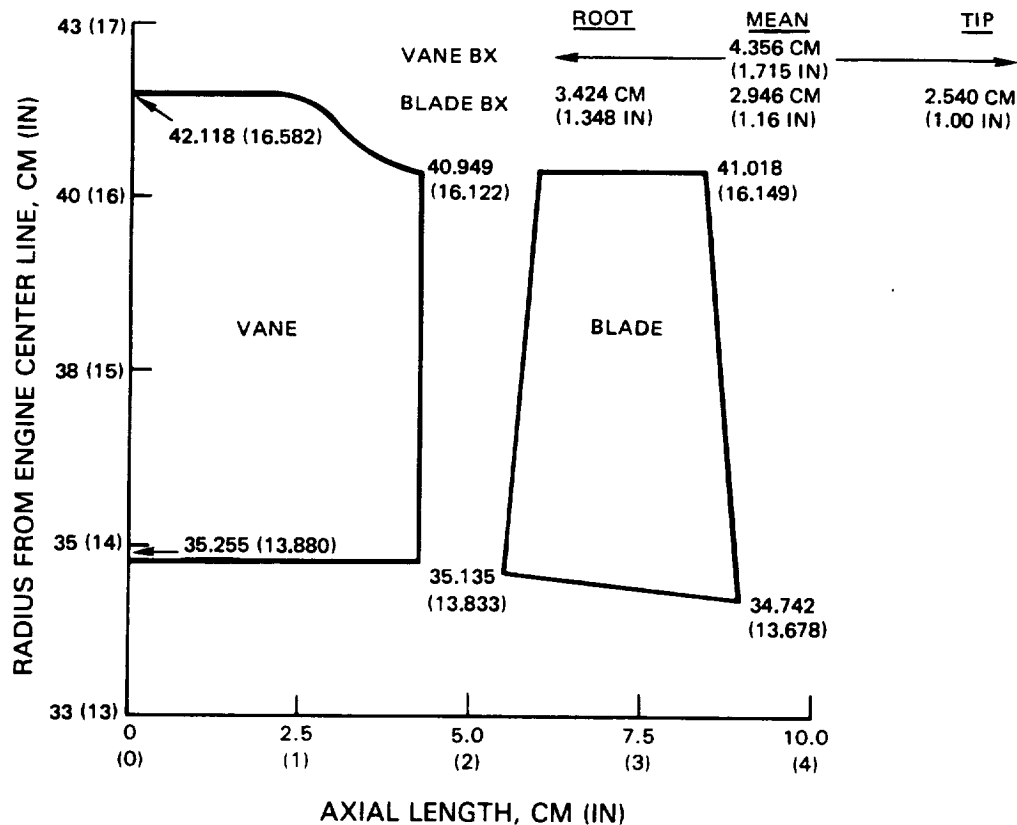


Figure 4.2.1-1 High-Pressure Turbine Flowpath Definition

The vanes are characterized by aerodynamic sections having a blunt leading edge and a long chord with the maximum airfoil thickness near the leading edge. The inner vane endwall is cylindrical, while the outer is contoured in an "S" shape (Figure 4.2.1-1). The large aerodynamic section thickness reduces the losses associated with the introduction of cooling flow and the S-wall design reduces endwall pressure losses. In addition, the number of vanes minimizes blockage as well as optimizes the positioning of the vanes with the combustor fuel injector nozzles.

The blades are highly tapered with a conical inner wall. Blade axial chord taper was selected to accommodate stress requirements. Also, the stage is defined with a high reaction level to enhance efficiency. On the basis of design analyses, it was shown that higher reaction levels produced higher efficiencies. The maximum allowable reaction level for this turbine design was limited to 43 percent because increasing the axial pressure load on the rotor resulted in excessive bearing loadings and consequent durability concerns. Experimental testing in the supporting Uncooled Rig Program demonstrated the benefit of the 43 percent reaction level in comparison to a lower level of 35 percent.

4.2.2 Airfoil Definition

Several analytical techniques were used to establish the turbine airfoil definitions. A streamline computer design simulation generated the radial aerodynamic environment. This information serves as input to the interactive airfoil design system for a definition of the external contour of the airfoil.

Analyses are then performed to ascertain pressure distribution and boundary layer characteristics. On the basis of these results, iterations of the airfoil shape are made to optimize pressure distribution, boundary layer and loss characteristics.

Using these methods, vane sections were analytically defined. The sections were designed so that the flow accelerated past the throat area with low, smooth backend diffusion. The uncovered turning and exit wedge angle were optimized to minimize pressure loss. Blade sections were designed to the same pressure distribution criteria as the vane. Uncovered turning and exit angle were optimized to reduce blade profile, trailing edge and shock losses. Results from the Supersonic Cascade Program verified the final airfoil shapes. Significant test results relating to the airfoil aerodynamic design are presented in Section 4.2.5.

Velocity triangle data pertaining to the final airfoil definitions are presented in Table 4.2.2-I. These triangles are similar to those used in the testing of turbine blades with a 43 percent reaction level (second build of the Uncooled Rig Program).

The assumed temperature profile for the combustor exit and the vane pressure loss profile used in the design is shown in Figure 4.2.2-1.

Figures 4.2.2-2 through 4.2.2-4 present the airfoil contours of the vane root, mean and tip sections, respectively, along with a summary of the section aerodynamics and corresponding static pressure distribution. Figure 4.2.2-5 shows a two-dimensional schematic of the vane section stacking.

TABLE 4.2.2-1

GAS TRIANGLES*

	<u>Root</u>	<u>Mean</u>	<u>Tip</u>
VANE			
α IN (deg)	90°	90°	90°
α OUT (deg)	11.6°	10.3°	9.1°
M IN	0.09	0.08	0.07
M OUT	1.0	0.92	0.85
θ GAS (deg)	78.4°	79.7°	80.4°
BLADE			
β IN (deg)	33.5°	42.7°	63.6°
β OUT (deg)	15.9°	16.9°	17.7°
Mr IN	0.36	0.25	0.14
Mr OUT	1.22	1.24	1.28
θ GAS (deg)	130.6°	120.4°	98.7°
α OUT (deg)	38.0°	43.8°	48.4°
M OUT (deg)	0.54	0.52	0.52

*Based on flat inlet temperature and flat loss profiles.

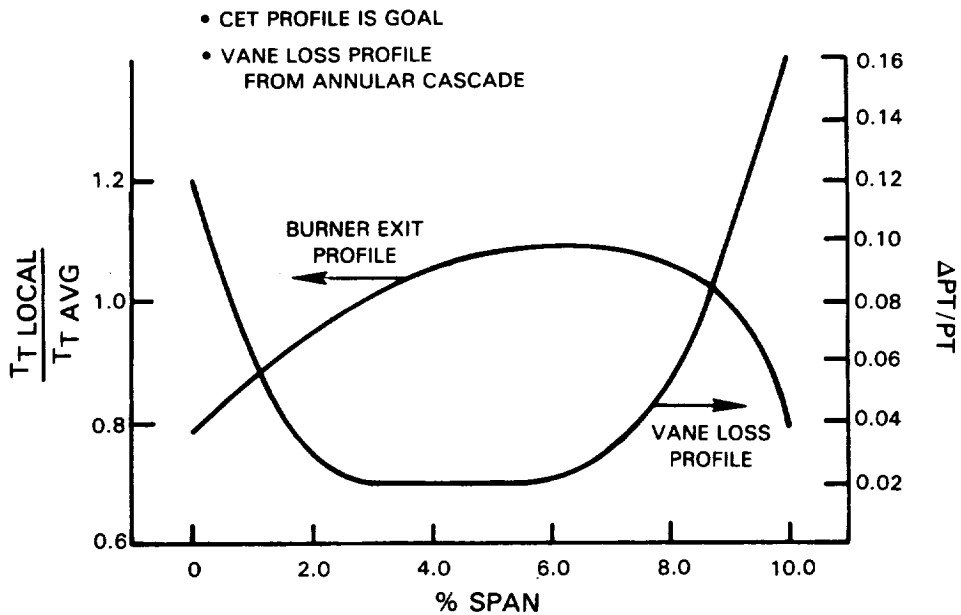


Figure 4.2.2-1 Vane Assumed Profiles For Inlet Temperature and Pressure Loss

CONTAINING SECTIONS OF POOR QUALITY.

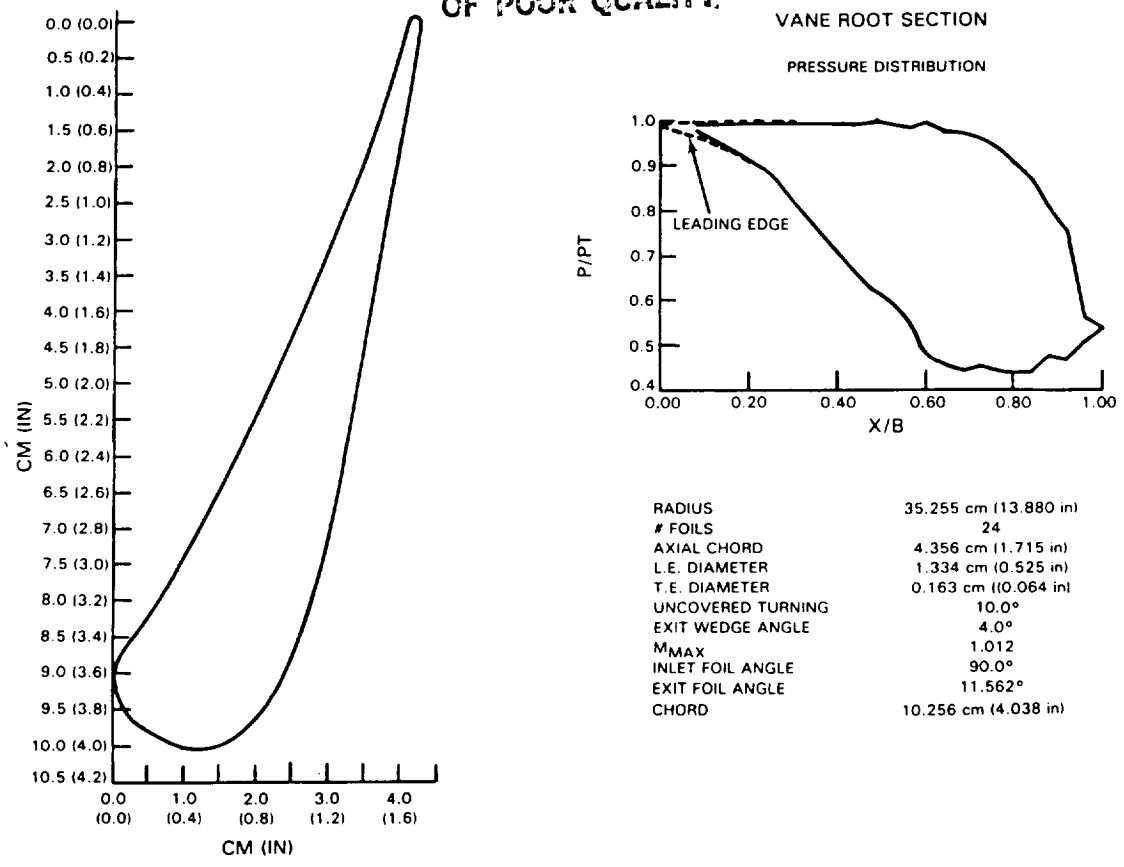


Figure 4.2.2-2 Vane Root Section Aerodynamic Contour and Pressure Distribution

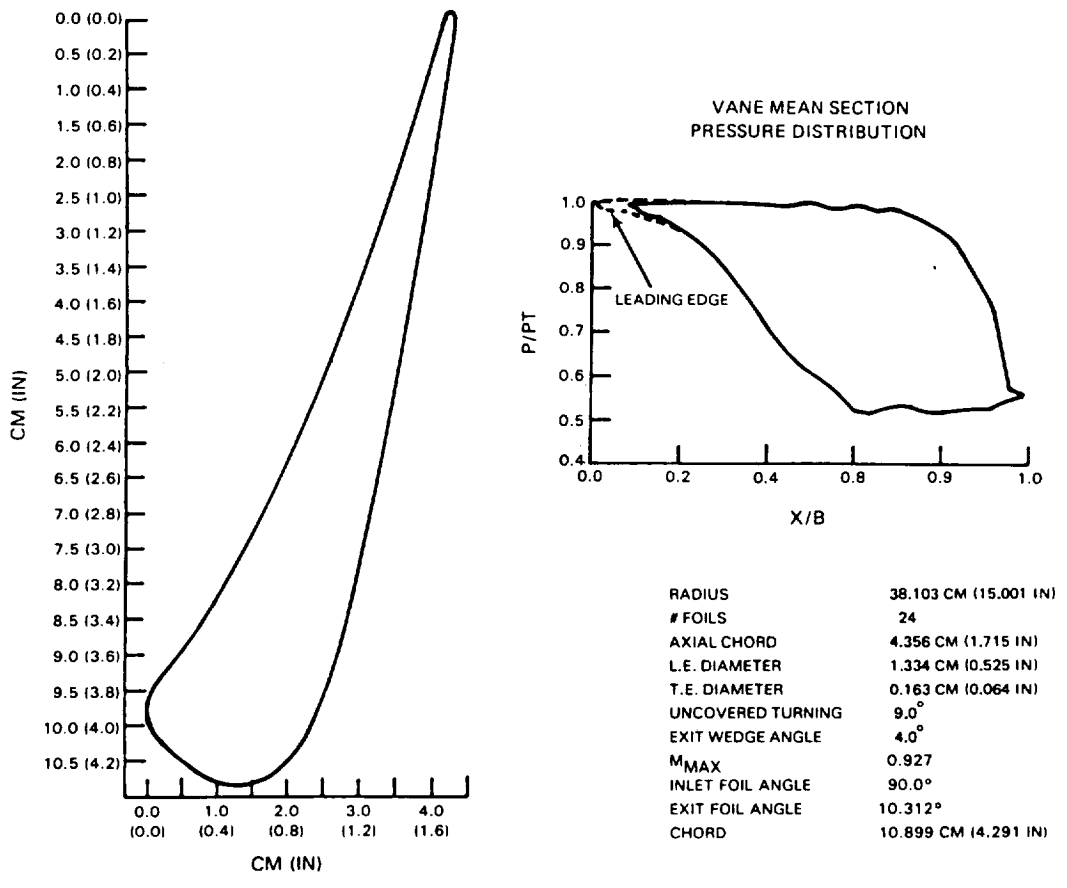


Figure 4.2.2-3 Vane Mean Section Aerodynamic Contour and Pressure Distribution

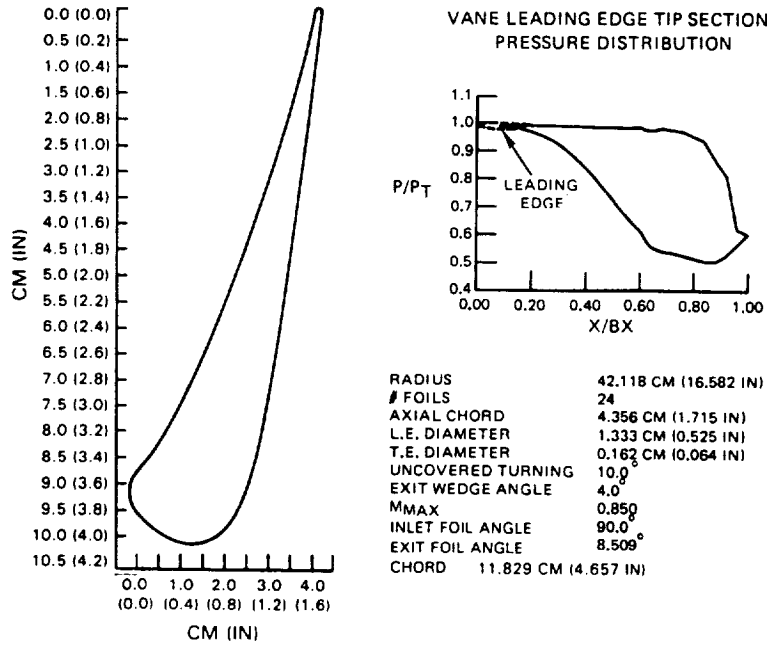


Figure 4.2.2-4 Vane Tip Section Aerodynamic Contour and Pressure Distribution

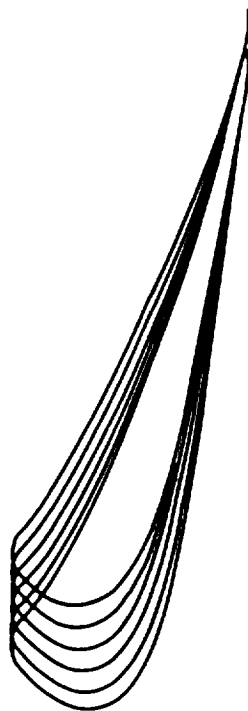


Figure 4.2.2-5 Turbine Vane Stacking

Similar design information is presented for the blade in Figures 4.2.2-6 through 4.2.2-12. As shown in Figure 4.2.2-6, the blade inlet angle has been adjusted to account for differences between a rig and engine environment (temperature, cooling and secondary airflows). The result is a blade design with the root and tip sections that are undercambered 5 and 10 degrees, respectively, and the mean section is overcambered 8 degrees in comparison to the rig contours.

Figures 4.2.2-7 through 4.2.2-11 present blade section contours for the root, one-quarter root, mean, one-quarter tip and tip section, respectively. These figures also provide a summary of the aerodynamic properties as well as the pressure distributions. Figure 4.2.2-12 shows the blade stacking.

Airfoil coordinates are given in Appendix A.

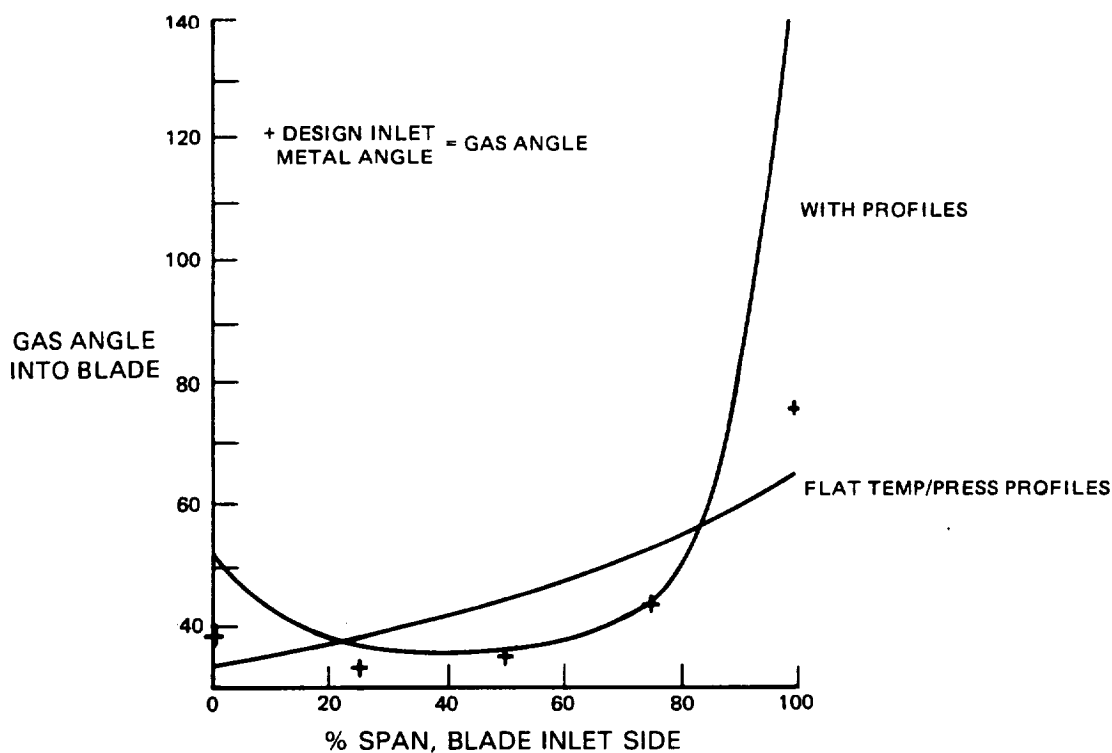


Figure 4.2.2-6 Effect of Inlet Temperature and Vane Loss Profile on Blade Inlet Angle

ORIGINAL PAGE IS
OF POOR QUALITY

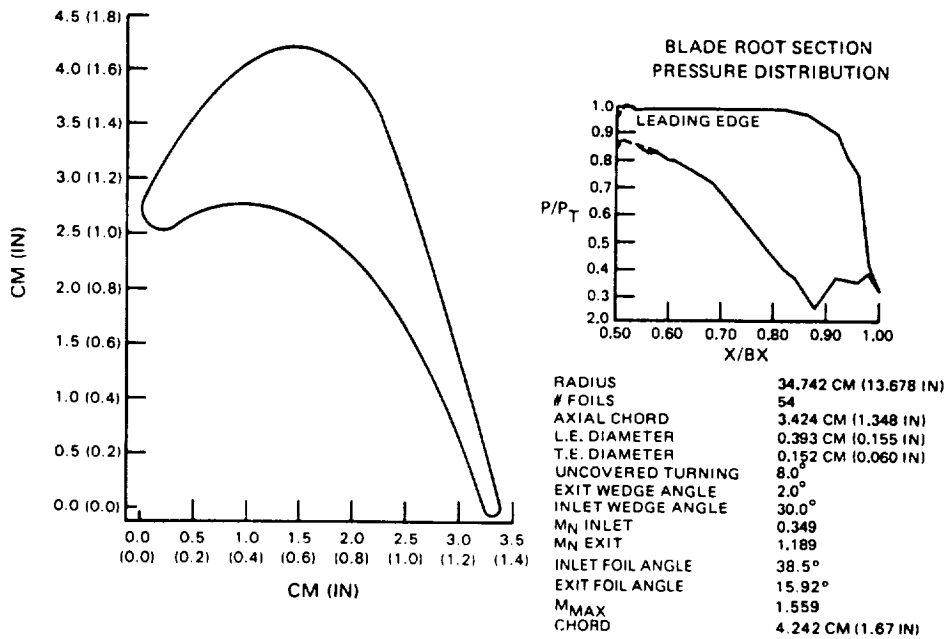


Figure 4.2.2-7 Blade Root Section Aerodynamic Contour and Pressure Distribution

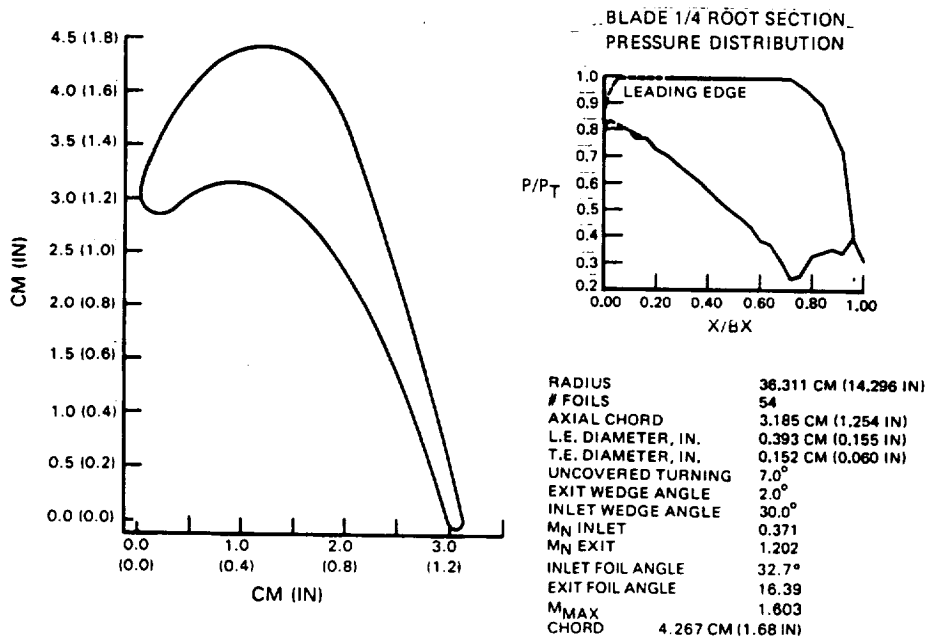


Figure 4.2.2-8 Blade One-Quarter Root Section Aerodynamic Contour and Pressure Distribution

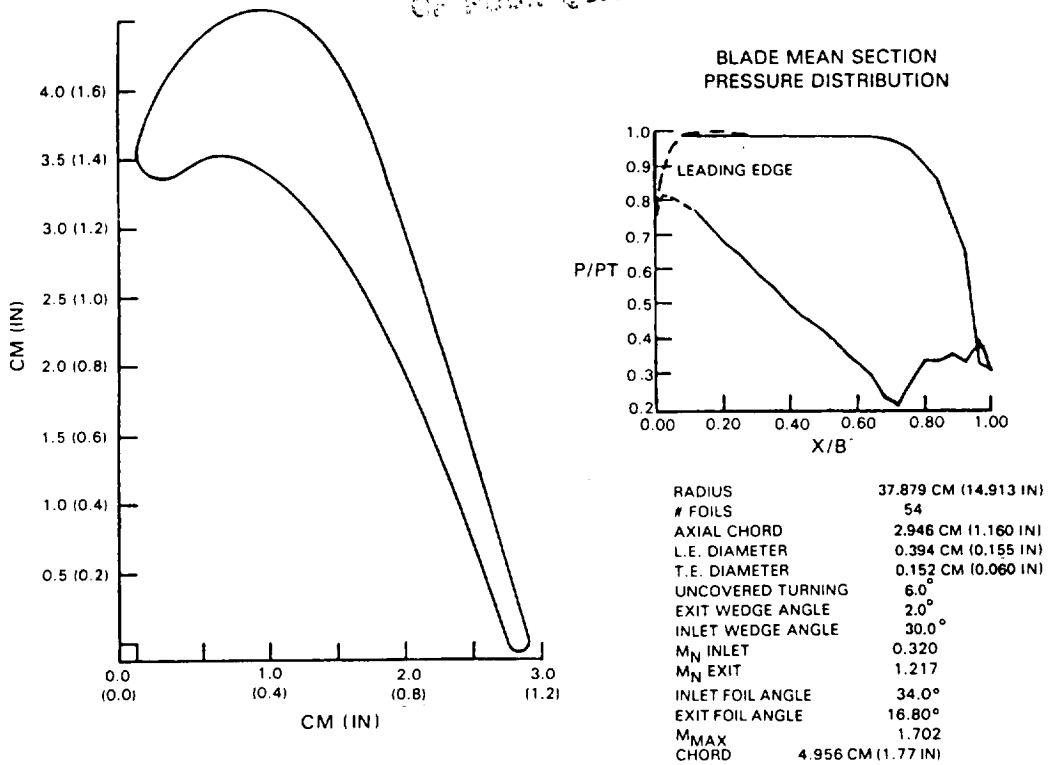


Figure 4.2.2-9 Blade Mean Section Aerodynamic Contour and Pressure Distribution

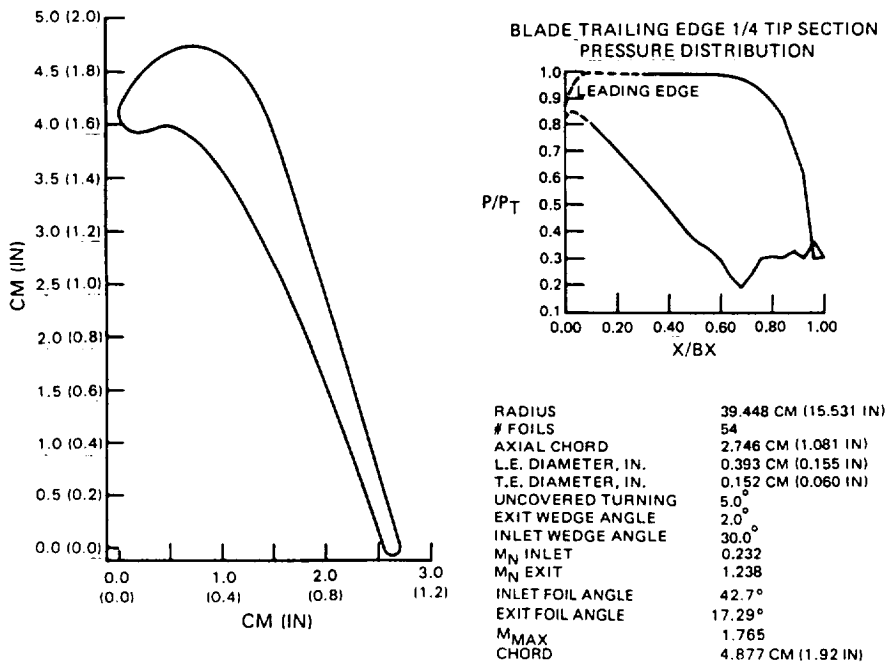


Figure 4.2.2-10 Blade One-Quarter Tip Section Aerodynamic Contour and Pressure Distribution

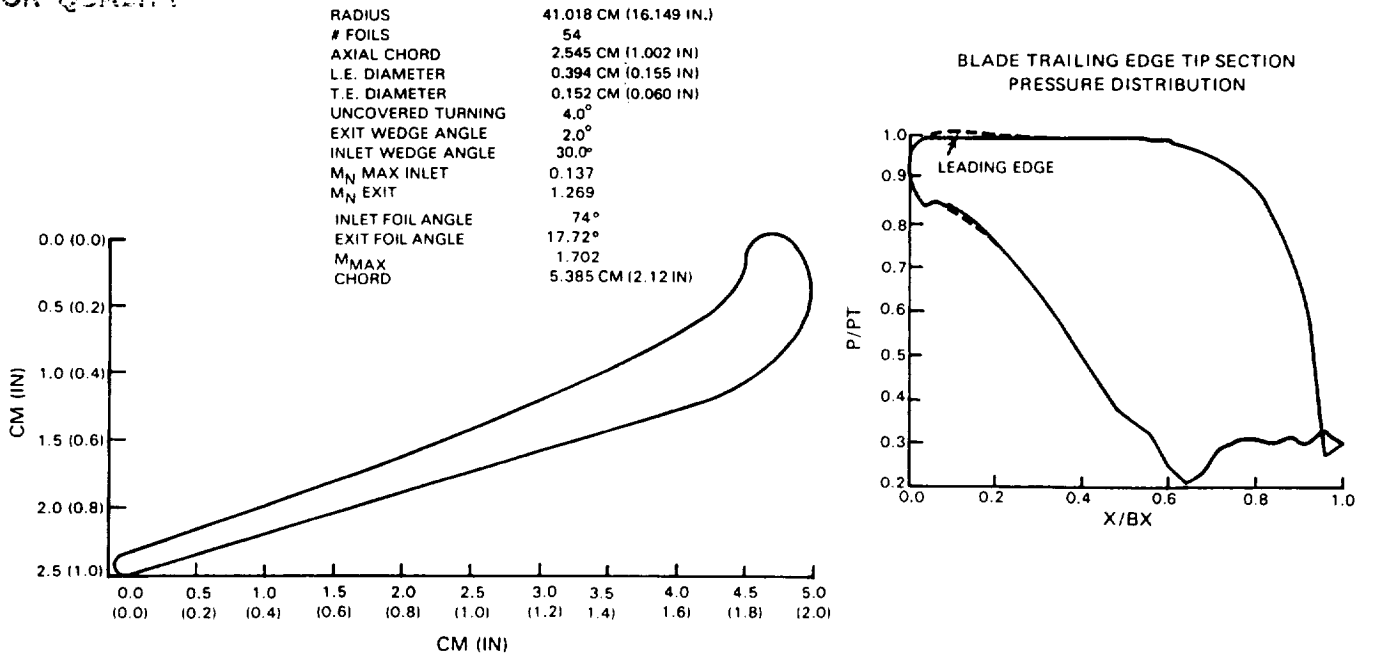


Figure 4.2.2-11 Blade Tip Section Aerodynamic Contour and Pressure Distribution

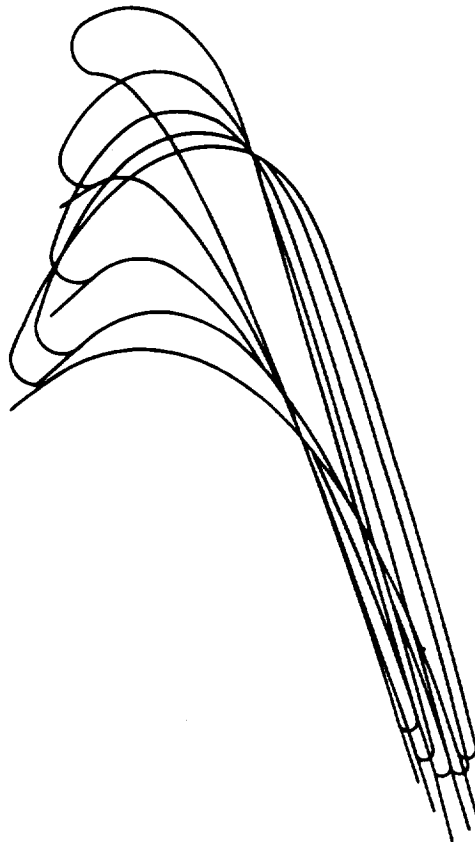


Figure 4.2.2-12 Turbine Blade Stacking

4.2.3 High-Pressure and Low-Pressure Turbine Matching

To achieve the desired low-pressure turbine inlet aerodynamic conditions in the integrated core/low spool, the high-pressure turbine blade stagger angle was opened 0.25 degree from its aerodynamic definition. As indicated in Table 4.2.3-1, the net result of restaggering is a slight penalty in high-pressure turbine efficiency.

TABLE 4.2.3-I

HIGH-PRESSURE TURBINE AERODYNAMICS AFTER RESTAGGERING

	HPT Designed (Initial IC/LS)	HPT Run At LPT FP	Restaggered HPT Run at LPT FP (Final IC/LS)
FPHPT IN	16.983	16.983	17,023
FPHPT OUT	66.562	68.165	68.165
PR HPT	3.98	4.093	4.084
HPT Reaction	43. percent	43.8 percent	42.4 percent
$\Delta\eta$ HPT	BASE	0 to -0.3 percent	0 to -0.15 percent
Mn HPT OUT	0.523	0.554	0.539
α HPT OUT	43.8 degrees	43.0 degrees	44.0 degrees
LPT Converg			
V1 ROOT	1.4	1.35	1.4
B1 ROOT	1.3	1.25	1.3

- Conclusion:

Restagger + 0.25 Degree To Get Back $\Delta\eta$ HPT, Bearing Load (i.e., Reaction), and LPT Aerodynamics

4.2.4 Aerodynamic Efficiency Status

The high-pressure turbine efficiency estimates, based on results acquired from the Uncooled Rig Program and the aerodynamic design, are summarized in Table 4.2.4-I. On the basis of these estimates, the efficiency goals for both the integrated core/low spool and flight propulsion system are attainable at the goal tip clearance 0.046 cm (0.0185 in) and exceeded at the status tip clearance 0.032 cm (0.0126 in). The component design efficiency level is also confirmed.

4.2.5 Supporting Technology Programs

In support of the high-pressure turbine aerodynamic design, several technology programs were conducted to experimentally assess the critical advanced design concepts. These programs included the Uncooled Rig Program, Supersonic Cascade Program and Leakage Program. Results acquired from these efforts provided the necessary technical guidance and insight to ensure a viable aerodynamic design.

TABLE 4.2.4-I

HIGH-PRESSURE TURBINE EFFICIENCY ESTIMATE BASED ON
UNCOOLED RIG TEST RESULTS
Aerodynamic Design Point
(10,668 m (35000 ft), 0.8 Mach No., Standard Day)

	<u>Flight Propulsion System (%)</u>	<u>Component Design (%)</u>	<u>Integrated Core/Low Spool (%)</u>
Uncooled Rig (Build 2)	91.1	91.1	91.1
Coating	-0.2	-0.2	-0.2
Cooling	-3.7	-3.8	-3.8
Trailing Edge Blowing	+1.1	+1.1	+1.1
Blade Restagger	-	-0.1	-0.1
Leakage	-	-	-0.1
Clearance	-	-	-0.2
Windage	-	-	-0.2
Part Quality	-	-	-0.8
Engine Rematch	-	-	-0.2
EFFICIENCY ESTIMATE AT:			
Goal Clearance 0.0472 cm (0.0186 in)	88.3	88.1	86.6
Status Clearance 0.0320 cm (0.0126 in)	88.8	-	87.1
GOAL EFFICIENCY (%)	88.2	-	86.7

The Uncooled Rig Program was basically directed towards establishing the uncooled aerodynamic efficiency base and verifying the principal aerodynamic design assumptions, specifically the benefits of increased stage reaction level and low ratio of throughflow to wheel speed (C_x/U). The Supersonic Cascade Program focused on determining the performance characteristics of different vane endwall geometries and blade configurations, including loss characteristics with cooling flow. The Leakage Program was structured to investigate potential leakage sources in the turbine design and define approaches to reduce leakage within the constraints of the component design and sealing concepts evaluated.

Salient results from these programs, which influenced the turbine aerodynamic design, are summarized in the following sections. A complete description of the results of each program is contained in the following NASA Technical Reports: Energy Efficient Engine High-Pressure Turbine Uncooled Rig Technology Program (CR-165149, Reference 1), Energy Efficient Engine High-Pressure Turbine Supersonic Cascade Technology Report (CR-165567, Reference 2), and Energy Efficient Engine High-Pressure Turbine Leakage Technology Report (CR-165202, Reference 3).

4.2.5.1 Uncooled Rig Technology Program

Test results obtained from the Uncooled Rig Program demonstrated that substantial efficiency gains could be achieved by designing a single stage turbine to operate at a low ratio of throughflow to wheel speed (C_x/U) with an attendant high blade attachment stress and at higher turbine reaction levels.

The benefits of decreasing the C_x/U value and increasing the AN^2 parameter, as established by rig testing, are summarized in Figure 4.2.5-1. As shown, the measured performance of the Energy Efficient Engine turbine configuration is clearly superior to turbines with AN^2 parameters at state-of-the-art levels. The benefit of operating at a low C_x/U translates into 1.15 percent increase in turbine efficiency over current performance levels.

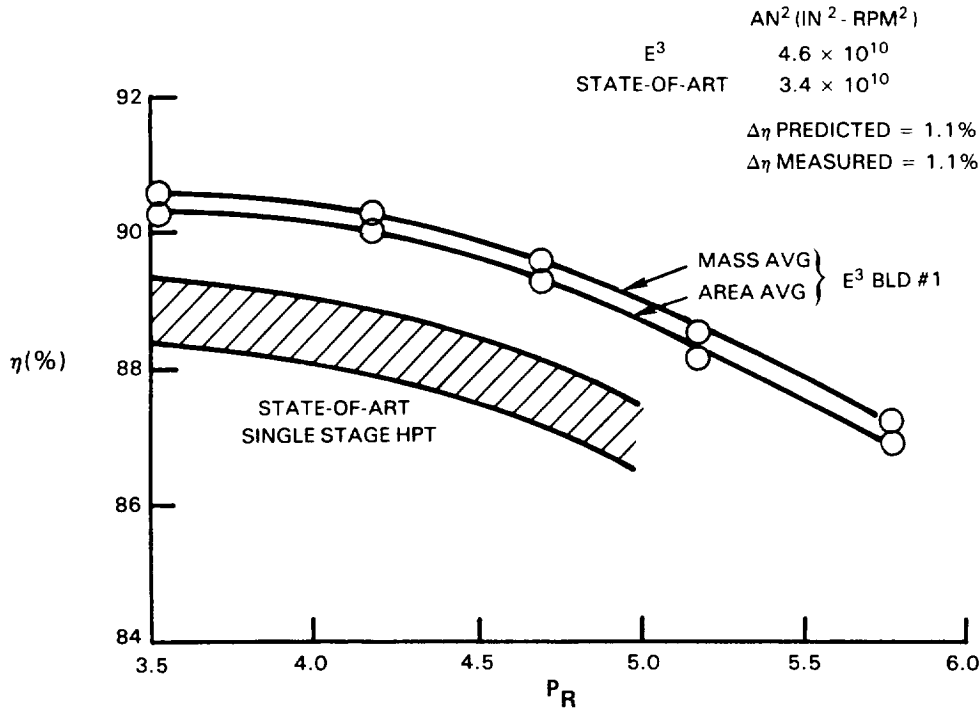


Figure 4.2.5-1 Turbine Uncooled Rig Performance Trends Showing Benefits of Decreasing the C_x/U and Increasing the AN^2 Parameter

Figure 4.2.5-2 shows the positive effect achieved by increasing the turbine stage reaction level. At the design point pressure ratio, testing with a higher reaction level -- 43 percent as opposed to the lower reaction level of 35 percent -- produced a 0.8 percent improvement in performance.

Table 4.2.5-I presents the predicted uncooled rig efficiency, along with the measured values. As indicated, the goals were surpassed. Overall, the results from this program have established the uncooled aerodynamic efficiency of the high-pressure turbine at 91.1 percent and have verified the feasibility of the advanced turbine aerodynamic design concepts.

ORIGINAL PAGE IS
OF POOR QUALITY

ORIGINAL PAGE IS
OF POOR QUALITY

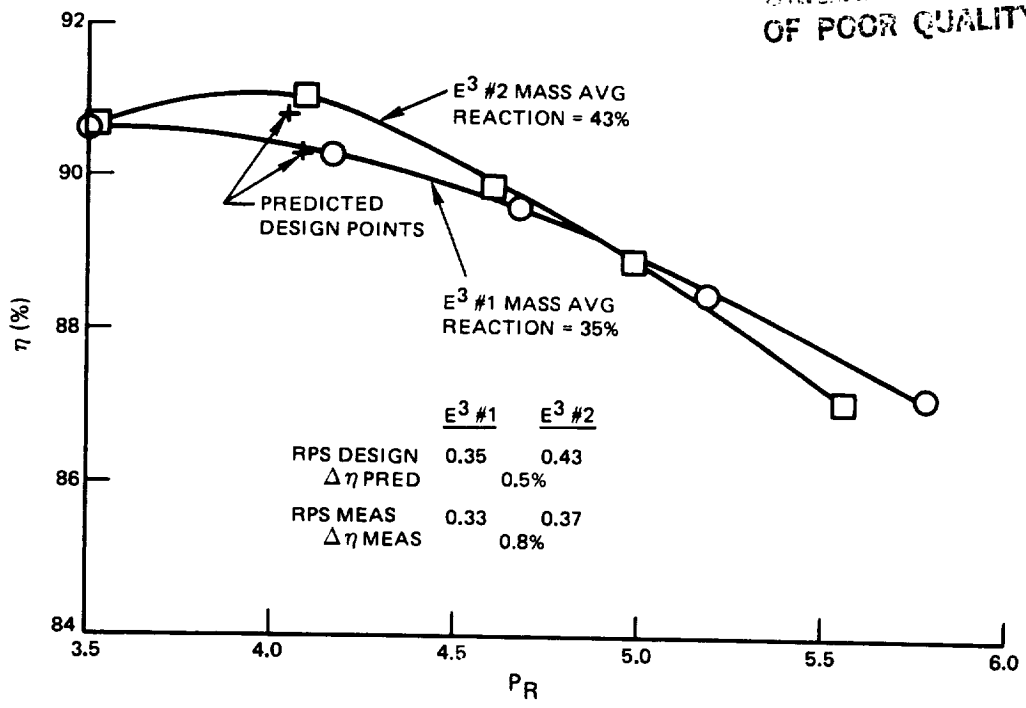


Figure 4.2.5-2 Efficiency Gains Associated with High Blade Reaction Levels

TABLE 4.2.5-I
TURBINE UNCOOLED RIG EFFICIENCY

	<u>Predicted (%)</u>	<u>Measured (%)</u>
Build 1	90.3	90.4
Build 2	90.8	91.1

4.2.5.2 Supersonic Cascade Program

In the Supersonic Cascade Program, two vane endwall geometries and three blade sections were evaluated to ascertain their influence on turbine performance. The vane endwall configurations included a contoured (S-wall) cascade and a straight wall cascade. Test results are presented in Figure 4.2.5-3, showing the spanwise distribution of total pressure loss for the two configurations. The data trends show that the S-wall design demonstrated substantially less pressure loss, a total of 17 percent, resulting primarily from the lower secondary loss in the S-wall cascade.

The ability to assess the losses of cooling and leakage flows is essential in order to properly predict the performance characteristics of a cooled turbine. To demonstrate the ability to predict these losses in a transonic environment, a cooled vane cascade test was conducted. In Figure 4.2.5-4, test data are compared to the analytical predictions. The good correlation of results verifies the ability of the design system to predict these effects.

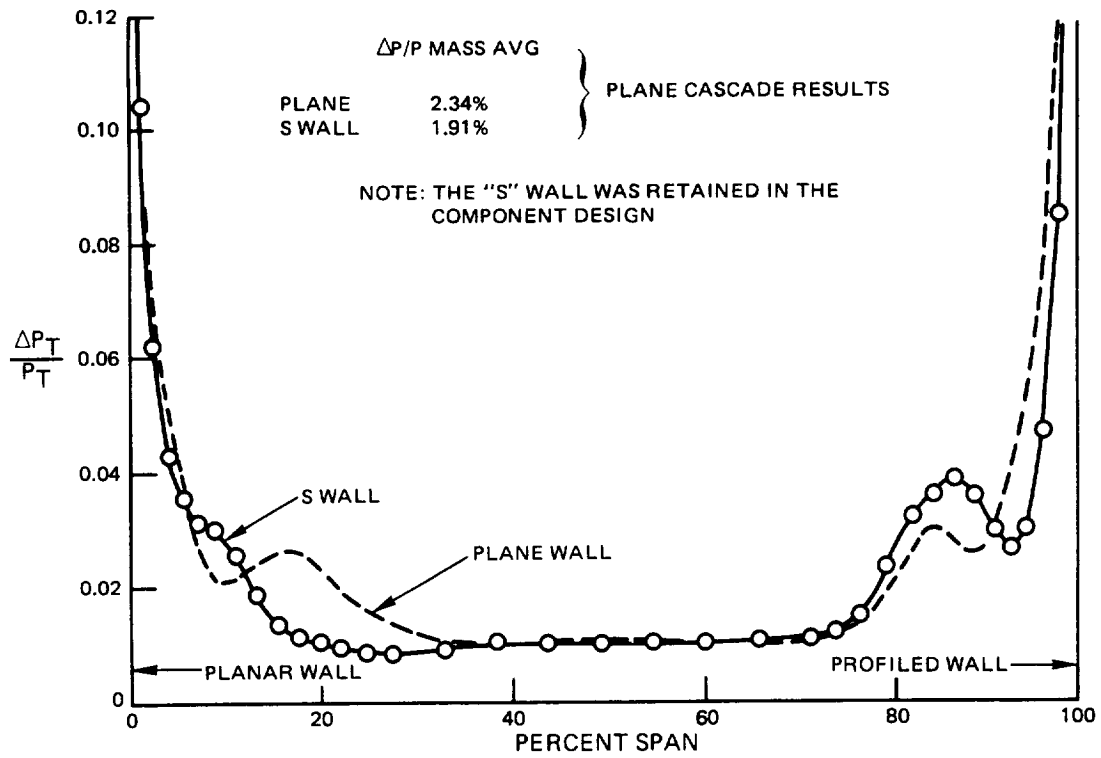


Figure 4.2.5-3 Spanwise Distribution of Total Pressure Loss for the Profiled Wall Cascade

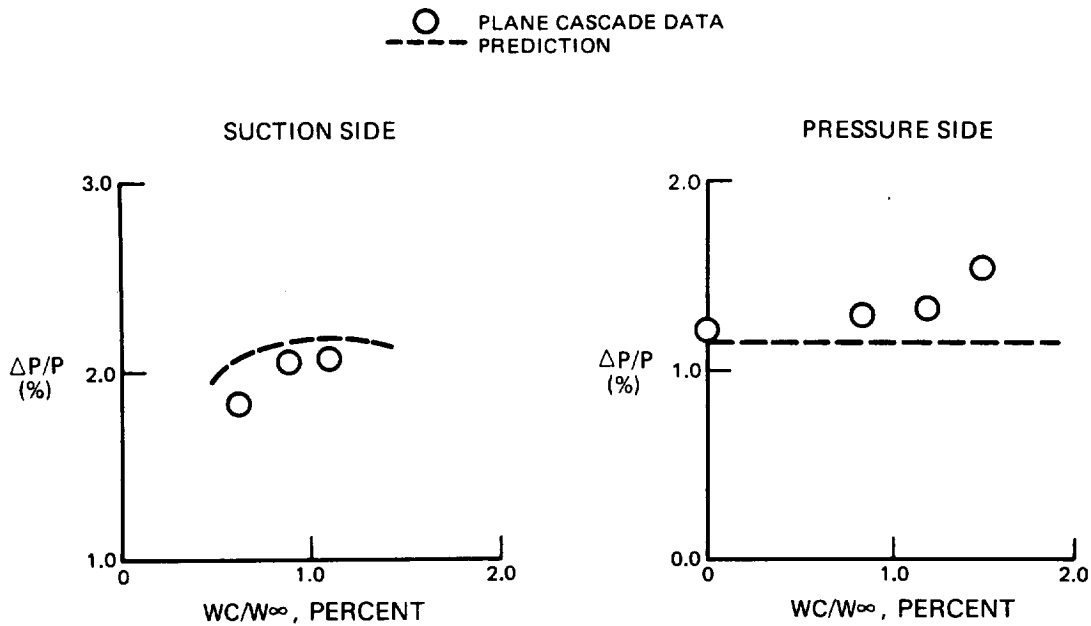


Figure 4.2.5-4 Predicted Vane Cooling Losses Compared to Test Results

ORIGINAL PAGE IS
OF POOR QUALITY

Blade cascades tested included overcambered and straightback designs which were evaluated against the candidate design (base blade configuration) for the Energy Efficient Engine high-pressure turbine. Cascade results demonstrated that no additional performance benefits were achieved by using the straightback design. Figure 4.2.5-5 shows the response of blade base pressure coefficient with trailing edge coolant injection and exit Mach numbers, and Figure 4.2.5-6 shows the effect of trailing edge ejected cooling flow on mean section total pressure loss. These results show that a significant performance improvement can be obtained with proper use of ejected cooling air.

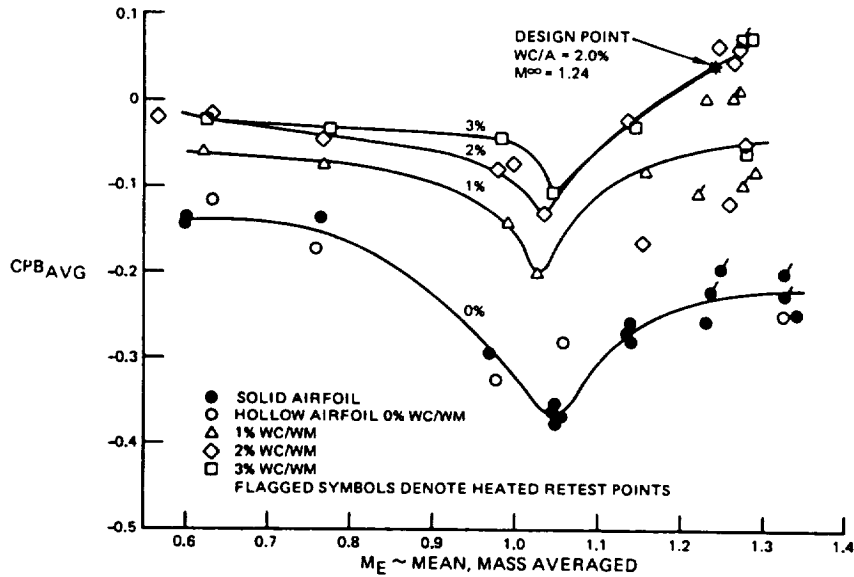


Figure 4.2.5-5 Effect of Trailing Edge Ejection Flow on Blade Pressure Coefficient

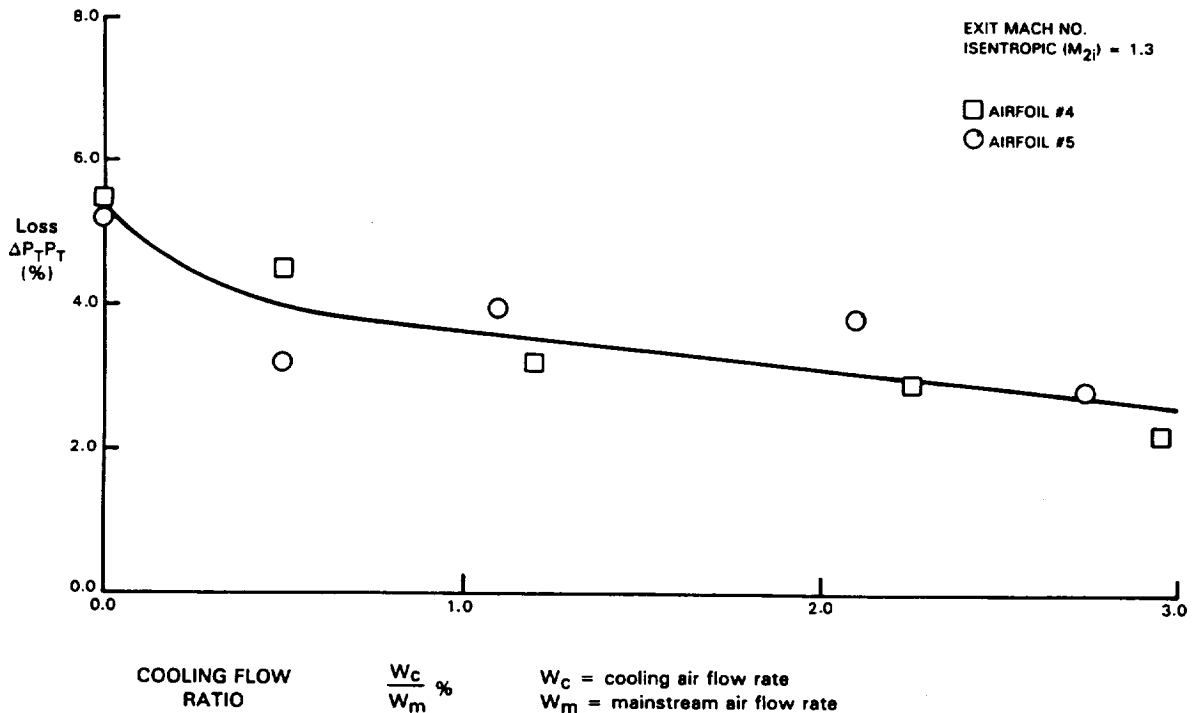


Figure 4.2.5-6 Plane Cascade Base Blade, Mean Section Trailing Edge Cooling Air Ejection

4.2.5.3 Leakage Program

The Leakage Program was conducted to evaluate techniques for leakage reduction in the high-pressure turbine. Based on this effort, the low leakage technology in the Energy Efficient Engine high-pressure turbine has been successfully substantiated. Test models were used to simulate component leak paths as well as to assess leakage reduction concepts. These models simulated the blade-disk attachment and the vane inner and outer platform attachment seals.

The results of blade-disk attachment testing disclosed that leakage in this area could be significantly reduced by paying careful attention to tolerances along the contact surfaces between the vibration damper and platform contact surface. As shown in Figure 4.2.5-7, attachment leakage is less than predicted, thereby demonstrating the effectiveness of the blade dampers in sealing the platforms.

Other tests were conducted to verify the full ring sideplate, W-seal design. The data presented in Figure 4.2.5-8 show that a flat rear sideplate against the disk face results in low leakage levels. Also, W-seals are effective in controlling leakage, as indicated by the results in Figure 4.2.5-9.

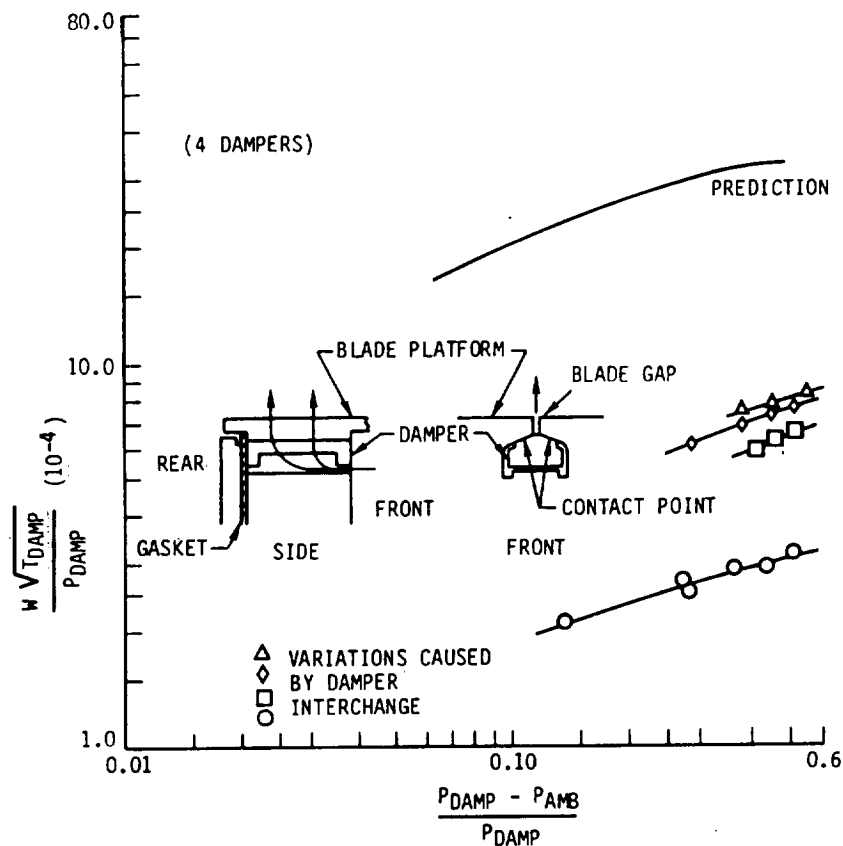


Figure 4.2.5-7 Results of Blade-Disk Model Testing Showing Leakage in the Attachment Area is Less Than Predicted

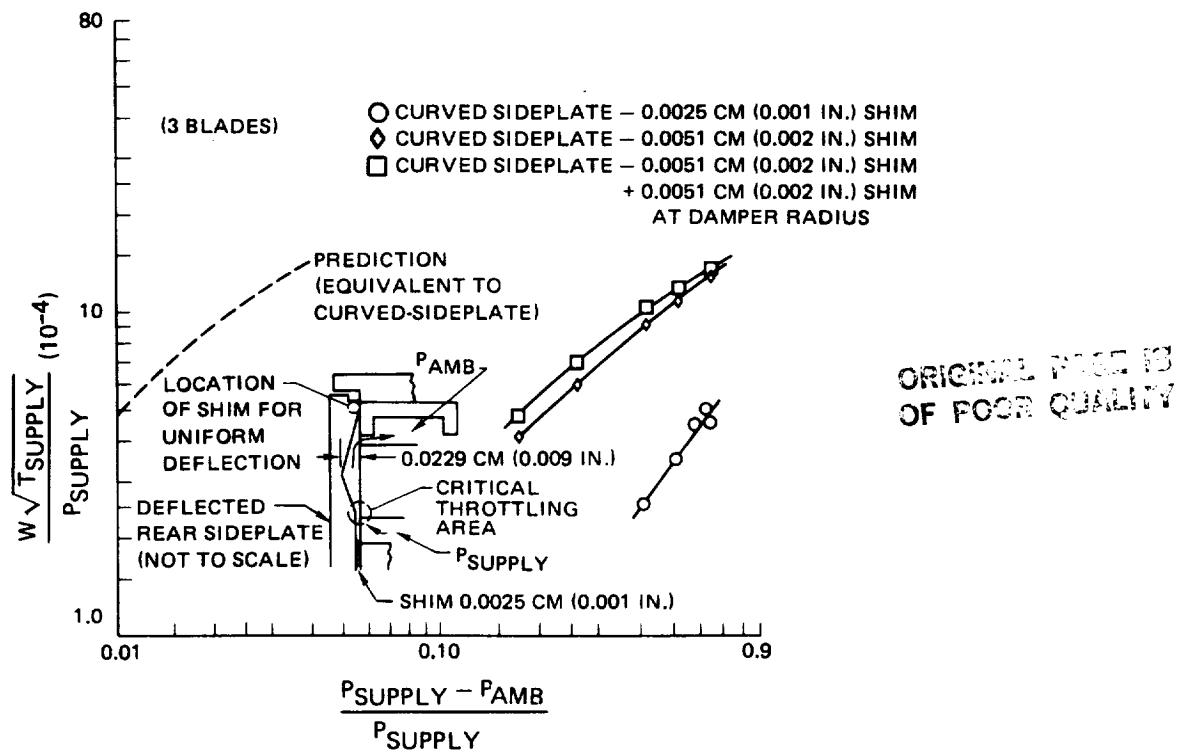


Figure 4.2.5-8 Sealing Effectiveness of Rear Sideplate Design

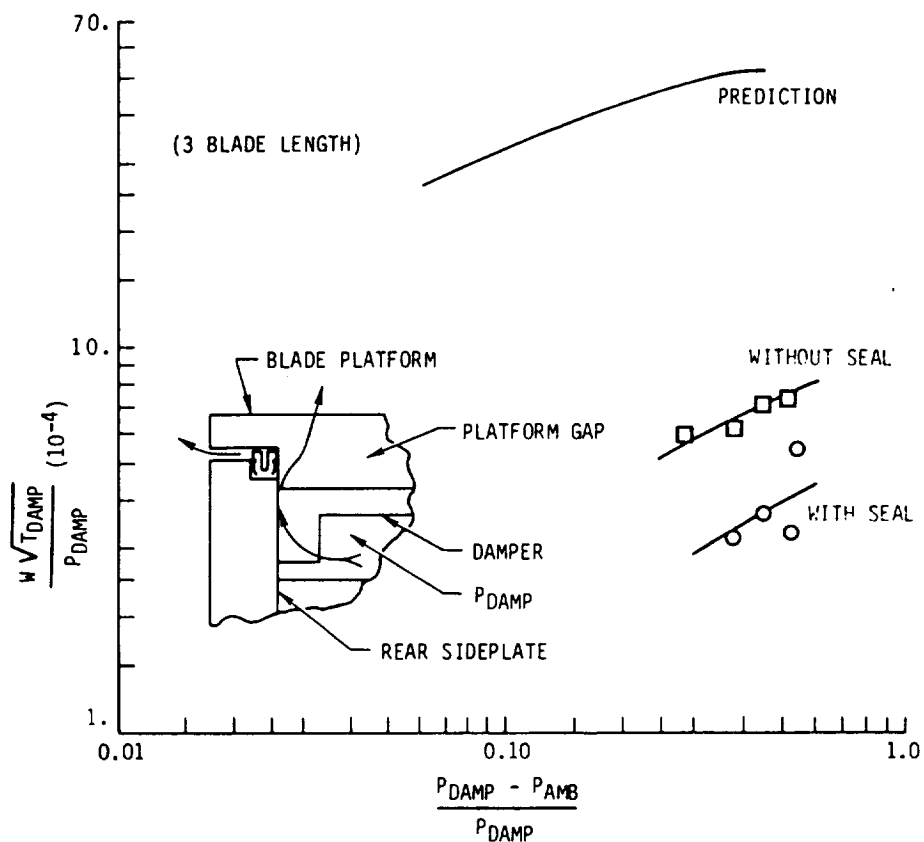
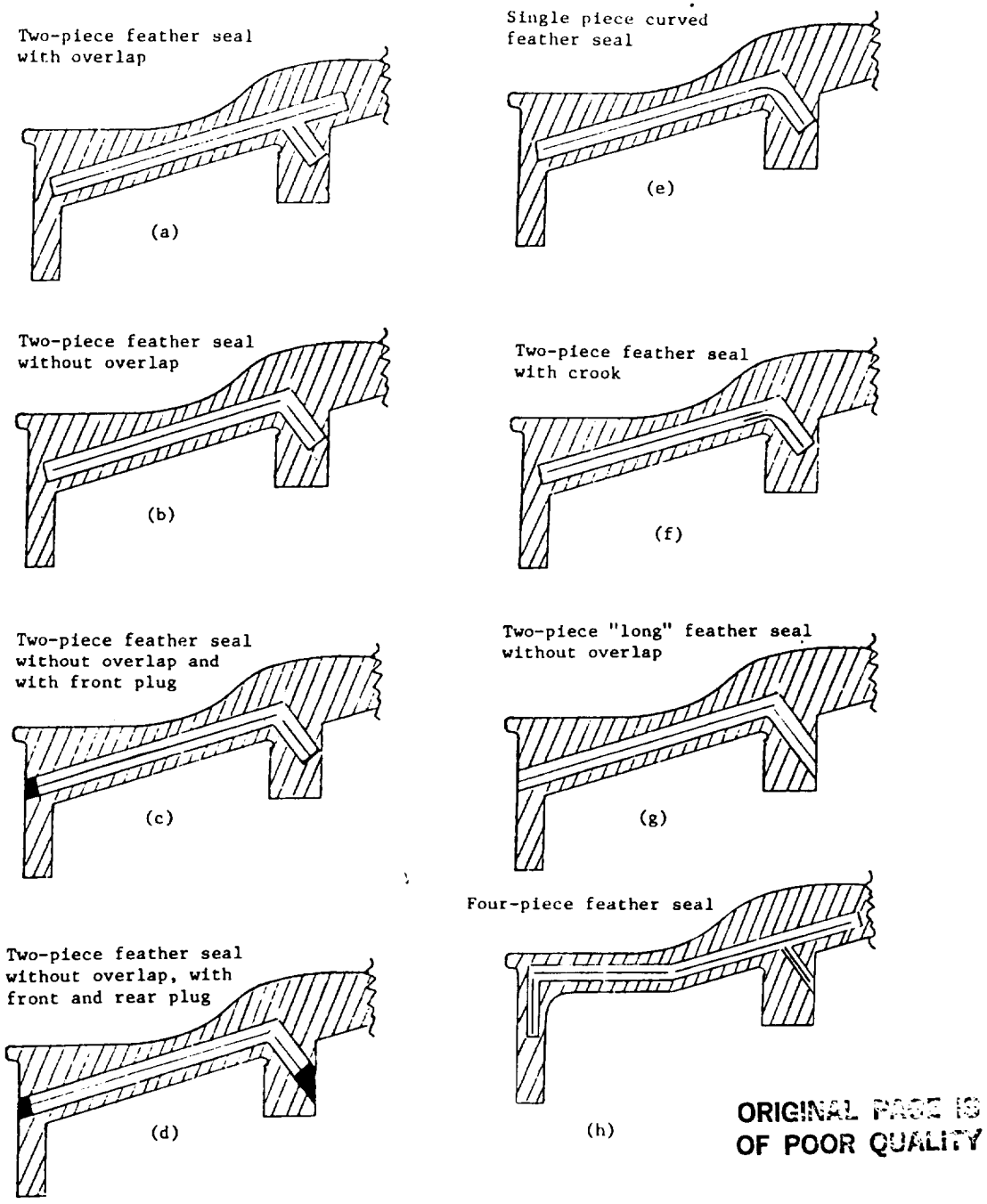


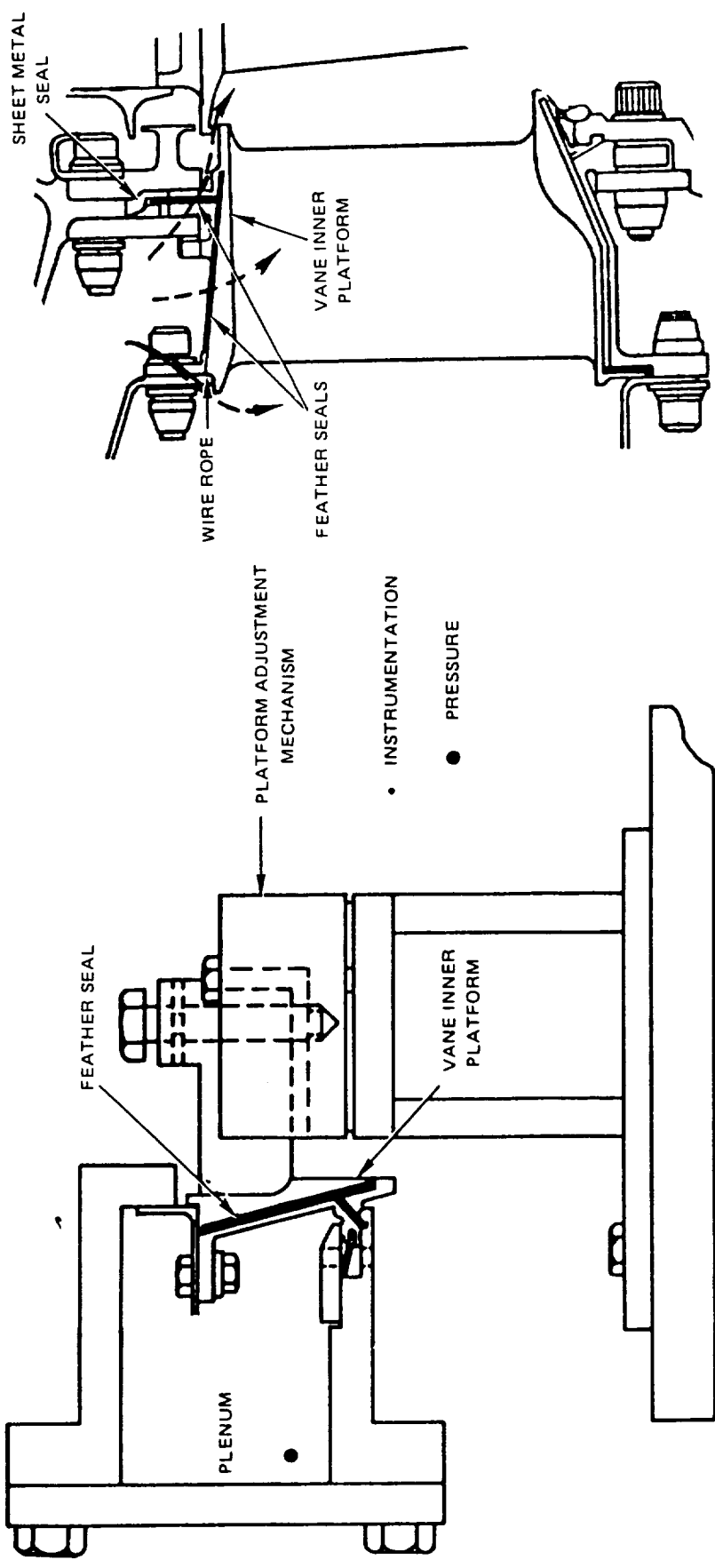
Figure 4.2.5-9 Results With and Without W-Seals in the Blade Platform Area

Leakage tests were also performed to assess the effectiveness of feather seal perturbations for leakage control in the vane inner and outer platform attachments. Figure 4.2.5-10 shows the various feather seal configurations tested, and Figure 4.2.5-11 presents the test rig arrangement, along with the major components. All of the test rigs incorporated gaps similar to those expected in the turbine component assembly. Testing demonstrated that significant reductions in leakage were achieved by eliminating the feather seal intersections and plugging the seal gaps. These results are shown in Figure 4.2.5-12 by the comparison of 0.025 to 0.050 cm (0.010 to 0.020 in) thick two piece overlapping seals in electrical discharge machined slots. In addition, the results indicated that minimizing surface waviness was essential for obtaining a good sealing surface. These results are presented in Figure 4.2.5-13.



ORIGINAL PAGE IS OF POOR QUALITY

Figure 4.2.5-10 Promising Feather Seal Configurations Evaluated



(a) RIG

(b) COMPONENT

Figure 4.2.5-11 Energy Efficient Engine High-Pressure Turbine Vane Inner Attachment Leakage Rig

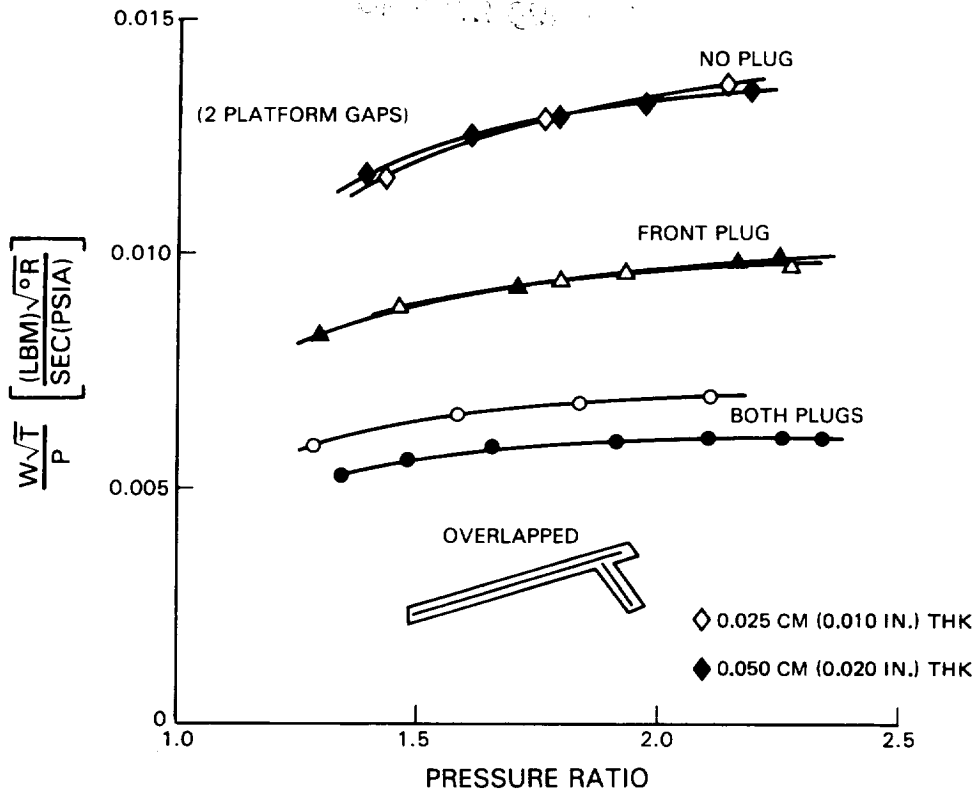


Figure 4.2.5-12 Comparison of 0.025 to 0.050 cm (0.010 to 0.020 in) Thick Two-Piece Overlapping Feather Seals

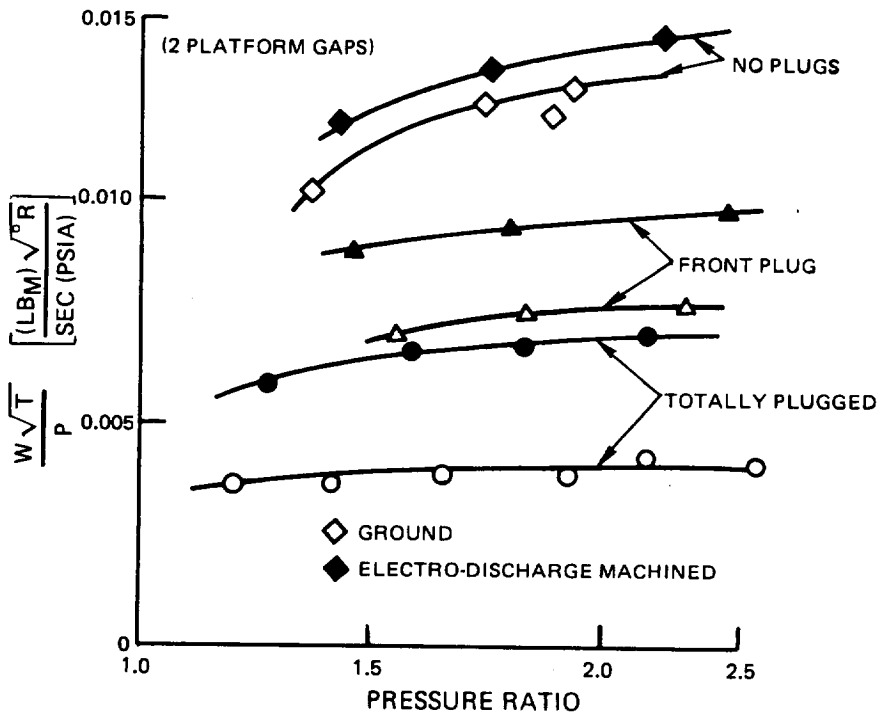


Figure 4.2.5-13 Two-piece Overlapped Seals in Ground Versus Electrodischarge Machined Slots

SECTION 5.0

AIRFOIL DURABILITY

5.1 OVERVIEW

The Energy Efficient Engine high-pressure turbine design emphasizes operation at a moderately high combustor exit temperature with a minimum of cooling to maximize fuel efficiency. This must be achieved, however, with no compromise in component durability.

Turbine airfoil durability goals for both vanes and blades are 10,000 hours of service life for the flight propulsion system and 50 hours hot section life at 28°C (84°F) day sea level takeoff conditions for the integrated core/low spool. The 10,000 hour goal is established in terms of international missions, and reflects an equivalent of 2200 missions. These goals are achieved through the combination of improved cooling effectiveness and advanced high-temperature capability materials.

5.2 TURBINE VANES

The thermal design, including durability assessment, of the turbine vanes is based on the combustor exit temperature profile shown in Figure 5.2-1. This profile represents an atypical worst case situation at hot spot locations, showing a nearly flat radial profile with a maximum temperature of 1888°C (3431°F) which reflects an appreciably high design pattern factor of 0.42 and a deteriorated engine condition.

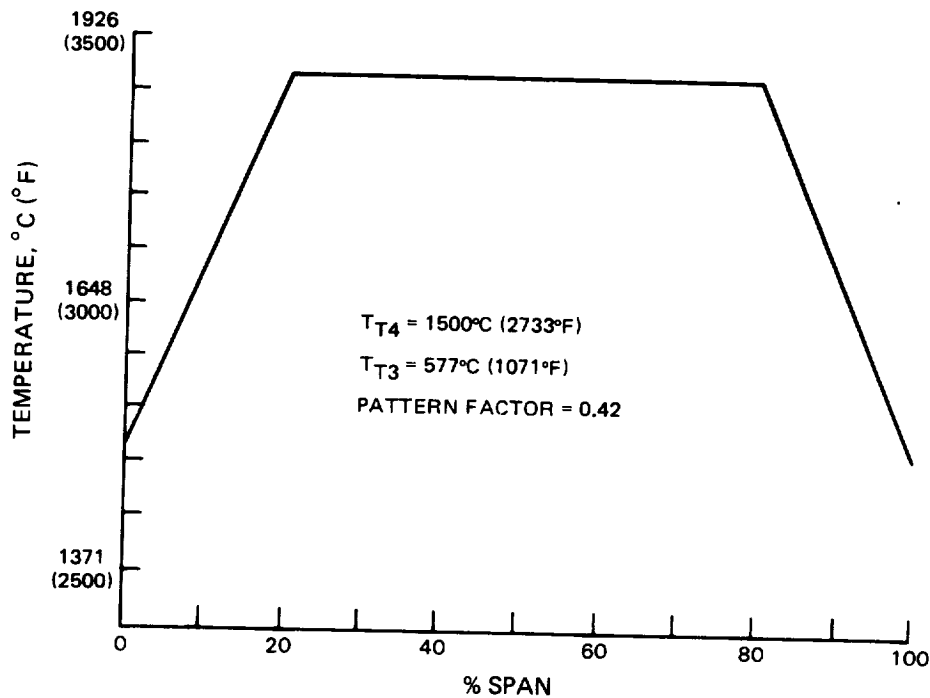


Figure 5.2-1 Combustor Exit Profile Used for Turbine Vane Durability Assessment for Flight Propulsion System at Hot Day Sea Level Takeoff Operating Conditions

5.2.1 Vane Cooling Management System

Vanes in the Energy Efficient Engine high-pressure turbine, as aerodynamically defined, are physically larger than turbine vanes in current gas-turbine engines because of the selection of a low number of airfoils. This increases vane surface area and causes inherently longer surfaces that must be cooled. In turn, the longer surfaces necessitate a greater number of film cooling rows to maintain acceptable metal surface temperature levels.

A diagram of the vane cooling system is presented in Figure 5.2.1-1. As indicated, the vane requires only a total of 6.41 percent of core engine inlet flow for cooling, excluding inner and outer platform surfaces. Internal surfaces are cooled by convection, while external surfaces are film cooled. In comparison to current commercial engines operating at similar turbine stator inlet temperatures, this represents a 1.2 percent reduction in cooling flow requirements.

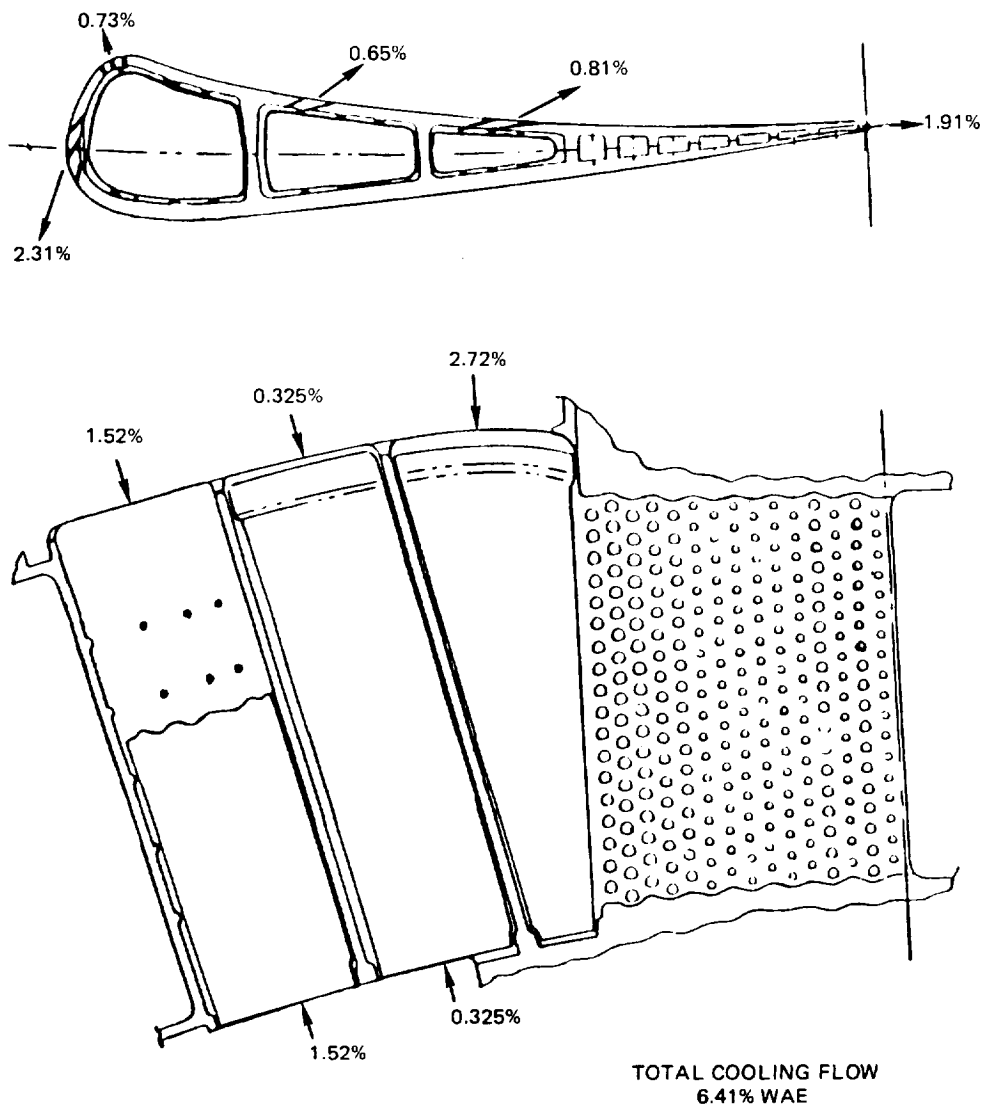


Figure 5.2.1-1 Turbine Vane Cooling Design

Cooling air enters the vane from the tip and the root at a pressure of 2,840,657 Pa (412 psia) and temperature of 577°C (1071°F) at the durability design condition of sea level takeoff, hot day. Exact percentages of flow are depicted in Figure 5.2.1-1. The coolant is distributed within the internal structure of the vane, which is designed with three cavities. These cavities are convectively cooled through the use of sheet metal impingement tubes that fit into the three cavities. To provide maximum strength against bulging deformation, two ribs tie the pressure wall and suction wall together. In addition, the vane trailing edge is convectively cooled by cooling air flowing through a series of pedestals or braces between the vane walls. Cooling flow passes around the pedestals and is discharged through a slot in the trailing edge.

The front cavity impingement tube is supplied cooling air to convectively cool the walls of the cavity. After the internal surface is cooled, the coolant is discharged through an array of showerhead holes in the leading edge as well as a set of holes downstream of the leading edge on the suction wall to provide a cooling film over the external surface. The showerhead holes are angled radially, as opposed to the axial angular orientation of the film cooling holes on the suction and pressure walls, for more effective heat transfer in the thick leading edge region.

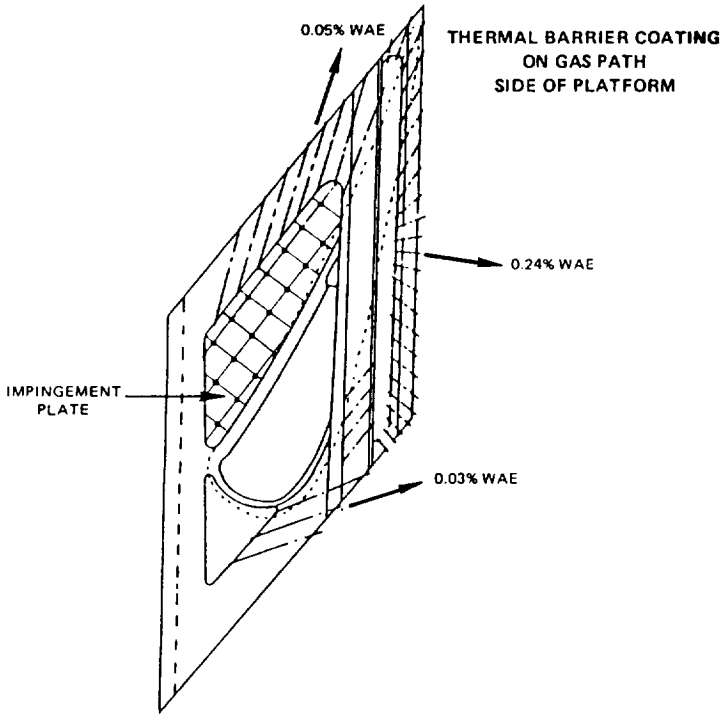
The middle and rear cavities also contain impingement tubes from which numerous cooling air jets are impinged against the vane inside surface. Cooling air flows in a chordwise direction and is discharged through axially-angled film holes in order to provide film cooling. A portion of the cooling air in the rear cavity is channeled through the trailing edge pedestal and discharged at the vane trailing edge. The size and spacing of the pedestals have been selected to provide the desired convective cooling and cooling flow levels.

Because of the somewhat unusual aerodynamic contour of the vane, the stagnation point on the airfoil appears on the pressure surface. This surface is film cooled to offset this heat load by two sets of two rows of holes, approximately 0.058 cm (0.023 in) in diameter. The suction surface incorporates three rows of cooling holes, approximately 0.050 cm (0.020 in) in diameter.

The cooling scheme, including cooling hole arrangement and flow distribution for the inner and outer vane platforms, is shown in Figures 5.2.1-2 and 5.2.1-3, respectively. The outer platform requires nearly 0.5 percent flow, while the inner platform requires 0.32 percent flow. The platform cooling scheme is based on Pratt & Whitney Aircraft experience and utilizes impingement cooling from under the platform and convection cooling from drilled holes. The large size of the airfoil makes exclusive use of convection cooling infeasible because of the increased friction loss resulting from the longer holes. Also, the requirement for more vane material to accommodate these longer holes would result in a significant increase in weight.

Impingement cooling is employed for the portion of the platform adjacent to the pressure side. Cooling holes are incorporated on the side and aft rails. If required, additional impingement cooling can be provided on the platform suction side. The heat transfer coefficients used for inner and outer platform analysis are shown in Figures 5.2.1-4 and 5.2.1-5.

VANE I.D. PLATFORM COOLING FLOW 0.32%



VANE O.D. PLATFORM COOLING FLOW 0.49%

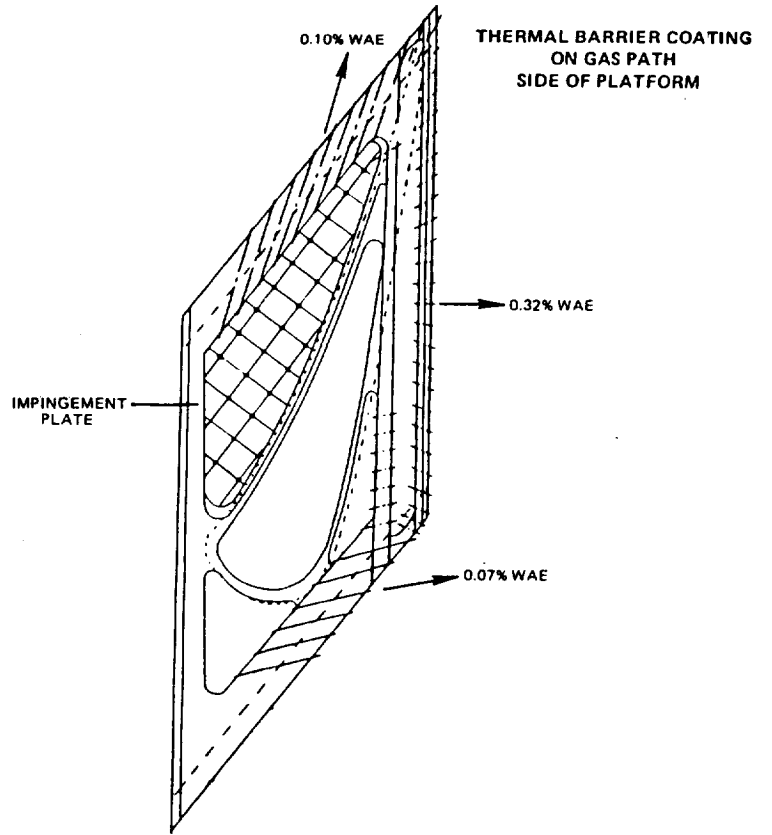


Figure 5.2.1-2 Turbine Vane Inner Platform Cooling Scheme

Figure 5.2.1-3 Turbine Vane Outer Platform Cooling Scheme

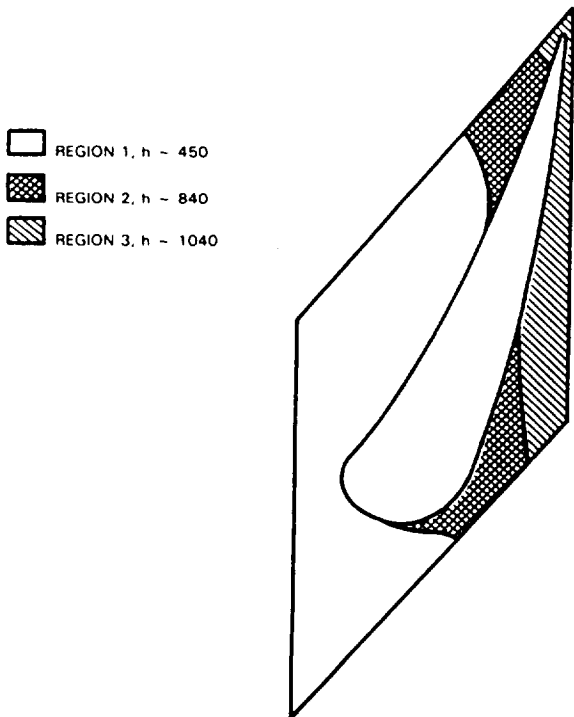


Figure 5.2.1-4 Turbine Vane Inner Platform Heat Transfer Coefficients

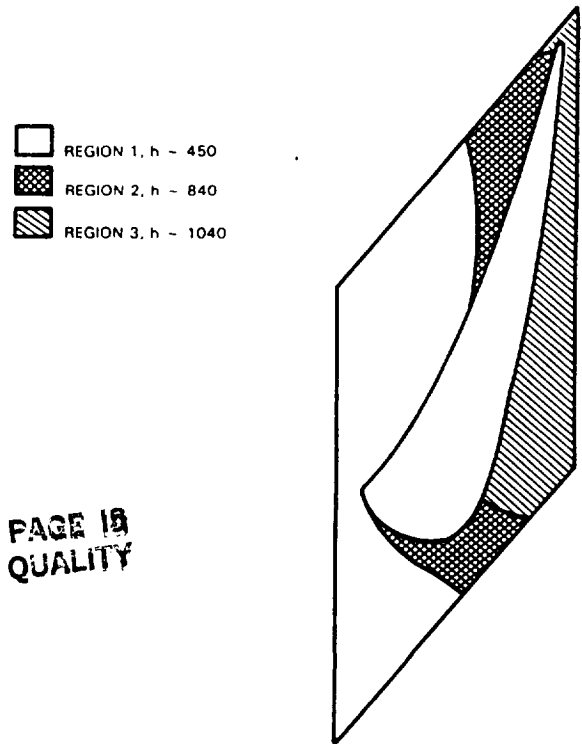


Figure 5.2.1-5 Turbine Vane Outer Platform Heat Transfer Coefficients

ORIGINAL PAGE IS OF POOR QUALITY

An assessment of the effectiveness of the vane cooling management system is summarized in Figures 5.2.1-6 through 5.2.1-10. The effectiveness of the film over the long suction wall is compared to two-dimensional flow on a flat plate in Figure 5.2.1-6. As shown, the Energy Efficient Engine design is conservative relative to the flow on a flat plate. Results of a thermal analysis, using the combustor exit profile shown in Figure 5.2-1, are presented in Figure 5.2.1-7. As shown by this isotherm plot, the highest calculated metal temperature is 1226°C (2239°F) on the suction side wall adjacent to the third cavity.

The effectiveness of the film cooling technique for the pressure and suction surfaces is corroborated by the film temperature distributions. A profile of the pressure surface film temperature is presented in Figure 5.2.1-8 and a similar profile of the suction surface film temperature distribution is shown in Figure 5.2.1-9. Of particular importance in Figure 5.2.1-9 is the fact that the leading edge film holes provide effective film protection for the entire suction surface with 2.31 percent of the total engine flow. A resulting profile for vane surface temperature is presented in Figure 5.2.1-10. The heat transfer coefficients used in the profile analysis are shown in Figure 5.2.1-11.

5.2.2 Vane Materials

A summary of the turbine vane materials and coating is presented in Table 5.2.2-1. The base alloy is SC 2000 nickel base single crystal material, which affords both high strength and high temperature capability. For the integrated core/low spool, vanes will be fabricated from PWA 1480 single crystal material. This material provides an approximate 10°C (50°F) metal temperature advantage over directionally solidified material (PWA 1422) used for turbine airfoils in modern Pratt & Whitney Aircraft commercial engines. The impingement tubes are of Inconel 625 sheet metal stock.

The external surface of the vane is coated with an oxidation-erosion resistant coating, PWA 270 (NiCoCrAl_y). A thermal barrier coating (PWA 264) is applied to the hot gas surface of the platform.

The materials and coatings planned for the flight propulsion system are advanced derivatives of those selected for the integrated core/low spool. The base alloy is a second-generation nickel base single crystal material (SC 2000). This material will provide an additional 10°C (50°F) metal temperature improvement over the PWA 1480 material.

For the flight propulsion system vane, both the internal and external surfaces are coated. The external surface is coated with an advanced overlay coating (PWA 286) that provides improved resistance to oxidation and erosion. An aluminide coating (PWA 275) is also applied for the internal cavity to enhance oxidation resistance. The platforms are coated with an advanced thermal barrier coating (TBC 100) for added temperature capability.

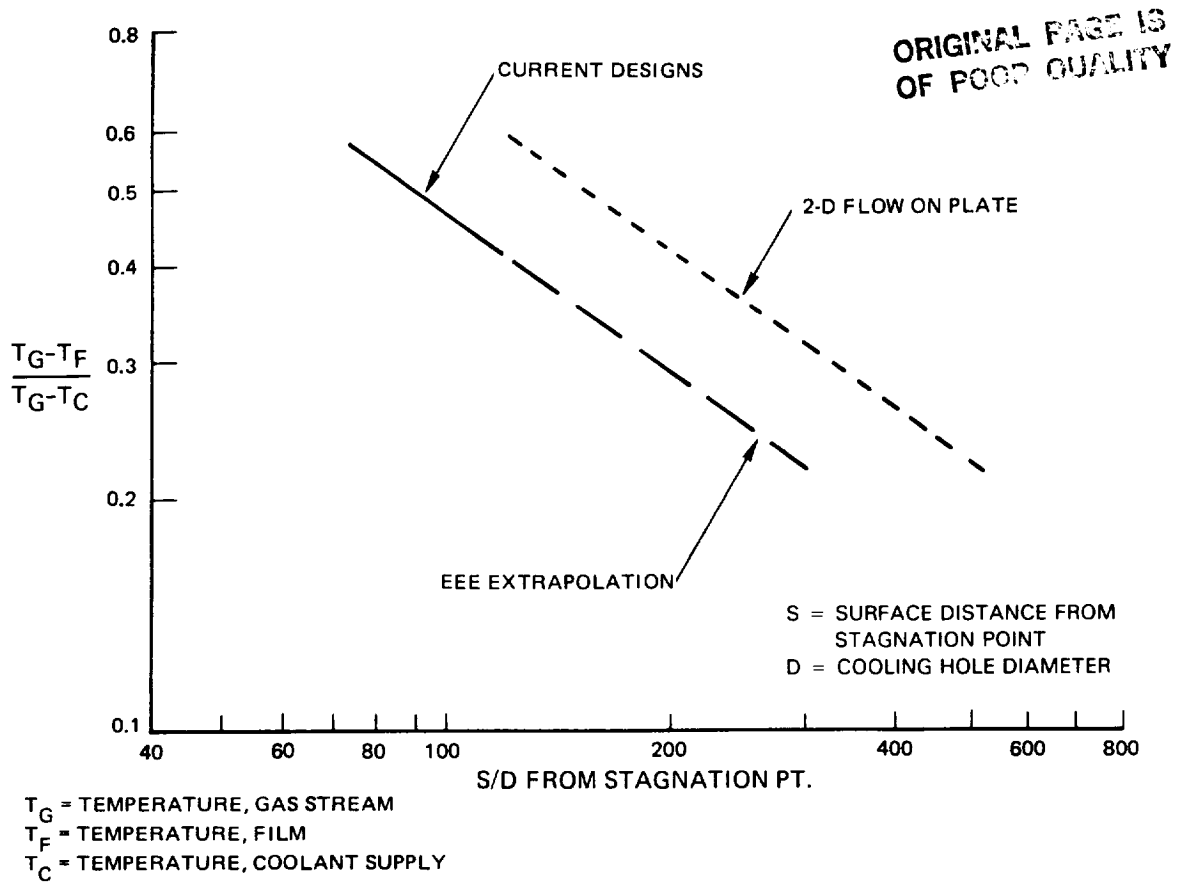


Figure 5.2.1-6 Suction Surface Film Effectiveness

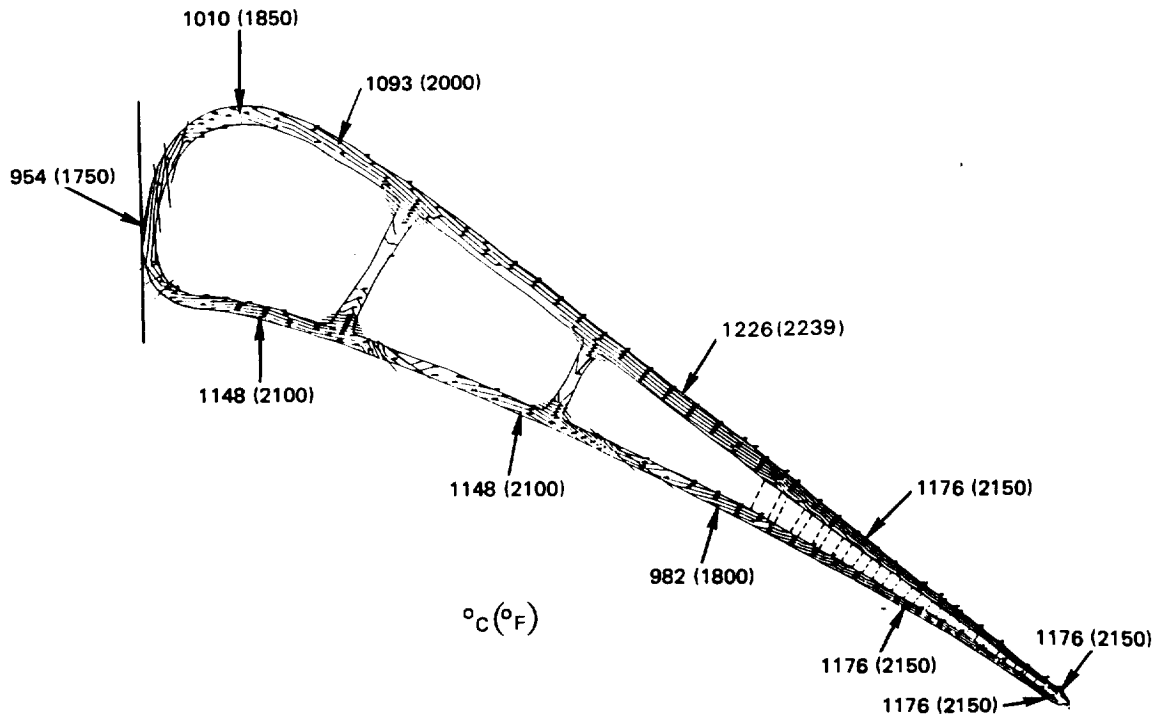


Figure 5.2.1-7 Vane Thermal Analysis Results

ORIGINAL PAGE IS
OF POOR QUALITY

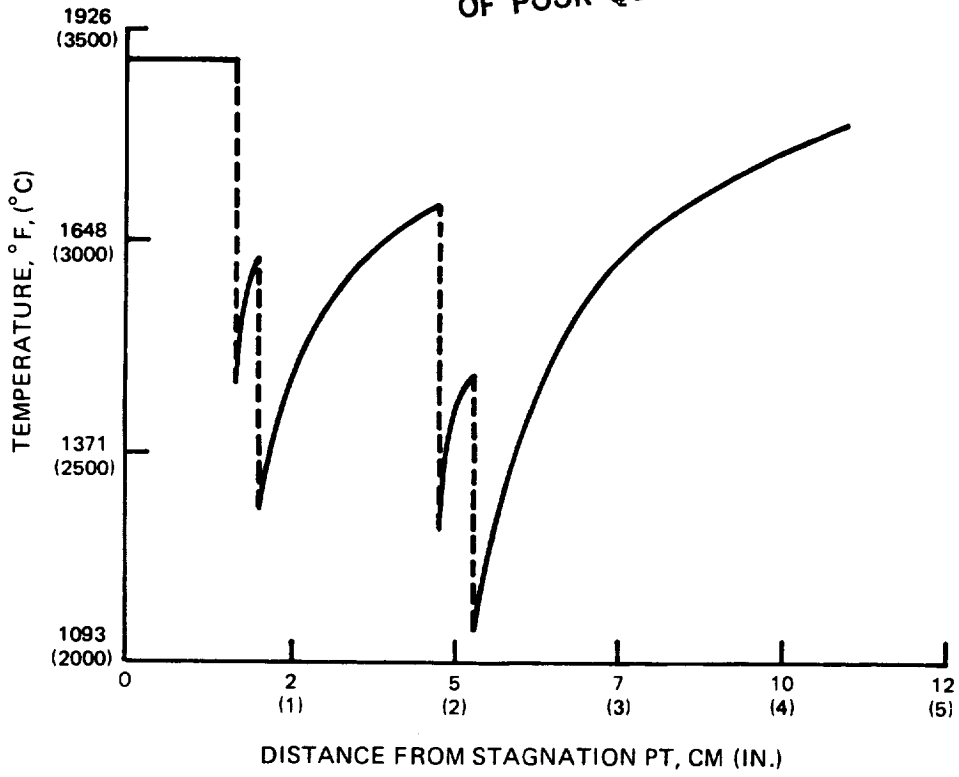


Figure 5.2.1-8 Pressure Wall Film Temperatures

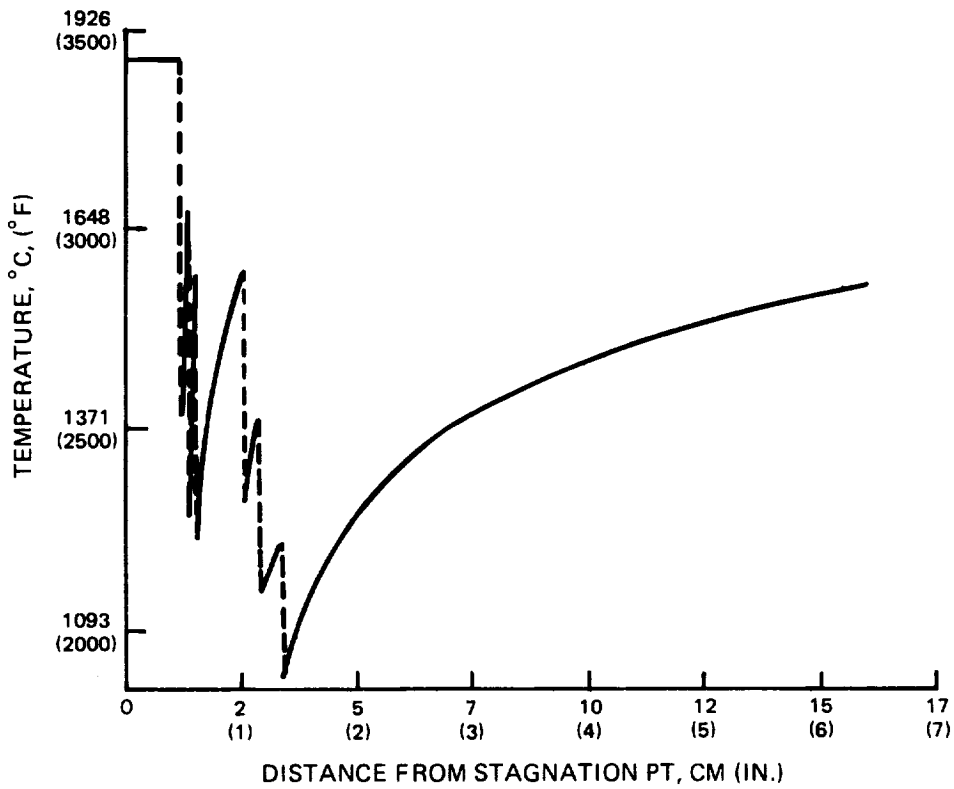


Figure 5.2.1-9 Suction Wall Film Temperatures

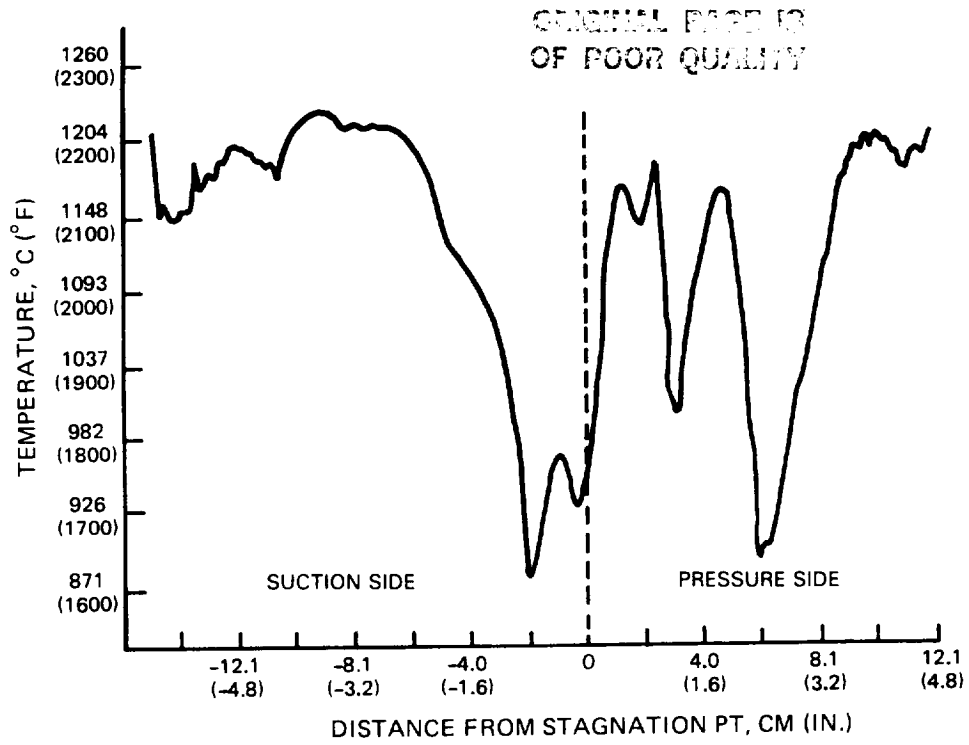


Figure 5.2.1-10 Vane Surface Temperature Profile

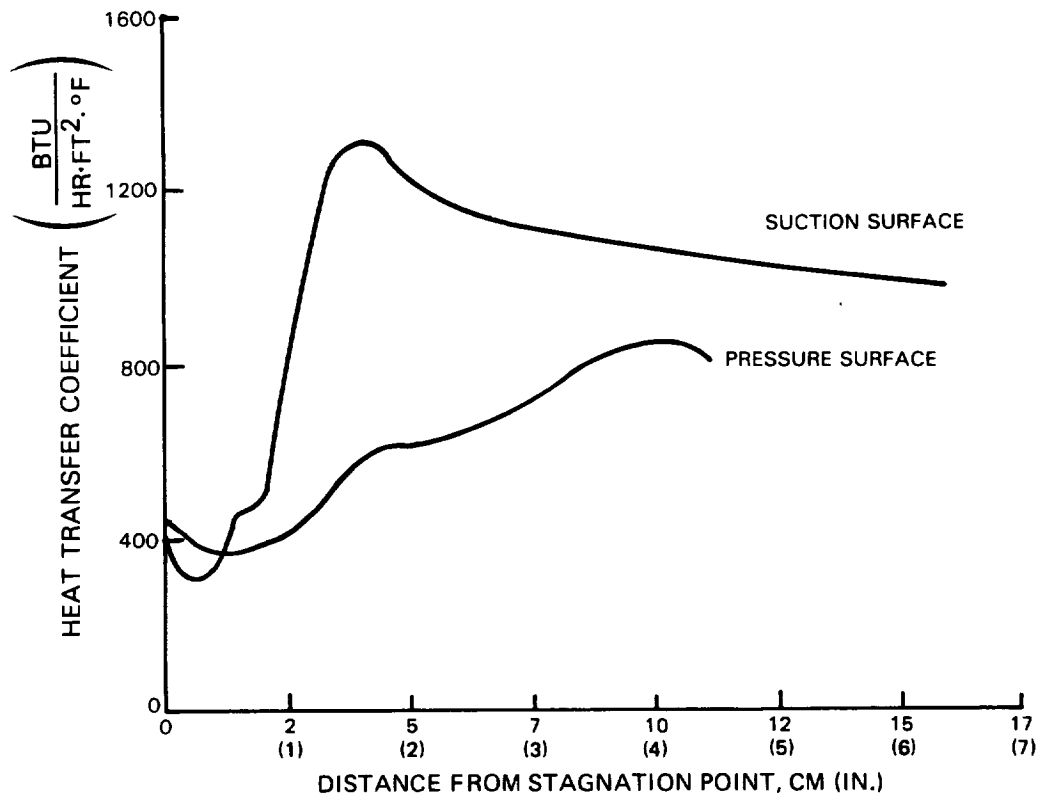


Figure 5.2.1-11 Vane Surface Heat Transfer Coefficients Used to Determine Surface Temperature Profiles

TABLE 5.2.2-I

VANE MATERIALS AND COATINGS

	<u>Flight Propulsion System</u>	<u>Integrated Core/Low Spool</u>
Base Alloy	SC 2000 (Advanced Single Crystal)	PWA 1480 (Single Crystal)
External Coating	PWA 286 (Advanced NiCoCrAlY Overlay)	PWA 270 (NiCoCrAlY)
Internal Coating	PWA 275 (Aluminide)	None
Platform Coating	TBC 100 (Advanced Ceramic Thermal Barrier Coating)	PWA 264 (Ceramic Thermal Barrier Coating)

5.2.3 Turbine Vane Durability Assessment

To evaluate vane durability characteristics, estimates of strain were made during transient engine operation. Transient strains essentially cause two strain cycles per flight mission, and the effects of both were included in estimating cyclic life. Results show that the vane leading edge experiences the greatest total strain range (0.7 percent). The relative strain at the leading edge during the two strain excursions -- takeoff and reverse thrust -- as opposed to other flight modes, is indicated in Figure 5.2.3-1. Strain ranges for the other areas of the vane are identified in Figure 5.2.3-2.

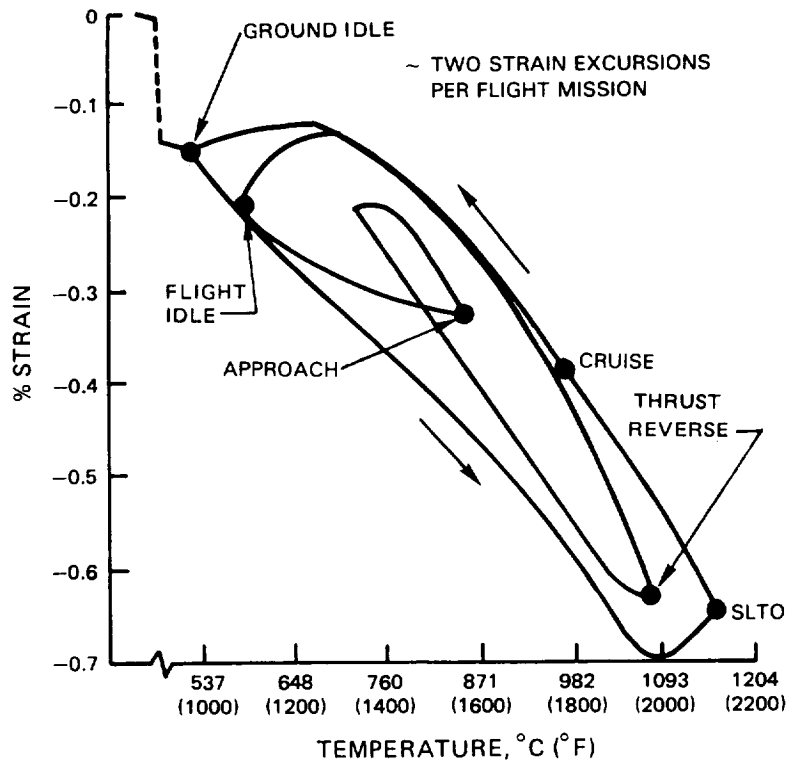
The calculated vane life for the flight propulsion system and the integrated core/low spool is presented in Table 5.2.3-I. Oxidation life and cracking life exceed the goal values by 1000 hours or 300 cycles.

5.3 TURBINE BLADES

The thermal design of the turbine blades was based on the exit temperature average profile produced by the vanes. This profile is shown in Figure 5.3-1, and as indicated, the peak of the profile (gas path temperature of 1425°C (2598°F)) occurs at the 65 percent span location. Consequently, the design of the blade cooling system was tailored to match the spanwise temperature ranges reflected by this profile in combination with the stress profile.

5.3.1 Blade Cooling Management System

The turbine blade cooling system design for the Energy Efficient Engine, like the vane, relies on the efficient management of coolant to maintain acceptable metal temperatures with minimum cooling air. The cooling system design was verified by the results acquired from a supporting flow visualization model test program.



ORIGINAL STRAIN
OF FOUR QUARTERS

Figure 5.2.3-1 Vane Limiting Strain Cycle

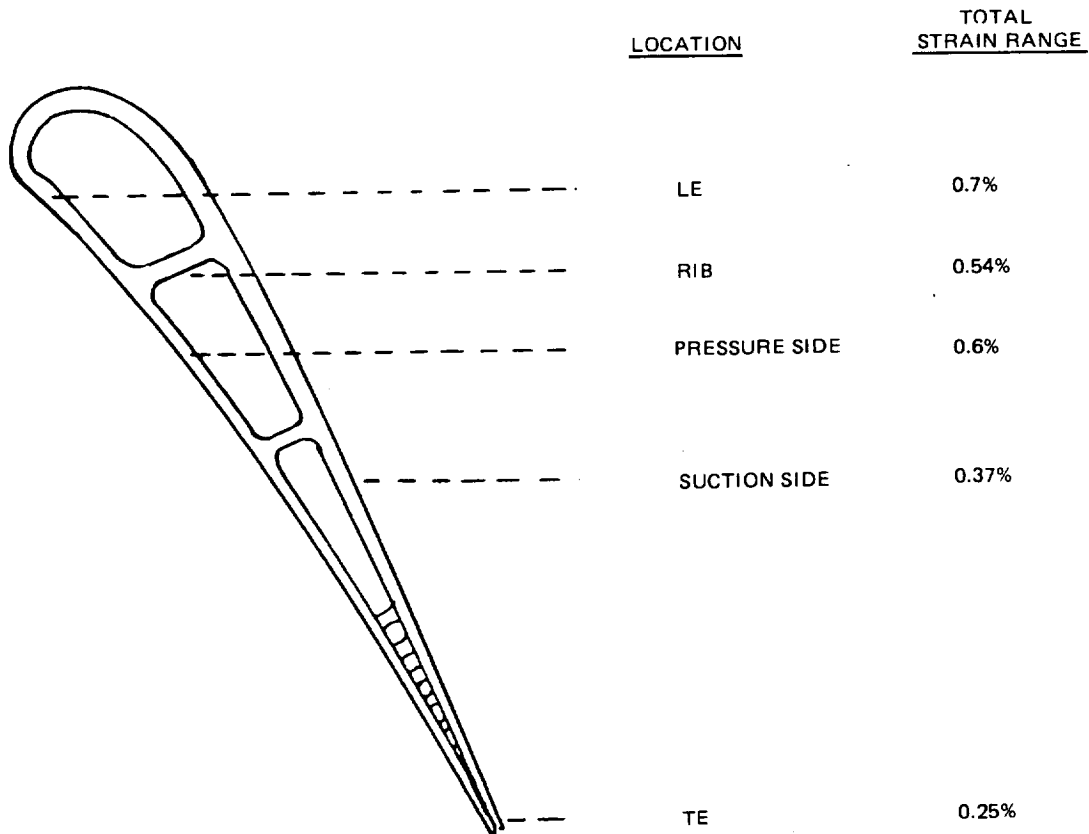


Figure 5.2.3-2 Predicted Strain

TABLE 5.2.3-I

**ORIGINAL PAGE IS
OF POOR QUALITY**

VANE LIFE

FLIGHT PROPULSION SYSTEM

	<u>Required</u>	<u>Calculated</u>
Oxidation	6000 Hours*	7000 Hours*
Cracking	10000 Hours (2200 Flight Missions)	11000 Hours (2500 Flight Missions)

INTEGRATED CORE/LOW SPOOL

Oxidation	50 Hours (Hot Time)	100 Hours (Hot Time)
-----------	---------------------	----------------------

*10,000 hours achieved with one recoating

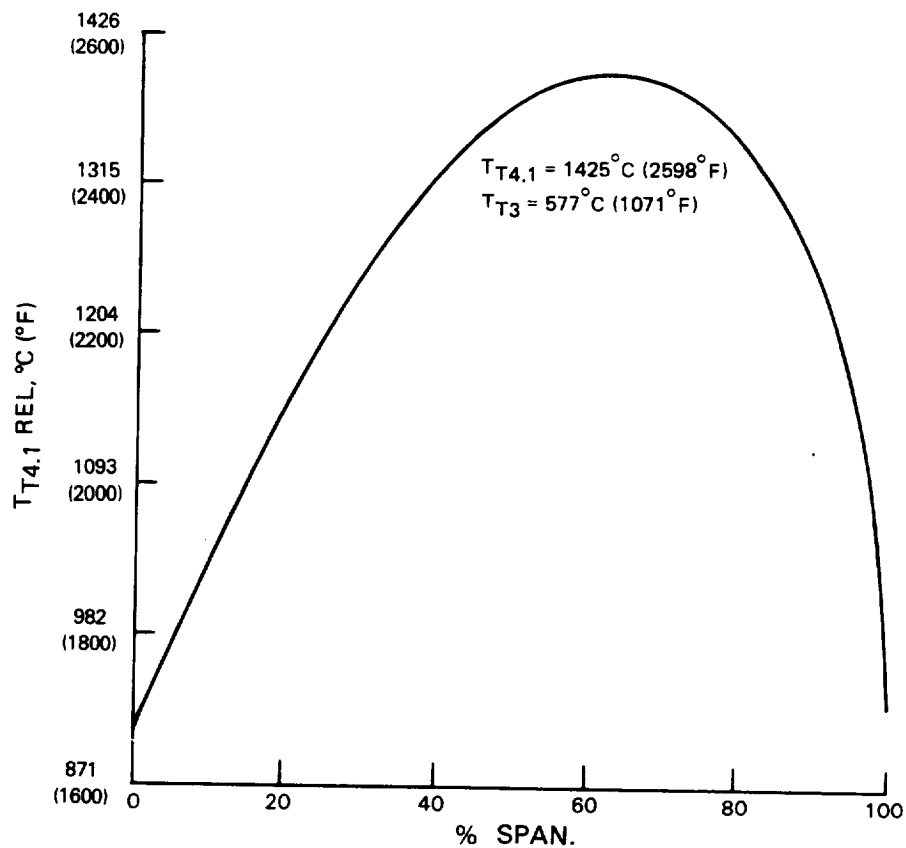
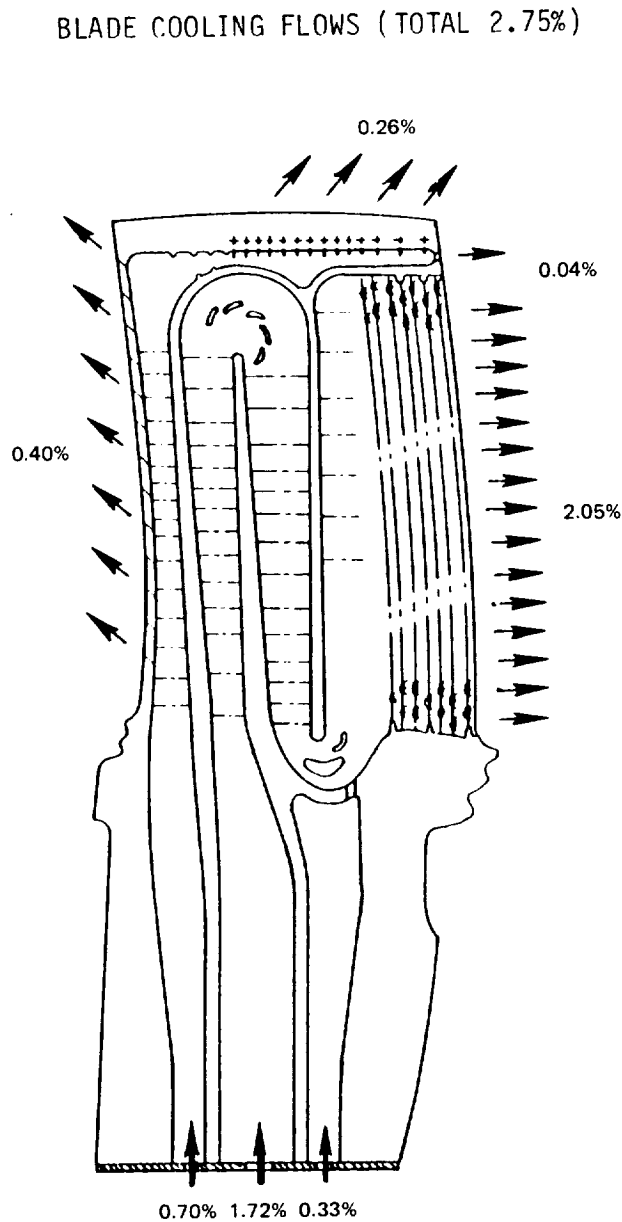


Figure 5.3-1 Turbine Vane Exit Profile for Flight Propulsion System at Hot Day Sea Level Takeoff Operating Conditions

A schematic of the blade cooling design is presented in Figure 5.3.1-1, showing the internal passages and distribution of cooling air. The blade internal geometry is cooled through convection, while external surfaces are locally film cooled from the leading edge showerhead holes and tip pressure side holes. There are no film cooling holes on either the pressure or suction surfaces of the airfoil.

The total cooling air requirement is 2.75 percent of the core engine inlet flow. As indicated in Figure 5.3.1-1, cooling air enters the blade through three root passages. The cooling flow is supplied to the blade root at a pressure of 1,661,646 Pa (241 psia) and a temperature of 556°C (1033°F) at the cooling design condition of hot day sea level takeoff.



ORIGINAL PAGE IS
OF POOR QUALITY

Figure 5.3.1-1 Turbine Blade Cooling System

The front passage supplies approximately 25 percent of the total blade flow to cool the leading edge and tip. This flow is discharged through a series of 0.038 to 0.050 cm (0.015 to 0.020 in) diameter showerhead holes at the leading edge and an array of 0.050 to 0.063 cm (0.020 to 0.025 in) diameter holes at the tip. Since the predicted gas temperatures are substantially lower at the airfoil span extremes, as shown earlier in Figure 5.3-1, the leading edge cooling hole pattern has been tailored to accommodate these temperature requirements. In addition, trip strips are integral with the internal passage design to promote a higher heat transfer rate.

The middle passage utilizes approximately two-thirds of the total blade cooling flow. Flow circulates through the internal cavity, making two spanwise excursions, and enters the trailing edge passage where it passes through an array of pedestals before being discharged into the gas path. Trip strips are also used in the passages to raise the heat transfer coefficient. At the tip and root sections, turning vanes are used to reduce aerodynamic flow separation and the attendant pressure loss penalty. Sizing of the flow areas was carefully selected to avoid areas of diffusion that could lead to flow separation and high pressure loss.

The third blade passage directs a small percentage of cooling air to cool a portion of the root area and supplements trailing edge cooling. Flow injection improves the flow distribution in the root turn area with essentially no penalty on the cooling supply pressure.

Verification of the coolant passage design was accomplished by the use of a five times size flow model (Reference 4), which duplicated the complete internal shape of the blade.

The capability of the cooling system design to maintain acceptable metal temperatures was confirmed by a thermal analysis. Figure 5.3.1-2 presents an isotherm plot of the blade mid-span section. As indicated, the average metal temperature is 954°C (1750°F). The highest predicted temperature is slightly above 1093°C (2000°F), and occurs on the suction wall surface near the first rib. A profile of pressure and suction surface temperatures is shown in Figure 5.3.1-3. The heat transfer coefficients used in the profile analysis are shown in Figure 5.3.1-4.

5.3.2 Blade Materials

A summary of the materials and coatings selected for the turbine blade is presented in Table 5.3.2-1 for the integrated core/low spool and flight propulsion system. For both applications, the base material and coatings are the same as for the turbine vane. The base material is an advanced nickel base single crystal alloy and the blade is coated with an advanced oxidation resistant coating. The major difference is that a thermal barrier coating on the platform is not required.

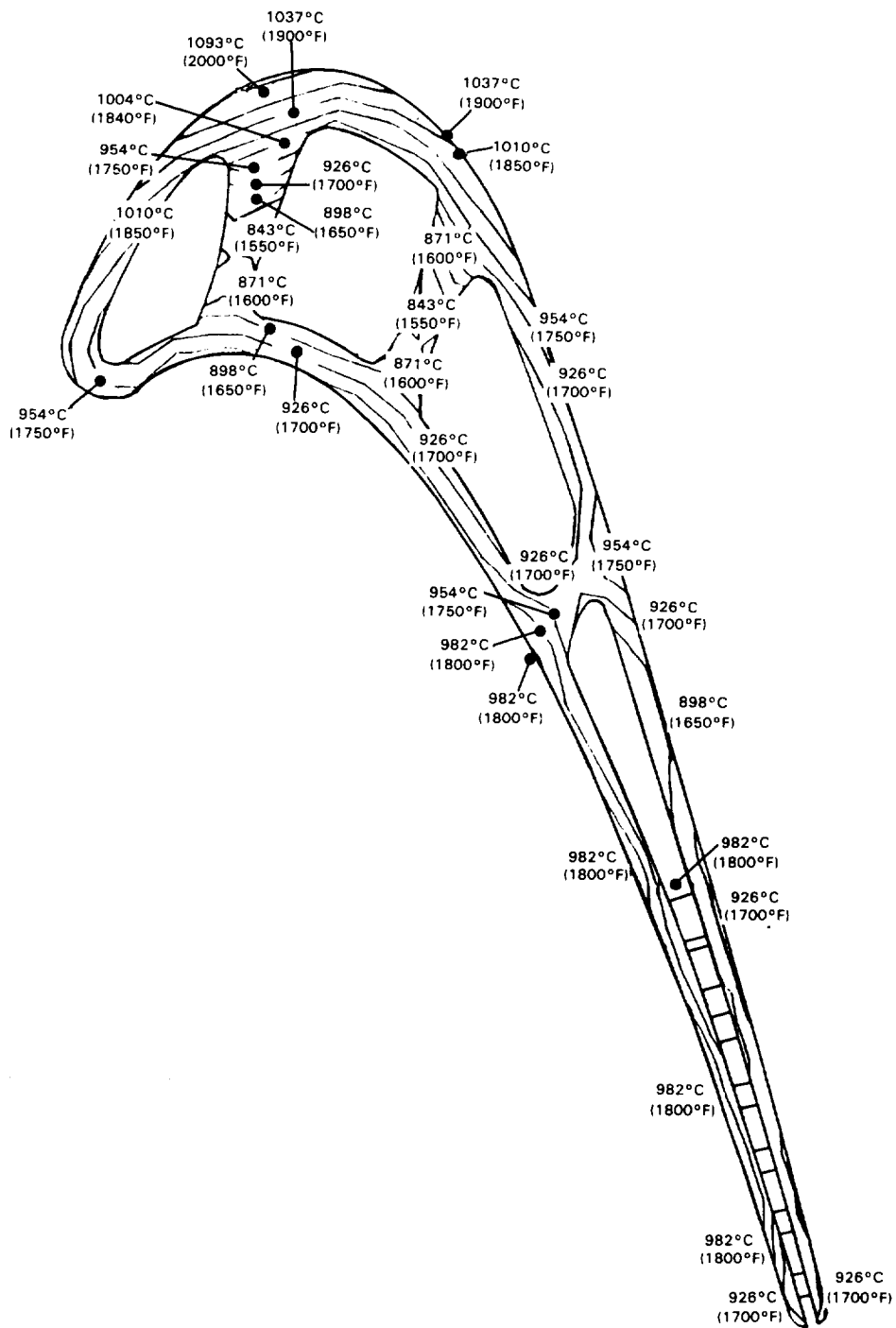


Figure 5.3.1-2 Blade Thermal Analysis Results (Midspan Location)

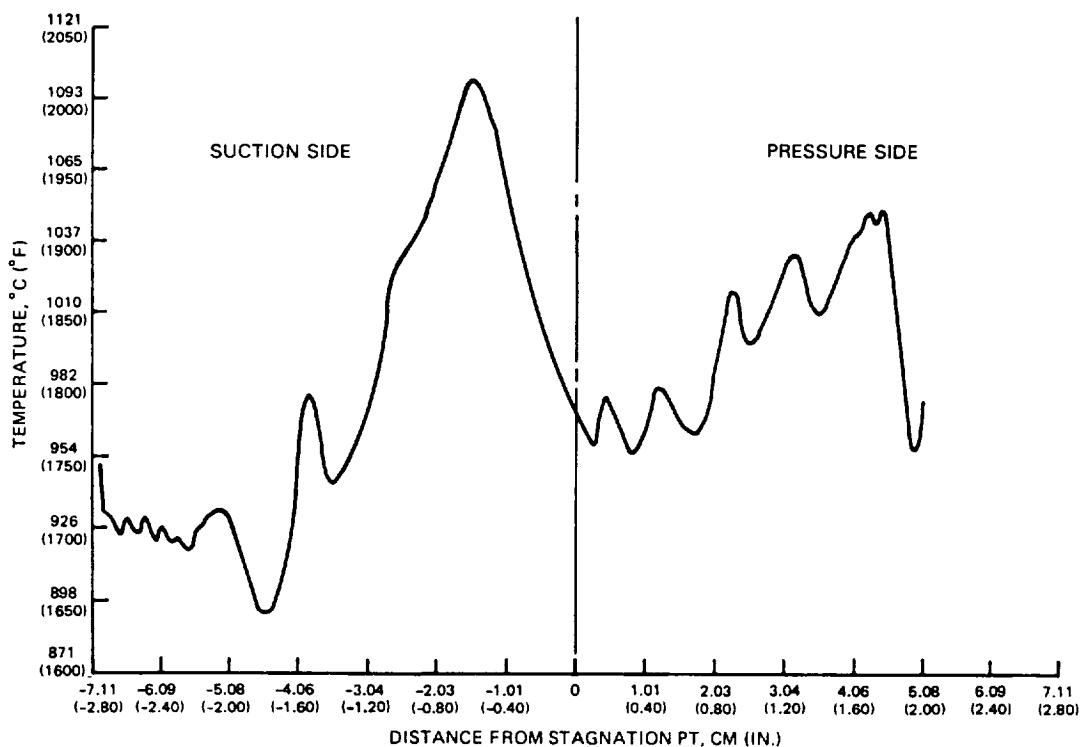


Figure 5.3.1-3 Surface Temperature Profile

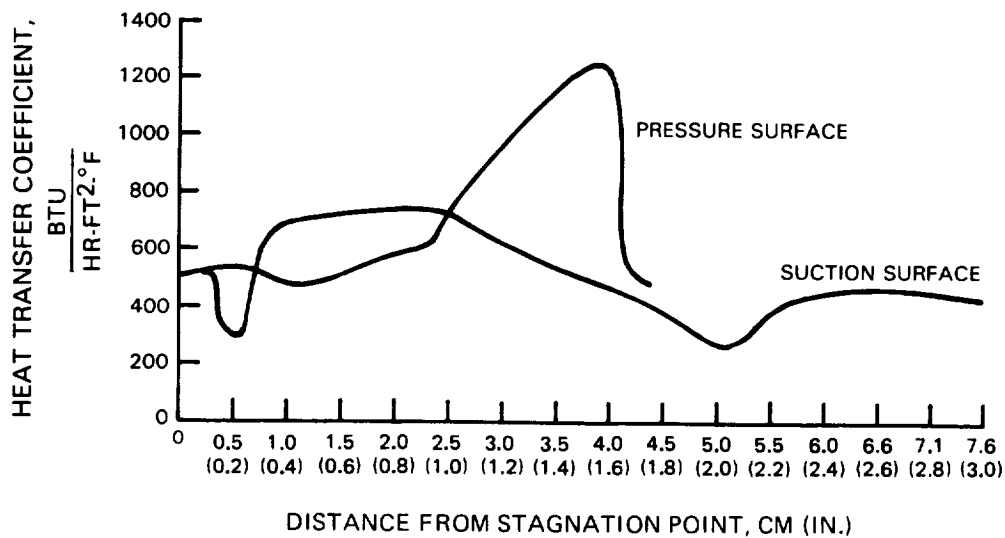


Figure 5.3.1-4 Blade Surface Heat Transfer Coefficients Used to Determine Surface Temperature Profiles

TABLE 5.3.2-I

BLADE MATERIALS

	<u>Flight Propulsion System</u>	<u>Integrated Core/Low Spool</u>
Base Alloy	SC 2000 (Advanced Single Crystal)	PWA 1480 (Single Crystal)
External Coating	PWA 286 (Advanced NiCoCrAlY)	PWA 270 (NiCoCrAlY)
Internal Coating	PWA 275 (Aluminide)	None

5.3.3 Turbine Blade Durability Assessment

An analysis of transient strains encountered during the flight cycle resulted in predicted lives that meet the durability goals. Characterization of blade strain properties showed that the first rib is subjected to the highest strain (0.55 percent range). Rib strain as a function of flight mode and corresponding operating temperature is shown in Figure 5.3.3-1. Strain ranges for other parts of the blade are indicated in Figure 5.3.3-2.

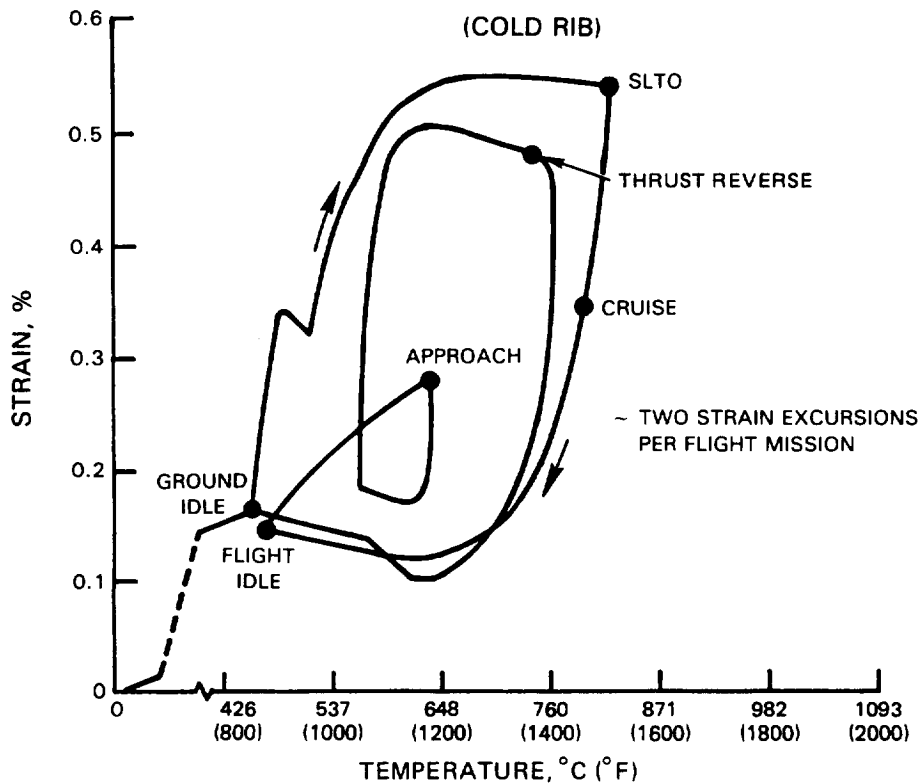


Figure 5.3.3-1 Blade Limiting Strain Cycle

ORIGINAL PAGE IS
OF POOR QUALITY

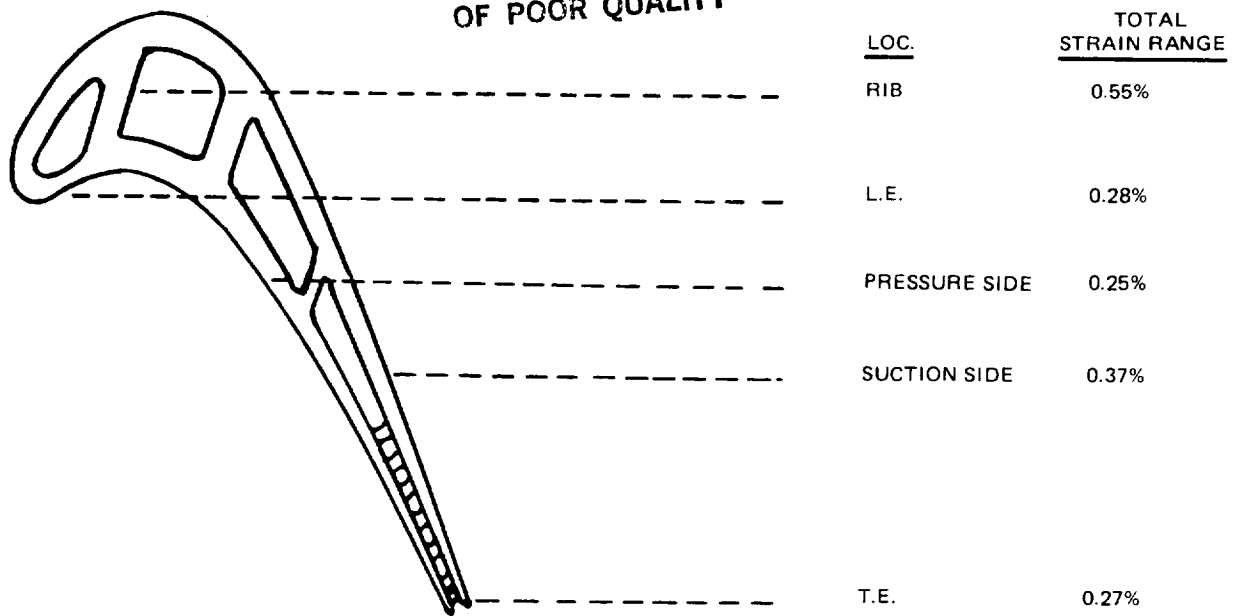


Figure 5.3.3-2 Predicted Strain

The calculated blade life for oxidation and cracking failure modes is tabulated in Table 5.3.3-I. Durability goals for both the integrated core/low spool and flight propulsion system are surpassed by an appreciable margin, as shown by these results. Cracking as a result of creep is defined as the life limiting failure mode. Figure 5.3.3-3 presents the calculated blade temperatures.

TABLE 5.3.3-I

BLADE LIFE

FLIGHT PROPULSION SYSTEM

	<u>Required</u>	<u>Calculated</u>
Oxidation	6,000 Hours	16,000 Hours
Cracking*	10,000 Hours (2200 Flight Missions)	16,000 Hours (3500 Flight Missions)

INTEGRATED CORE/LOW SPOOL

Oxidation	50 Hours (Hot Time)	400 Hours (Hot Time)
Creep	50 Hours (Hot Time)	80 Hours (Hot Time)

*Cracking due to interacting creep and low cycle fatigue

ORIGINAL PAGE IS
OF POOR QUALITY

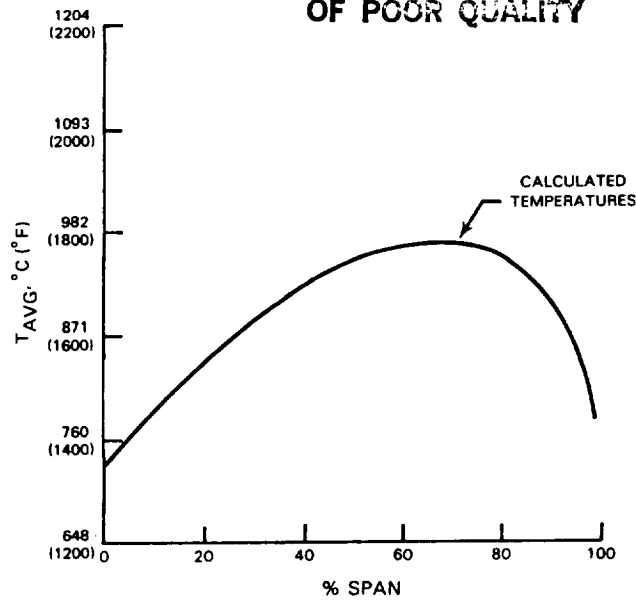


Figure 5.3.3-3 Calculated Blade Temperature for Flight Propulsion System at Hot Day Sea Level Takeoff Operating Conditions

As part of the durability assessment, blade life sensitivity to wall thickness tolerances was analyzed to evaluate the possible impact of core shifts. The predicted effects of wall thickness on blade life are summarized in Figure 5.3.3-4. Creep life is shown to be relatively insensitive to small tolerance variations with a single crystal material.

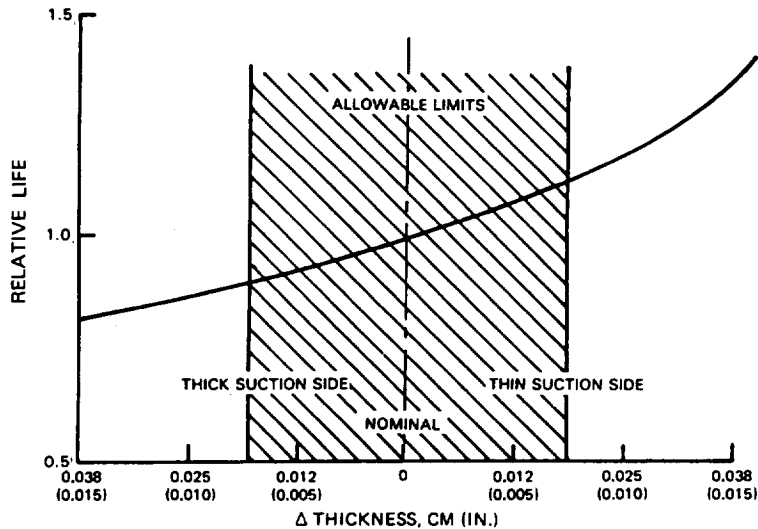


Figure 5.3.3-4 Effects of Wall Thickness Tolerance on Blade Life

SECTION 6.0

SECONDARY AIRFLOW SYSTEM

6.1 OVERVIEW

The high-pressure turbine secondary flow system is designed to maximize the use of secondary air for cooling and thrust balance as well as minimize parasitic leakage and the attendant performance penalty. The primary design features that enhance leakage control and contribute to a higher overall system performance include:

- o A tangential on-board injection (TOBI) system for positive blade coolant flow supply
- o Front rim cavity mini tangential on-board injection (TOBI) system
- o Boltless and full ring rotor sideplates
- o A multi knife-edge, stepped high-pressure compressor discharge seal.

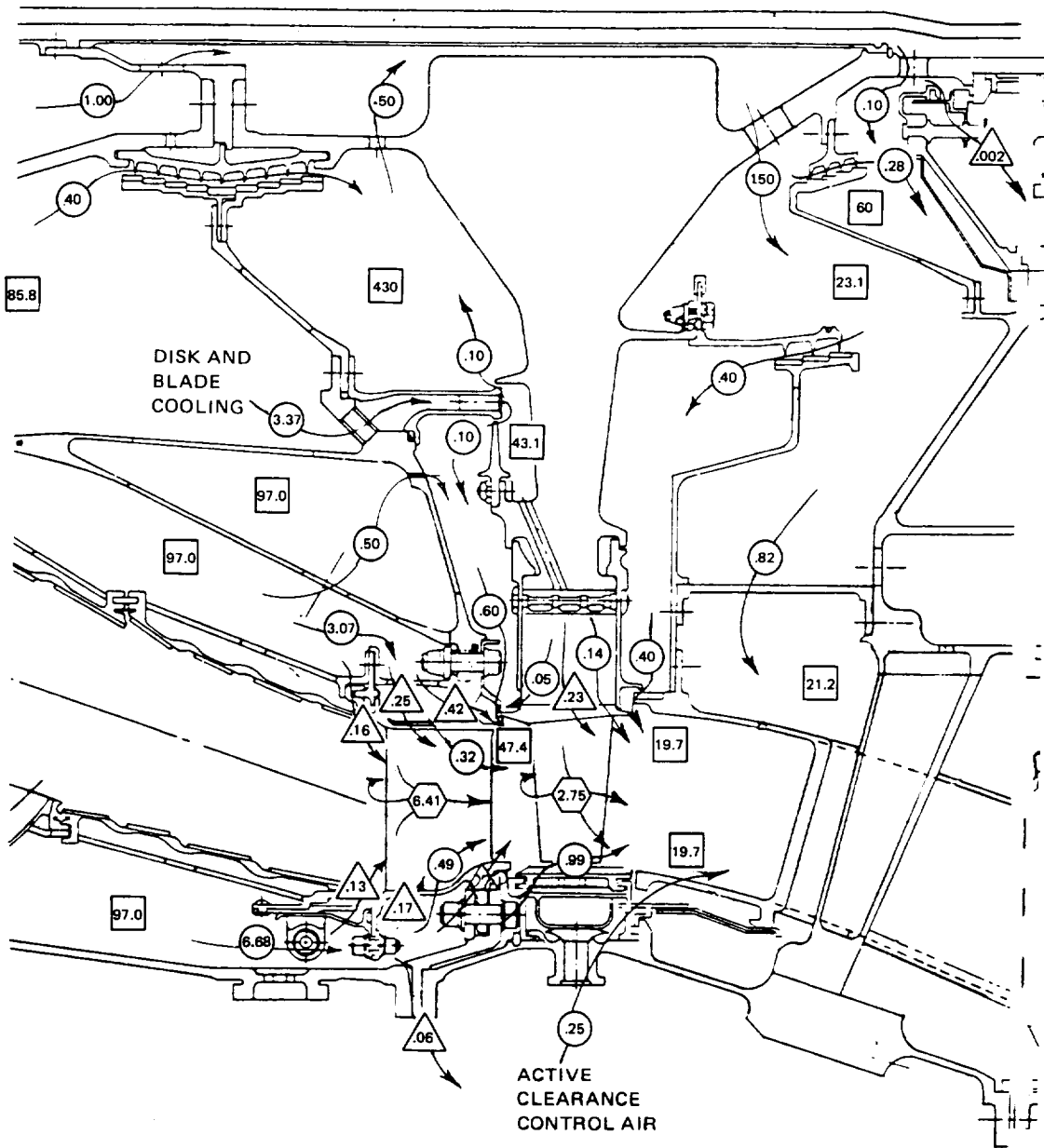
The benefits derived from these features, in conjunction with improved sealing concepts, result in the utilization of only 14.10 percent of the core engine inlet flow for cooling the high-pressure turbine disk, blades, vanes and case in the flight propulsion system.

Much of the sealing technology incorporated in the secondary flow system design has evolved from a leakage supporting technology program. This effort was instrumental in providing design guidance for the vane feather seals, blade damper seals and outer air seal. Significant results from the leakage program are described in Section 4.2.5.3.

6.2 SECONDARY FLOW SUMMARY

Figure 6.2-1 shows a secondary flow map of the high-pressure turbine, identifying cooling air flows, secondary cooling flows, leakage flow rates, and the static pressure at various points. Table 6.2-1 presents a status summary of the flow rates of the major turbine components in both the flight propulsion system and integrated core/low spool. Secondary flow totals for the flight propulsion system and integrated core/low spool are 14.10 and 14.56 percent of the total inlet flow, respectively. The slight difference in total flow is based on the assumption that the flight propulsion system will incorporate a higher level of feather seal technology in the vane and outer seals. These numbers differ from those shown for W_C/a in Table 3.3-I since they are status numbers and represent flows calculated after the parts were designed. Table 3.3-I lists the flows estimated before completion of the design.

The design features that contribute to these low flow rates are described in the following section.



- ⬡ AIR COOLING % W_{ae} AT ADP
- SECONDARY COOLING % W_{ae} AT ADP
- △ LEAKAGE FLOW % W_{ae} AT ADP
- STATIC PRESSURE % P_{T3} AT ADP

Figure 6.2-1 High-Pressure Turbine Secondary Flow System Map

TABLE 6.2-I

SECONDARY FLOW STATUS SUMMARY

	PERCENT W_{ae} AERODYNAMIC DESIGN POINT	
	<u>Flight Propulsion System</u>	<u>Integrated Core/ Low Spool</u>
DISK		
Front Rim Cavity	0.60	0.60
Rear Rim Cavity	<u>0.40</u>	<u>0.40</u>
Sub Total	1.00	1.00
BLADE		
Foil Cooling Flow	2.75	2.75
Sideplate Cooling	0.19	0.19
Leakage	<u>0.23</u>	<u>0.23</u>
Sub Total	3.17	3.17
VANE		
Foil Cooling Flow	6.41	6.41
Platform Cooling	0.81	0.81
Leakage	<u>1.40</u>	<u>1.83</u>
Sub Total	8.62	9.05
CASE		
Outer Air Seal Cooling	0.99	1.03
Active Clearance	0.25	0.25
Flange Leakage	<u>0.06</u>	<u>0.06</u>
Sub Total	1.30	1.34
TOTAL	<u>14.10</u>	<u>14.56</u>

6.3 SECONDARY FLOW SYSTEM DESIGN FEATURES

The main design features in the secondary flow system are shown in Figure 6.3-1. These include a blade coolant supply tangential on-board injection (TOBI) system, a front rim cavity mini tangential on-board injection (TOBI) system, boltless rotor sideplates, and a multi knife-edge, stepped high-pressure compressor discharge seal.

The blade tangential on-board injection system is a high efficiency cascade design to ensure positive supply of blade cooling air, which is furnished from the high-pressure compressor inner bleed. Since the system is pressure balanced, inner and outer seals are not necessary. Also, only a small percentage of air flow (0.1 percent of the total engine inlet flow) is required around the flow guides at the nozzle discharge plane. Furthermore, because the system is balanced to accommodate the gas path inner diameter pressure, cooling flow is insensitive to rim seal clearances.

The mini tangential on-board injection system shown in Figure 6.3-2 preswirls the front rim cavity and thereby reduces windage heat up that would increase front side plate temperature. The swirl field also provides a radial pressure gradient between the blade supply tangential on-board injection system and the gas path static pressure, thereby effectively linking the blade supply pressure to the gas path leading edge inner diameter pressure. This keeps the ratio of blade supply pressure to gas path inner static pressure fixed and independent of seal leakage, attachment leakage and blade flow area.

The full ring, boltless sideplate configuration adopted for the Energy Efficient Engine high-pressure turbine considerably reduces the leakage inherent in conventional segmented sideplates. A diagram of the blade coolant supply system, showing pressure and flow characteristics, is presented in Figure 6.3-3. The design blade cooling flow is 2.75 percent of core engine air flow and is supplied to the blade at an inlet pressure of 53.2 percent of the total pressure at the high-pressure compressor exit. The tangential on-board injection dump pressure of 43.1 percent of the total high-pressure compressor exit pressure is increased to 48.2 percent by the free vortex pressure recovery, and up to 53.2 percent by solid body rotation in the disk feed passages. As indicated, the full ring sideplate arrangement is very effective in reducing leakage. In addition, the use of W-seals at the interface of the rear plate and blade platform successfully controls leakage flow.

Other pertinent rotor and turbine case secondary flow features include the following:

- o Rim Seals -- These seals are positioned at the leading and trailing edge of the blade platform to isolate the disk cavity from the gas path. In essence, these serve as flow guides that function like fish-mouth seals to prevent hot gas ingestion and the resulting heat up of the disk rim.
- o High-Pressure Compressor Discharge Seal -- The compressor discharge seal is a nine knife-edge structure with an abradable seal land. This seal is designed to operate at a very close clearance 0.031 cm (0.0125 in), permitting minimum leakage flow. The calculated leakage flow rate is 0.4 percent of the total core engine flow.

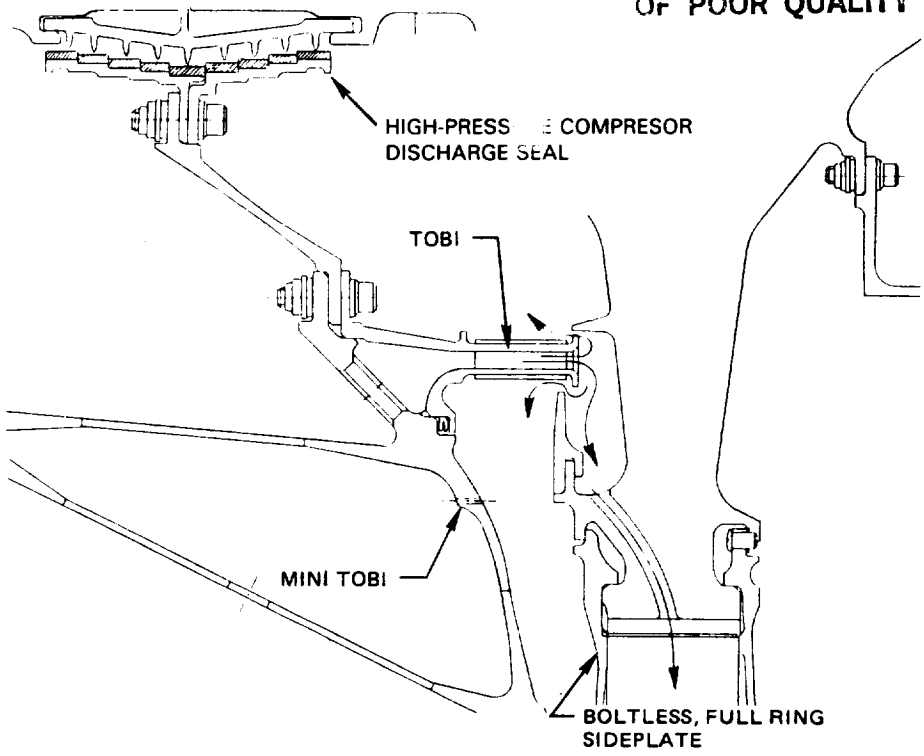


Figure 6.3-1 Secondary Flow System Design Features

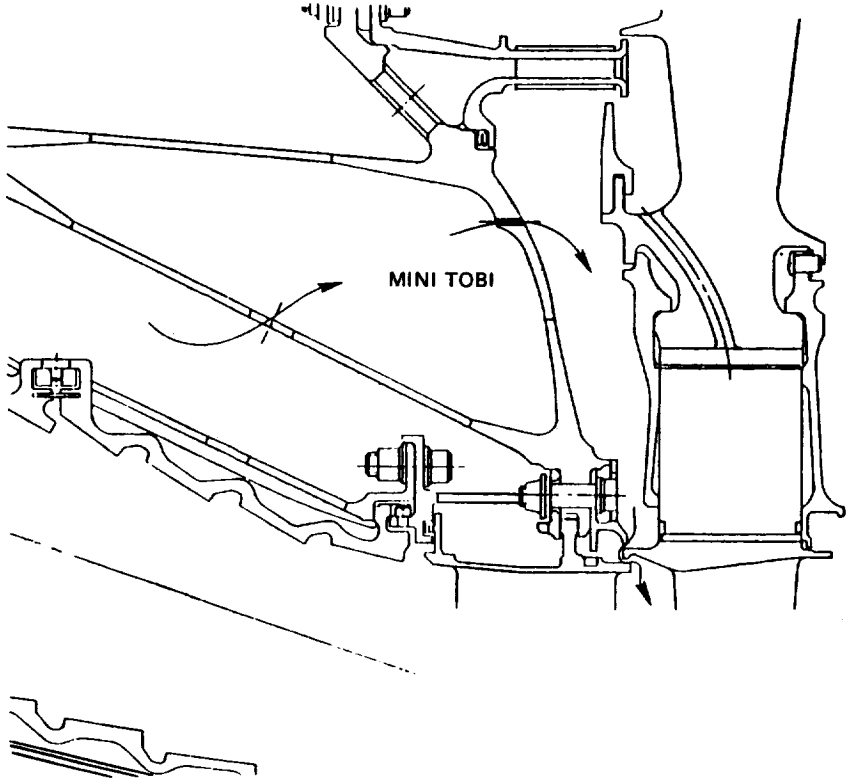


Figure 6.3-2 Mini Tangential On-Board Injection System

**ORIGINAL PAGE 13
OF PCOR QUALITY**

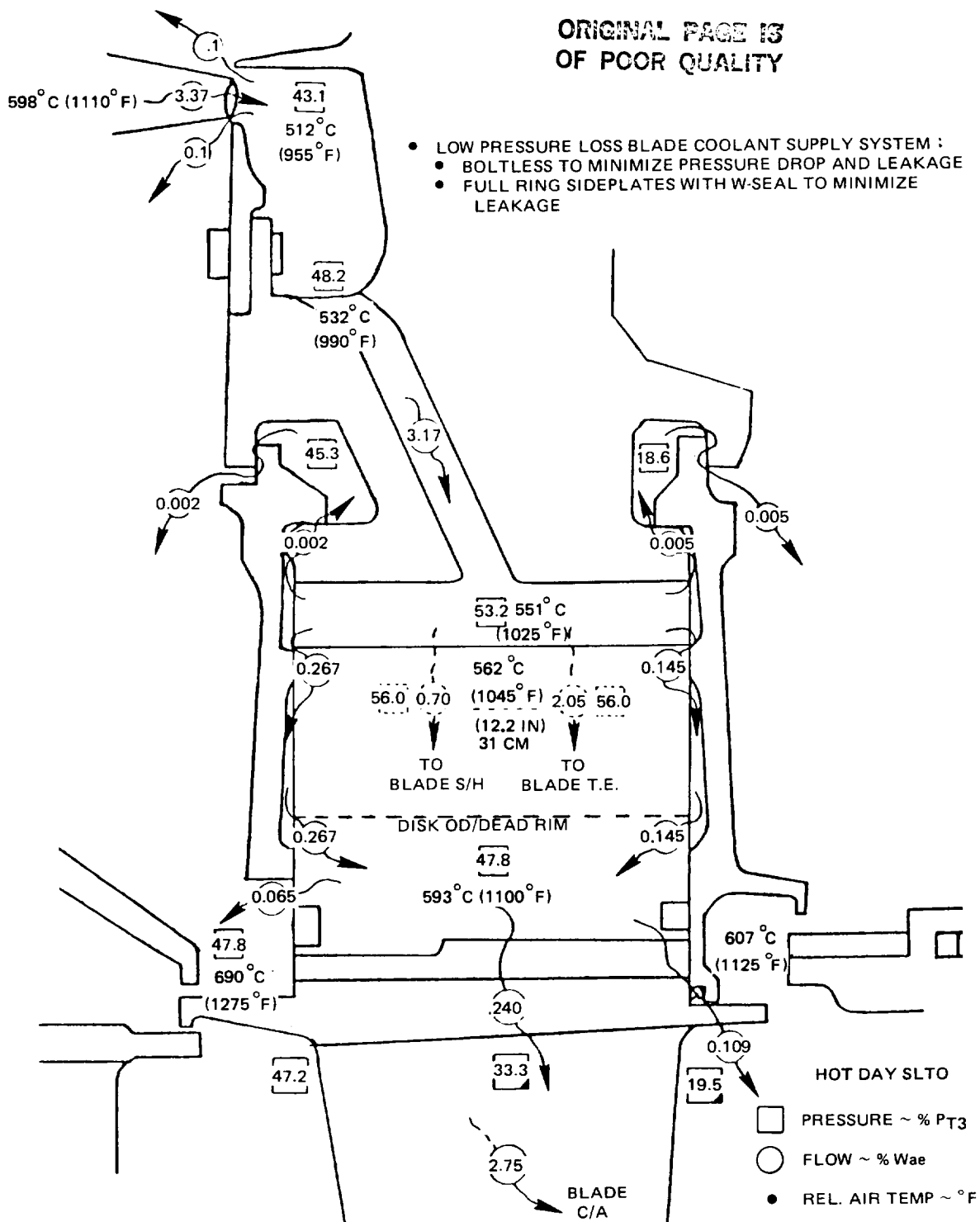


Figure 6.3-3 Flow Characteristics of Blade Coolant Supply System

- o Rear Seal -- A seal at the rear of the high-pressure turbine is used to provide thrust balance. The net thrust of the high-pressure rotor is presently calculated at 22,241 N (5000 lb) at sea level takeoff conditions.
- o Buffer Seal -- This seal, which is located in the proximity of the rear seal, is used to separate cool low-pressure compressor discharge air from high-pressure turbine bore cooling air for the rear bearing compartment.
- o Active Clearance Control System -- Turbine case active clearance control is achieved through an internal system supplied with a mixture of tenth and fifteenth-stage high-pressure compressor bleed flow, which totals 0.25 percent of the total engine inlet flow. The impingement of this air cools the full ring rails to control the clearance of the outer air seals. The thermal environment of the front and rear rails is precisely matched to prevent adverse thermal gradients.
- o Outer Air Seals -- These seals are ceramic coated and impingement cooled by combustor secondary cooling air. Since the pressure of this cooling air is relatively high, it is channeled to the intersegment gap to cool the exposed intermediate seal layer as well as prevent gas path ingestion.
- o W-Seals and Feather Seals -- Both sealing techniques have proved effective in minimizing leakage during experimental models tests. These seals are used extensively in the high-pressure turbine design.

6.4 Thermal Analysis

The effectiveness and adequacy of the secondary flow system has been verified on the basis of results acquired from thermal analyses. Figure 6.4-1 shows the detailed thermal model element breakup of the rotor and portions of the static structure required to establish boundary conditions. Figure 6.4-2 shows an example of time transient responses for the disk during a snap acceleration/deceleration. As expected, the rim thermal response is the fastest, while the bore response is slowest.

Turbine case and outer seal temperatures were generated with the thermal model shown in Figure 6.4-3. Results of the analysis are presented in Figure 6.4-4, which shows a time transient response of elements at the ceramic interface in the front and rear outer air seal rails for a snap acceleration/deceleration. The ceramic interface temperature is a key parameter for outer air seal structural integrity.

ORIGINAL PAGE IS
OF POOR QUALITY

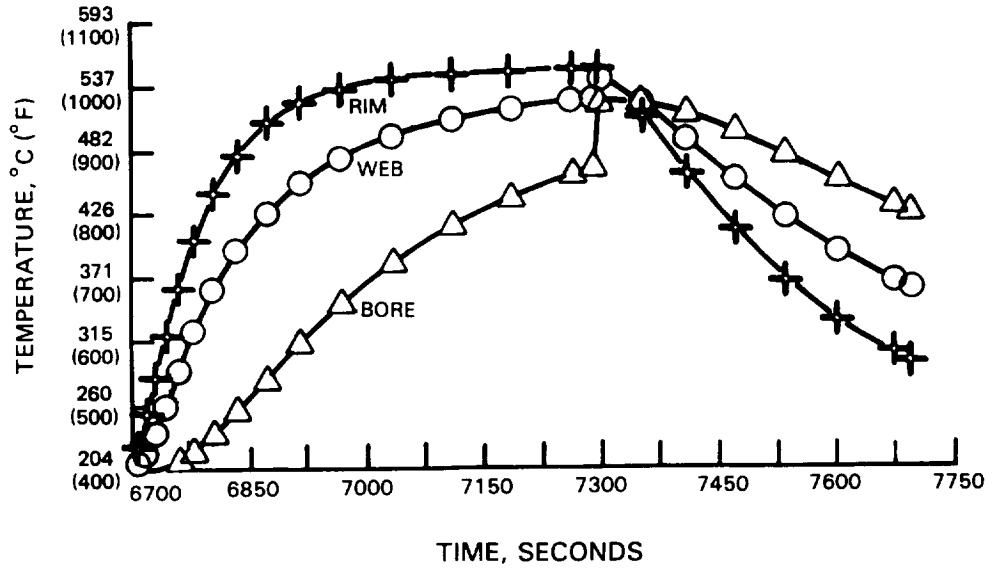
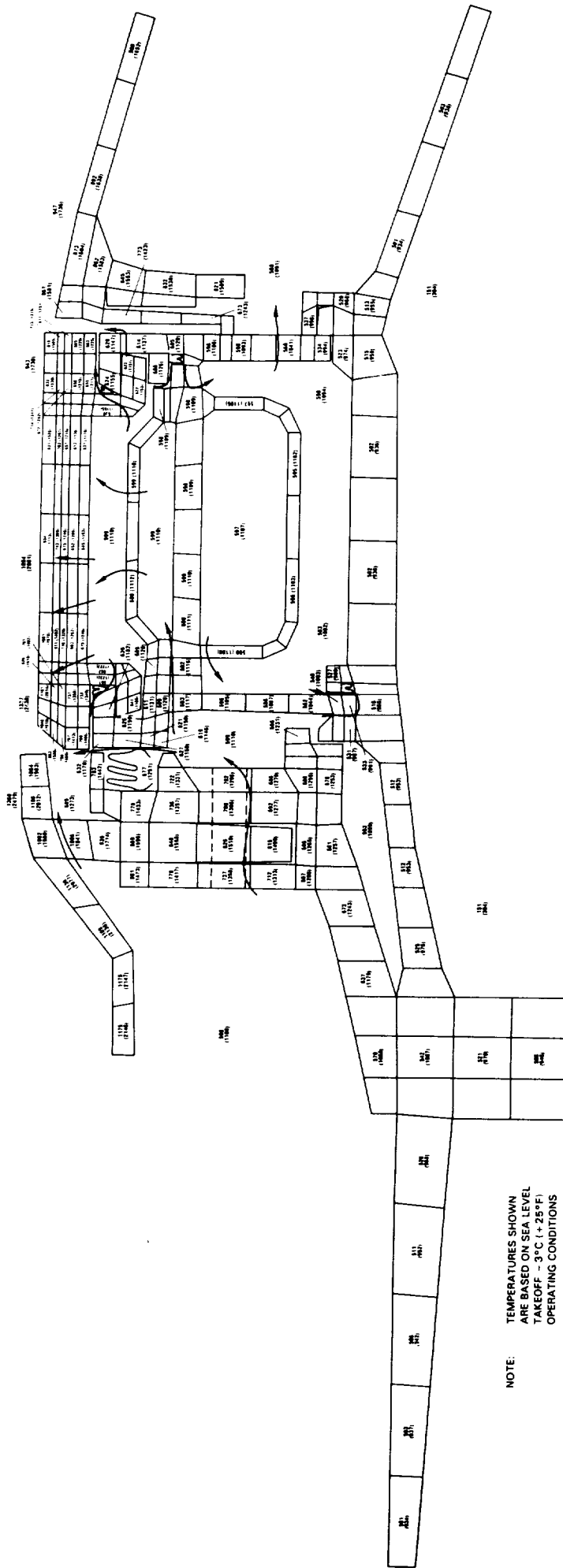


Figure 6.4-2 Typical Transient Response of Turbine Disk During Snap Acceleration/Deceleration

ORIGINAL PAGE IS
OF POOR QUALITY

ORIGINAL PAGE IS
OF POOR QUALITY



NOTE: TEMPERATURES SHOWN
ARE BASED ON SEA LEVEL
TAKEOFF - 3°C (+25°F)
OPERATING CONDITIONS

Figure 6.4-3 Detailed Turbine Case and Outer Airseal Model Used in Thermal Analysis

FOLDDOUT ERAME

2 FOLDDOUT ERAME

ORIGINAL PAGE IS
OF POOR QUALITY

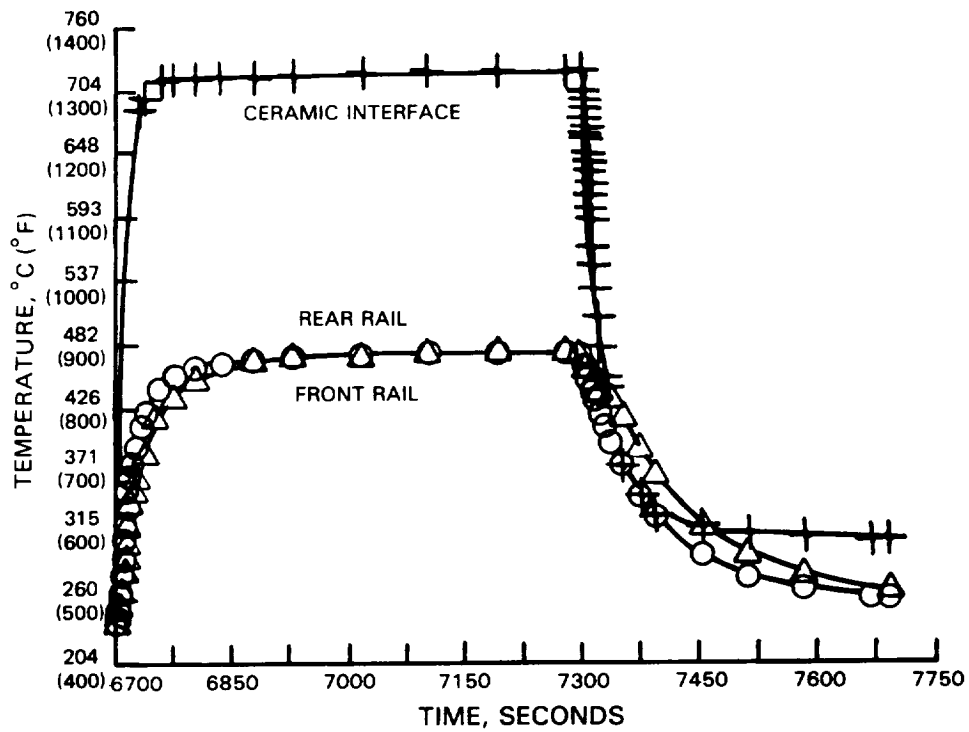


Figure 6.4-4 Results of Temperature Analysis

SECTION 7.0

COMPONENT MECHANICAL DESIGN

7.1 OVERVIEW

The mechanical definition of the high-pressure turbine component evolved through an iterative process based on the results of the aerodynamic effort and various supporting technology programs. Where necessary, the turbine design for the flight propulsion system has been modified to meet specific requirements associated with the integrated core/low spool. The resultant configuration is illustrated in Figure 7.1-1. To facilitate design and analysis, the total effort was divided into the analysis of the following subassemblies: the rotor, vane and inner case, outer case and outer airseal, and number 4 and 5 bearing compartment.

7.2 TURBINE ROTOR ASSEMBLY

7.2.1 General Description

The high-pressure turbine rotor assembly is illustrated in Figure 7.2.1-1. The primary elements in this assembly are the blade, disk, disk sideplates, vortex plate and high-pressure turbine to high-pressure compressor bolted joint. Design details pertaining to these components are discussed in the following sections.

The Energy Efficient Engine high-pressure rotor construction is different from most previous Pratt & Whitney Aircraft designs in that the rotor is straddle mounted. This arrangement eliminates the bearing compartment forward of the high-pressure turbine disk and places it after the disk. The advantage of straddle mounting the rotor is shown by the results of a dynamics analysis. A stiff high rotor equipped with a soft effective front spring mount (No. 3 bearing) eliminates any high critical speed response in the engine operating range, as indicated in Figure 7.2.1-2.

Figure 7.2.1-3 shows that the most serious critical speed mode is a free-free mode with 100 percent strain energy. This mode occurs well above the rotor red line speed at 27,600 rpm. A pitch mode with 4.2 percent rotor strain energy occurs at 7450 and a bounce mode occurs at 4950 rpm, respectively, which are both below idle speed.

Another possible critical mode is during startup when a stationary rotor becomes bowed as a result of thermals from residual heat in a nonoperating engine. This mode occurs below idle. Acceptable bowed rotor start characteristics are achieved with the aid of viscous film dampers on the bearing outer races.

A significant concern in the design of the joint between the turbine front hub and compressor rear hub was to provide adequate joint strength to prevent separation in the event of blade loss and ensuing high rotor imbalance loads.

High strength, cobalt alloy MP 159 was selected as the bolt material for this joint. Bolt tensile stress at steady state conditions was calculated to be 863,918,440 Pa (125,300 psi), and assembly tensile stress was 1,118,336,560 Pa (162,200 psi). Steady state thread shear stress was 364,045,440 Pa (52,800 psi) and assembly principal shear was 847,370,920 Pa (122,900 psi). All stresses were within allowable limits for this material.

ORIGINAL PAGE IS
OF POOR QUALITY

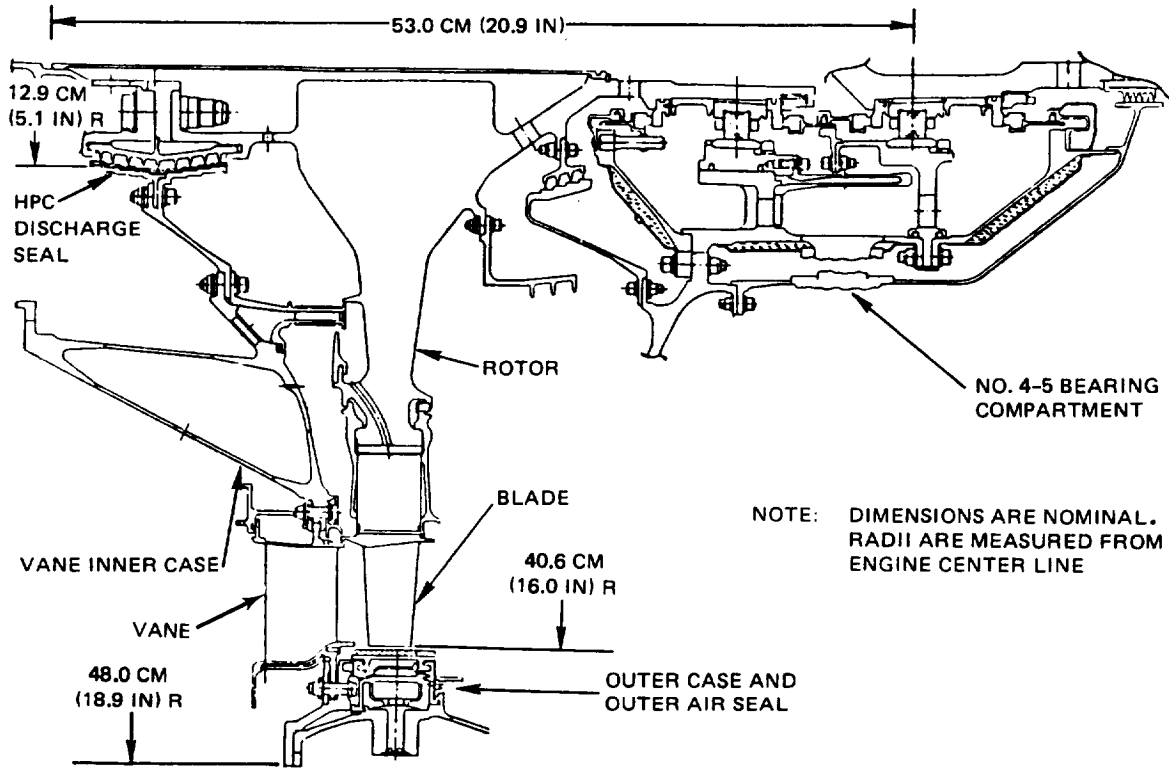


Figure 7.1-1 High-Pressure Turbine Mechanical Configuration

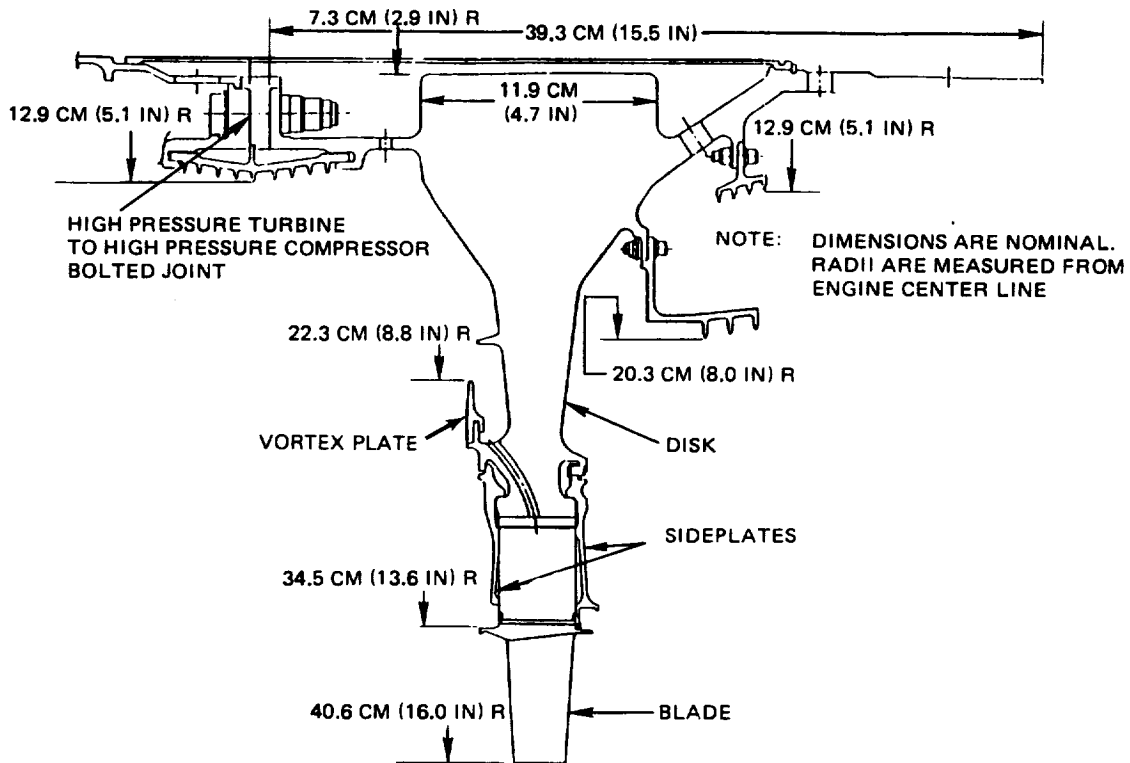


Figure 7.2.1-1 High-Pressure Turbine Rotor Assembly

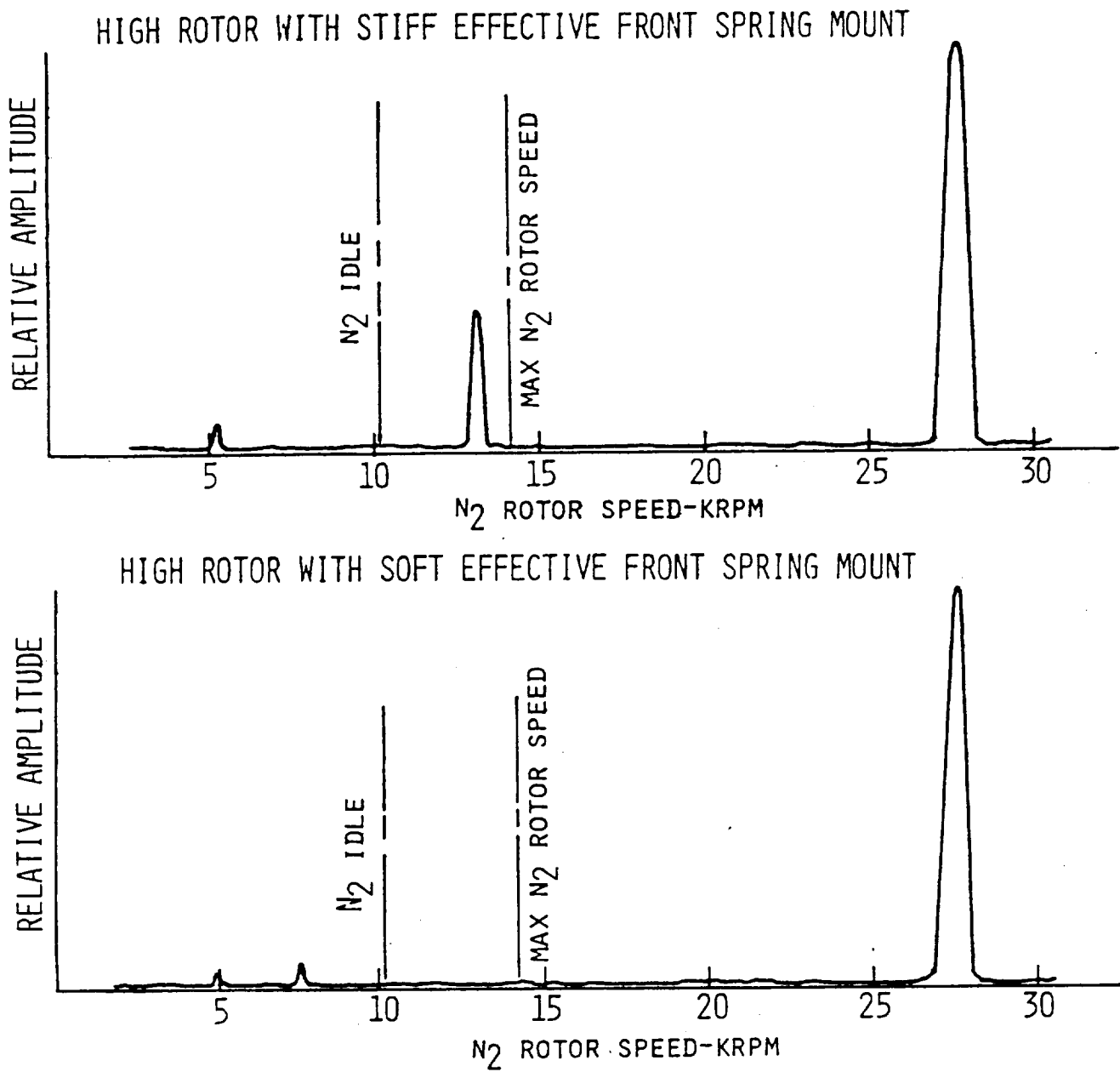
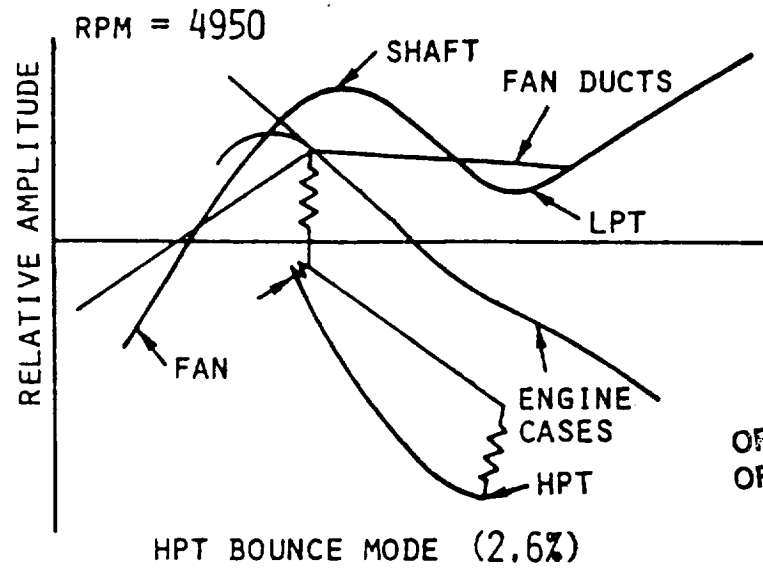


Figure 7.2.1-2 Energy Efficient Engine High Rotor Imbalance Response



ORIGINAL PAGE IS
OF POOR QUALITY

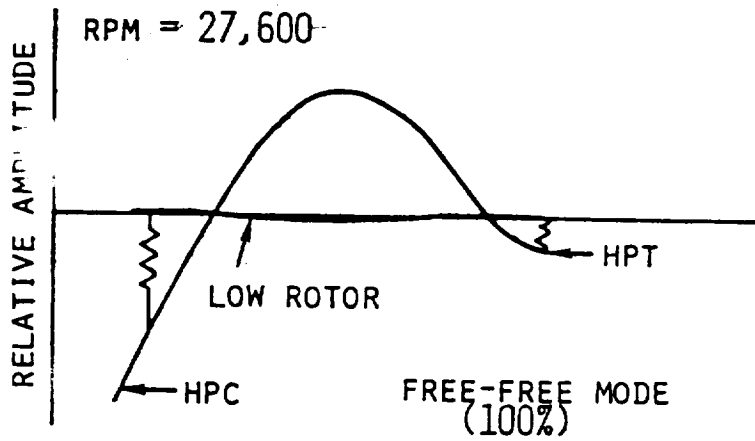
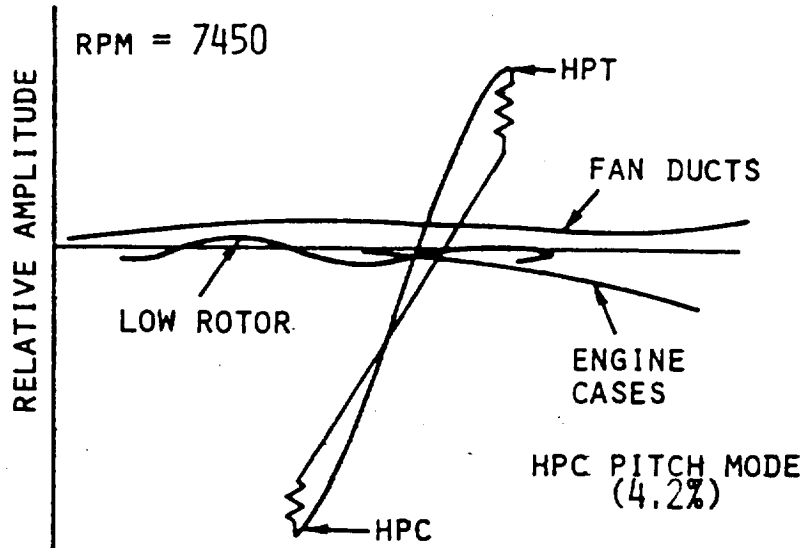


Figure 7.2.1-3 Energy Efficient Engine High Rotor Critical Speeds and Mode Shapes (% Rotor Strain Energy)

7.2.2 Blades

7.2.2.1 Mechanical Design Features

The high-pressure turbine blade mechanical design is shown in Figure 7.2.2-1. The mechanical design features of the blade are tailored to accommodate the increased AN^2 parameter, the benefits of which were demonstrated in the high-pressure turbine Uncooled Rig Program, as discussed in Section 4.1.2.1. The corresponding increased wheel speed associated with the higher AN^2 , however, results in a higher stress load. To compensate for these higher stresses, the blade is constructed from advanced high strength and high temperature capability materials. It is also tapered, incorporates a slight degree of tilt and has minimum wall thickness. The calculated average stress loads are shown in Table 7.2.2-I.

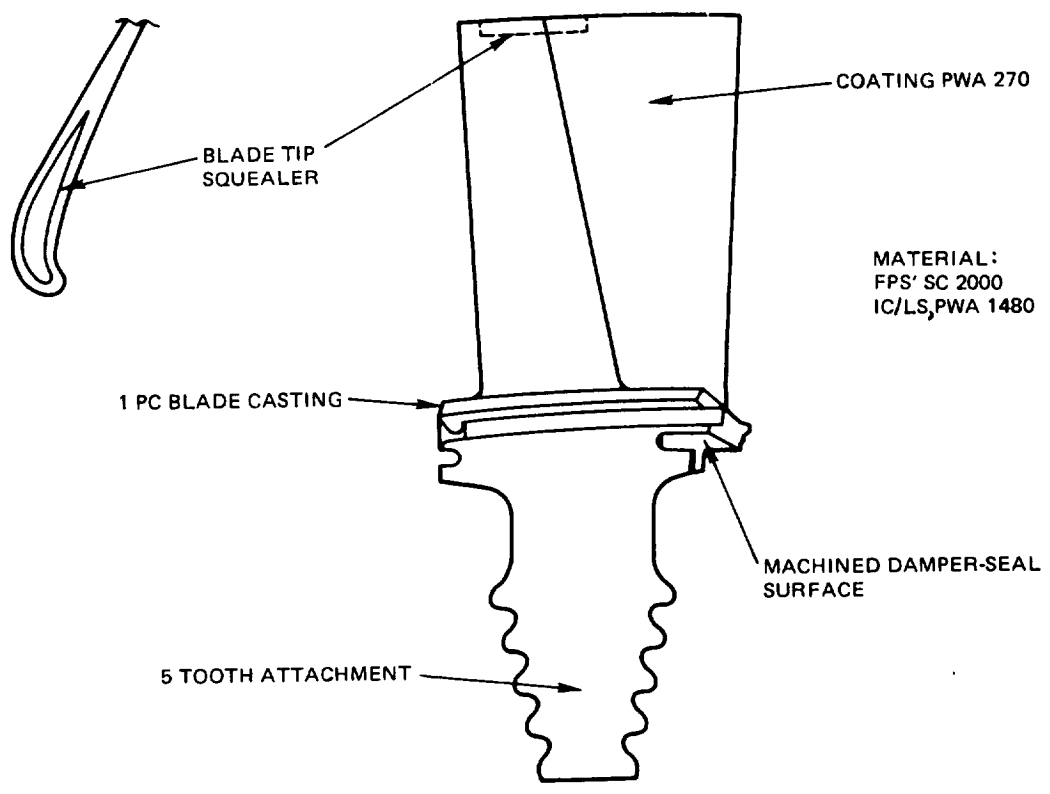


Figure 7.2.2-1 Turbine Blade Mechanical Configuration

TABLE 7.2.2-I
HIGH-PRESSURE TURBINE BLADE STRESS SUMMARY

Calculated Force/Area Stress MPa (kpsi)*

Root	325,434 (47.2)
One-Quarter Root	287,513 (41.7)
Mean	230,286 (33.4)
Extended Neck	310,266 (45.0)

*Sea level takeoff condition, 28°C (84°F), high-pressure rotor speed = 14,045 revolutions per minute (rpm)

The blade is constructed from a one-piece casting of a nickel base single crystal alloy. An advanced overlay coating is also used on the airfoil surface to provide additional resistance from oxidation and erosion. The materials selected for the blade are SC 2000 for the flight propulsion system and PWA 1480 for the integrated core/low spool. SC 2000 is a second-generation single crystal alloy still under development. It has improved stress rupture, creep, thermal fatigue, notch fatigue strength, and coated oxidation resistance over currently used directionally-solidified alloys. PWA 1480 is a currently available first-generation single crystal alloy with a 10°C (50°F) lower temperature capability than SC 2000. The blades for the integrated core/low spool were designed based on SC 2000 properties and cooling requirements, then checked to ensure that they met the integrated core/low spool life goals. Although PWA 270 coating is planned for use in the flight propulsion system to enhance blade life, it is not required for the experimental hardware.

Taper is used to control the radial distribution of blade mass so centrifugal forces due to wheel speed can be held to an acceptable level. The degree of taper in the blade design is illustrated in Figures 7.2.2-2, and was determined as part of an analysis that assessed the combined effects of taper, wall thickness, and blade tilt on airfoil stresses.

The degree of tilt in the airfoil design was established through an analysis aimed at balancing the stresses resulting from gas bending loads as well as those associated with centrifugal loads. Gas bending loads dominate at low engine speed whereas centrifugal loads dominate at high engine speeds. The degree of tilt in the blade design to accomplish the desired stress balance is shown in Figure 7.2.2-3.

Blade wall thickness and cooling passage ribs were also tailored to provide the desired distribution of radial mass. Figure 7.2.2-4 shows the nominal thicknesses established for the root, mean and tip sections. The thin trailing edge wall thickness of 0.0508 cm (0.020 in) including coating thickness was dictated by the aerodynamic concern to maintain a trailing edge wedge angle of 2 degrees and a cooling air discharge slot width of 0.050 cm (0.020 in).

The internal cooling configuration of the blade required provisions to support the ceramic core through the blade tip, while the blade is being cast (Figure 7.2.2-5). Following casting, these holes are plugged by welding in closure plugs.

A blade tip squealer and abrasive tip cap have been selected in order to decrease the amount of performance deterioration that would normally result in the event of blade tip rubs (see Section 7.6 for further discussion on blade tip clearances). The blade tip squealer was designed to be compatible with the tip cap configuration by incorporating a 0.127 cm (0.050 in) nominal wall thickness, which will provide adequate surface area for the application of an abrasive grit. The predicted performance gain expected by using only the squealer with a 0.088 cm (0.035 in) wall thickness is approximately 0.4 percent. Increasing the wall thickness to 0.127 cm (0.050 in) decreases this performance gain by 0.1 percent. However, using an abrasive tip cap will more than offset this slight performance penalty. The blade tip squealer design is shown in Figure 7.2.2-6.

CRITICAL PAIR IS OF POOR QUALITY

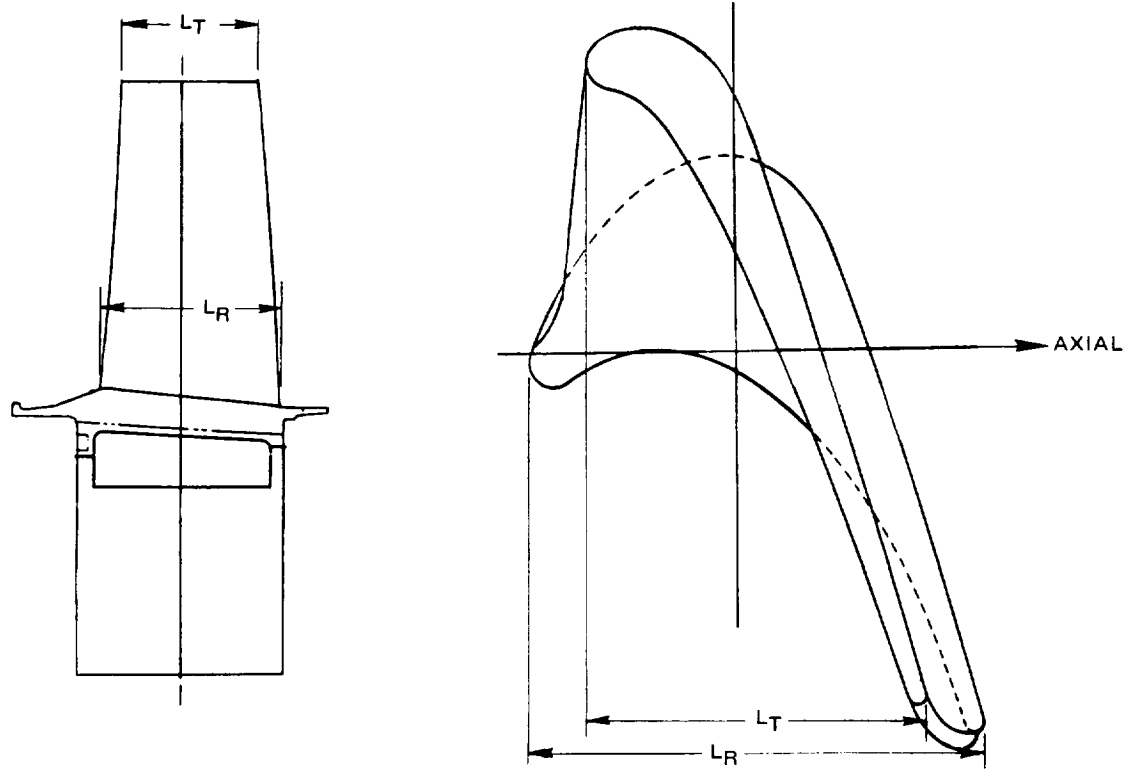


Figure 7.2.2-2 Radial Taper in Turbine Blade To Minimize Stress

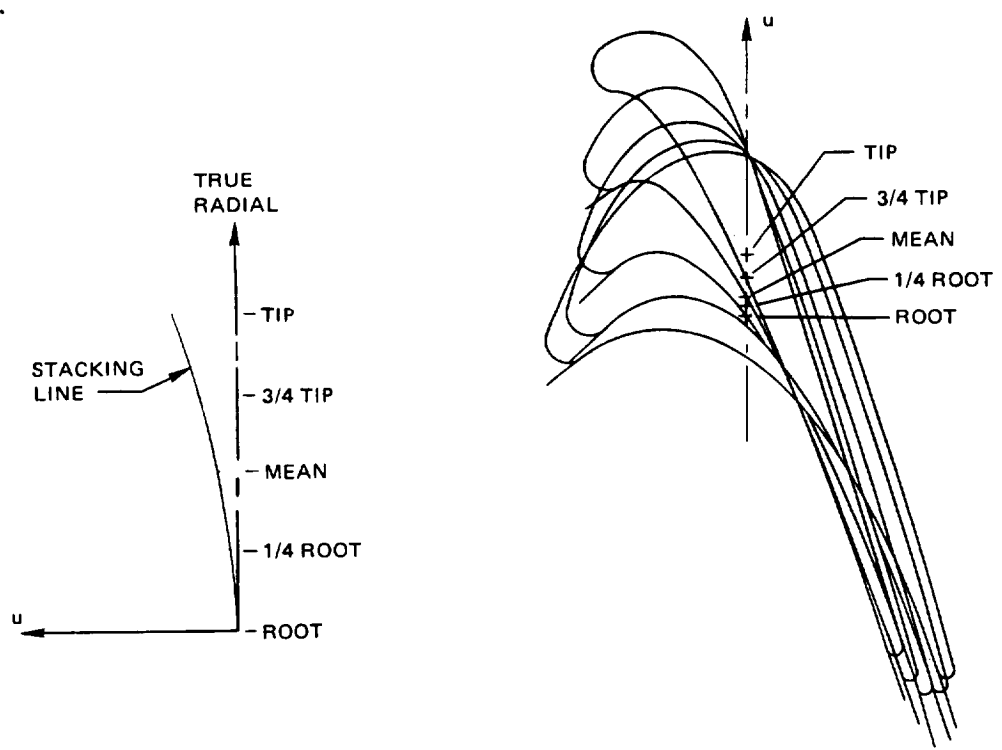


Figure 7.2.2-3 Degree of Tilt in the High-Pressure Turbine Blade To Achieve the Desired Balance Between Gas Bending Load Stresses and Stresses Resulting from Centrifugal Loads

ORIGINAL PAGE IS
OF POOR QUALITY

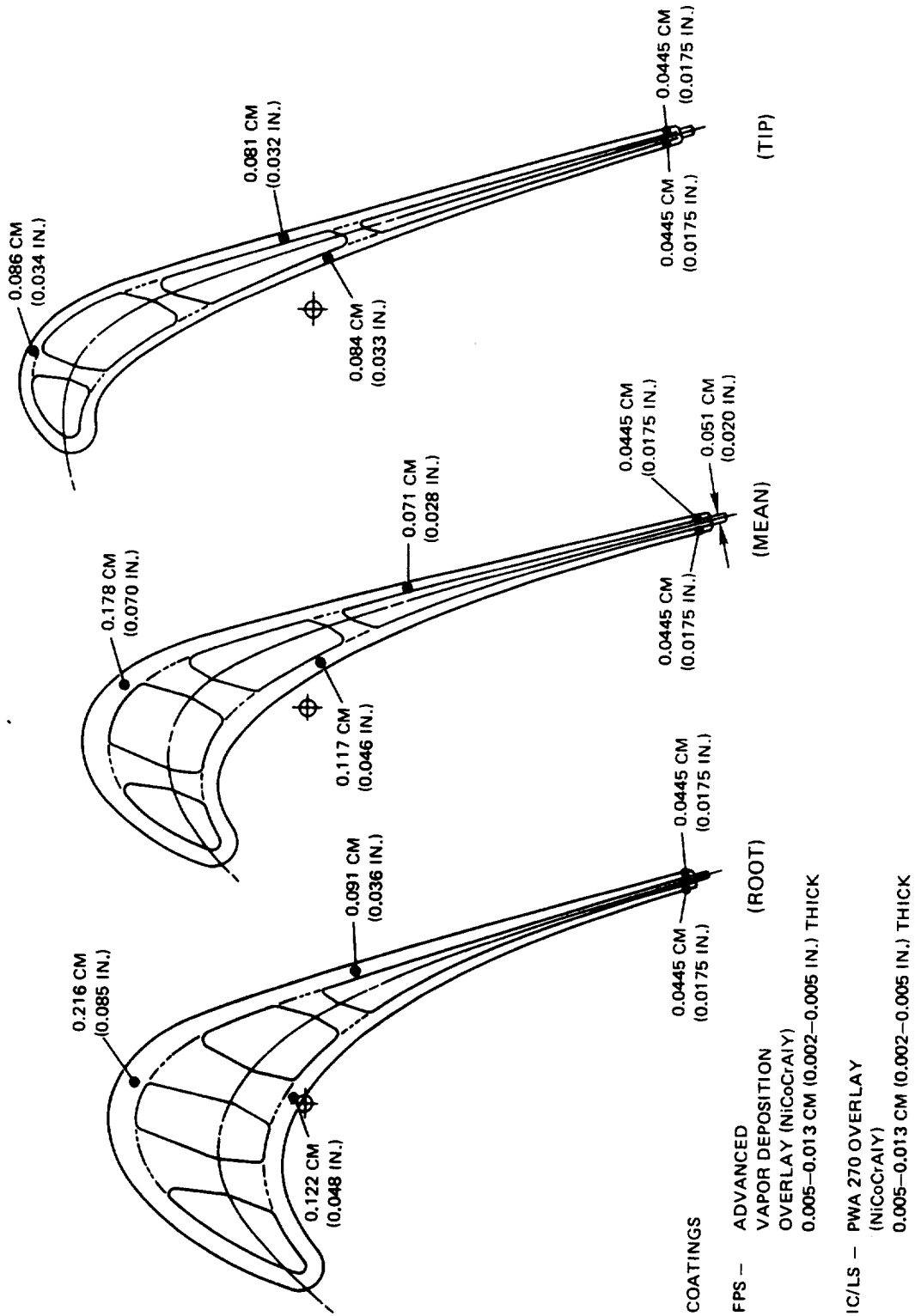


Figure 7.2.2-4 Uncoated Blade Wall Thickness and Internal Rib Design

ORIGINAL PAGE IS
OF POOR QUALITY

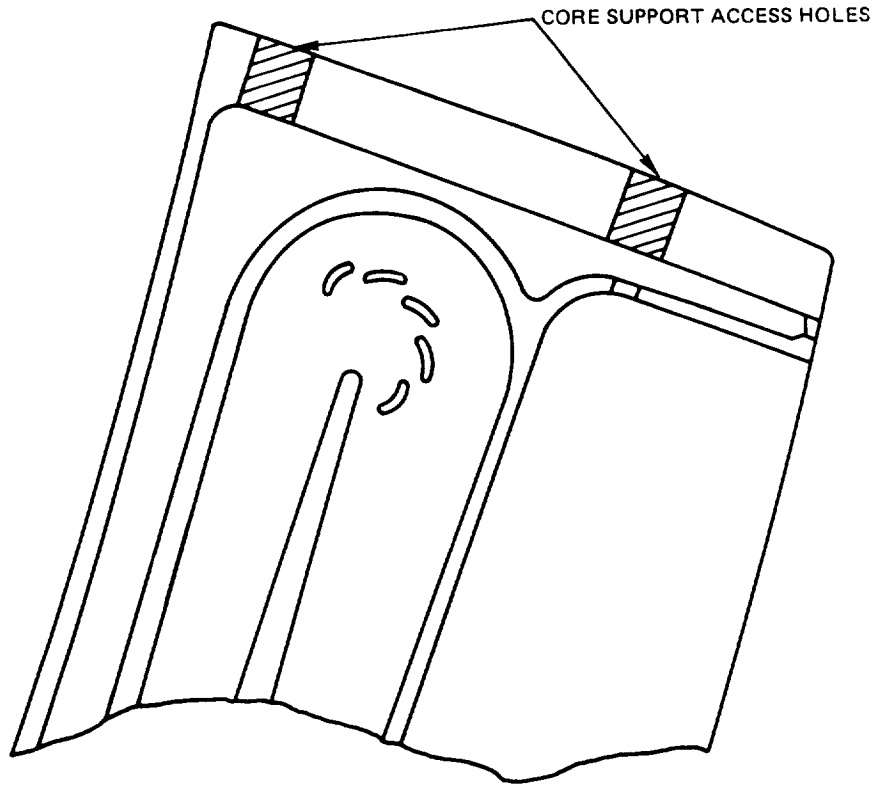


Figure 7.2.2-5 Core Support Method

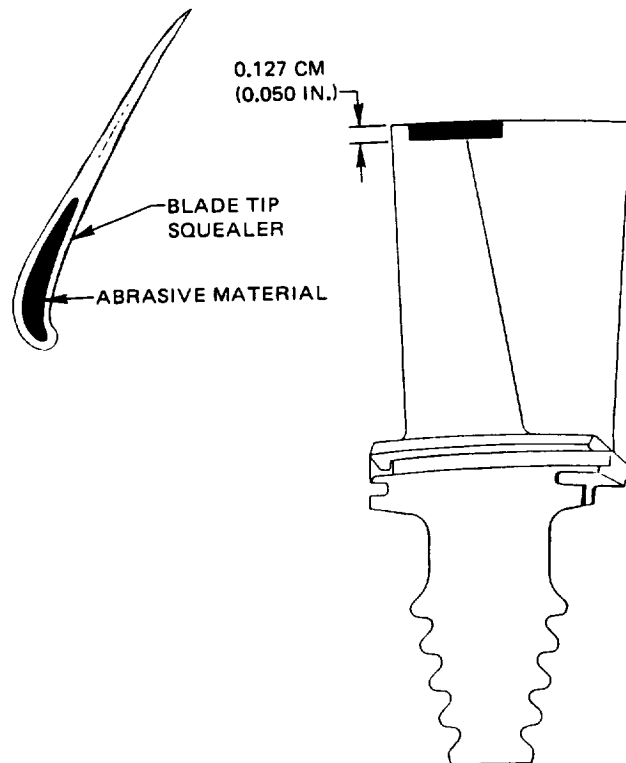


Figure 7.2.2-6 Blade Tip Squealer Geometry

7.2.2.2 Airfoil Vibration Analysis

A structural analysis of the single crystal blade was performed using the NASTRAN analytical technique. This technique uses a three-dimensional finite element analysis capable of showing airfoil vibratory response in terms of mode shape and natural frequency.

A graphical display of the high-pressure turbine blade defined by the NASTRAN technique is presented in Figure 7.2.2-7. The model utilizes plane stress elements for the airfoil skin and ribs, while the blade neck is simulated with beam elements. Attachment flexibilities are included as springrates to ground.

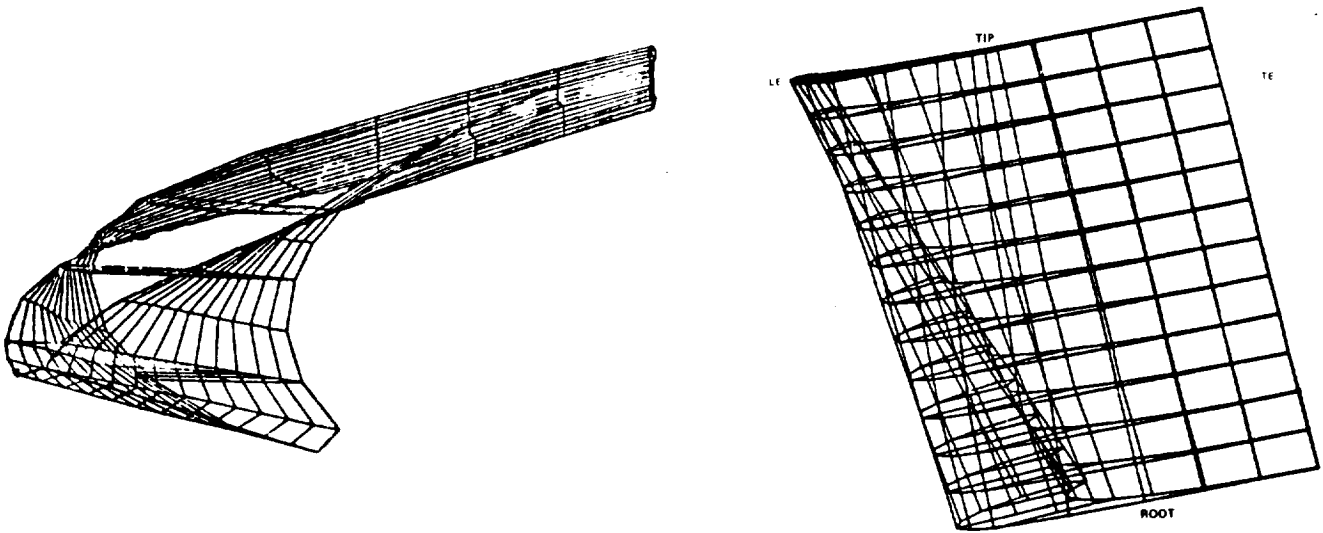


Figure 7.2.2-7 Graphical Display of Turbine Blade Defined by the NASTRAN Analytical Technique

In addition, this model included the unique stiffness properties associated with the single crystal atomic orientation whose characteristics could not be evaluated by using the classical beam analytical models for blade vibration. This enabled optimizing the crystallographic orientation of the blade to ensure sufficient margin from critical vibratory excitations throughout the engine operating range.

The initial NASTRAN blade analysis was based on an engine configuration which had 14 struts in the transition duct downstream of the high-pressure turbine. Also, the single crystal axes orientation was arbitrarily aligned with the engine axis system (primary axis in the radial direction, secondary in the axial direction (see Figure 7.2.2-8)), recognizing that the secondary axis $\langle 010 \rangle$ and $\langle 100 \rangle$ could be re-oriented spacially, if required. Results of this initial analysis indicated unacceptable frequency margins in the engine operating range.

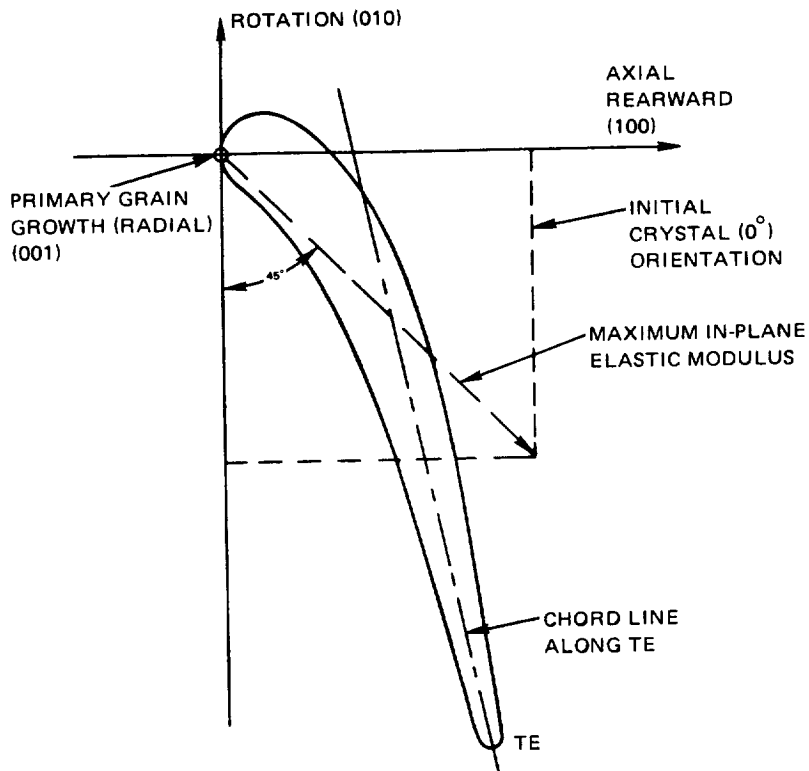


Figure 7.2.2-8 Single Crystal Major Axes Orientation

Figure 7.2.2-9 presents the estimated vibratory frequencies for the first five modes of blade vibration. The critical engine order lines of 14E and 24E, which correspond to turbine transition duct strut and first-stage turbine vane passing frequencies, respectively, are shown with the estimated frequency margins in the cruise-to-redline high-pressure rotor speed range. As indicated, there is insufficient margin between the 14E order line and the third vibratory mode (7.3 percent) and the 24E order line and fifth vibratory mode (2.6 percent).

Analysis of blade vibrations in these five resonant modes indicated that the trailing edge region from mid-span to tip was the area of greatest vibrational magnitude. This can be seen in the airfoil isodeflection characteristics illustrated in Figures 7.2.2-10 through 7.2.2-14.

To achieve acceptable margins, two methods of corrective action were taken. The first was an engine configurational change to reduce the number of transition duct struts from 14 to 11. This resulted in an 11E order line significantly below the 14E line, and permitted tuning of both first and second modes so that adequate margin was provided for the first mode below minimum cruise engine speed and for the second mode above redline speed.

ORIGINAL PAGE IS
OF POOR QUALITY

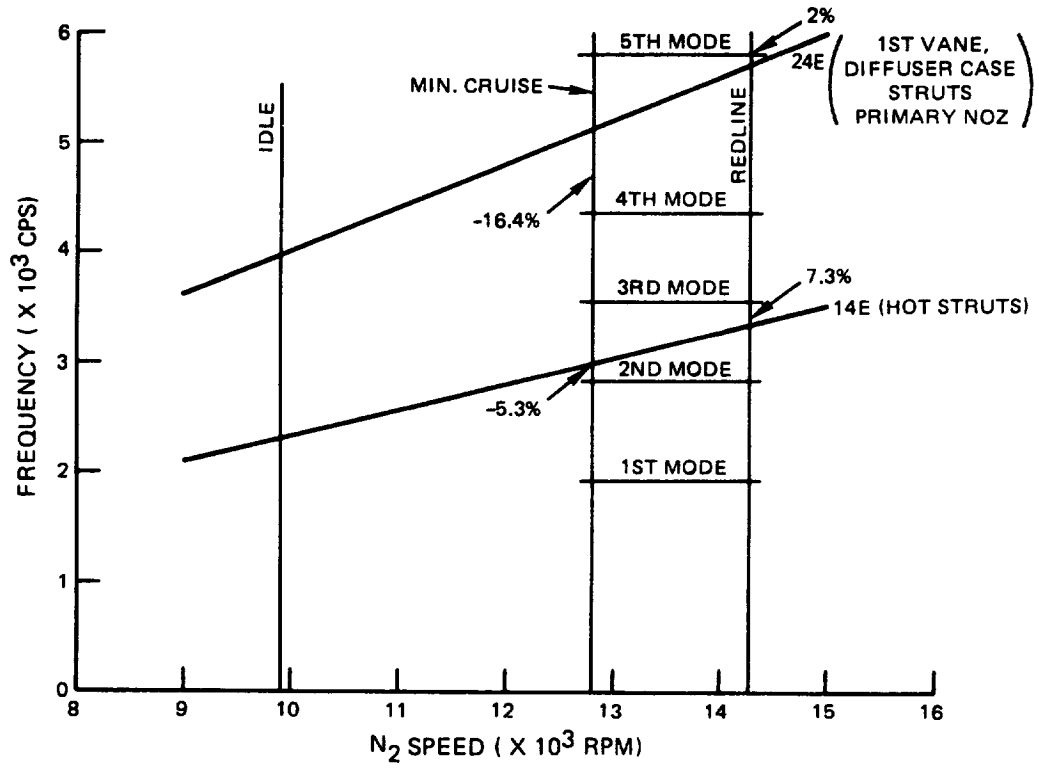


Figure 7.2.2-9 High-Pressure Turbine Resonance Diagram

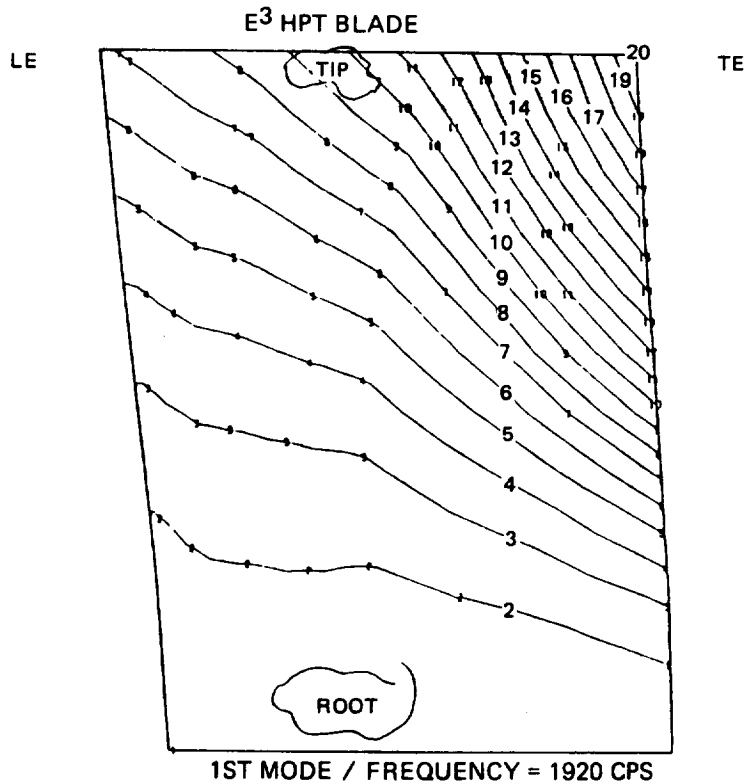


Figure 7.2.2-10 Blade Vibration Characteristics in First Mode

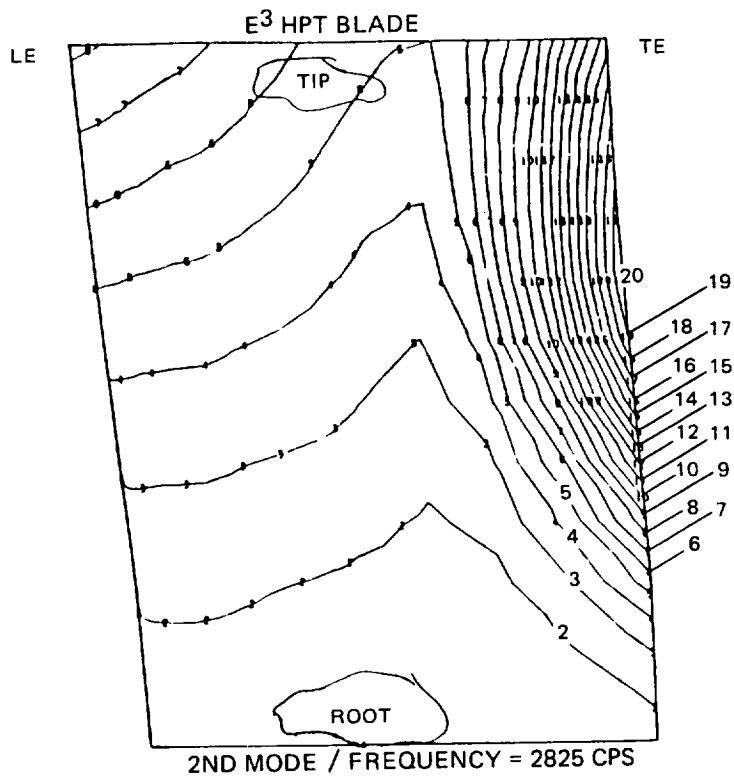


Figure 7.2.2-11 Blade Vibration Characteristics in Second Mode

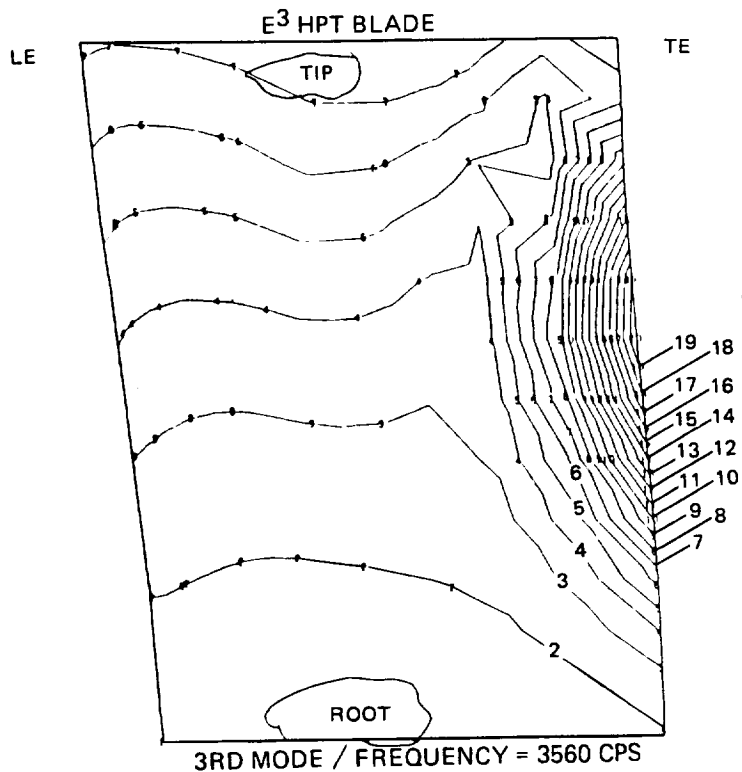


Figure 7.2.2-12 Blade Vibration Characteristics in Third Mode

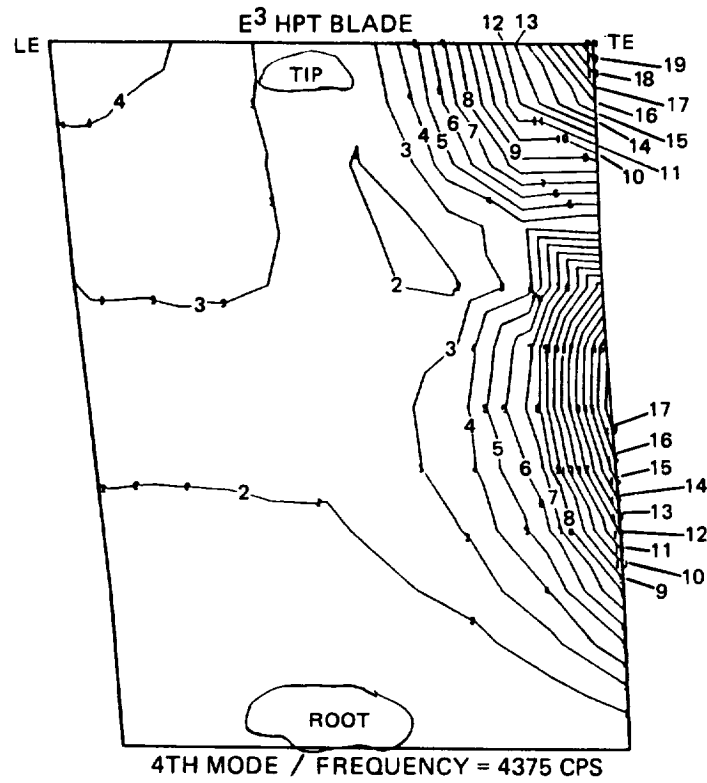


Figure 7.2.2-13 Blade Vibration Characteristics in Fourth Mode

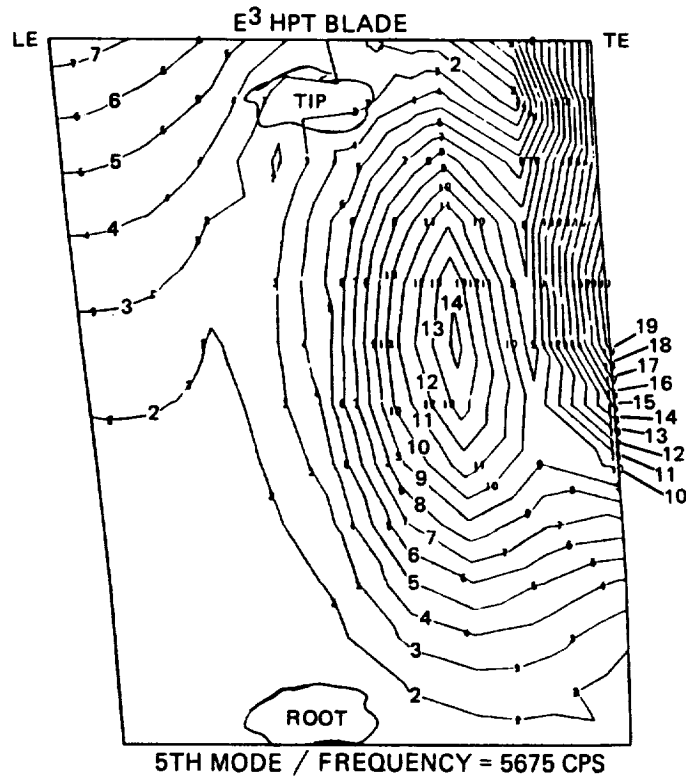


Figure 7.2.2-14 Blade Vibration Characteristics in Fifth Mode

The second area of corrective action, which was required to provide adequate frequency margin at redline speed for both the 11E second mode and 24E fifth mode resonances, involved investigation of the impact of single crystal secondary axis orientation on blade vibration characteristics. Figure 7.2.2-15 shows how the modulus of elasticity varies along the secondary axis of the crystalline structure, thereby indicating that re-orientation of the secondary crystallographic axis could be expected to affect the frequencies of the various vibratory modes. To determine this variation, the crystal was rotated about the radial axis $\langle 001 \rangle$ in a clockwise manner. The resulting mode frequencies were plotted as a function of this rotation angle. The results are shown in Figures 7.2.2-16. The final requirement for crystal secondary axis control was predicated on obtaining the highest second and fifth mode frequencies. This was obtained by rotating the crystal secondary axis 25 degrees. Because of the significant trailing edge clockwise motion in these modes, it was necessary to align the maximum in-plane modulus of elasticity with chord line "A" running through the blade trailing edge, as shown in Figure 7.2.2-17.

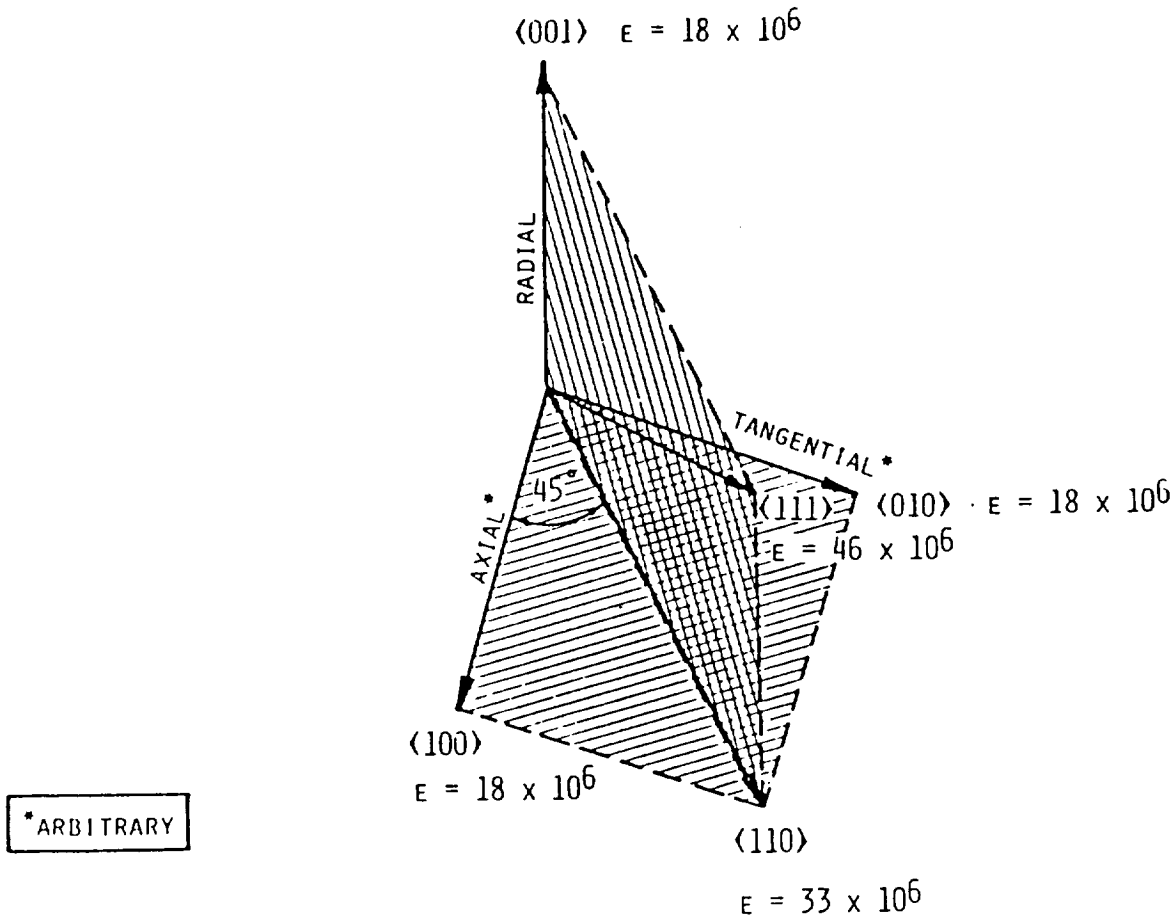


Figure 7.2.2-15 Crystallographic Orientation

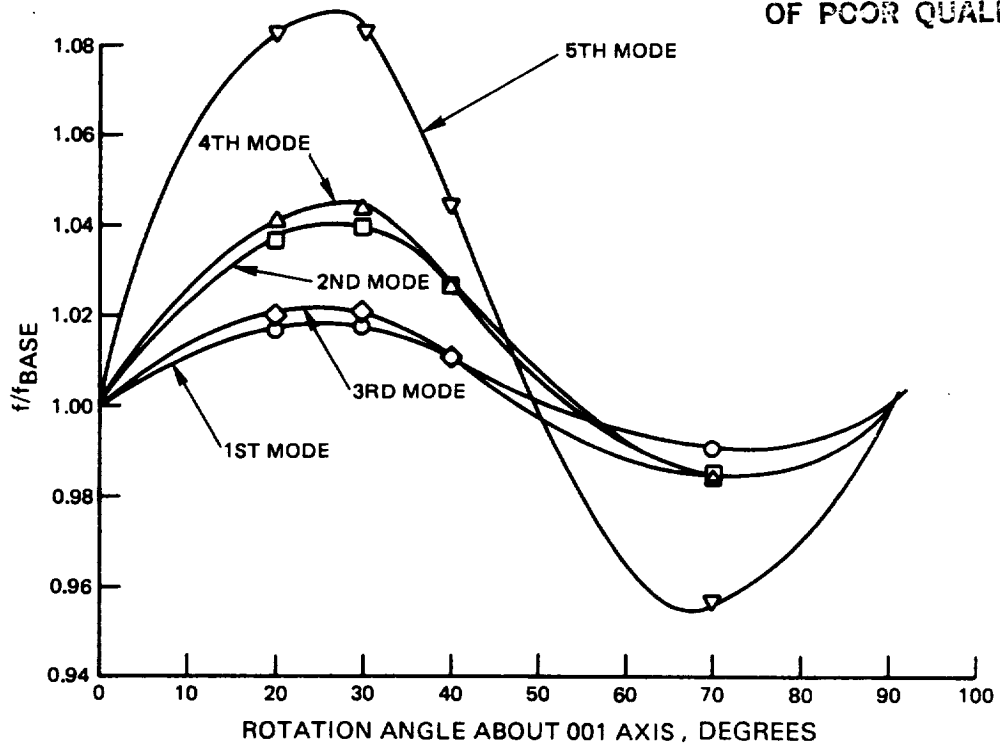


Figure 7.2.2-16 Predicted Frequencies Versus Crystal Secondary Orientation Angle

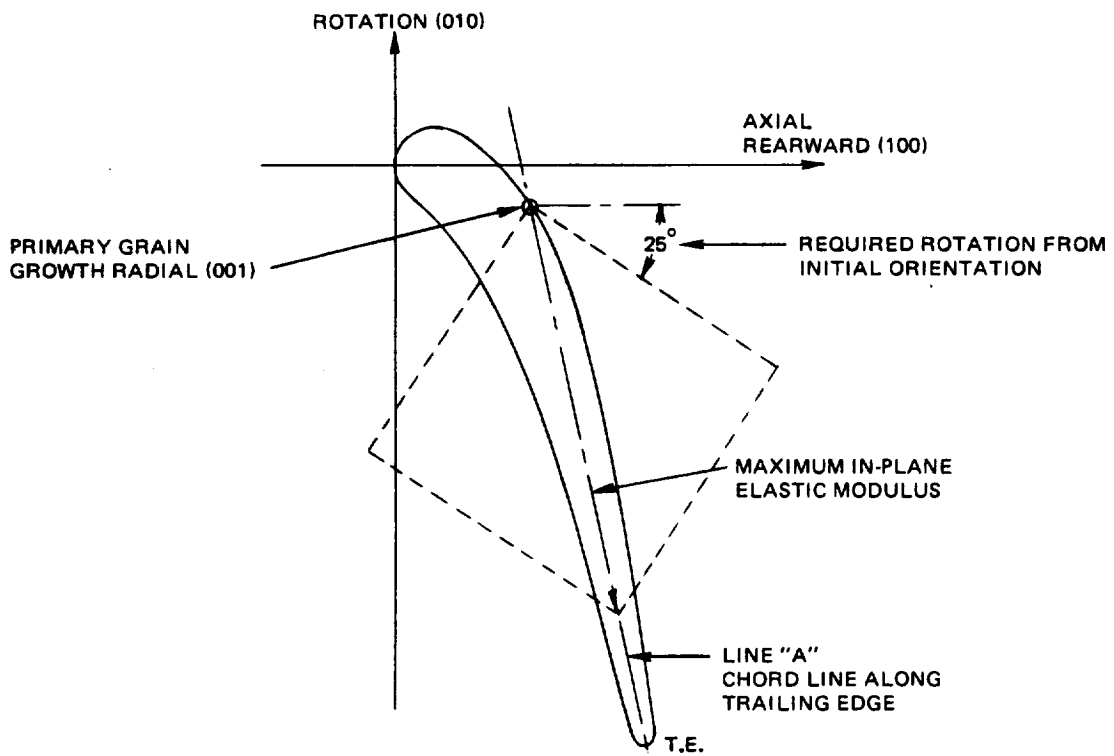


Figure 7.2.2-17 Axial Shift in Crystal Orientation

An analysis of this modified configuration demonstrated acceptable frequency margins for both 11E and 24E engine order lines. The results are presented in the resonance diagram in Figure 7.2.2-18.

Blade platform frequencies were calculated to ensure that no vane passing resonances would occur in the engine operating range. Both 11E and 24E resonances were predicted to be well above redline speed.

The reduced velocity flutter parameter for the high-pressure turbine blades is 2.1, which is well below the established design limit for shroudless turbine blades. The long chord and high frequency characteristics of the blade contribute to this stability. Blade damper load was set at 4448 N (1000 lb) to provide effective control of both buffet stress and resonant stress. The buffet stress analysis assumed that the combustor liner pressure drop was 2.5 percent of total pressure at the high-pressure compressor exit location.

Axial gapping between the blade, first vane, and hot strut was also analyzed. The spacing along a streamline at the outer diameter between the blade trailing edge and the hot strut leading edge was established at three times the maximum thickness of the strut. The axial meanline gap between the blade leading edge and the first vane trailing edge was established at approximately 0.33 times the vane meanline axial chord.

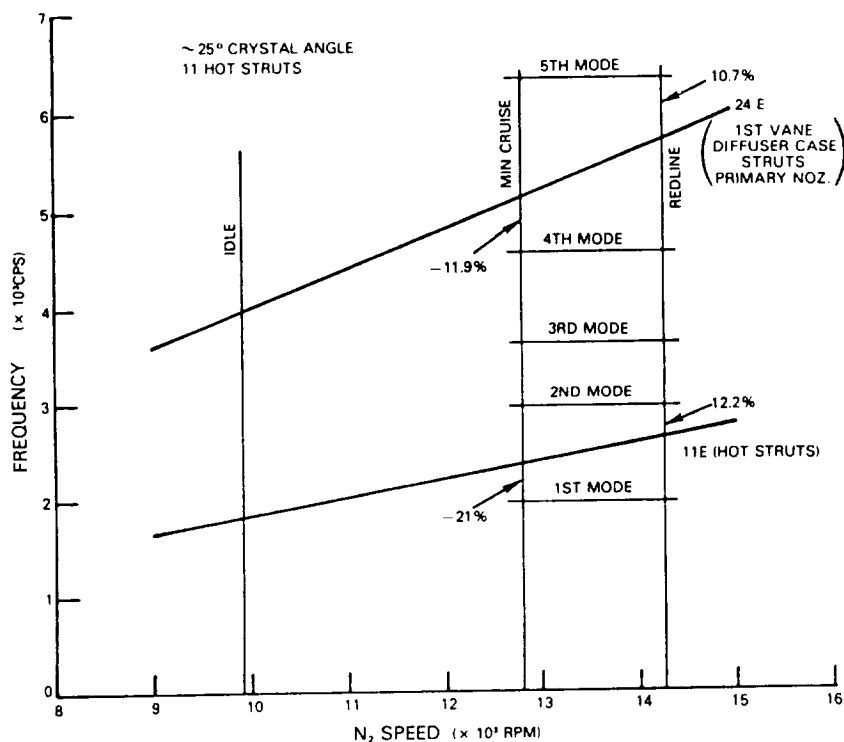


Figure 7.2.2-18 Predicted Frequency with Modified Configuration

7.2.3 Blade Attachment

7.2.3.1 Mechanical Design Features

The attachment for the high-pressure turbine blade is a five-tooth firtree design that evolved from a four-tooth design during the preliminary design effort for the high-pressure turbine component. Primary contributing factors to this change consisted of: (1) a flowpath revision that increased the platform pull by 20 percent, and (2) a blade neck extension of 0.584 cm (0.23 in), which increased neck pull by 50 percent. With the original four-tooth configuration, the combination of these factors increased the concentrated stress in the attachment above the allowable level. Consequently, the five-tooth geometry was adopted.

7.2.3.2 Structural Analysis

A stress analysis of the blade attachment geometry was conducted by using a finite element technique. Results are summarized in Table 7.2.3-1 for the nominal stresses of shear, bending, bearing, and tension. These results are based on the most stress-limiting tooth in the firtree geometry.

As indicated by these results, the predicted shear and bearing stresses exceed the maximum allowable limit by 8 and 11 percent, respectively. The remaining values are substantially below limit, with the exception of tension, which is only marginally higher than the acceptable limit. However, rig testing of single crystal root attachment specimens has been successfully conducted both at and above these stress levels with no evidence of material distress. On the basis of these experimental data, the blade attachment configuration is structurally adequate and the predictions are somewhat conservative.

Additional stress analyses were performed using two-dimensional finite element technology to ensure concentrated attachment stresses provided adequate life in the integrated core/low spool and the flight propulsion system. Life goals are 1000 and 12,000 cycles, respectively, assuming the appropriate materials. The results of this analysis are presented in Figure 7.2.3-1. Estimates for the integrated core/low spool show that all stresses are below the maximum level, thereby attaining the 1000 cycle goal. However, for the higher cyclic life requirements of the flight propulsion system, blade stresses are lower than the allowable limit but stresses are also higher on the disk by approximately the same percentage. This result suggests that the disk broach geometry can be optimized to achieve the desired stress balance between the blade and disk to meet the 12,000 cycle life goal.

TABLE 7.2.3-I
BLADE ATTACHMENT STRESS SUMMARY

<u>Stress Mode</u>	<u>Location</u>	<u>% Above (Or Below) Design System</u>
Shear	Blade	+11*
	Disk	-21
Bending	Blade	-48
	Disk	-63
Bearing	Blade	+ 8*
	Disk	-17
Tension	Blade	+ 2
	Disk	+ 1

*Rig testing has been conducted at these levels without material distress.

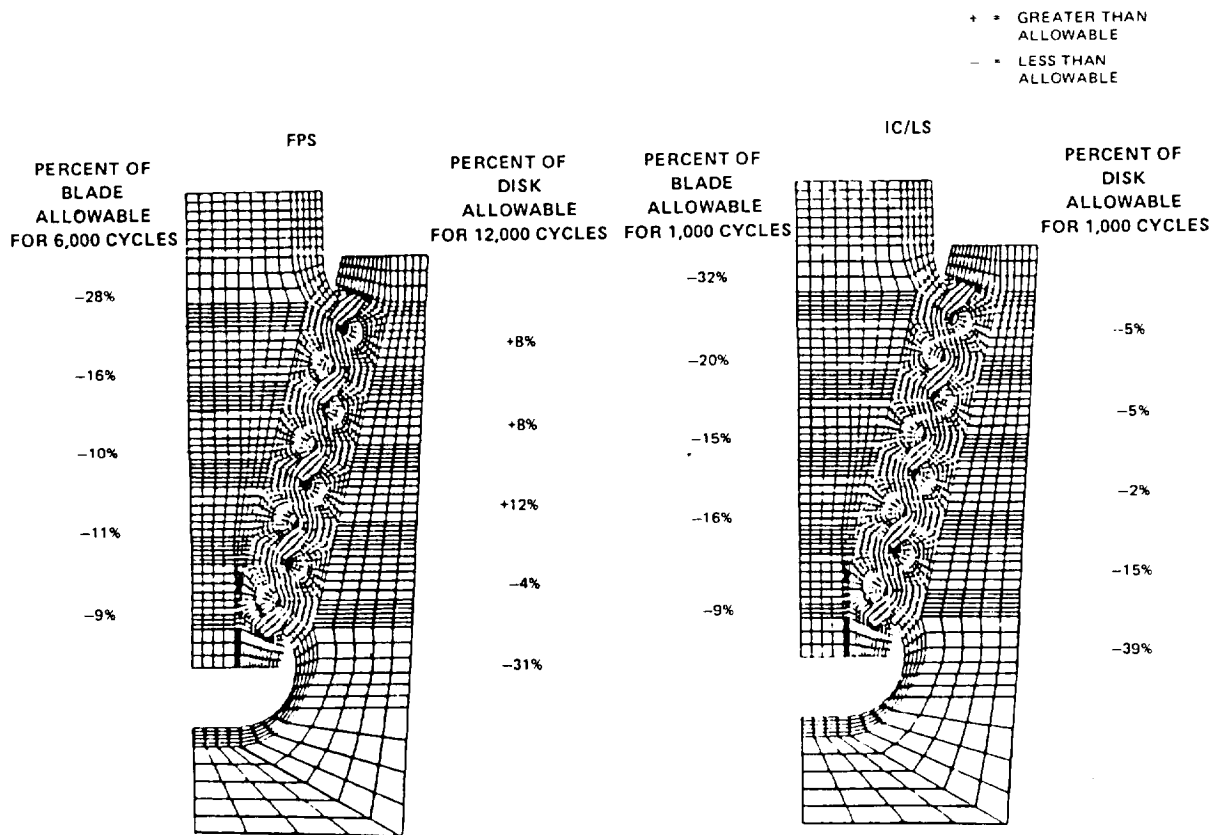


Figure 7.2.3-1 Blade Attachment Stress Results

7.2.4 Disk

7.2.4.1 Mechanical Design Features

The high-pressure turbine disk that evolved from the detailed design effort is illustrated in Figure 7.2.4-1. Design requirements for this disk were defined by the high rim speed that resulted from the high AN^2 parameter selected for the basic turbine aerodynamics. Characteristics of the disk required by this parameter are a thick bore region and use of advanced high strength materials.

The disk rim features firtree attachments to hold the blades, shelves to support the boltless front and rear sideplates, a flange to support the vortex plate, and curved elliptical cooling air supply holes which transport the cooling air from the tangential on-board injection nozzle to the blade roots.

The design was based on flight propulsion system requirements and the use of advanced MERL 80 material. This same disk configuration will be used in the integrated core/low spool. However, the material will be PWA 1099, which has adequate mechanical properties to meet the life requirements of the demonstrator vehicle and is currently available.

Details of the elliptical cooling air supply hole are illustrated in Figure 7.2.4-2. This design was predicated on the desire to keep rim width to a minimum (i.e., minimize material mass in the rim area), control rim breakout stress concentrations, and provide the required coolant air flow to the blade root. Again, because of the high rim speeds, the primary concern was stress concentration in the rim area.

7.2.4.2 Structural Analysis

Results of a stress analysis for the areas of the rim, blade attachment, and sideplates indicated that average tangential stresses are within allowable limits for the flight propulsion system disk and slightly less than allowable for the integrated core/low spool to meet its 1000 cycle life requirement. Further refinement will bring these stresses within allowable limits. Burst margin is adequate. Disk web thickness was controlled to avoid possible low order (2E through 4E) first coupled mode resonances occurring at high speed. First coupled mode vibration is defined as that mode shape of the disk and blade where disk deflection is in a fore and aft direction and accompanies (coupled) bending of the blade (see Figure 7.2.4-3). Principal life and stress characteristics are shown in Table 7.2.4-I.

TABLE 7.2.4-I
DISK LIFE AND STRESS SUMMARY

	<u>Flight Propulsion System</u>	<u>Integrated Core/ Low Spool</u>
Bore Life ($\times 10^{-3}$ cycles)	35	8.5
Rim Life ($\times 10^{-3}$ cycles)	100	80
Burst Margin	1.22	1.244
Average Tangential Stress MPa (kpsi)	796,349 (115.5)	759,462 (110.15)

ORIGINAL PAGE IS
OF POOR QUALITY

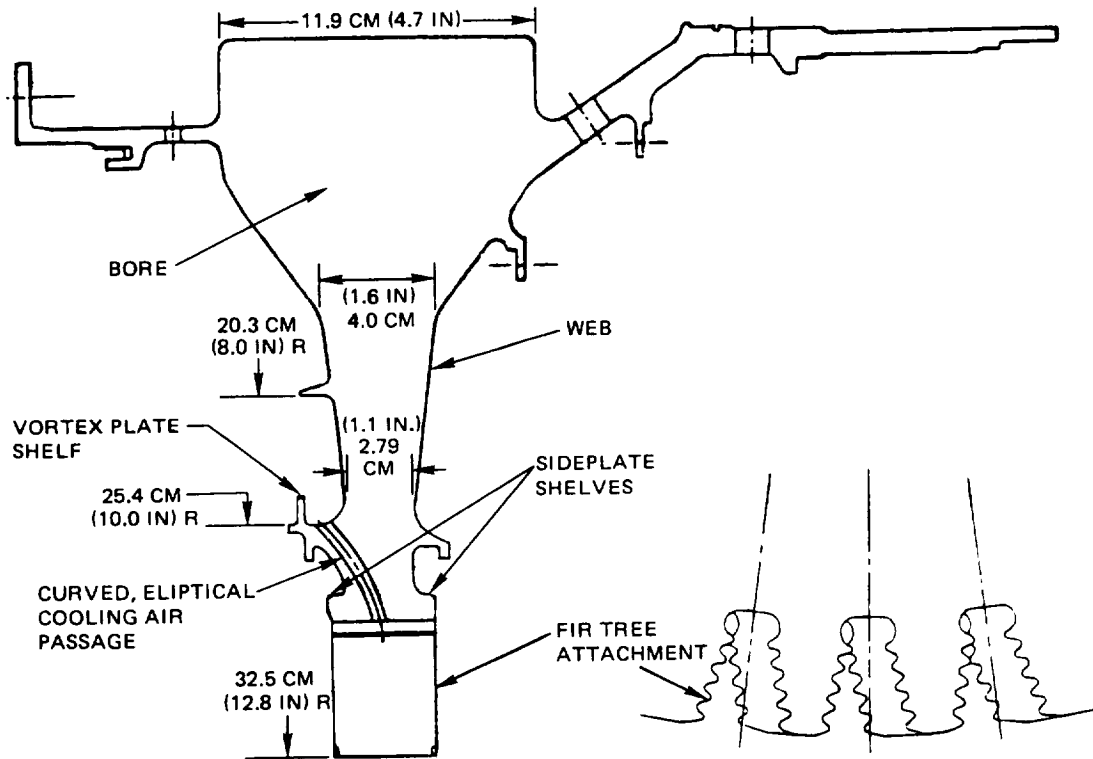


Figure 7.2.4-1 High-Pressure Turbine Disk Design Features

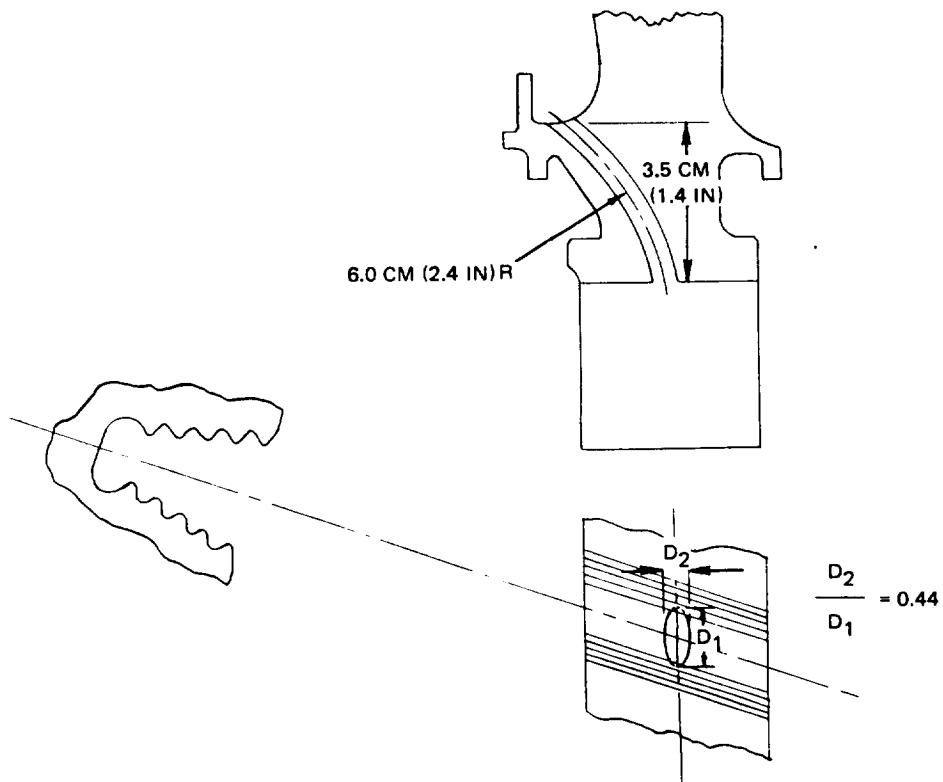


Figure 7.2.4-2 Elliptical Cooling Air Supply Hole

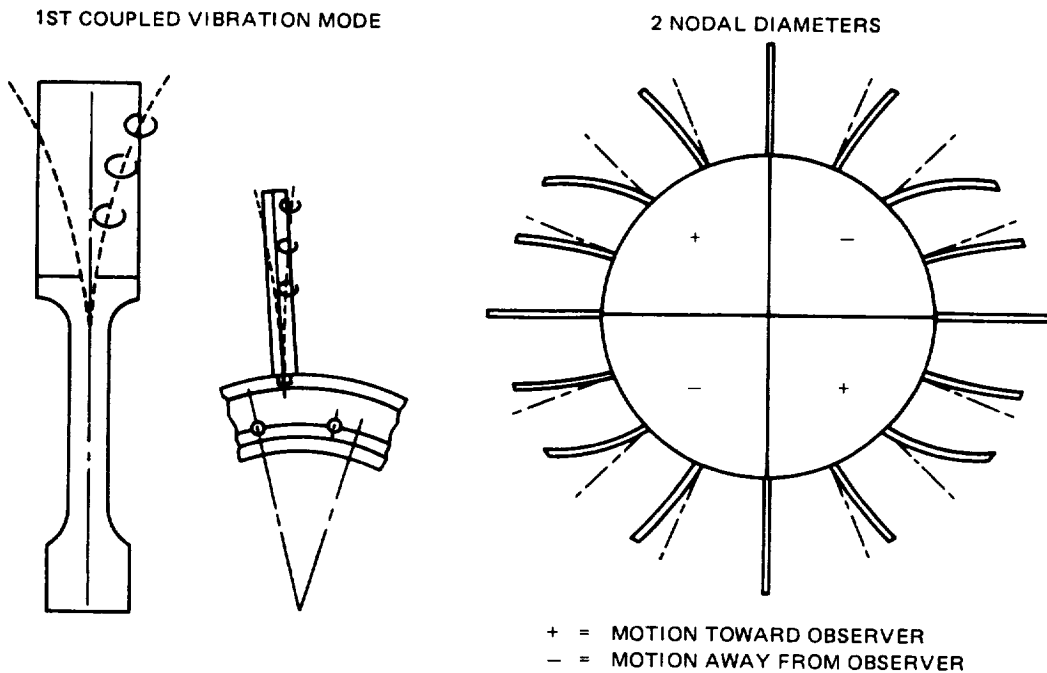


Figure 7.2.4-3 Schematic Showing Disk and Blade Deflections Caused by First Coupled Mode Vibration

Low cycle fatigue (LCF) requirements for the disk, sideplates and vortex plate were set at 12,000 cycles. In order to assess disk low cycle fatigue characteristics, a finite element analysis was undertaken. Figure 7.2.4-4 shows the finite element break-up used, along with the boundary conditions assumed for the analysis. To account for stresses generated along the curved elliptical cooling air passage, a three-dimensional boundary integral equation analytical model was used. The combined results of these analyses are summarized in Figure 7.2.4-5, which shows the low cycle fatigue lives for the critical areas of the turbine rim. As shown, calculated lives in three critical areas exceed requirements. Since the low cycle fatigue properties of notched MERL 80 and PWA 1099 materials are identical, the same life is predicted for both the flight propulsion system and the integrated core/low spool.

7.2.5 Sideplates and Vortex Plate

7.2.5.1 Mechanical Design Features

The disk sideplates and vortex plate are illustrated in Figure 7.2.5-1. The full ring sideplates perform a dual function -- blade retention and sealing in the rim areas. Axial loads at the critical sealing areas are generated by centrifugal loads, acting on the sideplates that are canted away from the disk rim. Undesireable retention holes in the sideplates were eliminated by designing the sideplates to be trapped by bayonet connectors (engaged lugs and slots) instead of conventional bolting arrangements. Stress analysis showed that conventional bolting designs resulted in unacceptably high bolt and bolt hole stresses. Leakage is controlled by damper seals sealing axially along the blade platform and by a W-seal trapped by the blade and rear sideplate. Typical sideplate loads are shown in Figure 7.2.5-2.

ORIGINAL PAGE IS
OF POOR QUALITY

$F_{PULL} = 8,594,446 \text{ N (1,932,117.8 lbs)}$ AT $R = 34.01 \text{ CM (13.39 IN)}$

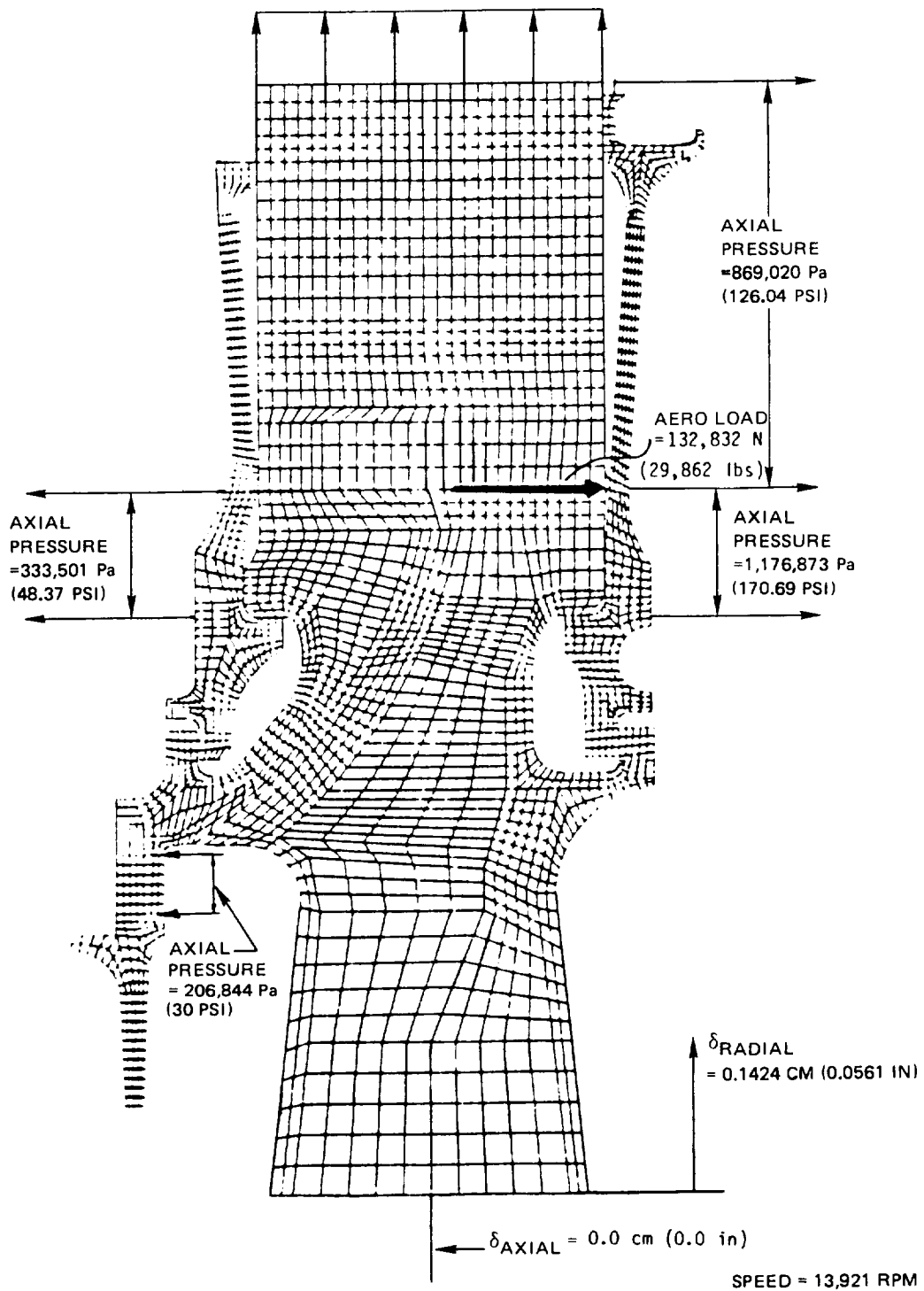


Figure 7.2.4-4 Boundary Conditions Used in Disk Structural Analysis

C-2

ORIGINAL PAGE IS
OF POOR QUALITY

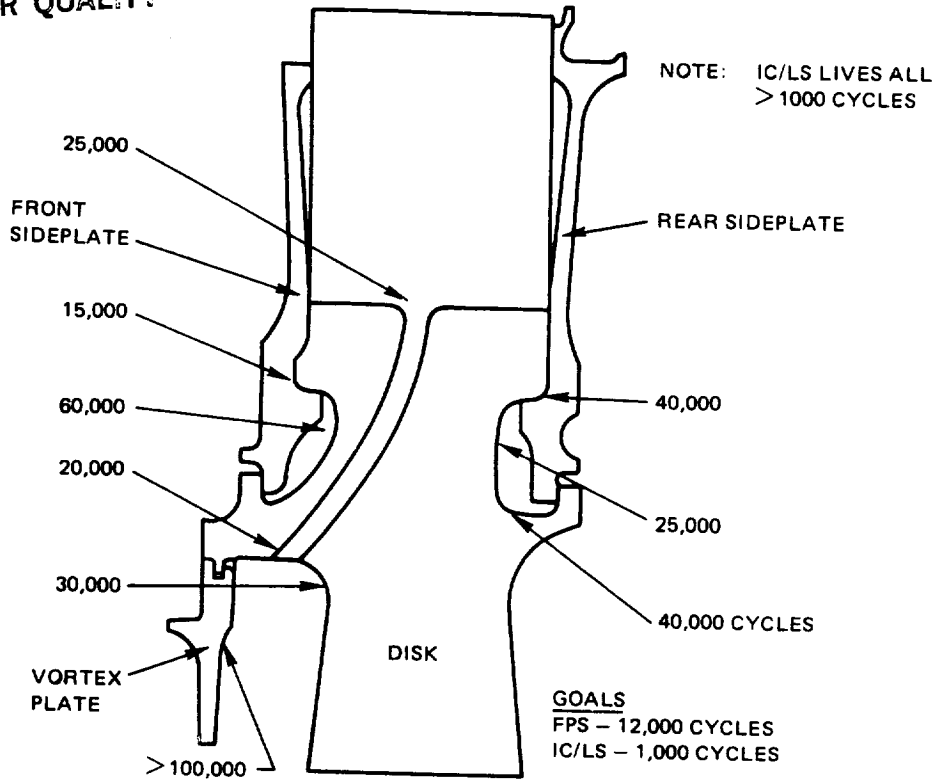


Figure 7.2.4-5 Flight Propulsion System Disk and Sideplate Calculated Minimum Low Cycle Fatigue Life Levels

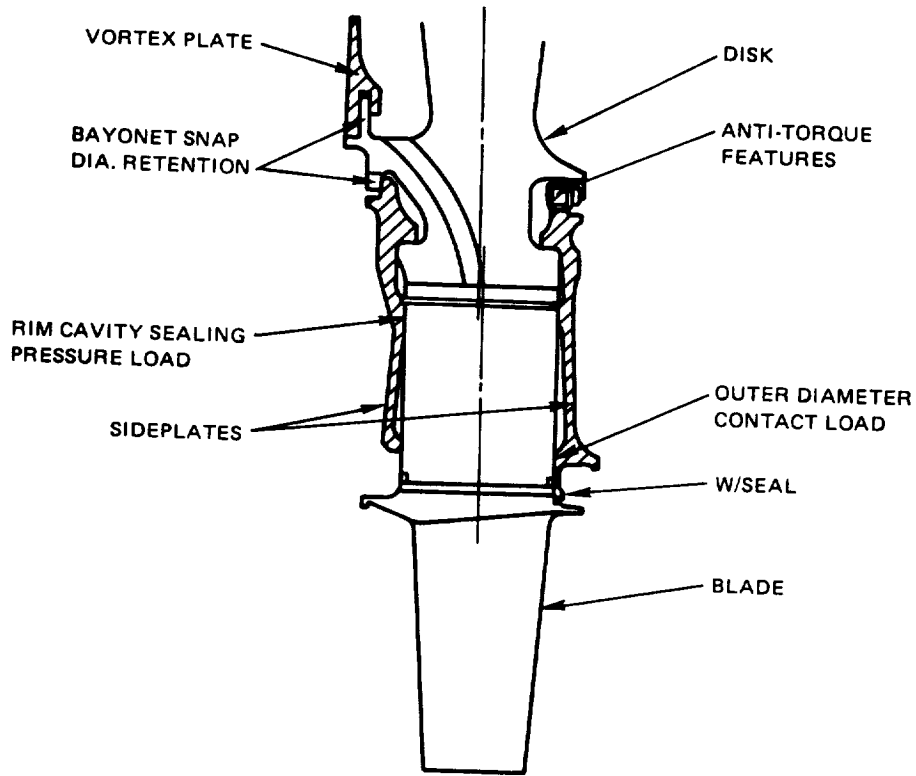


Figure 7.2.5-1 Disk Sideplate and Vortex Plate Design

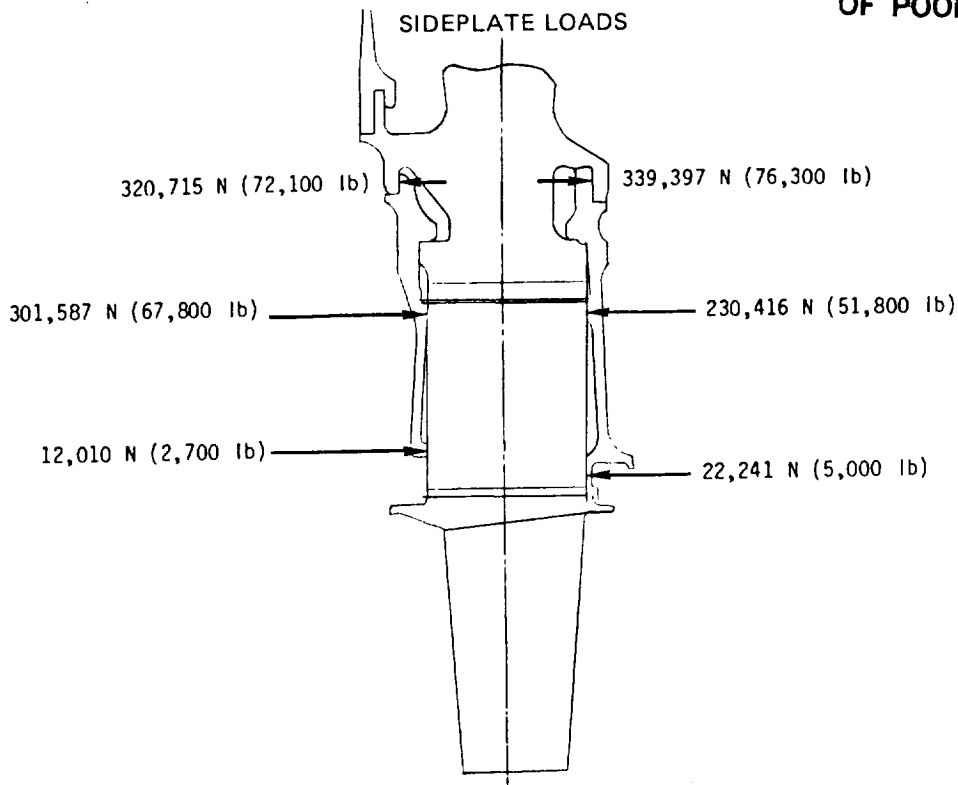


Figure 7.2.5-2 Typical Sideplate Loads

There are several other advantages with the boltless sideplate configuration. These include elimination of broach angle/bolt compatibility problems, reduction in rim cavity size requirements and elimination of flow restrictions caused by the proximity of the bolt to the rim cooling air source.

Anti-torque features are provided by the blade metering plates that engage the front sideplate and by torque pins for the rear sideplate. The assembly sequence, depicted in Figure 7.2.5-3, consists of the following steps. The front sideplate is assembled first by heating the disk, then placing the plate into position through the bayonet arrangement and rotating the plate 20 degrees to engage the disk slots and sideplate lugs. The turbine blades, which are installed next, lock the front sideplate in place by extension of the blade meter plate located at the bottom of the blade root attachment. The rear sideplate assembly is similar to the front sideplate. After it has been rotated into position, anti-torque pins are positioned to lock the plate. Figure 7.2.5-4 illustrates the anti-torque pin details.

The function of the vortex plate is to contain the blade cooling air and provide a passage for free-vortex pressure rise to augment the pressure of cooling flow exiting the tangential on-board injection nozzle. Pumping action through the curved elliptical hole further raises the pressure before entering the blade root cavity. The vortex plate is fastened to the disk in the same manner as the front sideplate. The retaining feature is boltless, thereby eliminates the need for windage covers and provides a clean external design. Anti-torque for the vortex plate is provided through use of a blind rivet.

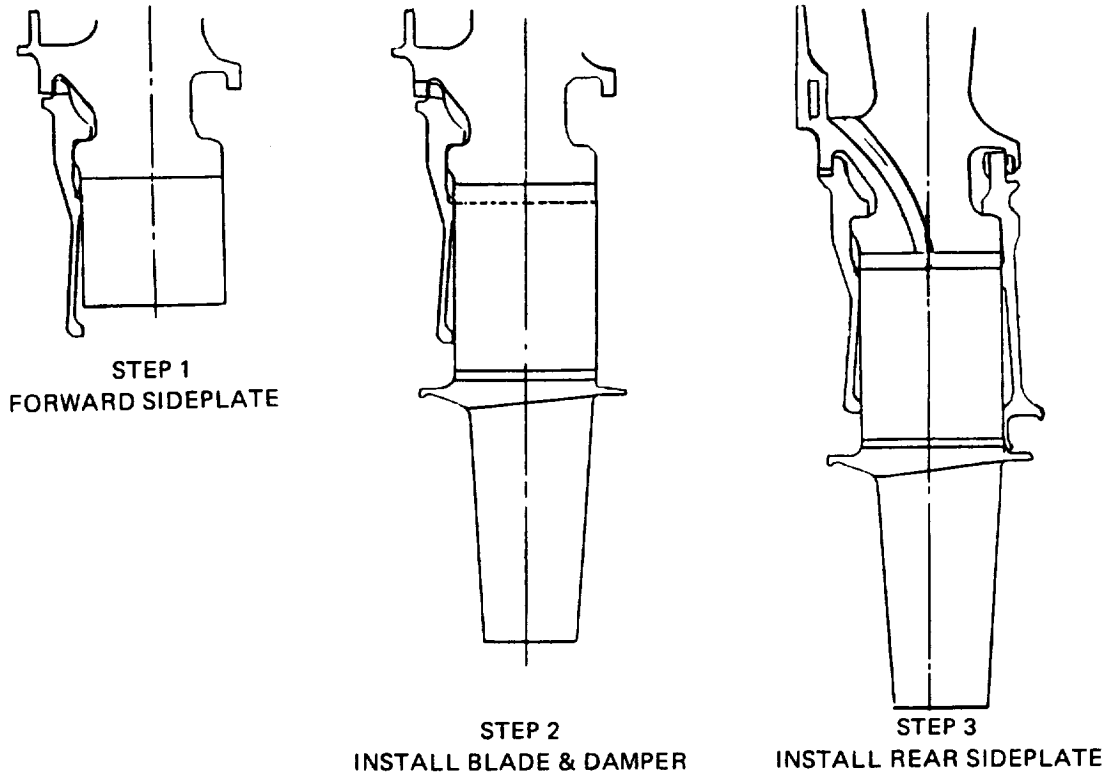


Figure 7.2.5-3 Blade and Sideplate Assembly Sequence

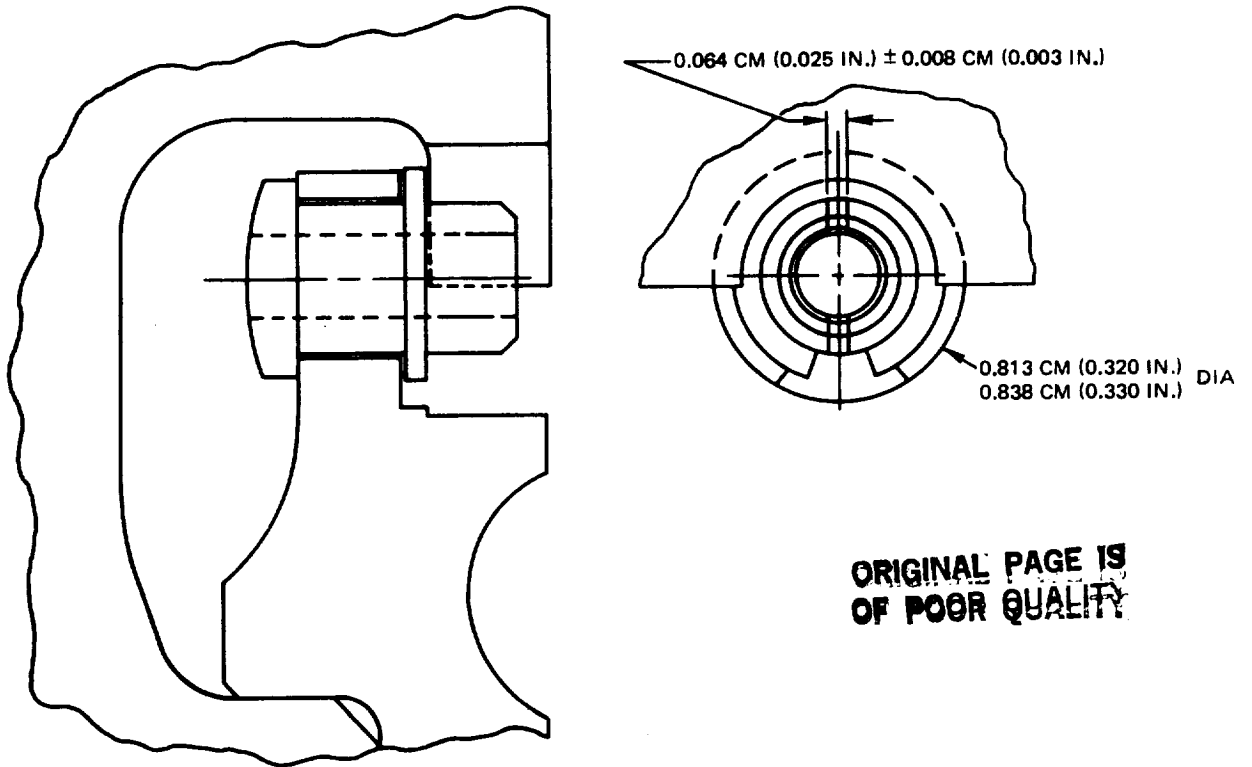


Figure 7.2.5-4 Anti-Torque Pin Details

7.2.5.2 Structural Analysis

A detailed finite element analysis of the sideplates and vortex plate was conducted concurrently with that for the disk to determine stress rupture and low cycle fatigue lives. The analysis identified critical stress locations at the front sideplate and rear sideplate snap diameter fillets where centrifugal loading of the plates are transmitted to the disk. The limiting low cycle fatigue lives at these corresponding highest stress locations are shown in Figure 7.2.4-5. Vortex plate stresses are relatively low resulting in high low cycle fatigue lives.

The limiting stress rupture points occur on the front sideplate outer diameter where the temperature is at 732°C (1350°F) and also at the front sideplate snap diameter fillet where the temperature is down to 593°C (1100°F), but the stress is higher than at the outer diameter. Stress rupture lives at both of these locations is greater than 1000 hours at hot day sea level takeoff conditions. Stresses at all other sideplate and vortex plate locations are lower than the above two and therefore have stress rupture lives greater than 1000 hours.

A buckling analysis of the front sideplate was also conducted to assess the possible effects of thermal gradients encountered during the flight cycle. This analysis indicated that no buckling occurs at any point in time during the flight cycle.

7.2.6 Air Seals

7.2.6.1 Mechanical Design Features

The high-pressure turbine rotor includes three knife-edge air seals. These seals are illustrated in Figure 7.2.6-1 and include the high-pressure compressor discharge seal, the No. 4 bearing compartment buffer seal and the thrust balance seal located on the rear side of the rotor. To avoid adding a bore to support the thrust balance seal, it has been designed within its self-sustaining radius, and thrust balance tuning is obtained by varying the pressure within the piston area cavity.

7.2.6.2 Structural Analysis

Vibratory characteristics of both the stationary and rotating parts of the seals were analyzed to ensure adequate resonance margin, coincidence margin and flutter stability in the engine operating range.

The resonance characteristics of rotating and stationary members were analyzed to ensure that a frequency margin to resonance exists at all speeds through redline to prevent vibratory excitation from the rotor.

Coincidence studies were also completed to confirm adequate coincidence margins. Coincidence occurs when the mode shape of the rotating member matches the mode shape of the stationary member at the same operating condition. At such a coincidence, energy transfer can occur from one member to the other, leading to excessive deflection and self destruction.

Analyses were also conducted on the seals, concerning aerodynamic flutter. Stability criteria expressed as stability energy must be met for both rotating and stationary members in order for the seals to be acceptable.

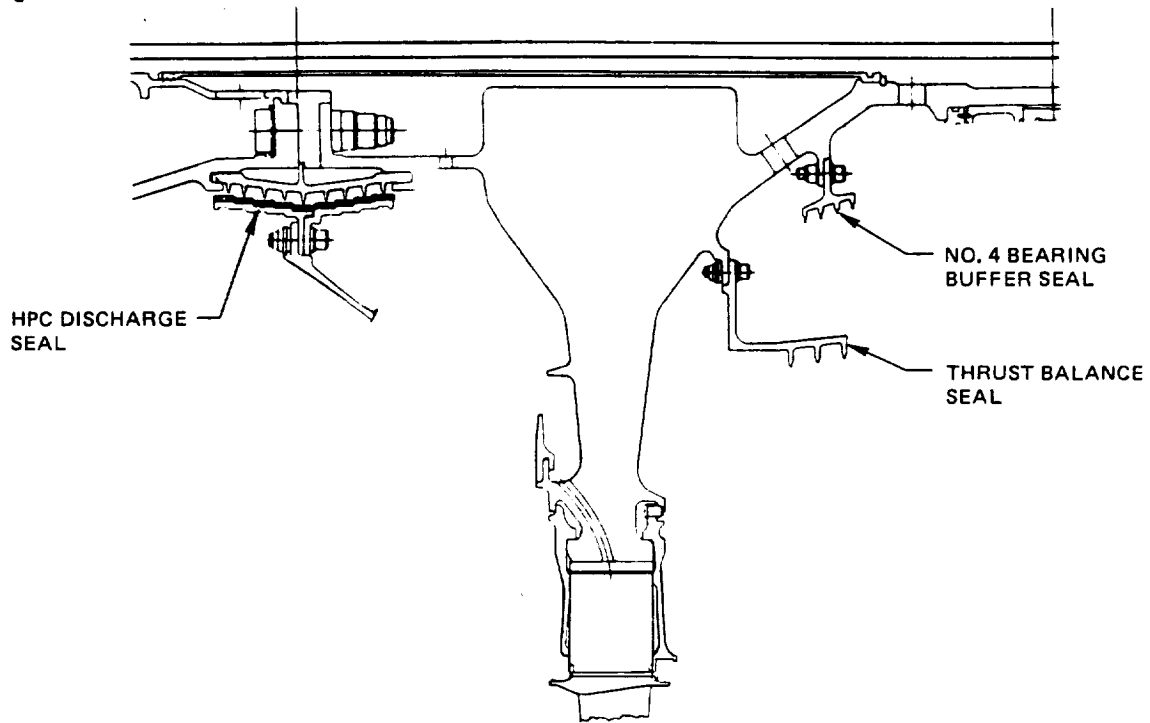


Figure 7.2.6-1 Turbine Seal Designs

The rear thrust balance seal assembly is shown in Figure 7.2.6-2, and locations for axial and radial restraint are depicted. A frequency response analysis of the assembly indicated that margins for resonance and coincidence met or exceeded requirements for commercial applications. The predicted resonance margins are 46 percent for the stationary seal land and 20 percent for the rotating knife-edge seal. The estimated coincidence margin for this seal assembly is 69 percent. The resonance and coincidence curves are shown in Figures 7.2.6-3 and 7.2.6-4. Frequencies divided by nodal diameter are plotted as a function of nodal diameter with the point of limiting margin indicated. Maximum stability energy was calculated to be less than 0.0005 cm-k_g/cm (0.001 in-lb/in), predicting flutter free operation. The dimensions shown in Figure 7.2.6-2 are minimum requirements for vibration-free operation.

As an added precaution to vibratory excitation, dampers were designed for both the rotating and non-rotating members. Their configurations are shown in Figure 7.2.6-2.

Details of the No. 4 bearing buffer seal assembly are shown in Figure 7.2.6-5. Predicted resonance margins for this seal are 37 percent for the stationary seal land and greater than 100 percent for the rotating knife-edge seal, both well in excess of commercial requirements. Coincidence margin for this seal is 48 percent, as shown in Figures 7.2.6-6 and 7.2.6-7. Like the thrust balance seal, the Number 4 bearing buffer seal has a calculated maximum stability energy less than 0.0005 cm-k_g/cm (0.001 in-lb/in) and is predicted to be free from flutter. Again, the dimensions shown in Figure 7.2.6-5 are minimum requirements to ensure vibration-free operation.

As with the thrust balance seal, damper rings were designed for the buffer air seal as a precautionary measure, to prevent vibratory excitation. The dampers were provided in the form of split rings fitting in grooves in the forward and aft sides of the seal, as shown in Figure 7.2.6-5.

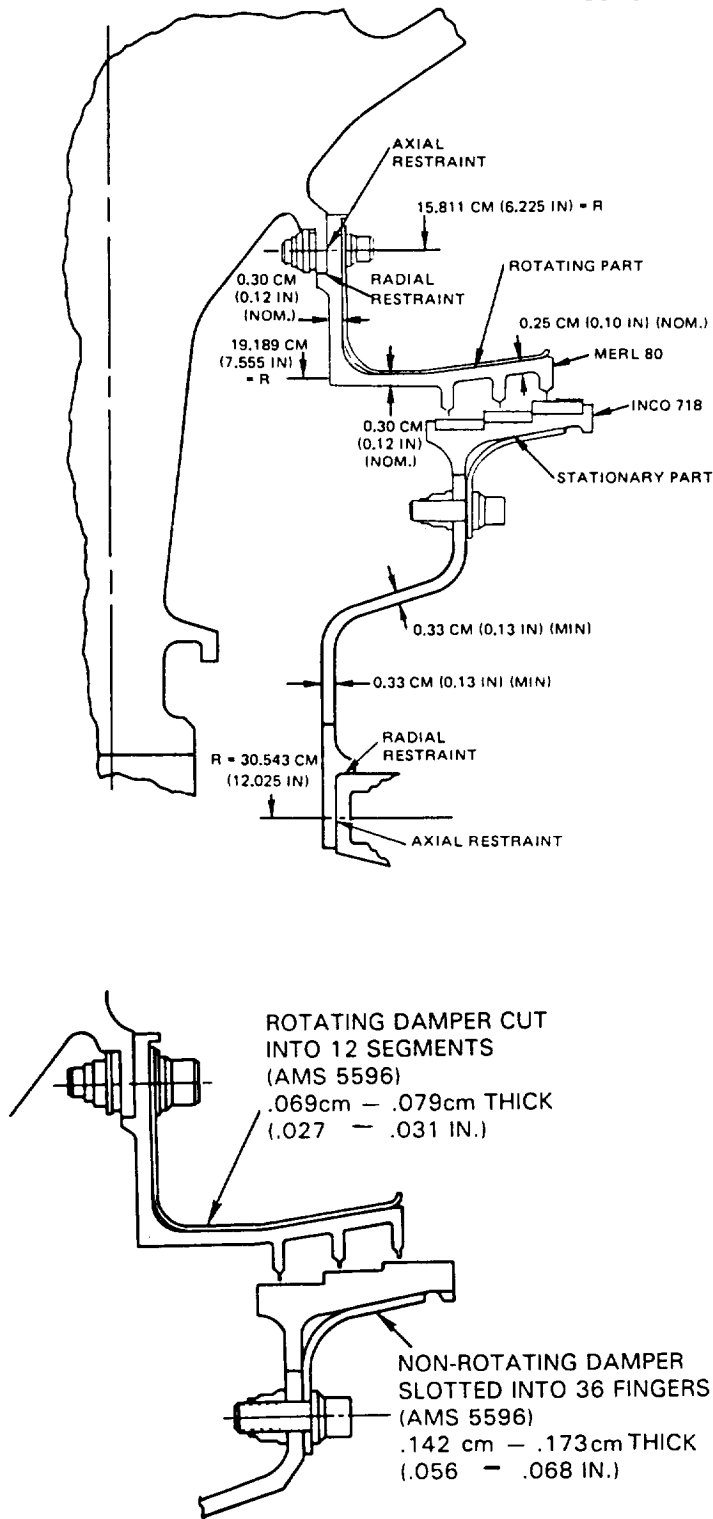


Figure 7.2.6-2 Rear Thrust Balance Seal

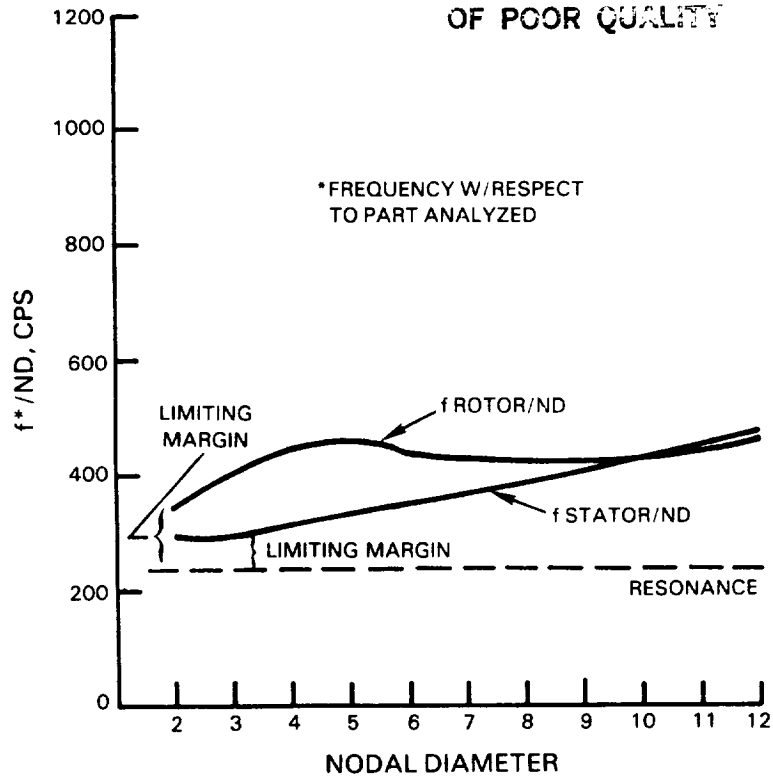


Figure 7.2.6-3 Thrust Balance Seal Rotor and Stator Resonance Diagram

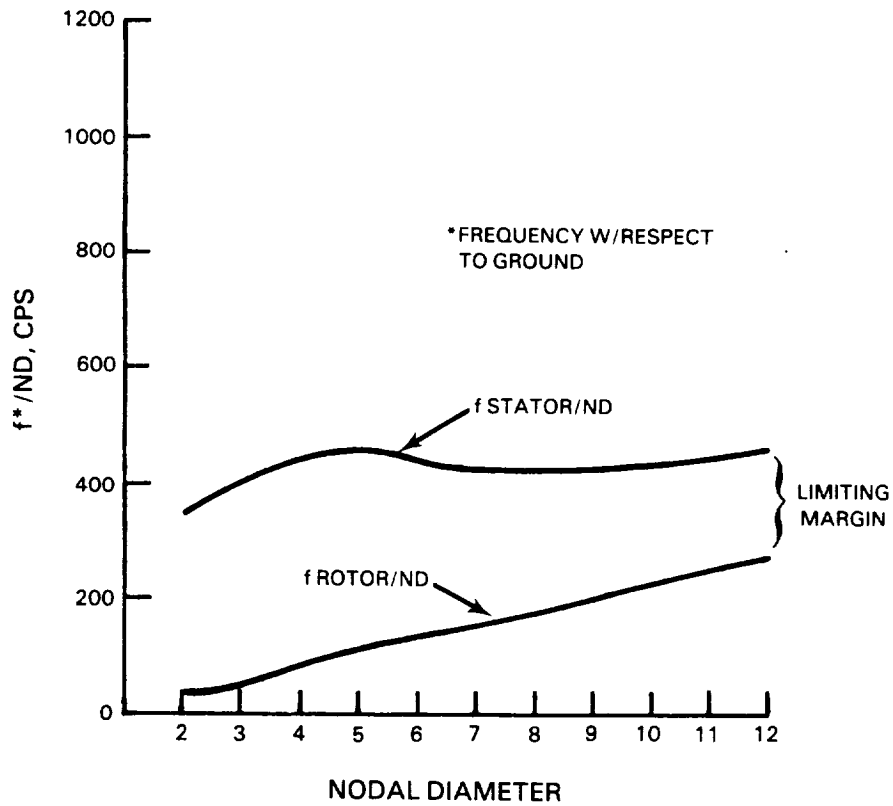
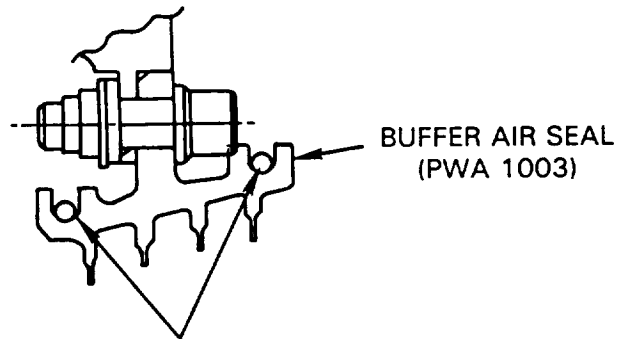
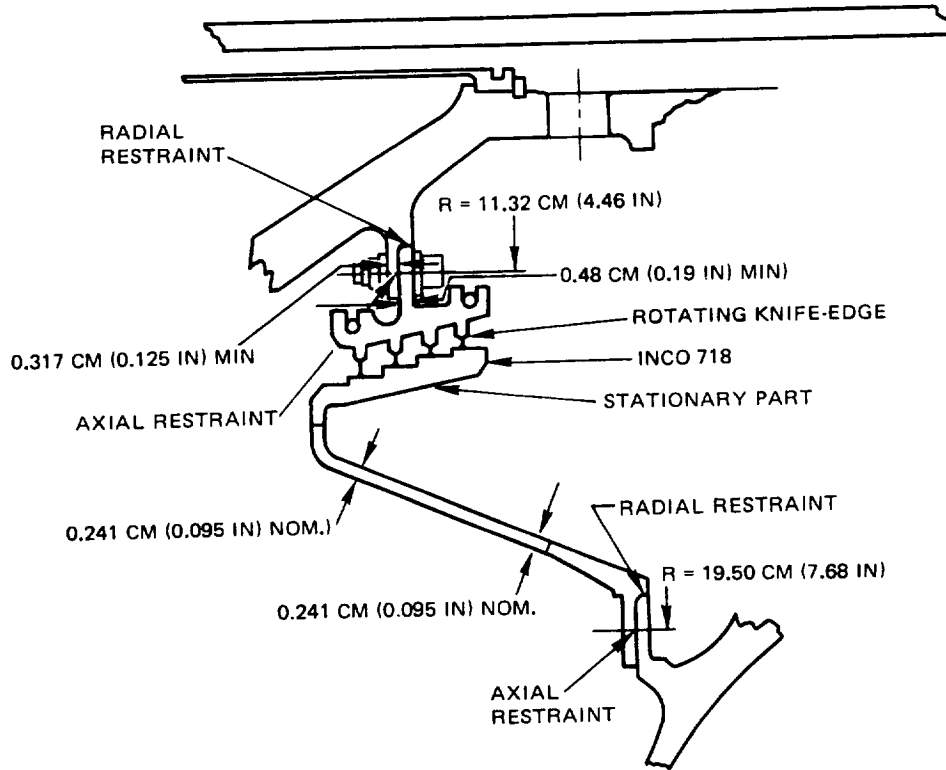


Figure 7.2.6-4 Thrust Balance Seal Rotor and Stator Coincidence Diagram



SPLIT RING DAMPERS
(AMS 5699)

.229cm-.234cm DIA
(.090 IN.-.092 IN.)

Figure 7.2.6-5 Number 4 Bearing Buffer Seal Assembly

ORIGINAL PROJECT
OF POOR QUALITY

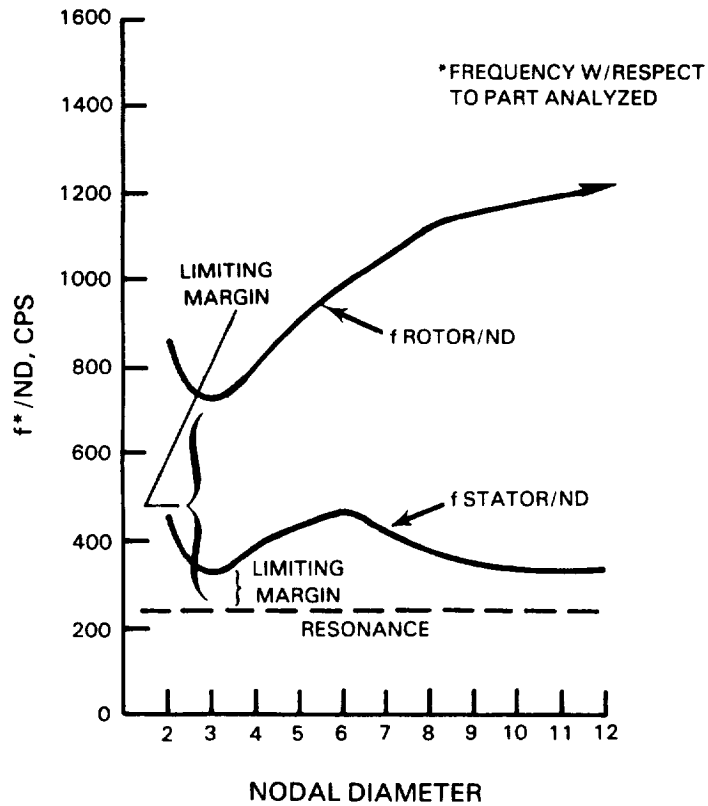


Figure 7.2.6-6 Number 4 Bearing Buffer Seal Rotor and Stator Resonance Diagram

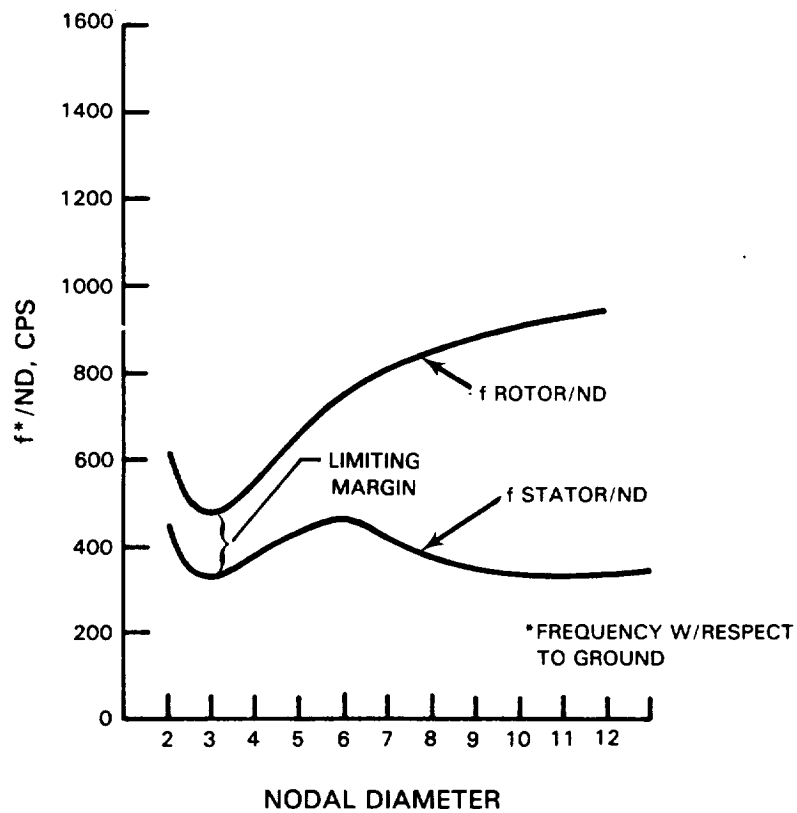


Figure 7.2.6-7 Number 4 Bearing Buffer Seal Rotor and Stator Coincidence Diagram

**ORIGINAL PAGE IS
OF POOR QUALITY**

The analysis of resonance and coincidence characteristics of the high-pressure compressor discharge seal, shown in Figure 7.2.6-8, indicated more than adequate frequency margins throughout the engine operating range. Predicted margins are 35 percent for the stationary seal land and greater than 100 percent for the rotating knife-edge seal. The coincidence margin for the seal assembly is greater than 100 percent, as shown in Figures 7.2.6-9 and 7.2.6-10. Minimum dimensions to ensure vibration-free operation are shown in Figure 7.2.6-8.

Again as a precautionary measure, sheet metal finger dampers were provided for the non-rotating portion of the seal, as shown in Figure 7.2.6-8.

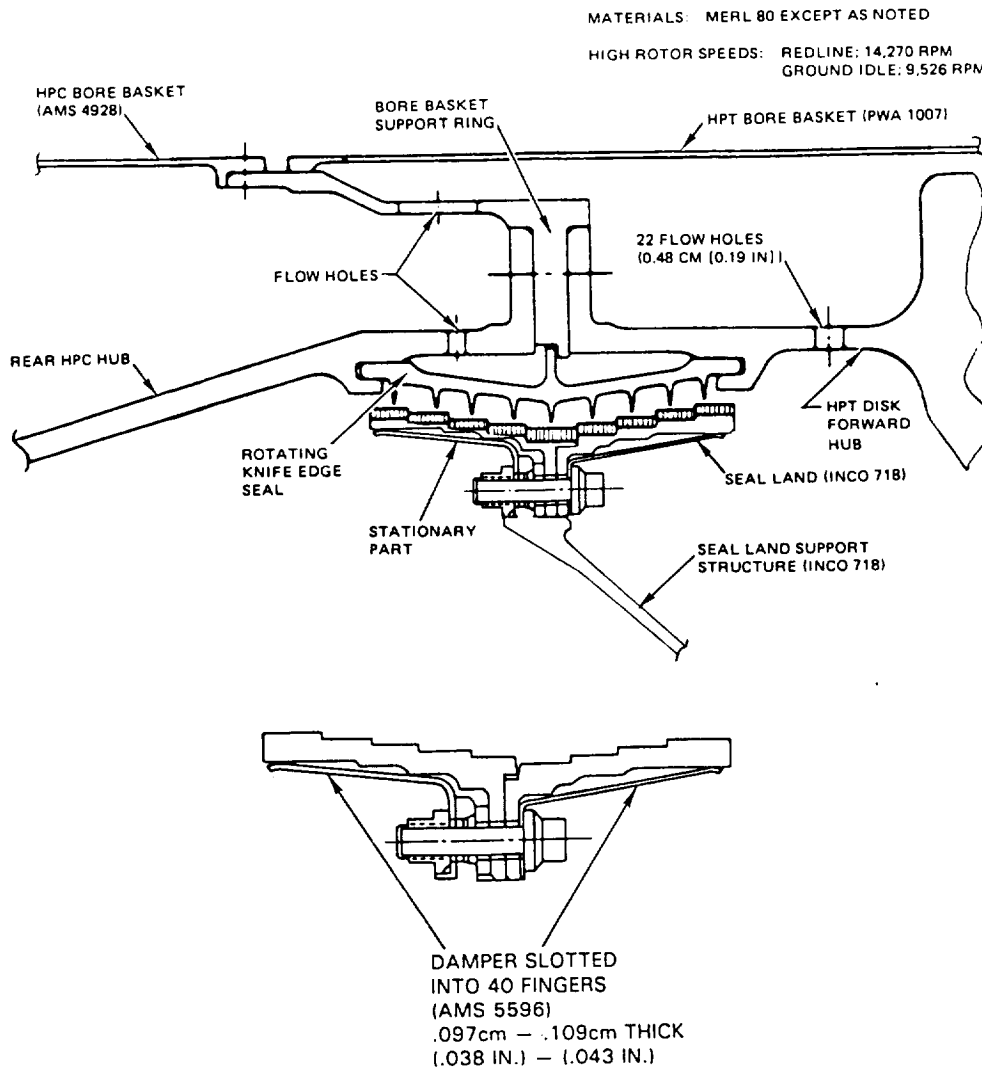


Figure 7.2.6-8 High-Pressure Compressor Discharge Seal Assembly

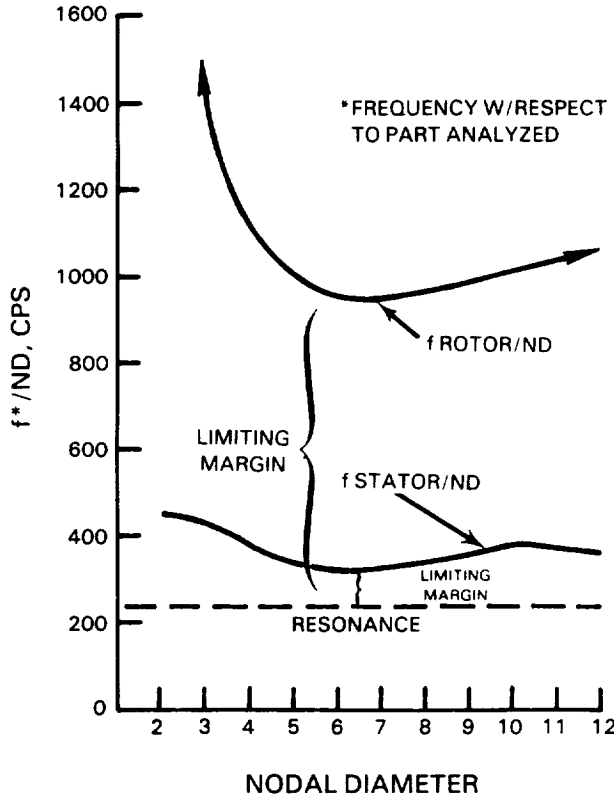


Figure 7.2.6-9 High-Pressure Compressor Discharge Seal Rotor and Stator Resonance Diagram

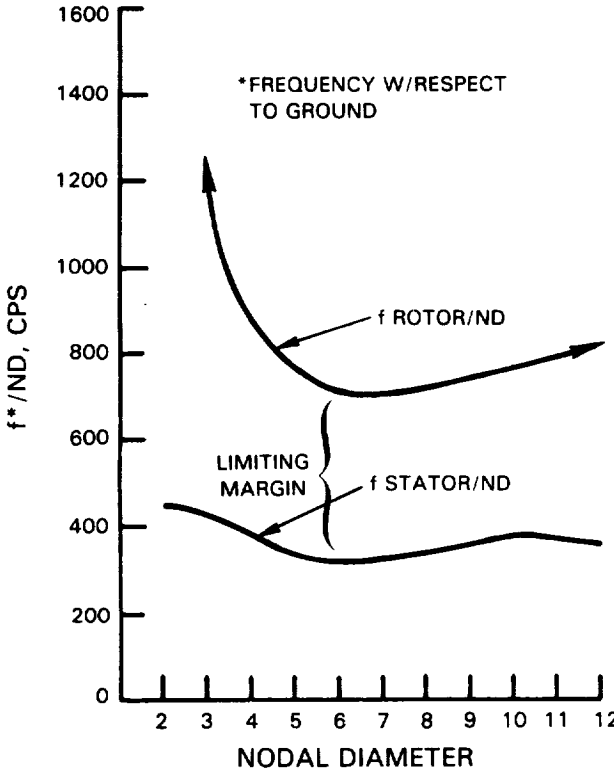


Figure 7.2.6-10 High-Pressure Compressor Discharge Seal Rotor and Stator Coincidence Diagram

7.3 VANE AND INNER CASE

7.3.1 General Description

The vane and inner case assembly is illustrated in Figure 7.3.1-1. The primary elements are the vanes and the vane support structure, the tangential on-board injection (TOBI) system, and the high-pressure compressor discharge seal support structure. Design details relating to these elements are described in the following sections.

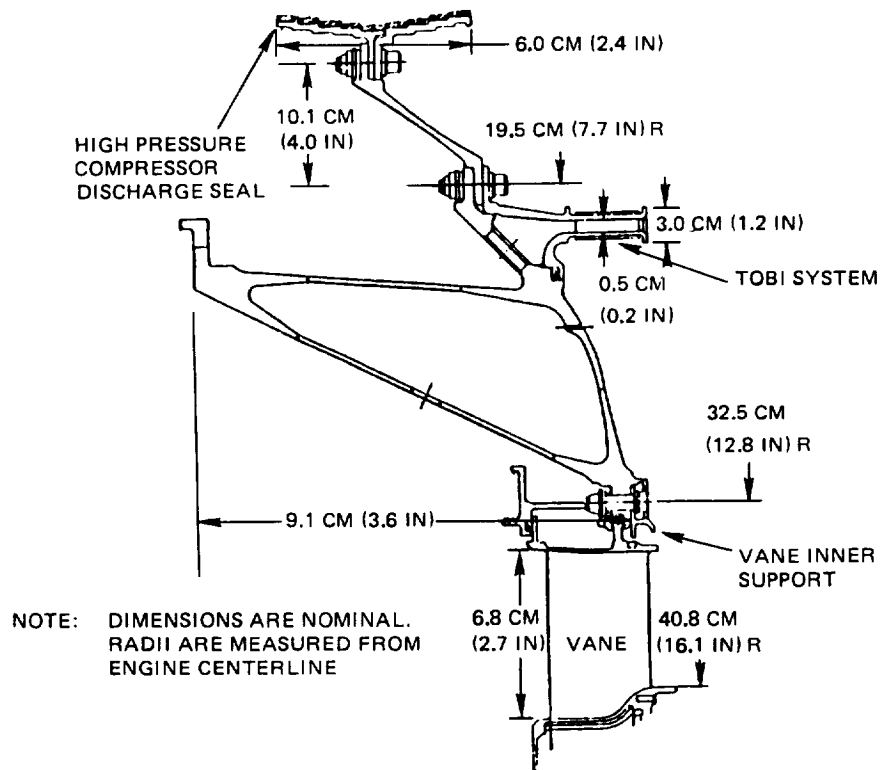


Figure 7.3.1-1 High-Pressure Turbine Vane and Inner Case Mechanical Design

7.3.2 Vanes

7.3.2.1 Mechanical Design Features

The turbine vane assembly, shown in Figure 7.3.2-1, comprises 24 vanes supported at the outer surface by bolts through the two holes in the outer flange. These bolts absorb the radial loads as well as provide circumferential restraint. This avoids excessive torque loads at the inner support structure and improper loading of the diffuser case struts. To minimize leakage caused by vane twisting, both the inner and outer surfaces are clamped along a chordal cut. By having a chordal cut, axial tilting of the vane, introduced by differential axial growth between the inner case and outer combustor case, is allowed to occur without binding up or opening a leak path.

Vane platforms are sealed by feather seals inserted into various slots on the platform surfaces, as shown in Figure 7.3.2-2, to prevent leakage of compressor discharge air into the turbine flowpath. Results from the leakage supporting technology program were incorporated in the design by minimizing feather seal slot intersections, plugging end gaps, and controlling slot straightness.

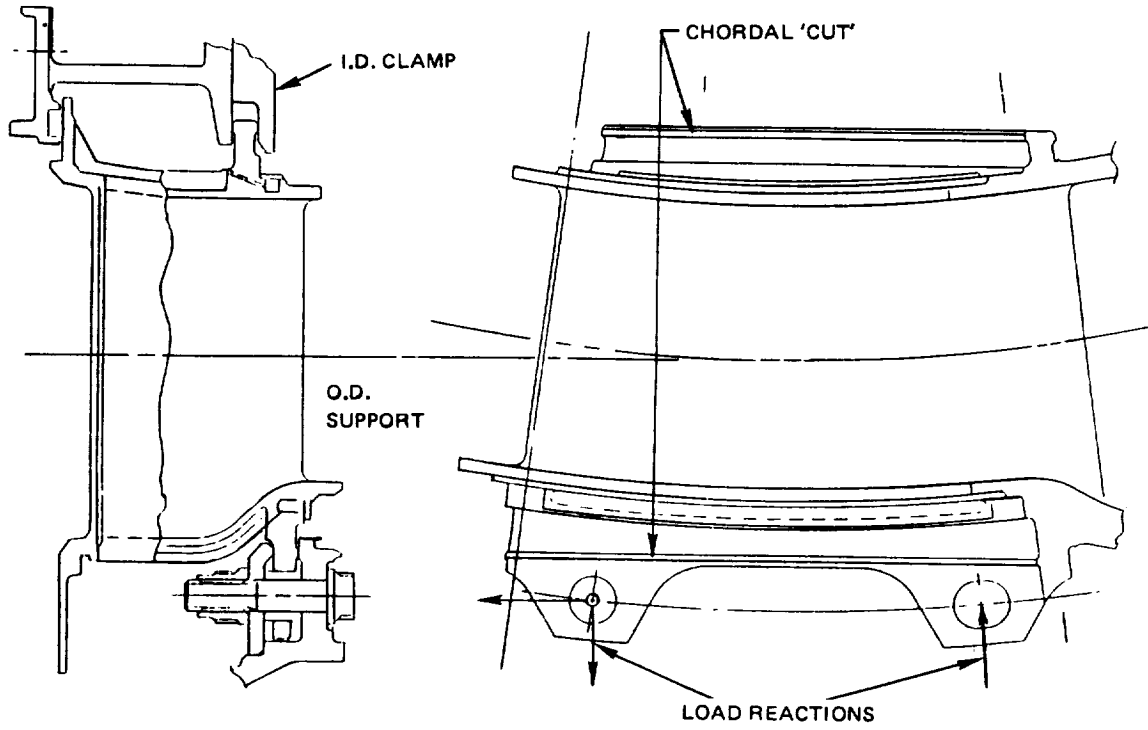


Figure 7.3.2-1 Turbine Vane Assembly

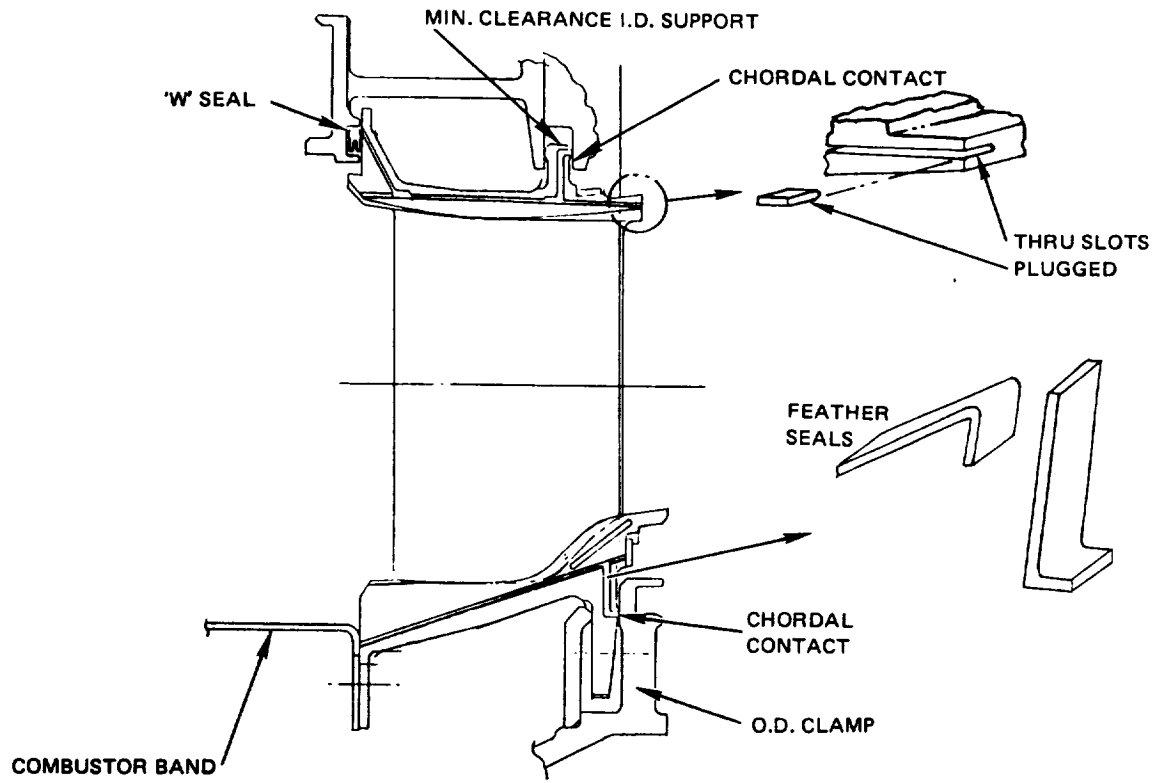


Figure 7.3.2-2 Design Approach to Vane Leakage Control

The vane materials and coatings selected for the flight propulsion system and integrated core/low spool are presented in Table 7.3.2-I. The advanced materials and coatings noted for the flight propulsion system vanes are required to meet the aggressive durability and temperature goals. Durability and life goals for the integrated core/low spool permit the use of state-of-the-art materials. As shown, an internal coating is not required for the integrated core/low spool vanes. Airfoil minimum wall thickness data are shown in Figure 7.3.2-3. Nominal wall thickness at trailing edge including coating is 0.055 cm (0.022 in).

TABLE 7.3.2-I
VANE MATERIALS AND COATINGS

	<u>Flight Propulsion System</u>	<u>Integrated Core/ Low Spool</u>
Base Alloy	SC 2000 (advanced single crystal)	PWA 1480 (single crystal)
External Coating	PWA 286 (advanced NiCoCrAlY)	PWA 270 (NiCoCrAlY)
Internal Coating	PWA 275 (aluminide)	None
Platform Coating	TBC 100 (advanced ceramic thermal barrier coating)	PWA 264 (ceramic thermal barrier coating)

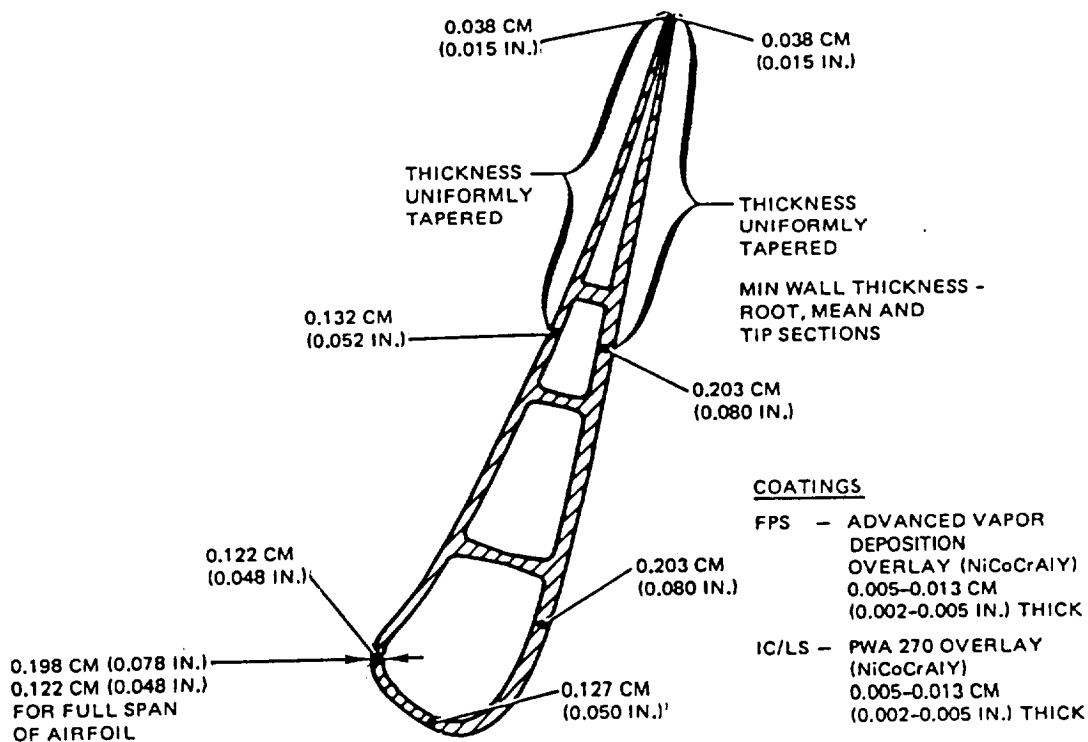


Figure 7.3.2-3 Uncoated Vane Minimum Wall Thickness Distribution

7.3.2.2 Structural Analysis

The structural analysis of the high-pressure turbine vanes is addressed as part of the durability studies. See Section 5.2.3 of this report.

7.3.3 Inner Support, Tangential On-Board Injection, and High-Pressure Compressor Seal Support

7.3.3.1 Mechanical Design Features

The high-pressure turbine inner support, tangential on-board injection system, and high-pressure compressor seal land support assembly are shown in Figure 7.3.3-1.

The inner vane support provides structural support to both the inner portion of the vane and the compressor discharge seal land. The inner portion of the vane is connected to the support through bolts that tie both the vane and inner combustor liner together into the support. The compressor discharge seal is supported from the inner region of the case through a bolt that also traps the primary tangential on-board injection nozzle. Air is brought into the center of this support case from the combustor area to supply air to the primary and secondary tangential on-board injection nozzle.

Although parts for the integrated core/low spool are designed using forgings and Inconel 718 welded construction, it is anticipated that cast materials would be used for a flight propulsion system.

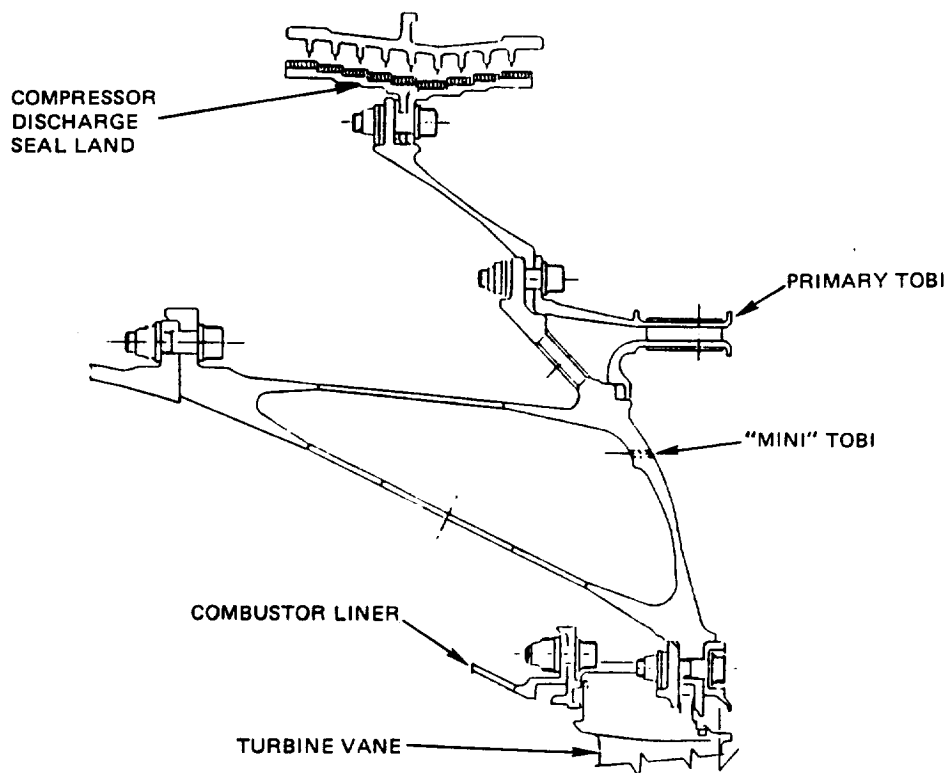


Figure 7.3.3-1 Turbine Inner Support, Tangential On-Board Injection System, and High-Pressure Compressor Seal Land Support System

The primary tangential on-board injection nozzle, shown in Figure 7.3.3-2, is designed to be fabricated from Hastelloy X material. The 36 vanes are brazed into slots in both the inner and outer walls. By keeping the primary tangential on-board injection nozzle a separate bolted-on unit, flexibility is provided for easy modification to provide proper flow. One way of modifying the flow is to cut back the trailing edge of the vanes and, thereby adjust the nozzle area.

The secondary (or mini) tangential on-board injection nozzle is shown in Figure 7.3.3-3. The primary purpose of this nozzle is to swirl the coolant flow to the front side of the turbine disk, thereby reducing windage heat up of the front side plate. The vortex action of this nozzle affects the pressure level of the pressure balanced tangential on-board injection system described in Section 6.4 of this report.

The high-pressure compressor discharge seal is designed to maintain minimum clearance at all operating conditions. By using a high expansion Tinidur material rotating member, the seal permits component assembly using a relatively large clearance that will close as parts heat up, providing a running clearance between 0.027 and 0.035 cm (0.011 and 0.014 in) depending on axial location. Clearances are set to ensure no rubs during maneuvers and to minimize the amount of rub during startup operation.

Figure 7.3.3-4 summarizes the seal clearances at two typical engine operating conditions. A more detailed discussion of clearances is presented in Section 7.6 of this report.

7.3.3.2 Structural Analysis

Vane durability analysis is discussed in Section 5.0 of this report. The major concern in the inner case design was to provide a lightweight design with suitable load-carrying ability for the first vane blow off loads, while at the same time minimizing deflections. Total blow off load of the first vanes, acting in an aft direction on the vane inner and outer attachment points, is 222,410 N (50,000 lb) at sea level takeoff. Half of this amount is taken by the inner case.

A detailed shell analysis was conducted at hot day sea level takeoff. At this condition, there is a large pressure load as well as thermal gradient. The resulting stresses are summarized in Figure 7.3.3-5, and as indicated, the values are quite low relative to the high strength of the Inconel 718 material. Thus, the impact from axial and radial deflections was the primary concern. The same shell analysis was used to determine the magnitude of these deflections, and the resulting axial deflections are summarized in Figure 7.3.3-6. Calculated radial clearances were not considered critical except at the compressor discharge seal, where maintenance of seal clearance tolerances is important. The critical axial deflection was at the vane inner support, as noted. Excessive axial motion at this location could create undesirable leakage flow paths in the vane platform and at the interface of the inner vane and blade platform.

ORIGINAL PAGE IS
OF POOR QUALITY

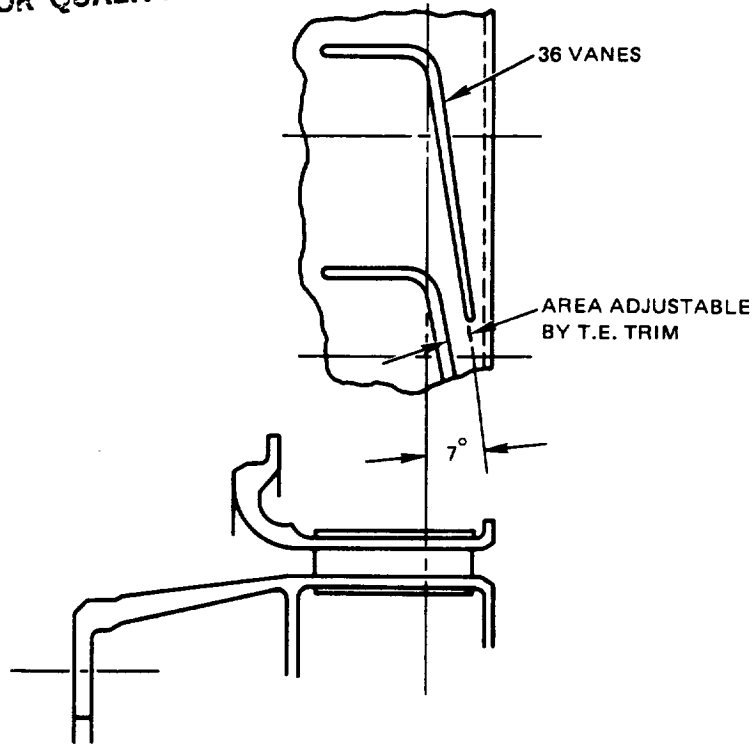


Figure 7.3.3-2 Nozzle Configuration for the Primary Tangential On-Board Injection System

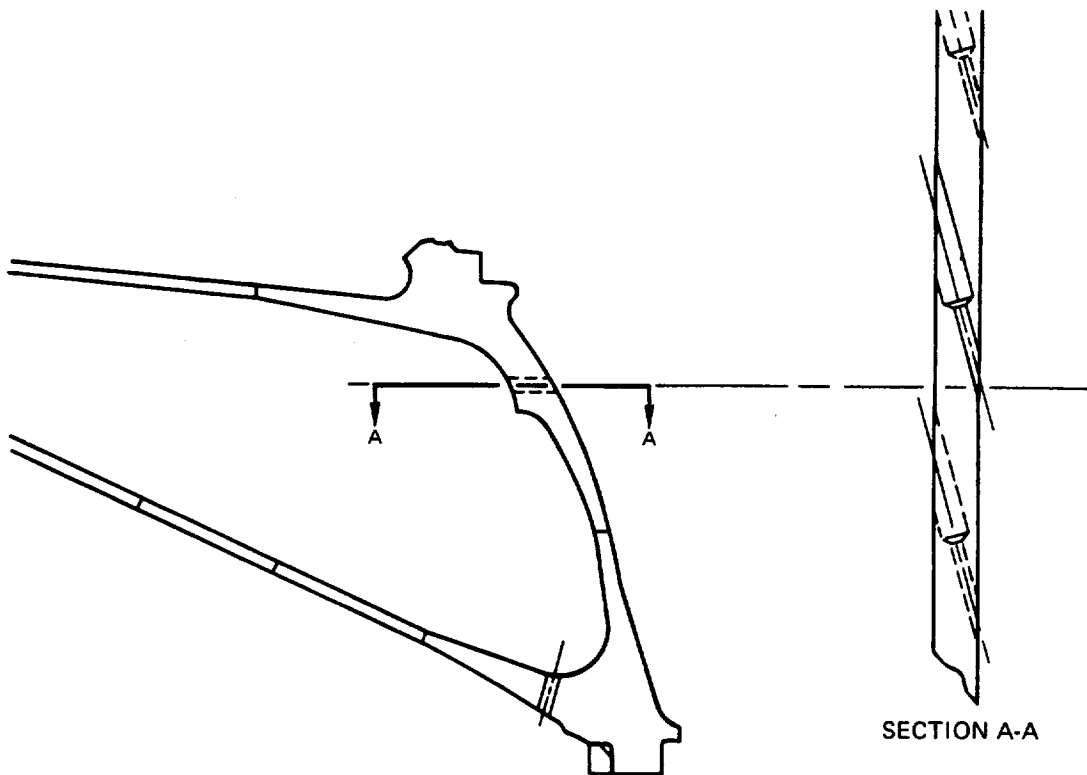
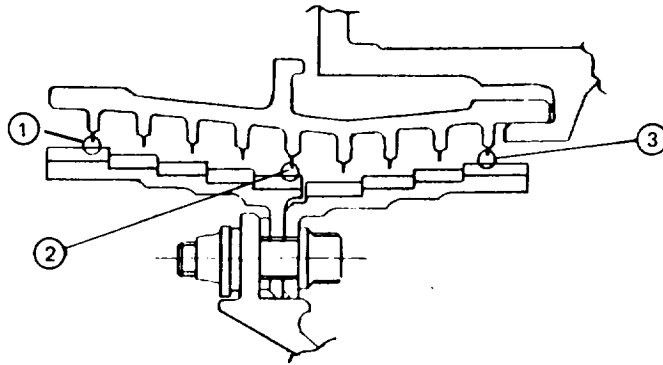


Figure 7.3.3-3 Nozzle Configuration for the Secondary or Mini Tangential On-Board Injection System

ORIGINAL FACE IS
OF POOR QUALITY

- MIN. ASSEMBLY CLEARANCE OF 0.038 CM (0.015 IN)
- DESIRED SLTO CLEARANCE OF 0.0317 CM (0.0125 IN)
- NO RUB AT MANEUVER 0.0193 CM (0.0076 IN)



• RESULTS

	①	②	③
COLD GAP PINCH PT	0.043 CM (0.017 IN)	0.073 CM (0.029 IN)	0.040 CM (0.016 IN)
AVG GAP @:	~ 60 SEC. DECEL.	~ 10-12 SEC. ACCEL.	~ 80 SEC. DECEL.
• ADP	0.030 CM (0.012 IN)	0.035 CM (0.014 IN)	0.027 CM (0.011 IN)
• SLTO	0.0317 CM (0.0125 IN)		

Figure 7.3.3-4 High-Pressure Compressor Discharge Seal Clearance Summary

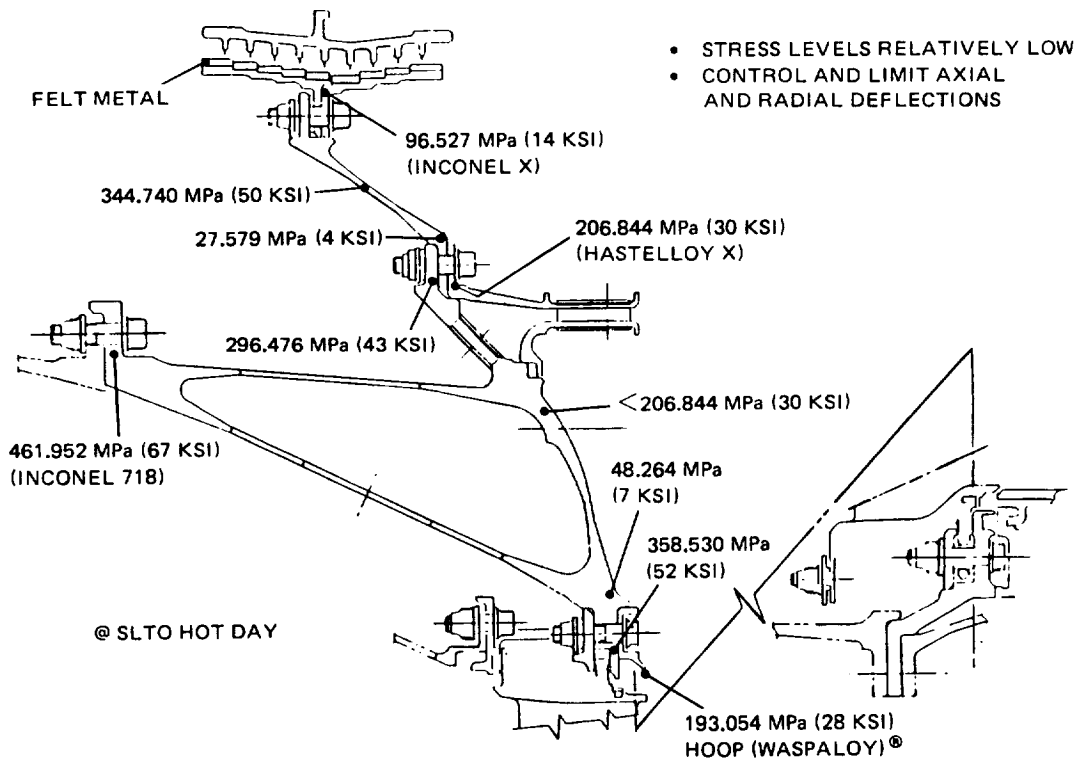


Figure 7.3.3-5 Inner Vane Case Stress Summary

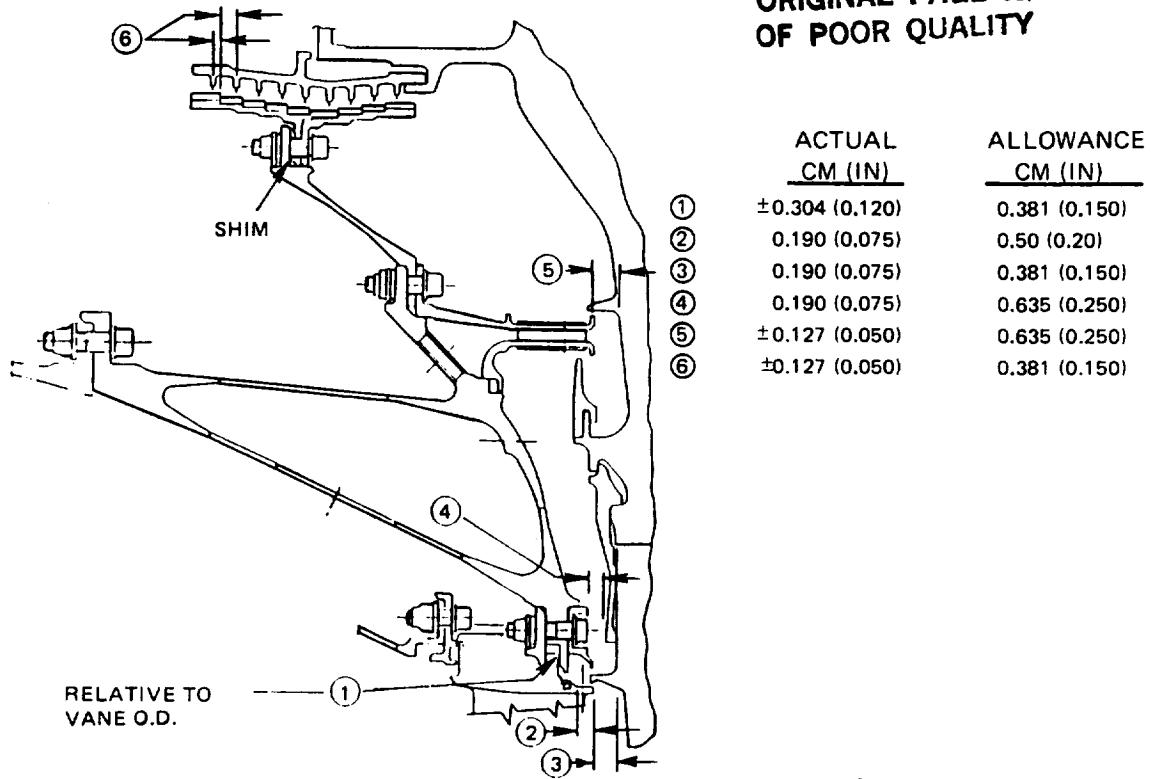


Figure 7.3.3-6 Case Structure Deflection Summary

7.4 OUTER CASE AND OUTER AIRSEAL

The high-pressure turbine outer case and outer airseal assembly is illustrated in Figure 7.4-1. The primary components of this assembly are the outer case, the front and rear outer airseal support rails, the ceramic outer airseal shoe, the cooling air impingement ring, and the active clearance control and cooling air manifolds. Design details relating to this assembly are discussed in the following sections.

7.4.1 Mechanical Design Features

The mechanical design features of the outer case and outer airseal are shown in Figure 7.4.1-1.

The outer case provides support for the outer diameter attachment of the inlet guide vane as well as support for the outer airseal shoes. The vane outer diameter support is carried through a flange and cone out to the flange connecting the turbine outer case to the rear combustor case. A W-seal is provided between this cone and the front surface of the outer airseal support rail. This W-seal prevents leakage of high-pressure compressor discharge air that is brought through the flange to provide cooling for the outer airseal shoes.

ORIGINAL PAGE IS
OF POOR QUALITY

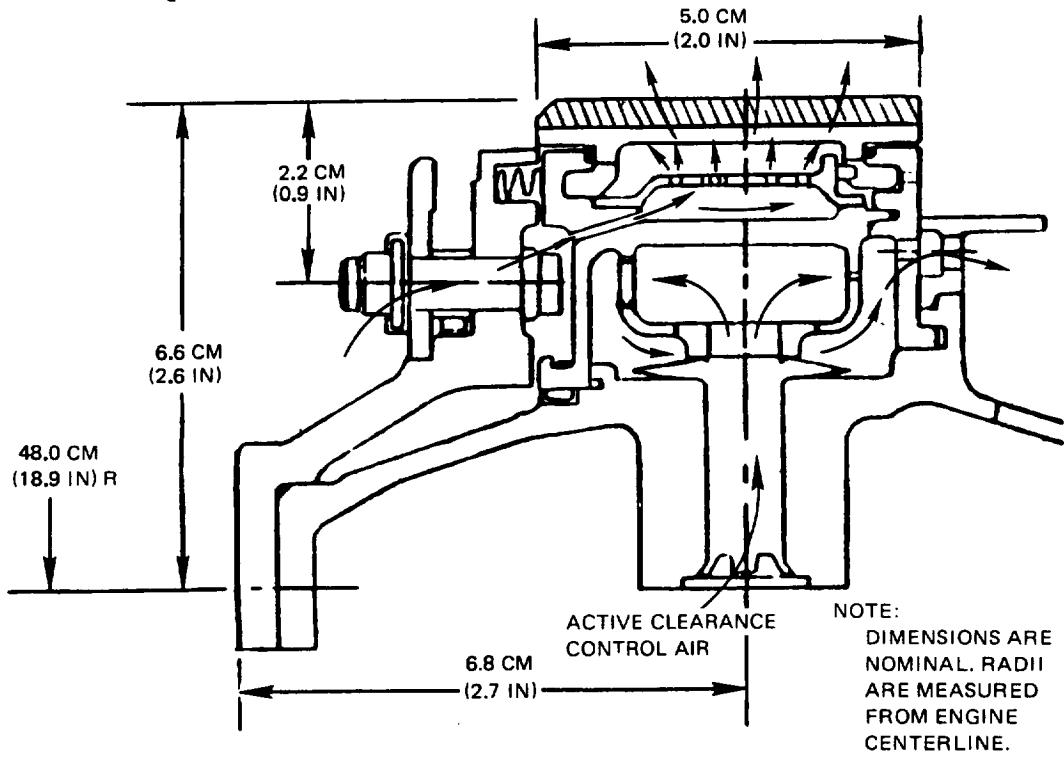


Figure 7.4-1 High-Pressure Turbine Outer Case and Outer Airseal Assembly

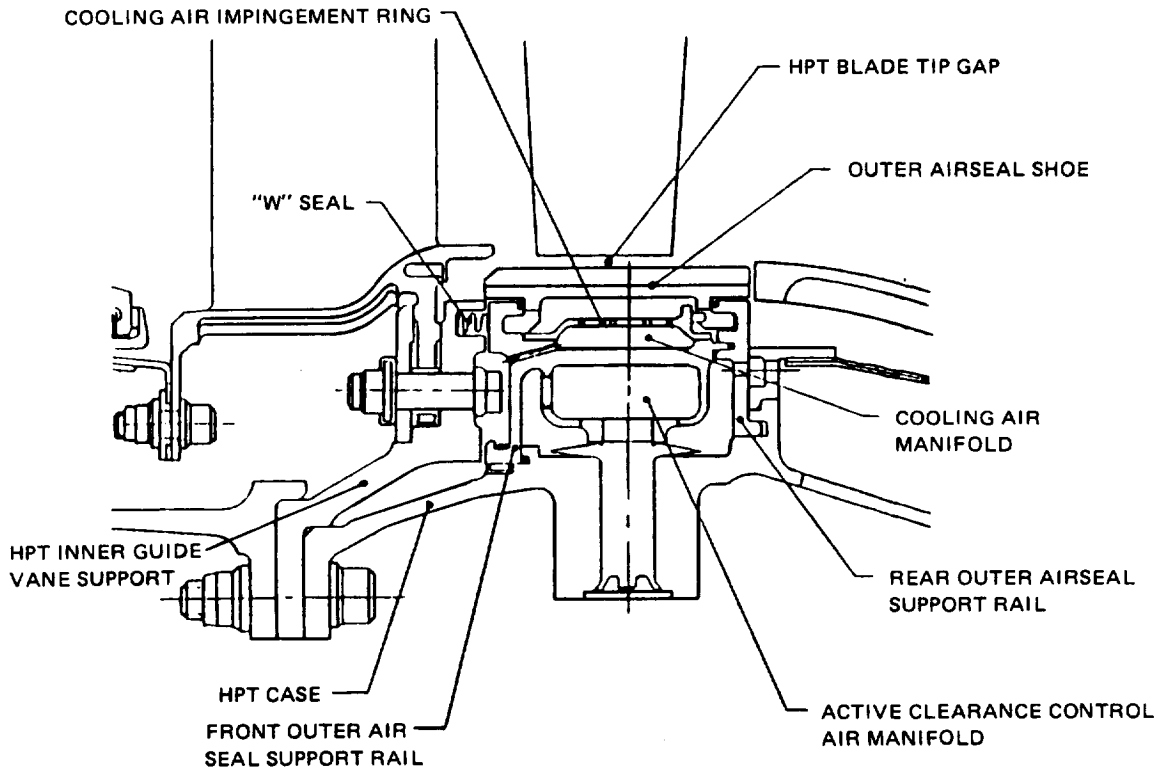


Figure 7.4.1-1 Mechanical Design Features

An internal active clearance control system is used for optimizing blade tip clearance during all engine operating conditions. This is accomplished by impinging controlled temperature air on the outer airseal support rails (Figure 7.4.1-1) to move the blade outer air seal shoes radially. Temperatures of the rear and front rails are kept similar for uniform deflection of both rails. The controlled temperature air enters the active clearance control manifold through eight bosses in the high-pressure turbine case, flows through holes in the active clearance control manifold to impinge on the outer airseal support rails, and axially discharges through holes in the rear outer airseal support rail to an annulus between the hot strut outer diameter fairing and the high-pressure turbine case. Further discussion of the active clearance control system is contained in Section 7.5 of this report.

The blade outer airseal shoe, shown in Figure 7.4.1-2, features a ceramic coating 0.327 cm (0.129 in) thick over a PWA 655 (cast Inconel 713) shoe nominally 0.254 cm (0.100 in) thick. Slots in the shoe reduce its spring rate. This prevents the ceramic material from being overstressed as it cools following engine transient operation.

To minimize cooling air leakage, W-seals are also used on the front and rear hook areas of the shoe and feather seals are used at the circumferential ship lap joint between shoes. The ship lap protects the feather seals from pressure pulses caused by the passing blades and serves as a backup (but less effective) seal. It also prevents a large step between shoes in the event of a blade rub. If one end of a shoe deflects due to a rub, the ship lap will force the end of the next adjacent shoe to deflect equally and simultaneously.

The shoes are held radially inward by the pressure differential across the shoes. Vibrations are damped by a combination of the axial spring load applied by the W-seals, pressure loadings and metal-to-metal contact in the ship lap and feather seal areas.

High-pressure compressor discharge air cools the outer airseal shoes (Figure 7.4.1-1). Air is metered through holes in the inlet guide vane support, passes through holes in the front outer airseal support rail to the cooling air manifold, then flows through radial holes in a circumferential impingement ring to cool the outer diameter of the outer airseal shoes.

After the outer airseal shoes are cooled, portions of the air flow to three different areas. The majority of the air flows through holes at one circumferential end of the shoes into the gap between shoes to prevent intrusion of gas path air into the gap and to lower the metal and ceramic temperatures adjacent to the gap. A small amount of the air leaks past the W-seals located between the outer airseal shoes and the support rails. Some of the air passes through axial holes in the hook area of the rear outer airseal support rail to maintain the temperature of the rear rail the same as that of the front rail.

The materials used in the outer case and outer airseal assembly are shown in Figure 7.4.1-3. Waspaloy and Inconel 718 materials were selected for the case wall and the common wall between the cooling air and active clearance control manifolds to provide the required dynamic resistance to satisfy the blade containment criteria, while maintaining an acceptable material thickness.

The ceramic is an abradable yttrium stabilized zirconia. The development goal is for 10:1 abradable volume ratio with grit imbedded blade tips.

ORIGINAL PAGE IS
OF POOR QUALITY

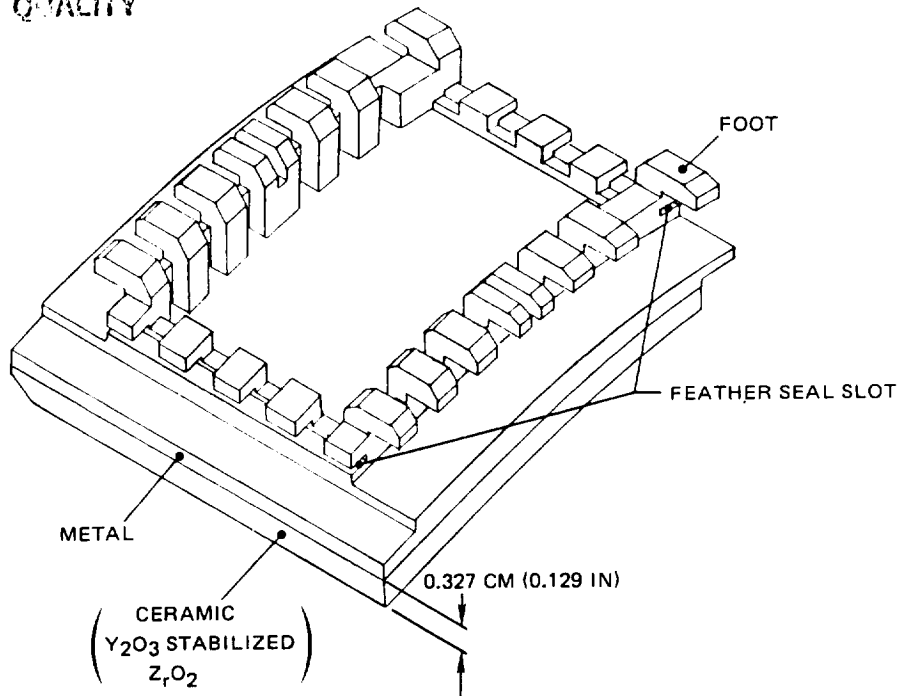


Figure 7.4.1-2 Details of the Outer Airseal Shoe Design

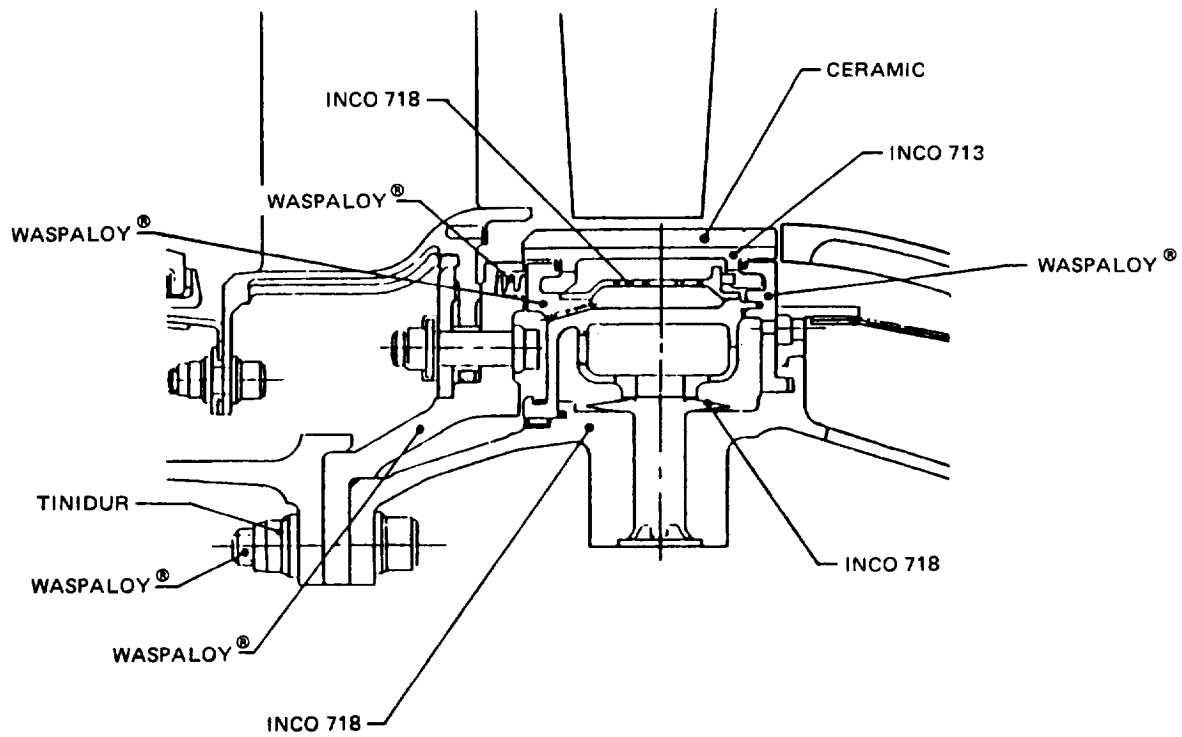


Figure 7.4.1-3 Outer Case and Outer Airseal Materials Map

7.4.2 Structural Analysis

Structural analysis of this assembly was accomplished through the use of the shell analysis model shown in Figure 7.4.2-1. This model includes pressure loadings, vane and shoe support reactions, and thermal gradients based on a steady-state sea level takeoff, hot day engine operating condition. Static pressures are shown in Figure 7.4.2-1 and the metal temperature distribution is shown in Figure 7.4.2-2.

Typical stresses resulting from this analysis are shown in Figure 7.4.2-3. All are well below allowables at the assumed steady-state condition, thereby satisfying both flight propulsion system and integrated core/low spool design requirements.

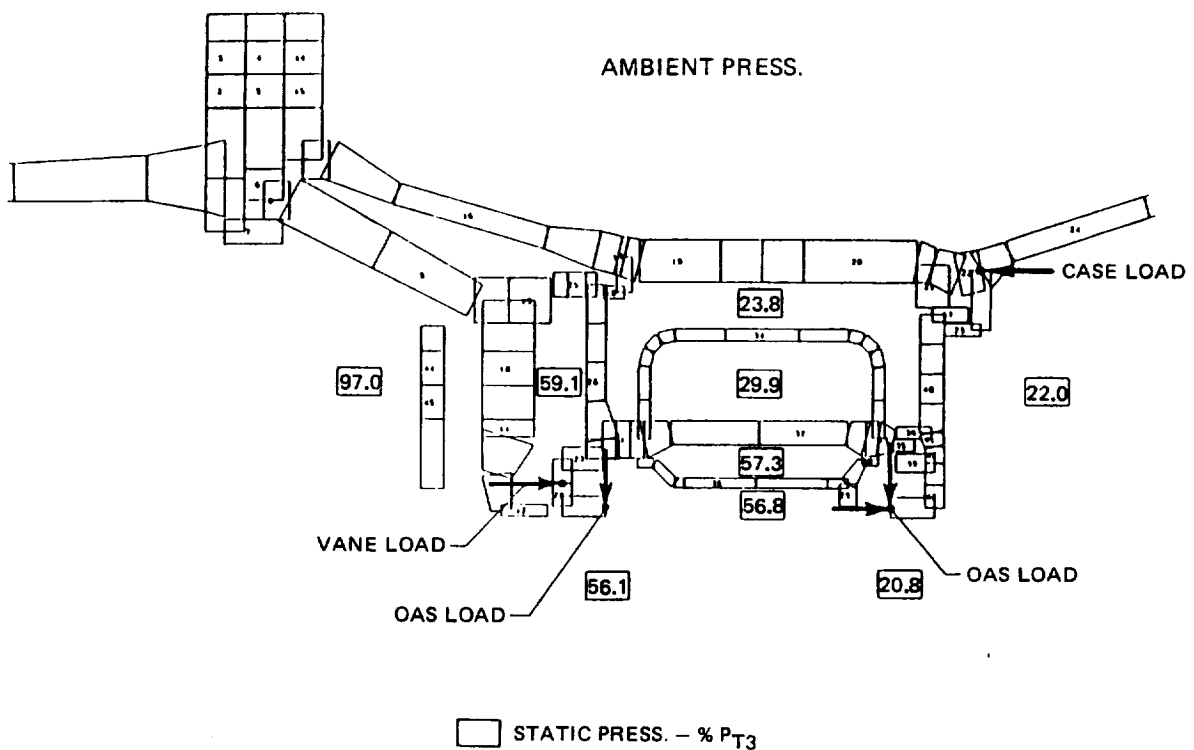


Figure 7.4.2-1 Shell Analysis Model

7.5 ACTIVE CLEARANCE CONTROL SYSTEM

Large turbine blade operating clearances have a deleterious affect on component efficiency, and consequently a negative impact on overall system fuel consumption. The goal, therefore, is to maintain tip clearances as close as possible, while avoiding rubs during normal operating conditions.

Since the high-pressure turbine in the Energy Efficient Engine is a high performance system, blade tip clearances are designed for minimum leakage. The goal blade tip clearances are 0.068 cm (0.027 in) at takeoff and 0.047 cm (0.0186 in) at cruise (the aerodynamic design point). To achieve optimum clearances during all flight conditions, the high-pressure turbine is designed with an active clearance control system.

ORIGINAL PAGE IS
OF POOR QUALITY

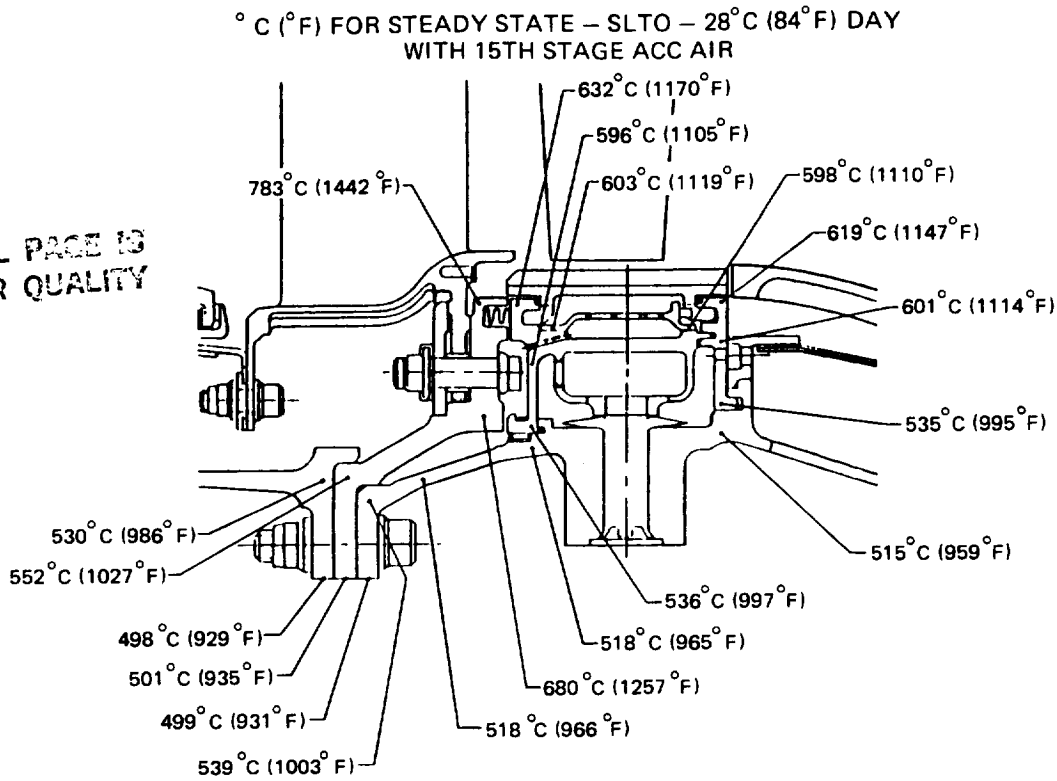


Figure 7.4.2-2 Temperature Map

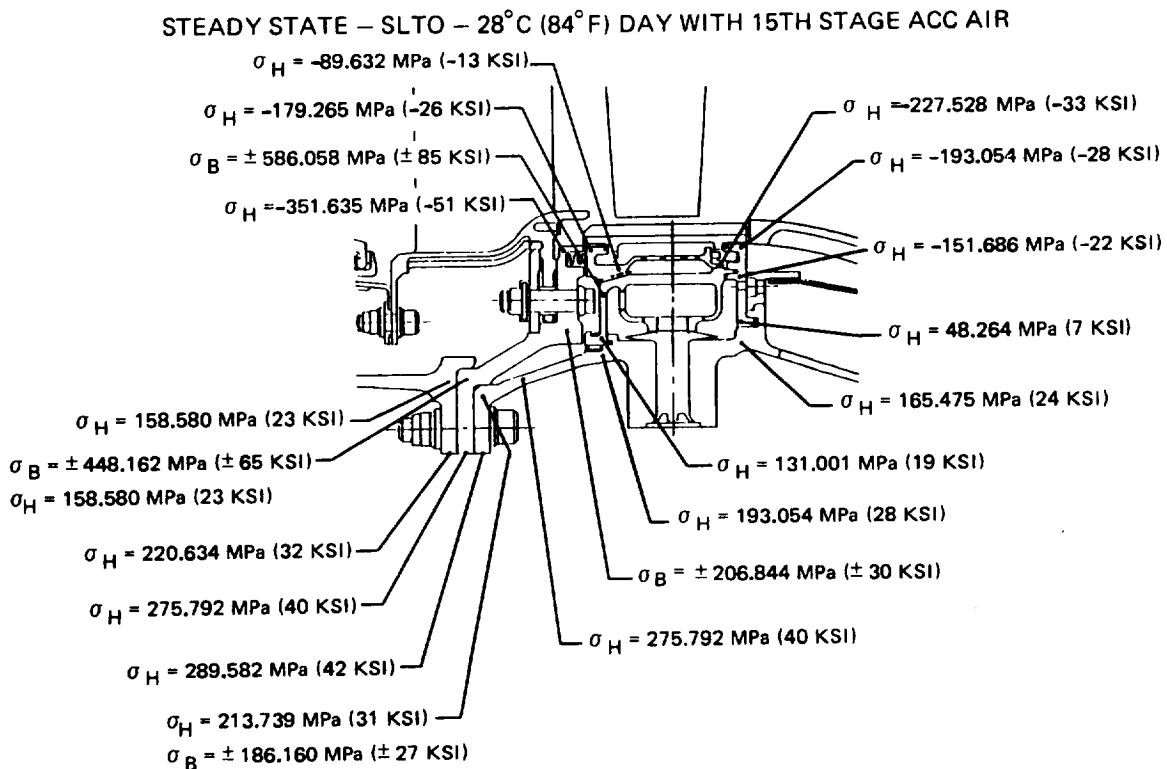


Figure 7.4.2-3 Stress Map

7.5.1 General Description

Clearance between the blade tip and outer air seal varies with engine operating conditions as a result in the changes in temperature and speed. With active clearance control, close turbine operating clearances are maintained by controlling the relative growth between the rotor and external cases. This is accomplished by changing the thermal expansion rate of the case through the introduction of controlled temperature cooling air.

The active clearance control system in the high-pressure turbine is shown schematically in Figure 7.5.1-1. In this system, the primary components are the outer case, front and rear outer airseal support rails, ceramic outer air seal shoe, cooling air impingement ring, and active clearance control and cooling air manifolds. Details pertaining to the mechanical design and structural analysis of these components are contained in Section 7.4.

Optimum blade tip clearances are achieved during all operating conditions by impinging controlled temperature air on the outer air seal support rails. The introduction of this cooler temperature air lowers the turbine case metal temperature and corresponding thermal expansion, thereby controlling the radial movement of the seal shoes towards the blade tip. Air for the active clearance control system is supplied from two sources in the high-pressure compressor: the tenth stage and the fifteenth stage. The mix of air from these sources is contingent on the engine operating condition and the desired gap closure.

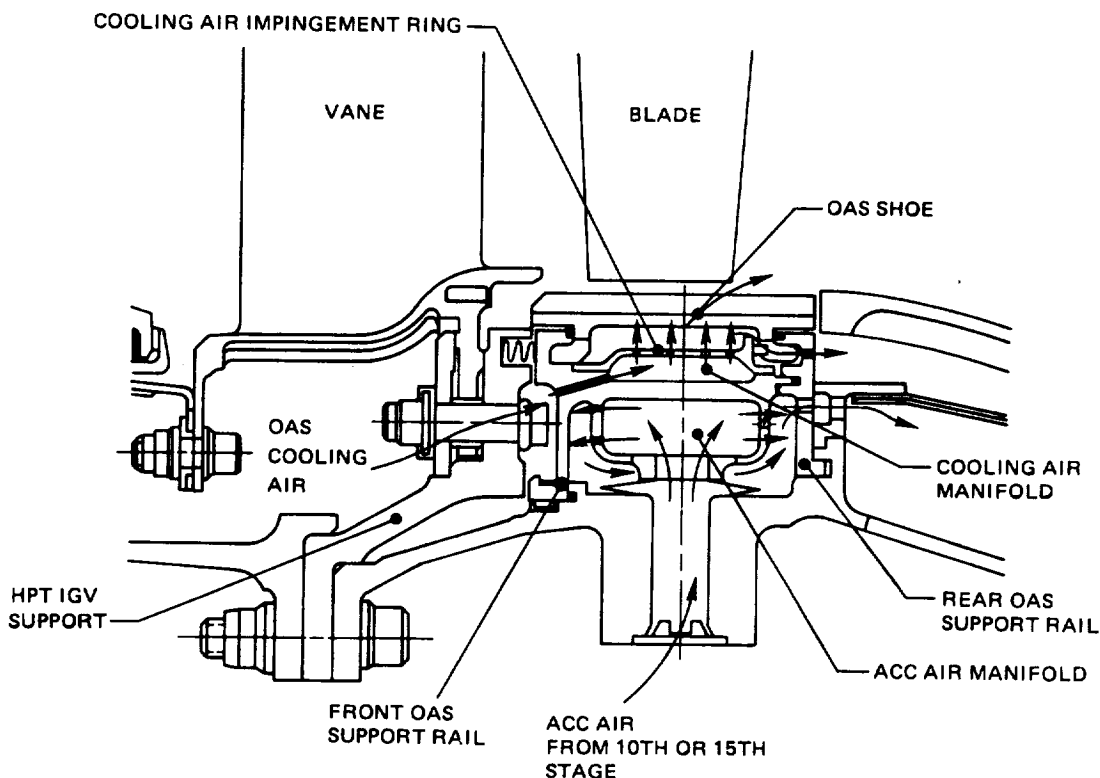


Figure 7.5.1-1 High-Pressure Turbine Active Clearance Control System

The high-pressure compressor bleed air enters the active clearance control manifold through eight bosses on the high-pressure turbine case. It then flows through holes in the active clearance control manifold to impinge on the outer air seal support rails. At this point, the air is discharged through holes in the rear outer air seal support rail into an annulus between the turbine intermediate case support strut outer diameter fairing and the high-pressure turbine case.

7.5.2 Blade Tip Clearance Definition

In general, the rotor structure grows at a more rapid rate than the turbine case during engine acceleration from idle to takeoff power because of the centrifugal forces acting on the rotor. This results in the smallest clearance, referred to as the pinch point gap, occurring shortly after acceleration to takeoff power. Figure 7.5.2-1 shows a typical radial growth time history for the rotor and case, indicating the occurrence of the pinch point.

An analysis of turbine rotor and case growth compatibility suggested that the pinch point occurring at takeoff could be eliminated by using fifteenth stage high-pressure compressor bleed air. However, it was not apparent that utilization of only fifteenth stage air would optimize clearances throughout the aircraft flight cycle.

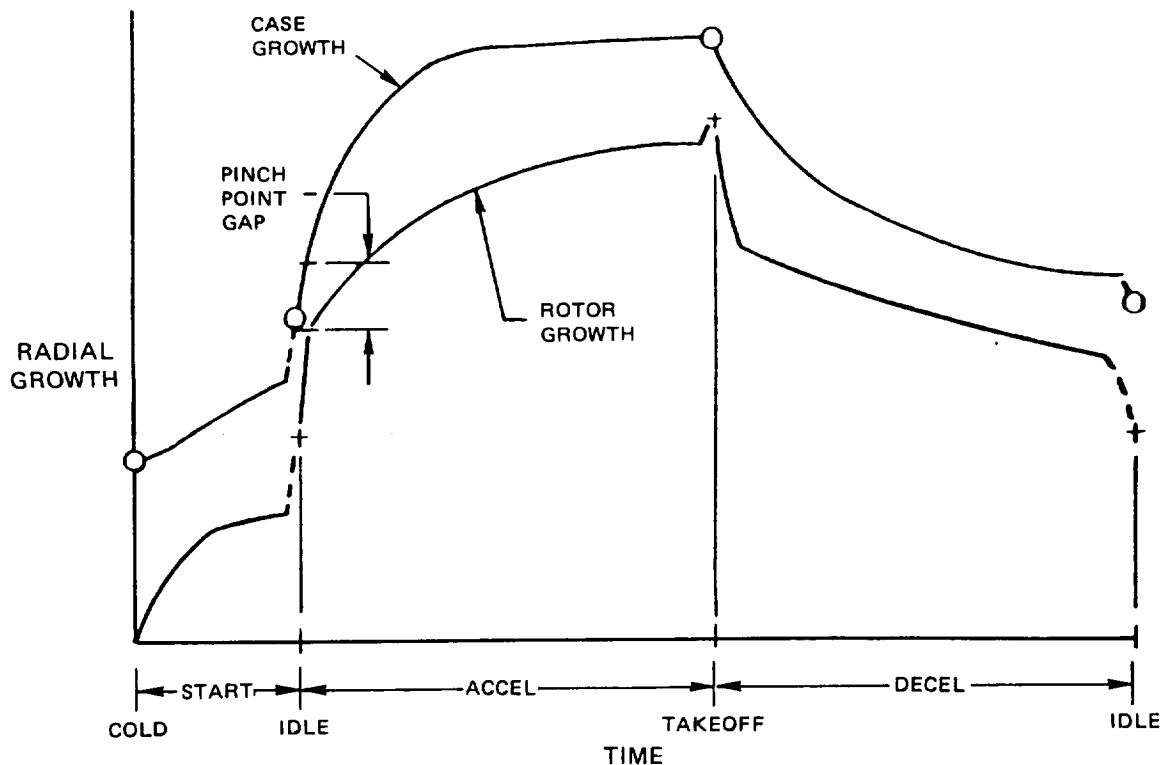


Figure 7.5.2-1 Typical Rotor and Case Growth History

As a result, a more comprehensive flight cycle analysis of rotor and case response growth was conducted. The analysis was based on the flight profile information presented in Table 7.5.2-I. In addition, the analysis assumed the use of two turbine case cooling schedules for active clearance control. Trends for rotor and case response with the two cooling schedules are presented in Figure 7.5.2-2.

The first schedule involved utilizing fifteenth stage high-compressor bleed air from idle through climb power until attaining an altitude of 6096 m (20,000 ft). At this point, cooling flow was switched to the tenth-stage bleed. As shown in Figure 7.5.2-2, this case cooling schedule provided the rapid case growth necessary to eliminate the pinch point at takeoff, but produced less than optimum clearance at both climb and cruise flight conditions.

TABLE 7.5.2-I
FLIGHT CYCLE FOR CLEARANCE ANALYSIS

DOMESTIC MISSION 1296 km (700 nm)			
Segment	Power Setting	Altitude/speed M/Mn (ft/Mach No.)	Time (min)
* Start and Idle-Taxi	Gr. idle	0/0	7.5
Takeoff	T.O.	0-457/0-0.39 (0-1500/0-0.39)	2.0
Climb	M. Cl.	457-10,668/0.39-0.80 (1500-35,000/0.39-0.80)	17.4
Cruise	0.85-0.82 M. Cr.	10,668/0.80 (35,000/0.80)	56.6
Descent	Fl. idle	10,668-457/0.80-0.39 (35,000-1500/0.80-0.39)	20.4
Approach/Landing	0.30 T.O. - Fl. idle	457-0/0.39-0.17 (1500-0/0.39-0.17)	2.0
Reverse	M. rev.	0/0.15	0.2
Idle-Taxi	Gr. idle	0/0	7.5
			113.6

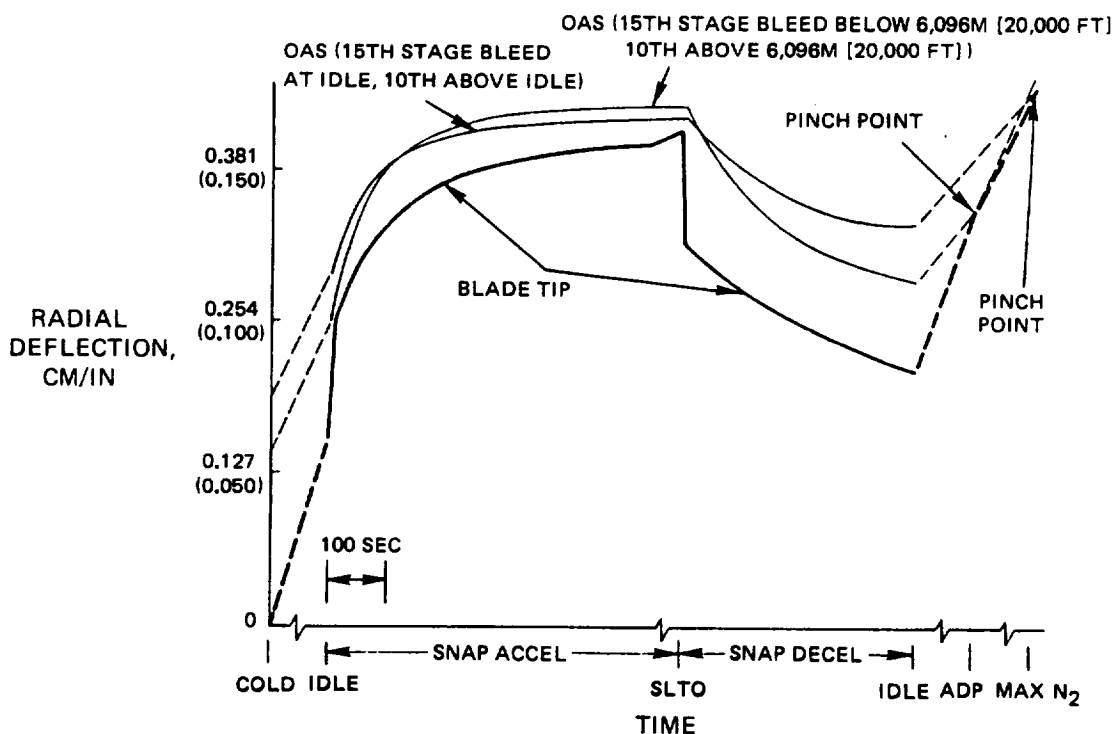


Figure 7.5.2-2 Rotor and Case Response with Two Cooling Bleed Schedules

The second cooling schedule assumed fifteenth-stage bleed air would be used through idle to eliminate the take off pinch point and tenth stage air would be used for the remainder of the flight cycle. This resulted in a second pinch point occurring at climb power (Figure 7.5.2-2). However, by mixing fifteenth and tenth stage air, this pinch point was eliminated. This effect is shown in Figure 7.5.2-3, along with the initial two cooling schedules for comparison. The final active clearance control bleed schedule is presented in Table 7.5.2-II. The resulting rotor and outer air seal response with this schedule is shown for the flight cycle in Figure 7.5.2-4.

Results from this analysis were used in establishing the high-pressure blade tip and seal gapping requirements as well as final blade tip operating clearances. Factors considered in establishing tip clearances include: (1) thermal and centrifugal gradients; (2) tolerances, eccentricities and rotor whirl; and (3) maneuver and cowl loads.

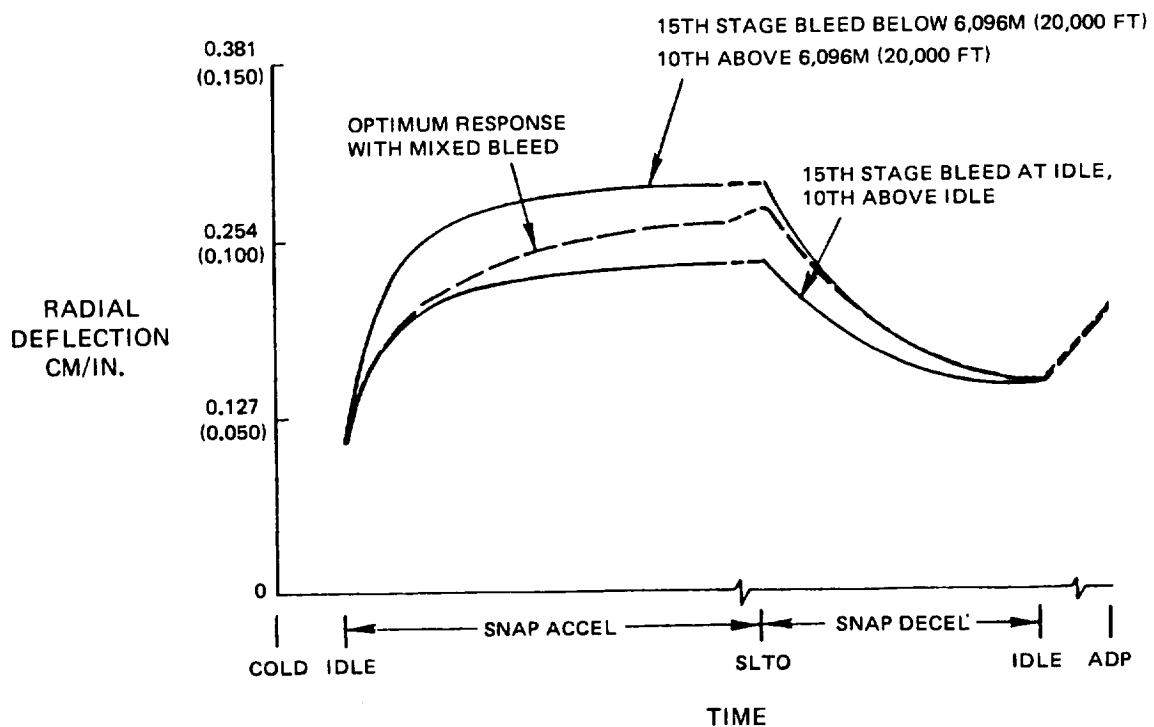


Figure 7.5.2-3 Effect of Mixed Bleed

TABLE 7.5.2-II

HIGH-PRESSURE TURBINE ACTIVE CLEARANCE CONTROL SYSTEM

	<u>Bleed System For ACC</u>
Idle	All 15th
ACCEL-SLTO	Mixed 10th and 15th
ADP	All 10th

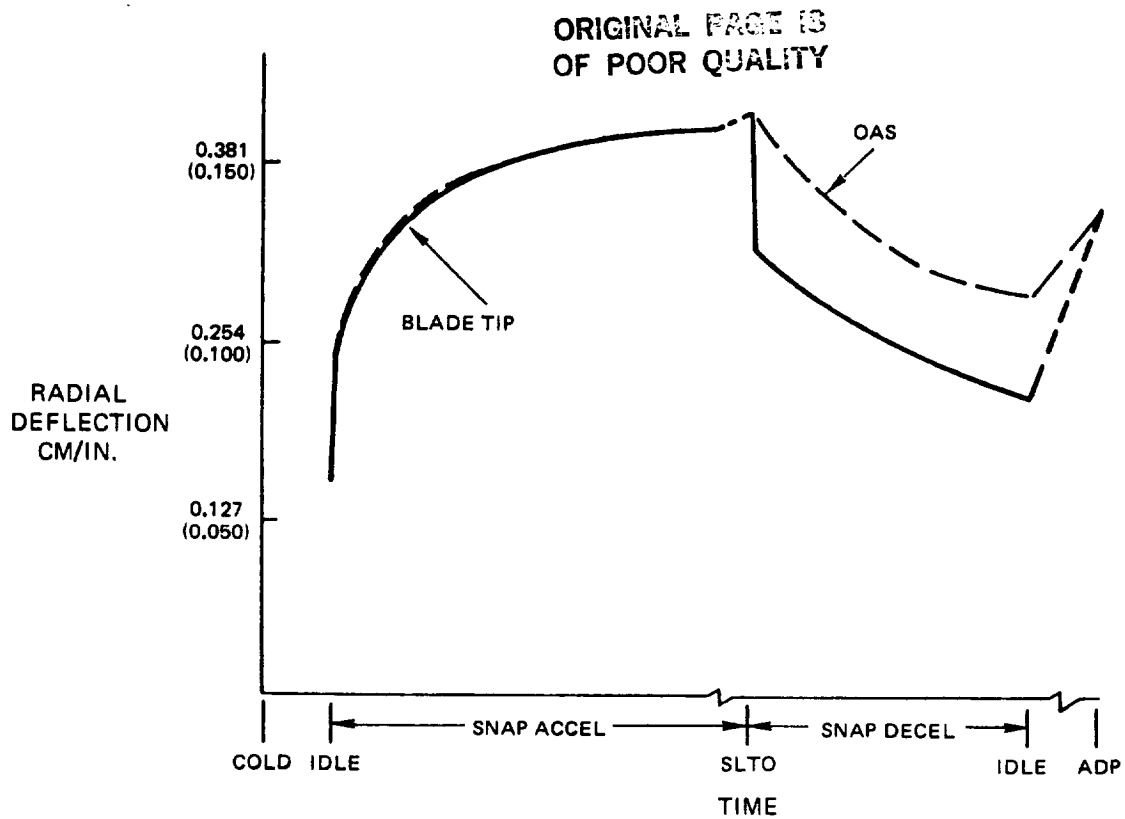


Figure 7.5.2-4 Rotor and Case Response with Optimum Mixed Cooling Bleed Schedule

A summary of the high-pressure turbine gapping requirements, the minimums needed to prevent a rub, is presented in Table 7.5.2-III for the flight conditions of idle, sea level takeoff and cruise. In arriving at these values, a number of considerations were used to establish a turbine build clearance. First, the clearance must be large enough to accommodate machining tolerances and eccentricities. Also, nominal unbalances in the rotor will produce additional rotor whirl motion for which more clearance must be provided. Furthermore, during the startup process, it is possible that the rotor can be bowed because of unsymmetric thermal gradients. Although this resultant motion is not very well defined, it is preferred to have the additional clearance to accommodate such motion. Finally, during flight conditions, additional deflection of the cases occur under normal maneuver and cowl aerodynamic loads. All these clearances are added up to provide the final gapping requirements.

The final blade tip clearances, using the active clearance control schedule of Table 7.5.2-II and recognizing the gap requirements of Table 7.5.2-III, are tabulated in Table 7.5.2-IV. The comparison of the clearance goal and predicted tip clearance status shows that the goals have been exceeded, thereby resulting in an improvement in turbine efficiency.

The rotor and seal response throughout the flight cycle is shown in Figure 7.5.2-5. The critical design point is the pinch point, which occurs approximately six seconds into the snap acceleration. The clearance of 0.034 cm (0.0134 in) is maintained throughout the acceleration segment. This results in the clearance during start to idle being greater than required and also results in the clearance at the aerodynamic design point being greater than the required 0.020 cm (0.0079 in). Although clearances at these two conditions are greater than required, they are still significantly less than the design goals.

TABLE 7.5.2-III

HIGH-PRESSURE TURBINE GAPPING REQUIREMENTS

	<u>Start-Idle</u> cm (in)	<u>ACCEL-SLTO</u> cm (in)	<u>ADP</u> cm (in)
Tolerances	0.0058 (0.0023)	0.0058 (0.0023)	0.0058 (0.0023)
Eccentricity	0.0086 (0.0034)	0.0086 (0.0034)	0.0086 (0.0034)
Rotor Whirl	0.0025 (0.0010)	0.0025 (0.0010)	0.0025 (0.0010)
Normal Maneuvers		0.0165 (0.0065)	0.0025 (0.0010)
Cowl Loads		0.0005 (0.0002)	0.0005 (0.0002)
Bowed Rotor Whirl	<u>0.0457 (0.0180)</u>		
TOTAL	0.0626 (0.0247)	0.0339 (0.0134)	0.0199 (0.0079)

TABLE 7.5.2-IV

HIGH-PRESSURE TURBINE TIP CLEARANCE RESULTS

	<u>Goal cm (in)</u>	<u>Status cm (in)</u>
Cold		0.1739 (0.0685)
Idle		0.1244 (0.049)
SLTO	0.0685 (0.027)	0.0340 (0.0134)
ADP	0.0472 (0.0186)	0.0320 (0.0126)

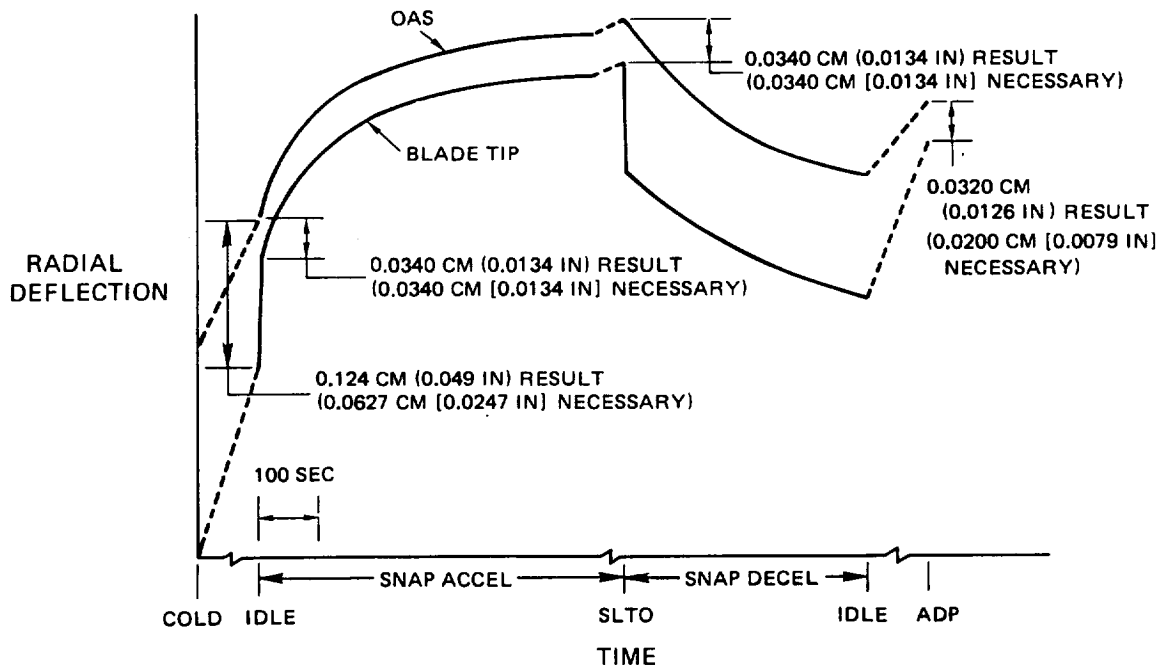


Figure 7.5.2-5 Resultant Blade Tip Clearances

7.6 NUMBER 4 AND 5 BEARING COMPARTMENT AND LUBRICATION SYSTEM

7.6.1 General Description

The number 4 and 5 bearing compartment for the Energy Efficient Engine high-pressure turbine incorporates existing service-proven technology and parts. The use of parts from current production engines minimizes expensive development and fabrication costs, and also reduces the degree of risk normally associated with the development of advanced technology hardware.

All parts in the number 4 and 5 bearing compartment meet Energy Efficient Engine design requirements, including mechanical stiffness, load carrying, imbalance, and high speed capability. Salient details of the number 4 and 5 bearing compartment for the integrated core/low spool are shown in Figures 7.6.1-1 and 7.6.1-2.

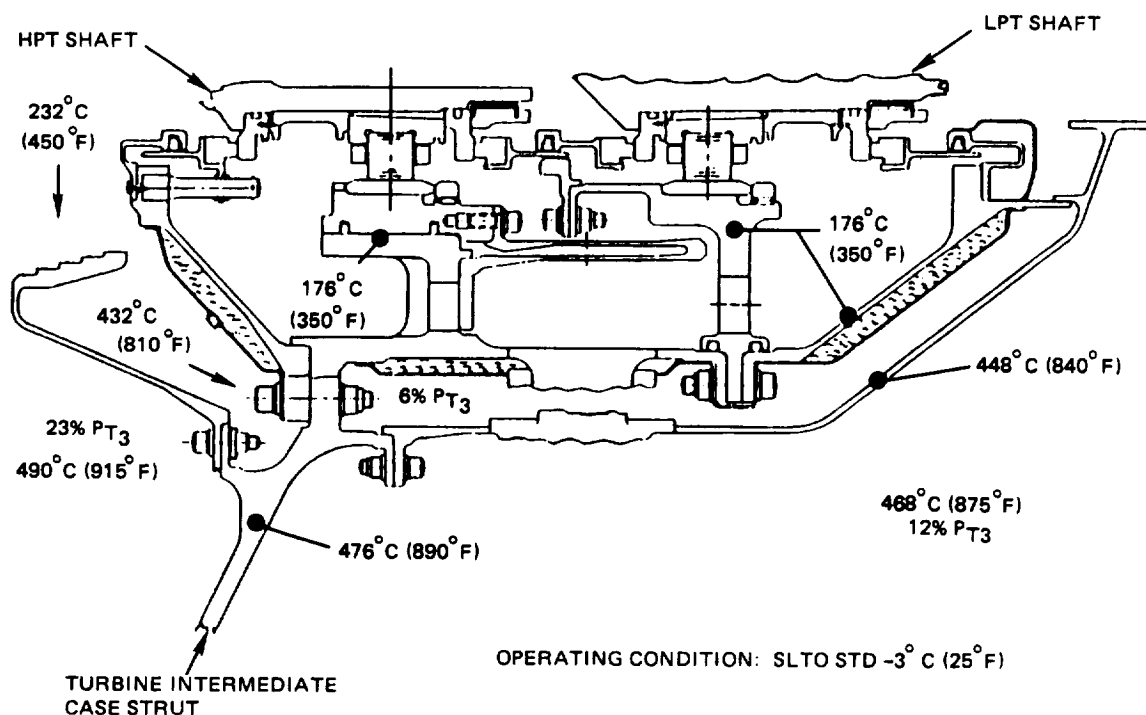


Figure 7.6.1-1 Integrated Core/Low Spool Number 4 and 5 Bearing Compartment - Temperature and Pressure Distribution at Sea Level Takeoff -3 C (+25°F) Operating Conditions

7.6.2 Bearing Mechanical Design Features

The number 4 and 5 bearings for the integrated core/low spool are the same as those used in a current Pratt & Whitney Aircraft engine. These bearings, in addition to meeting all established integrated core/low spool life requirements, have logged a significant amount of service experience, and, therefore provide a low risk base for application in the integrated core/low spool. In addition, the cost of designing, manufacturing and testing new bearings is eliminated. The bearings for the number 4 and 5 bearing compartment are discussed in the following paragraphs.

ORIGINAL PAGE IS
OF POOR QUALITY

E3 REAR COMPARTMENT

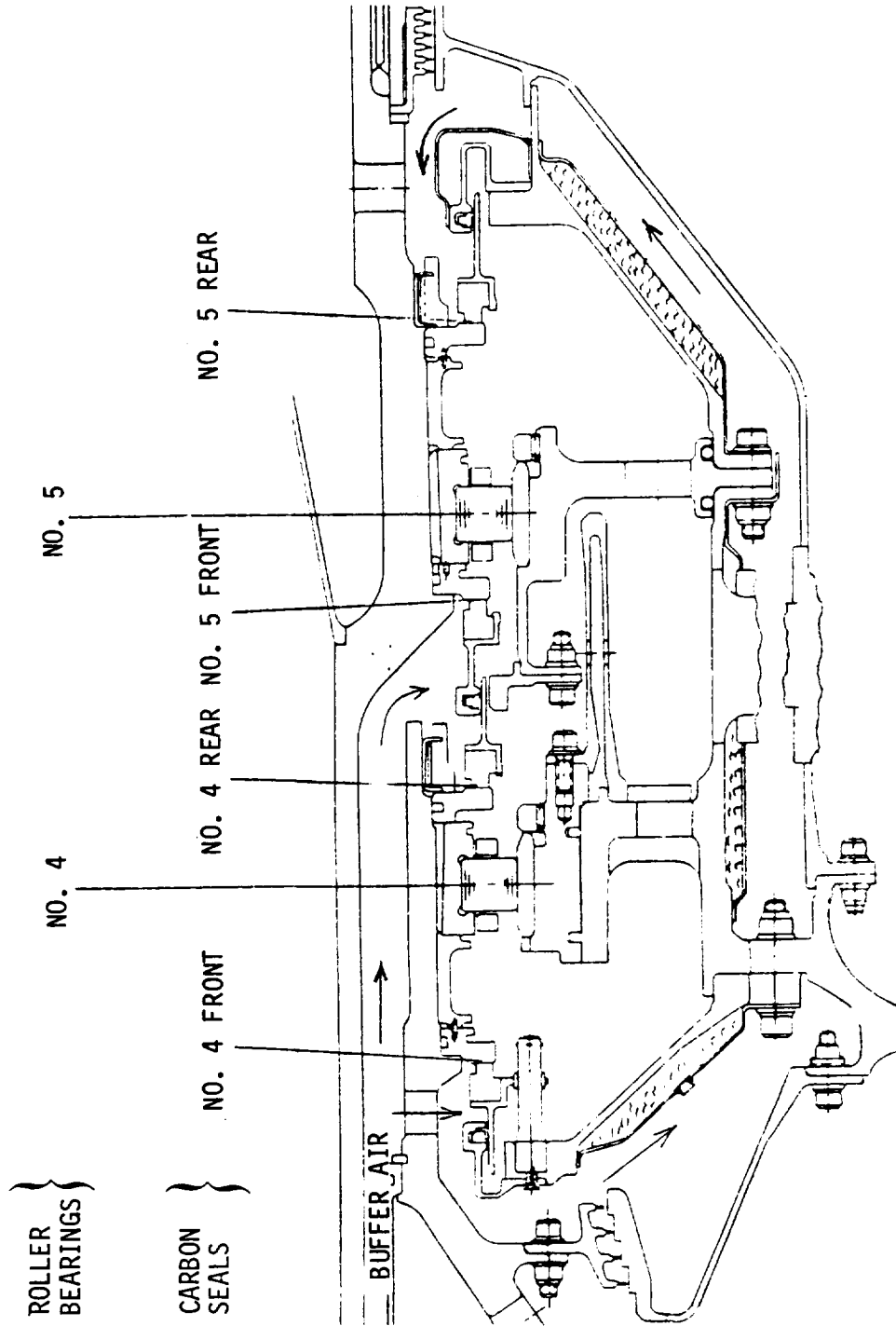


Figure 7.6.1-2 Number 4 and 5 Bearing Compartment Bearing and Seal Arrangement

The number 4 roller bearing for the integrated core/low spool measures 165 mm at the inner diameter and 222 mm at the outer diameter; has 16 mm diameter rollers and operates at 2.3×10^6 DN. The bearing is oil damped, spring centered, preloaded and under race cooled. The viscous oil damper and soft centering spring are incorporated to satisfy high rotor dynamic response criteria. The preloading benefit minimizes roller skidding. The under-race cooling feature provides positive cooling to manage thermal expansion throughout all operating conditions. Oil flow is 7 kg/min (16 lb/min) and heat generation is rated at 475,141 J/min (450 Btu/min). The expected B1 life of the number 4 bearing is greater than 500 hours, and the expected B10 life is greater than 2500 hours. This bearing may have to be optimized to meet flight propulsion system durability and life requirements.

The integrated core/low spool number 5 bearing is also a 165 mm inner diameter, 222 mm outer diameter size bearing, with 16 mm diameter rollers, but operates at much lower speed than the number 5 bearing; 0.64×10^6 DN. It has zero preload and reduced internal radial clearance. Its oil flow is 1 kg/min (4 lb/min) with a heat generation of 31,676 J/min (30 Btu/min). A viscous oil film damper has been incorporated on the outer ring to control low rotor vibratory response. Integrated core/low spool life rating for this bearing is B1 life greater than 10,000 hours and B10 life greater than 50,000 hours.

The results of a structural study to determine maximum stress and deflection are shown in Figure 7.6.2-1.

The number 5 bearing for the flight propulsion system is similar to the number 4 bearing, but with the inner diameter bore reduced to 160 mm and the outer diameter increased to 230 mm.

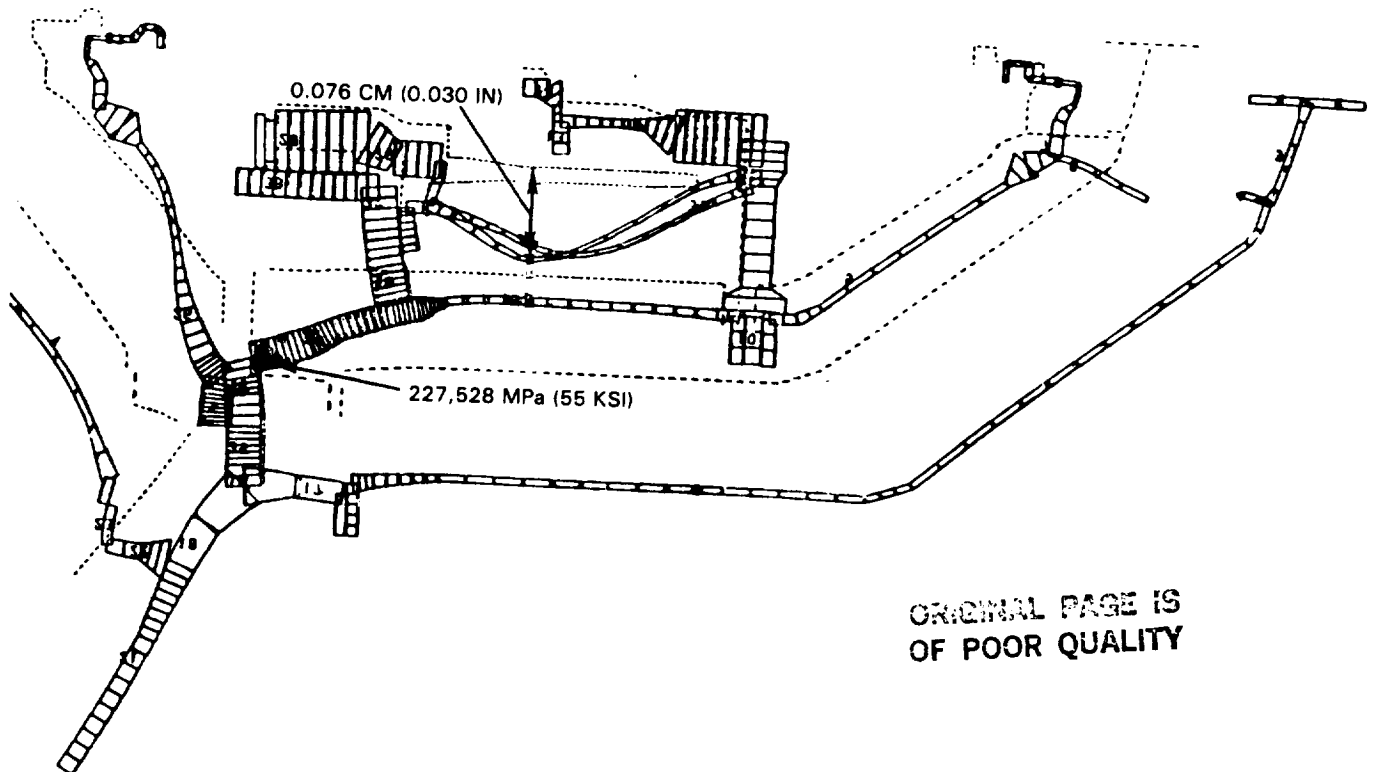


Figure 7.6.2-1 Number 4 and 5 Bearing Compartment - Locations of Maximum Stress and Deflection

7.6.3 Seals

The seals used in the number 4 and 5 bearing compartment of the integrated core/low spool are derived from existing service-proven designs for minimized risk and decreased cost. The operating environment of the integrated core/low spool is less severe than that of the existing design. Therefore, the seals more than adequately meet the life and durability requirements of the integrated core/low spool.

Carbon seals were selected in place of knife edge seals because of the increased radial deflection of the high-pressure turbine rotor associated with the oil-damped number 4 bearing. The resulting large radial gaps would be detrimental to labyrinth seal operation. Carbon seals minimize the breather flow and limit total engine oil consumption to 0.22 l/hr (0.06 gal/hr).

The seal arrangement in the number 4 and 5 bearing compartment consists of a number 4 front carbon seal, an intershaft seal consisting of back-to-back carbon seals, and a number 5 rear carbon seal. These seals are dry-face, short carbon with cooled rotating seal plates. Maximum surface rubbing speed is 135 m/sec (445 ft/sec) for the flight propulsion system and 140 m/sec (462 ft/sec) for the integrated core/low spool, operating in a low-temperature and low-pressure environment at 68,948 Pa (10 psi) seal pressure drop. Current engine experience on similar seals has been accumulated at this rubbing speed with seal pressure drops of 379,214 Pa (55 psi). The integrated core/low spool seals are derived from existing hardware. The seals used in the flight propulsion system feature a high quality carbon grade with excellent durability characteristics.

To reduce leakage, the low-pressure bearing compartments are buffered by cold low-pressure compressor air bleed discharge. The system features a single mainshaft deoiler in the front compartment. Air is introduced to the bearing compartment between the low and high-speed shafts. The buffering air is bled from the low-pressure compressor, routed through the center shaft, bled into the bearing compartment and then discharged through blowdown tubes to the deoiler in the main compartment. The main feature of this system is the self-regulating design, which eliminates the need for extensive valving and pumps.

Analysis of the seal pressure drop indicates that positive seal pressure can be obtained at all operating conditions. This positive seal pressure can be achieved at sea level idle conditions by either reducing the exit bleed flow or increasing the idle speed.

Integrated core/low spool seal operating conditions are summarized in Table 7.6.3-1. A summary of dry face seal pressure, temperature, and speed experience is presented in Figure 7.6.3-1.

7.6.4 Lubrication System

The lubrication system for the number 4 and 5 bearing compartment is part of a system that features positive oil management to provide sufficient cooling and lubrication flow. One of the main features of this system is the self-regulation arrangement, which eliminates the need for expensive pumps and extensive plumbing. As a result, the plumbing system is simplified, the size and number of scavenge pumps reduced, and the need for a pressure regulating valve eliminated.

TABLE 7.6.3-1

INTEGRATED CORE/LOW SPOOL SEAL OPERATING CONDITIONS

	High Rotor Seals			Low Rotor Seals		
	ADP	SLTO	IDLE	ADP	SLTO	IDLE
Rubbing Speed m/sec (ft/sec)	133 (439)	140 (462)	102 (335)	39 (129)	39 (129)	11 (37)
Seal Δp Pa (psi)	20,684 (3)	48,263-68948 (7-10)	<6894<(1)	20,684 (3)	48,263-68,948 (7-10)	<6894<(1)
Heat Generation (Btu/min)	131	139	93	26	24	7
Air Temperature °C (°F)		232 (450)		Front Rear	232 (450) 426 (800)	

• E³ IC/LS OPERATING CONDITIONS LESS SEVERE THAN EXPERIENCE

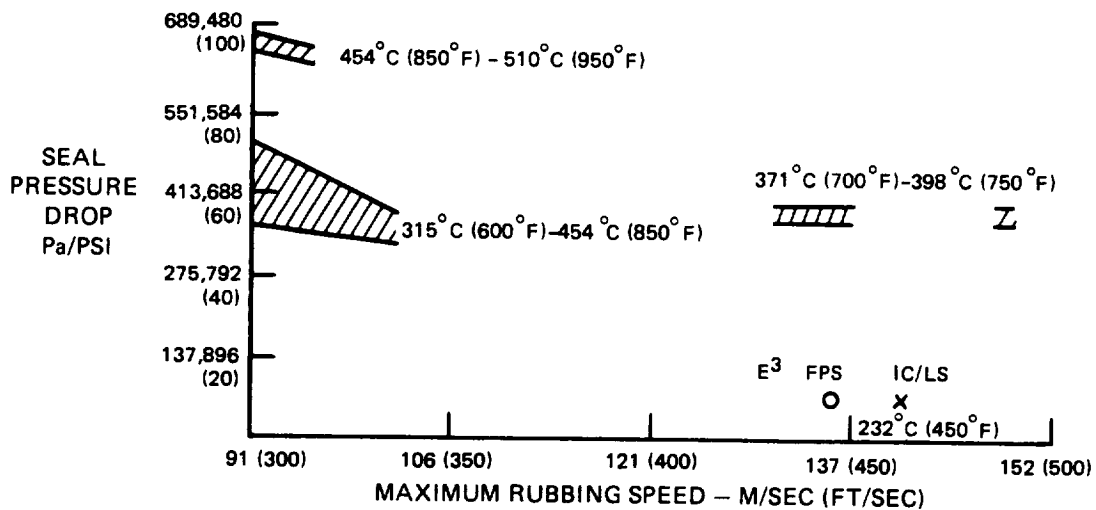


Figure 7.6.3-1 Dry Face Seal Pressure, Temperature and Speed Experience

An additional feature of the lubrication system is the blowdown system with oil and air scavenged together through the turbine transition duct strut. The integrated core/low spool uses two struts and the design ensures that the oil and air mixture flows through each of the struts without backing up through the scavenge lines. This design also eliminates the high cost of installing a complex internal plumbing arrangement within a single strut. With the plumbing divided between two struts, the fabrication cost and the associated operational risk are substantially reduced.

Oil is transported from the main engine oil pump to two radial oil scoops in the rear compartment, one scoop servicing the front bearing and the other servicing the rear. The scoop efficiency for the integrated core/low spool is 60 percent, which is commensurate with scoop efficiency levels of most current commercial engines. The scoop arrangement for the flight propulsion system is being refined for an efficiency increase.

Adequate leakage provisions have been supplied to ensure that no oil touches any of the hot parts. To address this requirement, an oil scupper line has been incorporated to provide a drain through which oil can be transported away from hot parts. This arrangement is depicted in Figure 7.6.4-1.

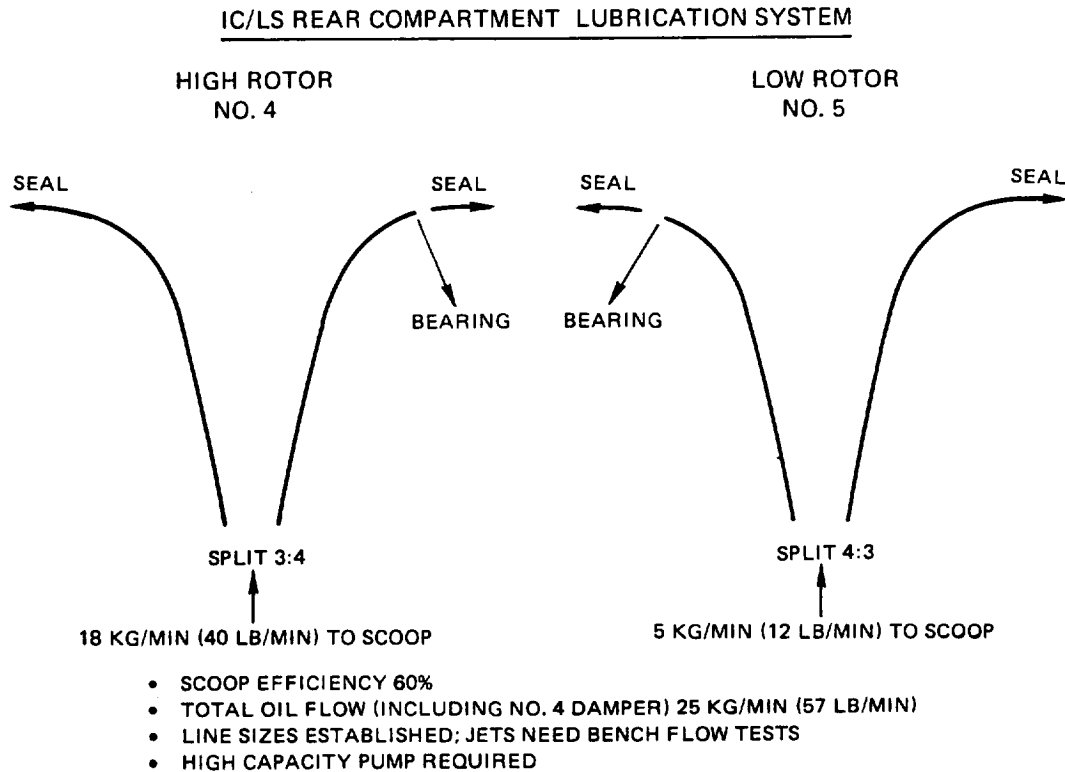


Figure 7.6.4.1 Oil Scupper Line for the Number 4 and 5 Bearing Compartment

7.7 TURBINE SYSTEM WEIGHT SUMMARY

Preliminary weight analyses were conducted for the high-pressure turbine as configured for the integrated core/low spool. Results of these analyses are presented in Table 7.7-I. A detailed weight assessment will not be performed until the final flight propulsion system preliminary design update.

TABLE 7.7-I
PRELIMINARY WEIGHT SUMMARY FOR INTEGRATED CORE/LOW SPOOL
HIGH-PRESSURE TURBINE COMPONENT

<u>Item</u>	<u>Weight</u> kgs/(lbs)	
Disk and Seals	150	(330)
Blade Assembly	32	(71)
Vane Assembly	26	(58)
Tangential On-Board Injection System (TOBI)	45	(99)
Outer Case Assembly	<u>106</u>	<u>(233)</u>
Total	359	(791)

SECTION 8.0 HIGH-PRESSURE TURBINE COMPONENT TEST RIG DESIGN

8.1 INTRODUCTION

The Energy Efficient Engine High-Pressure Turbine Component Rig was designed to establish the performance base for the turbine and verify the advanced aerodynamic/thermodynamic design concepts of the program. The rig design configuration incorporates structural criteria and mechanical constraints consistent with experimental hardware.

The following sections provide (1) a general description of the rig, including salient rig assembly and safety features, (2) information describing the mechanical design, and (3) a description of the instrumentation used to monitor turbine performance and rig structural integrity.

8.2 GENERAL DESCRIPTION AND MAJOR FEATURES

The turbine component rig is designed to test the full size high-pressure turbine component at the design differential pressure, but at reduced temperature and absolute pressure levels. It is intended to confirm the aerodynamic performance of full sized integrated core/low spool hardware prior to running the integrated core/low spool test. In addition, it will provide a check of predicted cooling and leakage flows and operation of the active clearance control system. A cross section of the rig is illustrated in Figure 8.2-1.

The rig assembly includes an inlet section, rotor and vane assembly, and exhaust section. The rotor and vane assemblies and active clearance control section are mainly component hardware (suitable for integrated core/low spool operation) while the inlet, exhaust and outer case sections are rig unique hardware. The rig features separate controls for all secondary flows as well as main flow. In addition, a separate system is provided for the active clearance control system, which covers an approximate 148°C (300°F) temperature range for clearance change. The main flow temperature will be 426°C (800°F) with the appropriate secondary air temperature ratio to simulate engine conditions. A circumferential traverse instrumentation ring has been provided to acquire a more thorough mapping behind the vanes and blades.

The rig incorporates an active clearance control system, which will be evaluated during testing. The internal hardware of the active clearance control system for the integrated core/low spool is also used in the rig.

Special consideration was given to the type of material used in certain areas of the rig. For example, rig hardware exposed to main and secondary airflow was designed using stainless steel or comparable rust-resistant alloys, to prevent contamination of coolant passages. High strength materials are used in the high temperature regions of the rig, while external rig hardware is of less expensive low carbon steel material.

ORIGINAL PAGE IS
OF POOR QUALITY

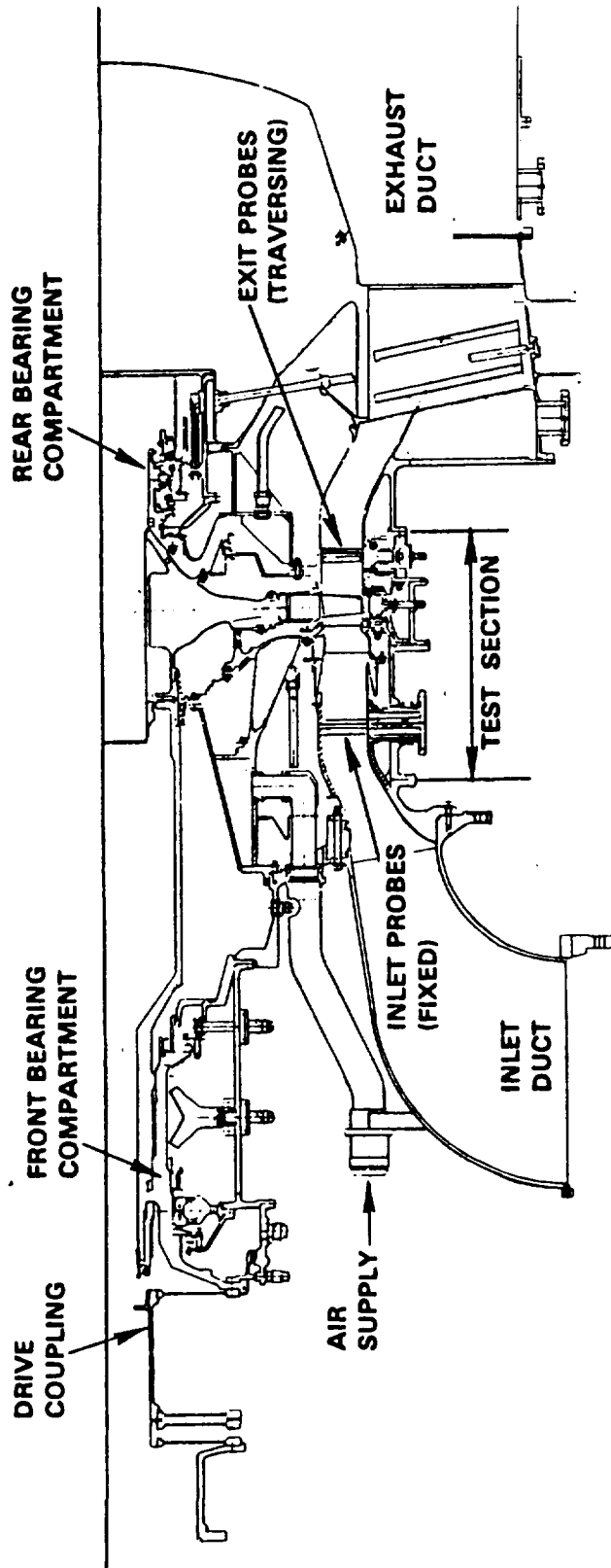


Figure 8.2-1 High-Pressure Turbine Component Test Rig

The rig safety systems are characterized by three primary modes. The first is an explosive system activated by the occurrence of an overspeed condition. The main stream airflow bypasses the rig and re-enters in the exhaust duct. The second system is a pop-valve, which also allows the airflow to bypass the rig. In addition to speed, the pop-valve can be excited by loss of oil flow, bearing compartment adverse pressure gradients, excessive vibration, and excessive bearing temperature. The third system is an alarm system, which is activated when the limits of various rig parameters are exceeded.

8.3 MECHANICAL DESIGN

8.3.1 Rotating Hardware

The rotating components in the rig consist of the front and rear bearing compartments, rotor shaft and rotor assembly.

The rig rotor design was analyzed for critical speeds and the rotor tie bolts were analyzed for blade loss capability. In addition, the rotor air seals were reviewed for resonance and coincidence. The critical speeds and mode shapes determined from the rotor dynamics study are shown in Figure 8.3.1-1. Because the mode shapes indicate a critical condition, a forced response analysis was conducted. The resultant bearing loads corresponding to 0.002 cm (0.001 in) of bearing support vibration at the speeds shown were judged to be acceptable (Table 8.3-1).

The calculated stress in the rotor tie bolts resulting from a blade loss situation is 482,636 MPa (70 kpsi), which is well under the 0.2-percent yield stress level of Inconel 718 material.

Seal dampers were provided for the rotor air seals as a conservative measure to avoid any resonance or coincidence problem, as discussed in Section 8.3.3.

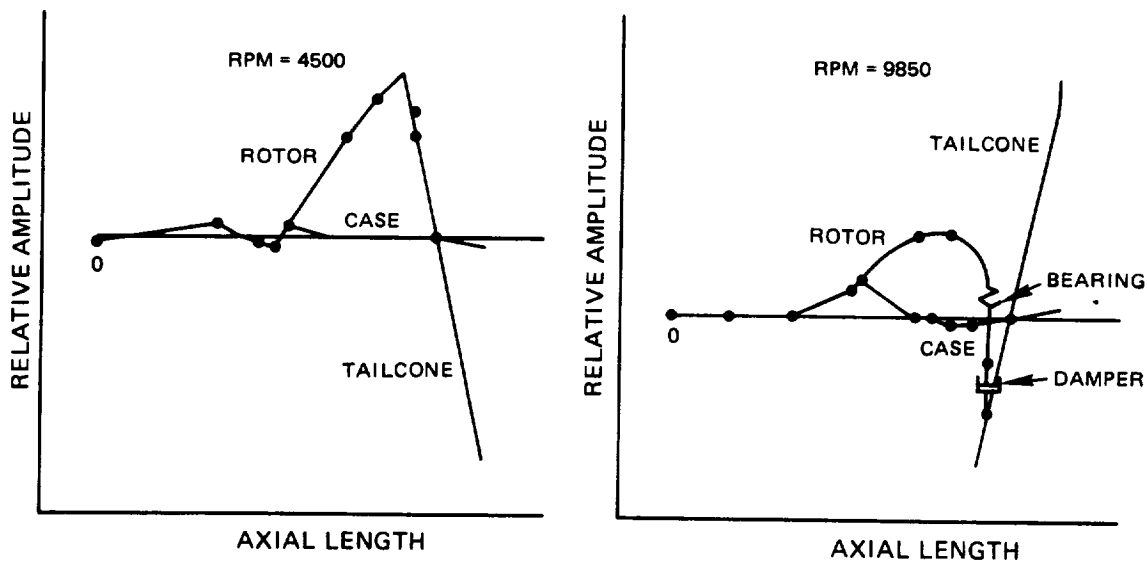


Figure 8.3.1-1 High-Pressure Turbine Component Test Rig Critical Speed and Mode Shapes

TABLE 8.3-I

HIGH-PRESSURE TURBINE COMPONENT RIG
FORCED RESPONSE RESULTS

Rotor Speed (rpm)	Bearing Loads for 0.002 cm (0.001 in) Bearing Support Vibration kg (lb)	
	Front Bearing	Rear Bearing
4500	34 (75)	138 (306)
9850	230 (508)	386 (851)

8.3.2 Bearings and Seals

The bearing compartments were designed using existing parts with minor modifications. Key features of the front and rear bearing compartments are described as follows.

The front bearing has a 220 mm bore and a 320 mm flanged outer diameter. Its maximum DN is 2.1×10^6 , and its maximum load is less than 4,535 kg (10,000 lb). The calculated B1 life is greater than 250 hours.

The front compartment seals are the dry face type with an oil-cooled carbon rubbing plate. Stackpole 2080 carbon grade seals are used for improved durability. Air temperature in the compartment is estimated to be 65°C (150 °F). The seal operating conditions are listed in Table 8.3.2.-I.

TABLE 8.3.2-I

FRONT COMPARTMENT OPERATING CONDITIONS

Condition	Seal Differential Pressure Pa (psi) (ΔP)		Rubbing Speed m/sec (ft/sec)
	FORWARD	REAR	
Aerodynamic Design Point (ADP)	227,528 (33)	220,633 (32)	121 (400)
Maximum Speed	262,002 (38)	255,107 (37)	134 (440)
Differential ΔP Range*	186,159-351,634 (27-51)	179,264-344,740 (26-50)	

* Range expected to be encountered during rig operation

The design of the rear compartment bearing for the rig is the same as that of the number 4 bearing for the integrated core/low spool. This oil-damped bearing has a 165 mm bore and a 222 mm outer diameter and is equipped with a soft centering spring. It also features preloading and under race oil cooling. Its maximum radial load is less than 453 kg (1000 lb), and its calculated B1 life is greater than 1000 hours. The maximum DN is 1.6×10^6 .

The design of the rear compartment forward seal is the same as that of the number 4 seal for the integrated core/low spool, and the rig rear seal is derived from the integrated core/low spool number 5 rear seal. Both are the dry-face type seal with oil cooled rubbing plates. Stackpole 2080 carbon grade seals are used for improved durability. The temperature of the surrounding air is maintained at 65°C (150°F). Operating conditions of the seals are shown in Table 8.3.2-II.

TABLE 8.3.2-II
OPERATING CONDITIONS OF THE REAR COMPARTMENT SEALS

<u>Condition</u>	<u>Seal ΔP Pa(psi) Both Seals</u>	<u>Rubbing Speed m/sec (ft/sec)</u>
ADP	41,368 (6)	89 (293)
Max Speed	41,368 (6)	98 (324)

Operating Requirement: 68,948 Pa (10 psia) Compartment Pressures

8.3.3 Air Seals

Extensive vibrational analysis was conducted on all high pressure drop, high speed air seals. Characteristics of the seals that were studied include resonance, coincidence and aerodynamic flutter.

A total of five air seals was reviewed in the study. These included the front and rear seals of the front bearing compartment and the three high-pressure turbine component design seals shown in Figure 7.2.6-1. These three seals, having been studied for their vibrational characteristics at integrated core/low spool conditions, were studied for response at rig speeds and pressure levels. The study results are as follows:

- o Front compartment front air seal (or thrust piston seal). Resonance and coincidence characteristics are as shown in Figures 8.3.3-1 and 8.3.3-2. Resonance margin for the stationary part of the seal is 60 percent and 45 percent for the rotating part. Coincidence margin is 46 percent.

A sheet metal damper of 0.170 cm (0.067 in) thick sheet metal was provided to the rotating member as a conservative measure to avoid any resonance. Aerodynamic flutter was considered unlikely for this seal because of the influence of the damper and relatively low pressure drop across the seal. The seal and its damper are shown in Figure 8.3.3-3.

ORIGINAL PAGE IS
OF POOR QUALITY

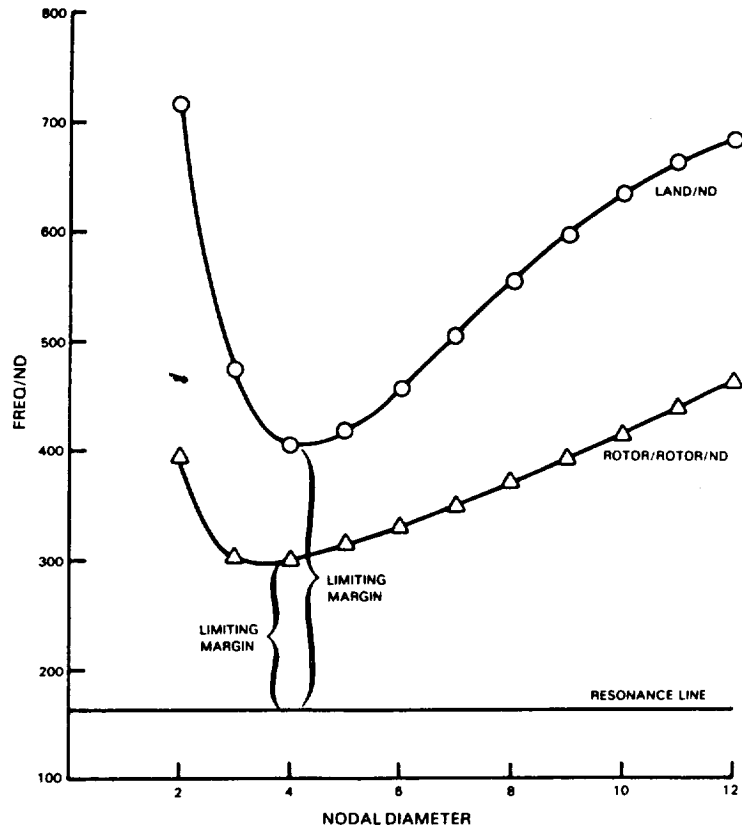


Figure 8.3.3-1 High-Pressure Turbine Rig Thrust Piston Seal Resonance

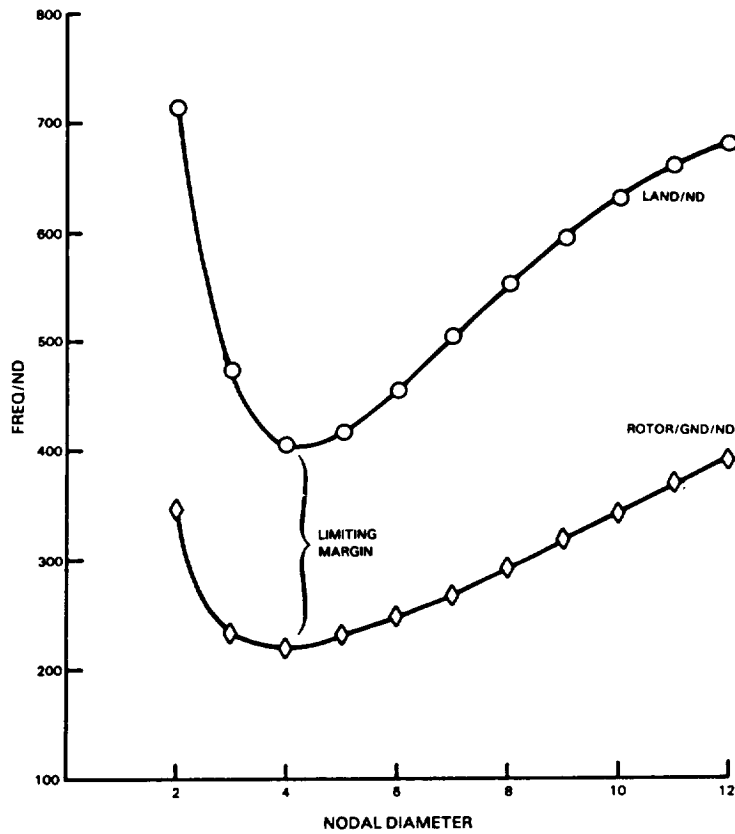


Figure 8.3.3-2 High-Pressure Turbine Rig Thrust Piston Seal Coincidence

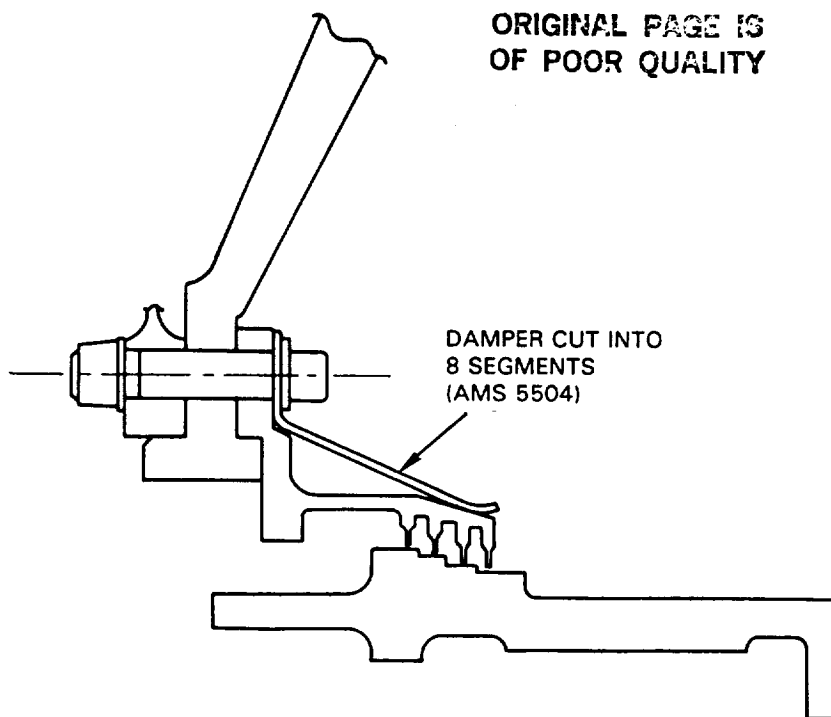


Figure 8.3.3-3 Front Compartment Front Airseal (Thrust Piston Seal)

- o Front compartment rear airseal. This seal's function is to act as a backup seal in the event of a malfunction of the carbon seal. A one-knife edge design was selected as best suited for this purpose in the unlikely event of a carbon seal failure.

Resonance and coincidence margins for this seal were found to be inadequate. Figures 8.3.3-4 and 8.3.3-5 indicate no margin near the three nodal diameter frequency mode for both resonance and coincidence. A damping feature was provided for this seal to avoid resonance or coincidence. The damper is constructed of 0.160 cm (0.063 in) thick sheet metal and is provided for both rotating and nonrotating members. The configuration of the seal with dampers is shown in Figure 8.3.3-6.

The addition of dampers to this seal, along with its single knife edge design, makes it a low risk for aerodynamic flutter.

- o High-pressure compressor discharge seal. Resonance margin for this seal, as shown in Figure 8.3.3-7, is 83 percent for the rotor and 68 percent for the stationary member. Coincidence margin is 11 percent, as shown in Figure 8.3.3-8. Flutter stability for this seal was analyzed for the integrated core/low spool application (Section 7.2.6.2) and found to be acceptable. The seal is therefore adequate for the rig application because of the same pressure drops. Sheet metal dampers 0.109 cm (0.043 in) thick were provided for the stationary member as a precautionary measure to provide additional safety margin. The seal configuration with dampers is shown in Figure 8.3.3-9.

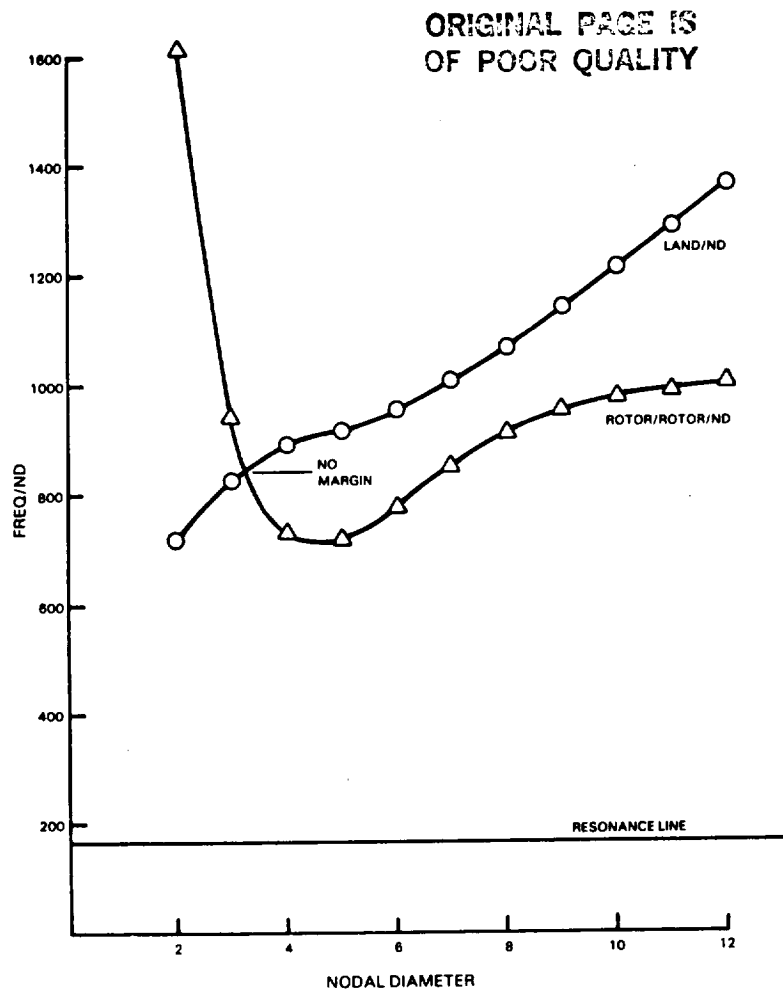


Figure 8.3.3-4 High-Pressure Turbine Rig Front Bearing Rear Seal Resonance

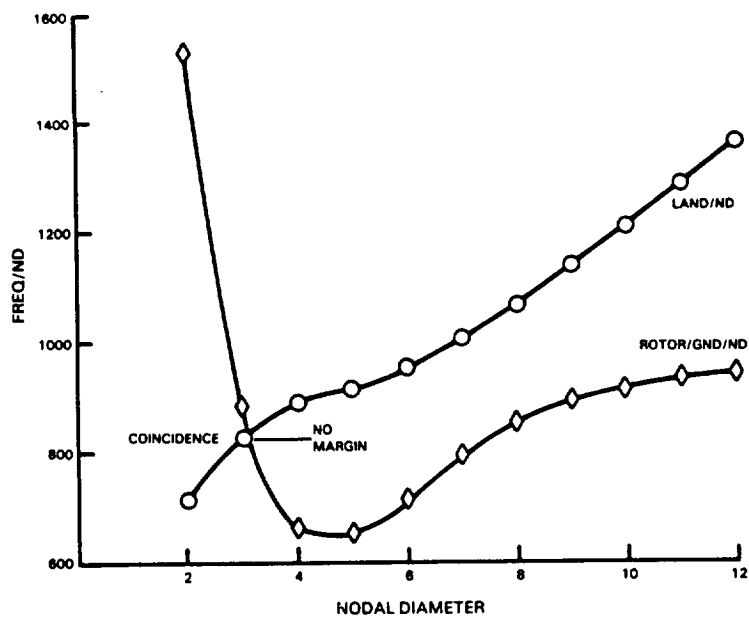


Figure 8.3.3-5 High-Pressure Turbine Rig Front Bearing Rear Seal Coincidence

ORIGINAL PAGE IS
OF POOR QUALITY

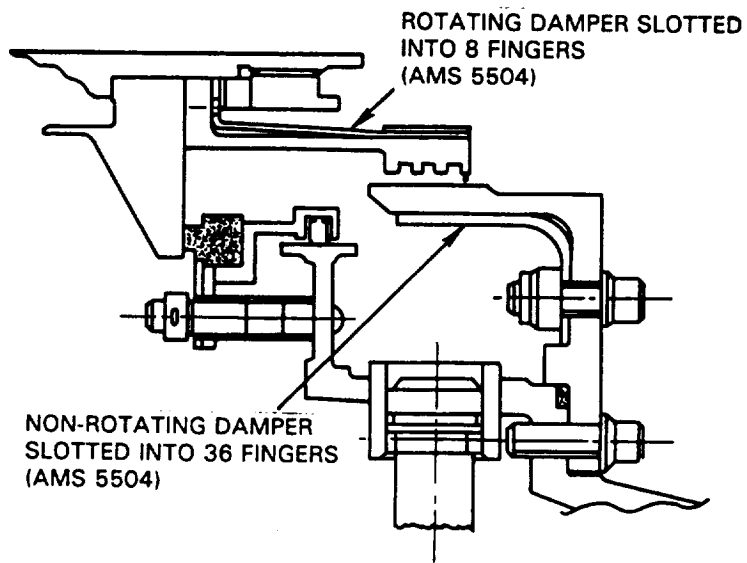


Figure 8.3.3-6 Front Compartment Rear Airseal

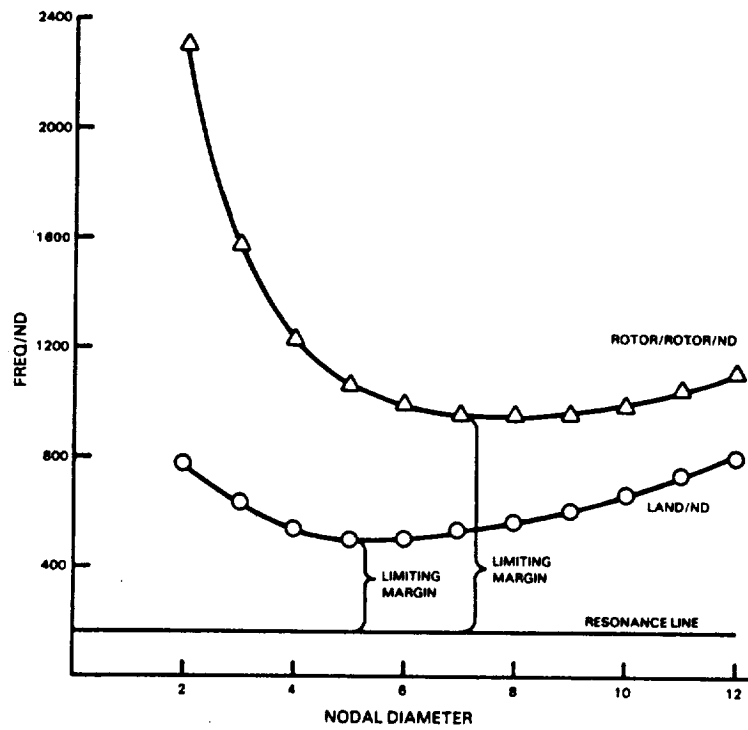


Figure 8.3.3-7 High-Pressure Turbine Rig High-Pressure Compressor Discharge Seal Resonance

ORIGINAL PAGE IS
OF POOR QUALITY

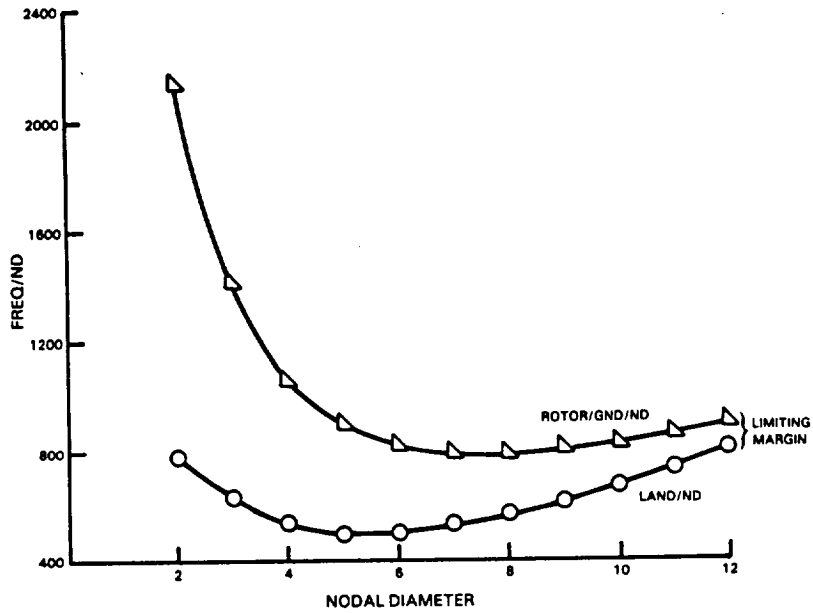


Figure 8.3.3-8 High-Pressure Turbine Rig High-Pressure Compressor Discharge Seal Coincidence

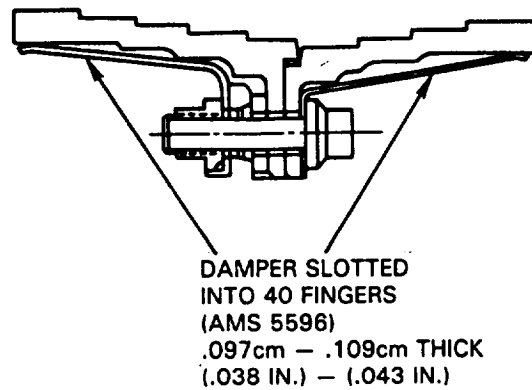


Figure 8.3.3-9 High-Pressure Compressor Discharge Seal

- o Thrust balance seal. The margin for resonance on the thrust balance seal is 20 percent for the rotor, as shown in Figure 8.3.3-10, and 56 percent for the stationary member. Coincidence margin is 21 percent, as shown in Figure 8.3.3-11.

A damper was provided for the rotating member, 0.073 cm (0.029 in) thick, as shown in Figure 8.3.3-12.

Flutter stability is adequate because of the analysis completed for integrated core/low spool and the similarity in rig and integrated core/low spool pressure drops. The addition of a damper provides additional confidence in flutter stability.

- o Number 4 bearing buffer air seal. Resonance margin for the buffer air seal was determined to be 53 percent for the stationary member and 75 percent for the rotating member, as shown in Figure 8.3.3-13. The coincidence margin was determined to be 46 percent, as shown in Figure 8.3.3-14.

Aerodynamic flutter was determined to be unlikely because of the low pressure drop across the seal. The analysis indicated no need for a damper on this seal.

The seal configuration is shown in Figure 8.3.3-15.

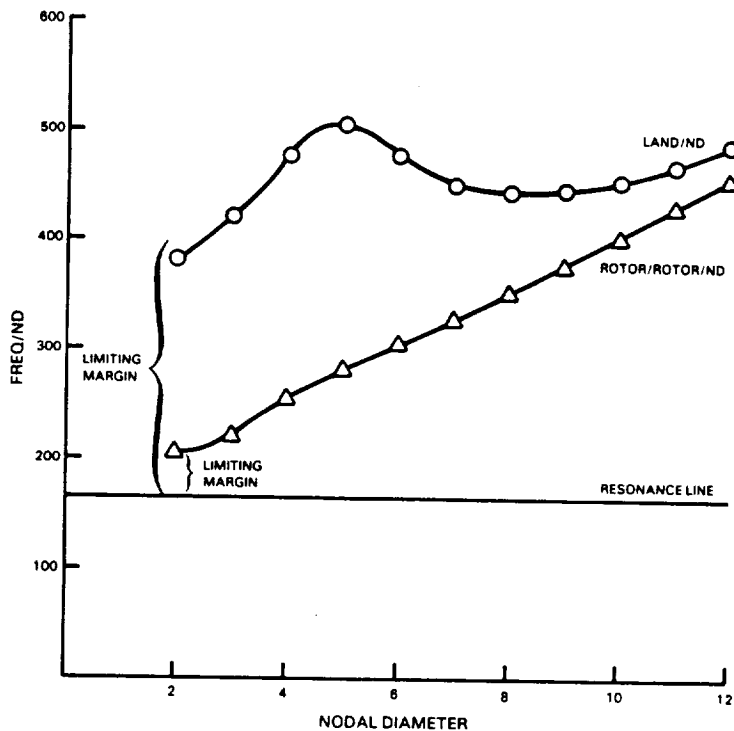


Figure 8.3.3-10 High-Pressure Turbine Rig Thrust Balance Seal Resonance

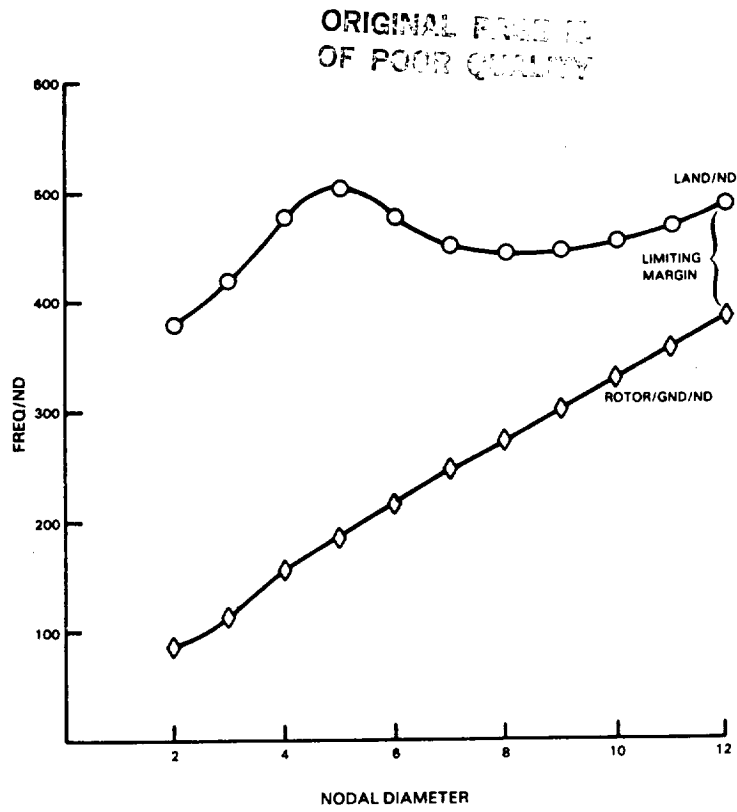


Figure 8.3.3-11 High-Pressure Turbine Rig Thrust Balance Seal Coincidence

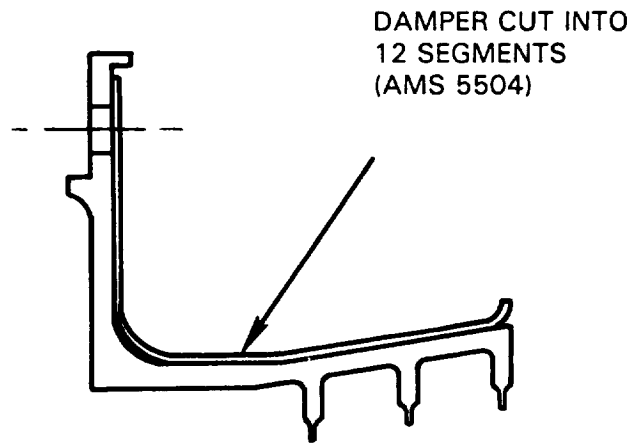


Figure 8.3.3-12 Thrust Balance Seal and Damper

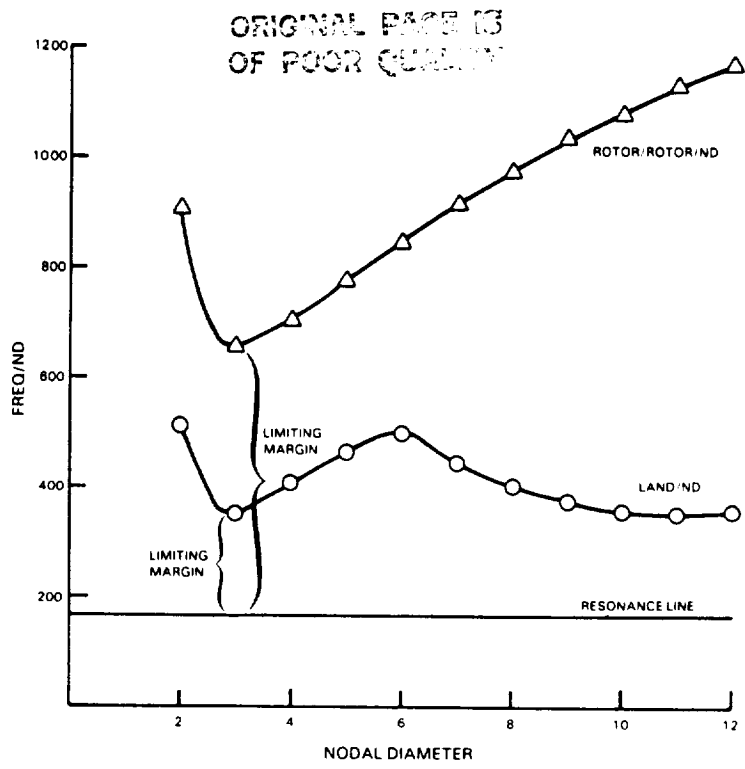


Figure 8.3.3-13 High-Pressure Turbine Rig Number 4 Bearing Buffer Seal Resonance

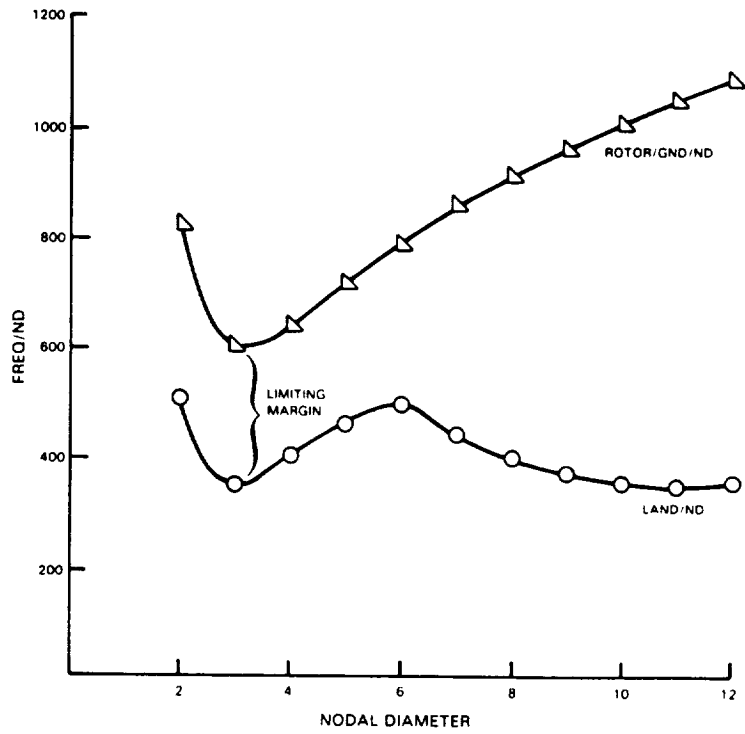


Figure 8.3.3-14 High-Pressure Turbine Rig Number 4 Bearing Buffer Seal Coincidence

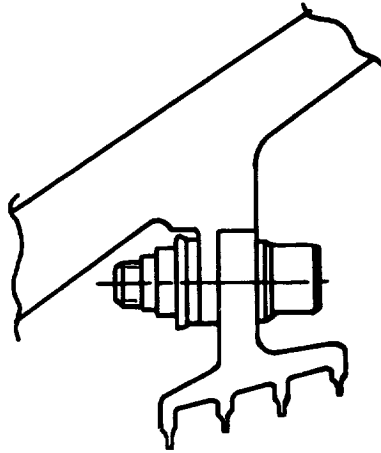


Figure 8.3.3-15 Number 4 Bearing Buffer Seal - Rig

8.3.4 Static Hardware

The rig static structure consists of the inlet and exit ducts, vanes and cases, including the active clearance control system.

The active clearance control system is used in the test program to evaluate its effectiveness during rig testing. The internal hardware of the active clearance control system for the integrated core/low spool is also used in the rig. The integrated core/low spool outer turbine case could not be used because of the requirement to place the exit probes in a specific axial location, which is incompatible with the case design. A rig-unique case was therefore designed to accommodate the required instrumentation. The material chosen for the rig case, Inconel 600, is a relatively low-cost nickel-based alloy that adequately matches the thermal expansion properties of PWA 1007 (Waspaloy) material in the integrated core/low spool. The rig design was analyzed to ensure that the outer air seal, over the turbine blade tip, moves out parallel to the rig centerline in order to maintain essential chordwise clearance between the blade tip and outer airseal platform during temperature excursions. The active clearance growth summary is shown in Figure 8.3.4-1.

8.4 SECONDARY FLOW SYSTEM AND THRUST BALANCE

The turbine component rig simulates engine cooling air and leakage flows and blade tip clearances, while preventing oil weepage from the bearing compartments and excessive thrust bearing loads. Figure 8.4-1 presents the rig secondary flows.

Sufficient rig instrumentation will allow measurement of these key flows. It will also provide confirmation of leakage and swirl field flows with static and total pressure sensors, cooling air temperatures and windage heat generation with thermocouples. Key thrust balance cavity pressures will be continuously monitored and processed to give an on-stand readout of thrust load.

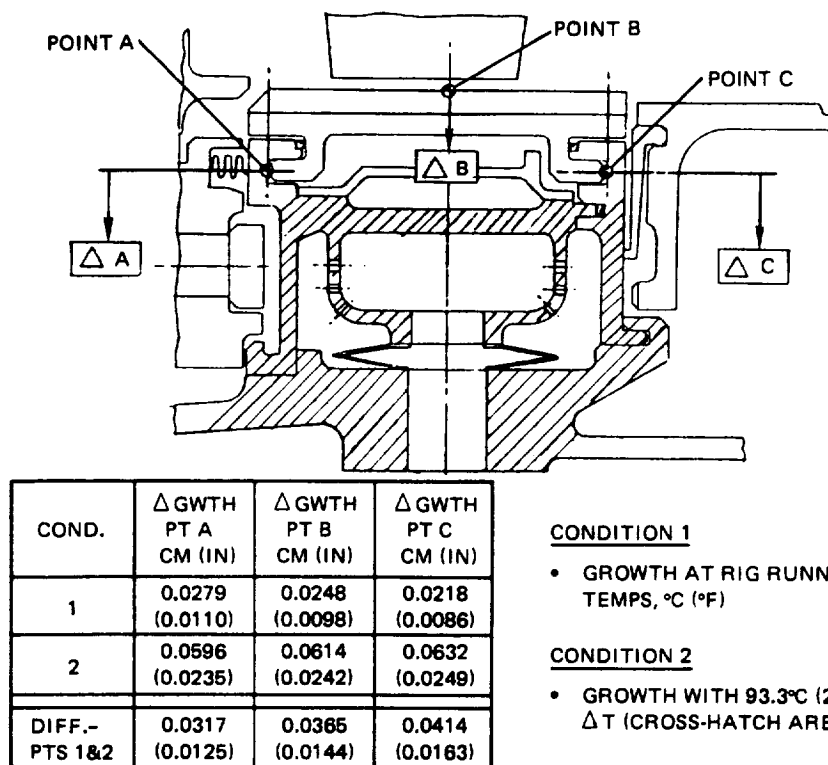


Figure 8.3.4-1 Active Clearance Control Growth Summary

The high-pressure compressor rear seal air supply will be injected tangentially to simulate the high-pressure compressor discharge bleed swirl in the engine. There will be separate control of the disk front rim cavity "mini" tangential on-board injection flow to change the swirl level and, hence, blade supply pressure. This will also affect thrust load. The temperature of the active clearance control air will also be controlled between 18°C (65°F) and 204°C (400°F). This control will change outer air seal (blade tip) clearances over the range available with the engine active clearance control system. The bearing compartments will be vacuum-pumped to provide a positive pressure gradient across the seals, thus preventing oil weepage. The rotor has been thrust-balanced so that the maximum load is 4009 kg (8839 lb).

8.5 RIG INSTRUMENTATION

The rig incorporates sufficient instrumentation to determine turbine aerodynamic performance and monitor rig structural integrity. This instrumentation was specifically selected or designed to maximize data acquisition capability without unduly perturbing the flow characteristics of the rig. This instrumentation measures overall stage performance and provides basic aerodynamic data as well as airfoil and endwall aerodynamic loading information. In addition, it monitors rig safety parameters and also records the performance of the "mini" tangential on-board injection system and active clearance control system. Both the cascade and the full-stage rigs have essentially the same instrumentation. A rig supervisory system will be employed to automatically control all of the secondary flow systems. All probes and wires are calibrated before installation.

The following sections describe rig performance and structural integrity instrumentation. A summary of rig instrumentation is presented in Table 8.5-I.

ORIGINAL PAGE IS
OF POOR QUALITY

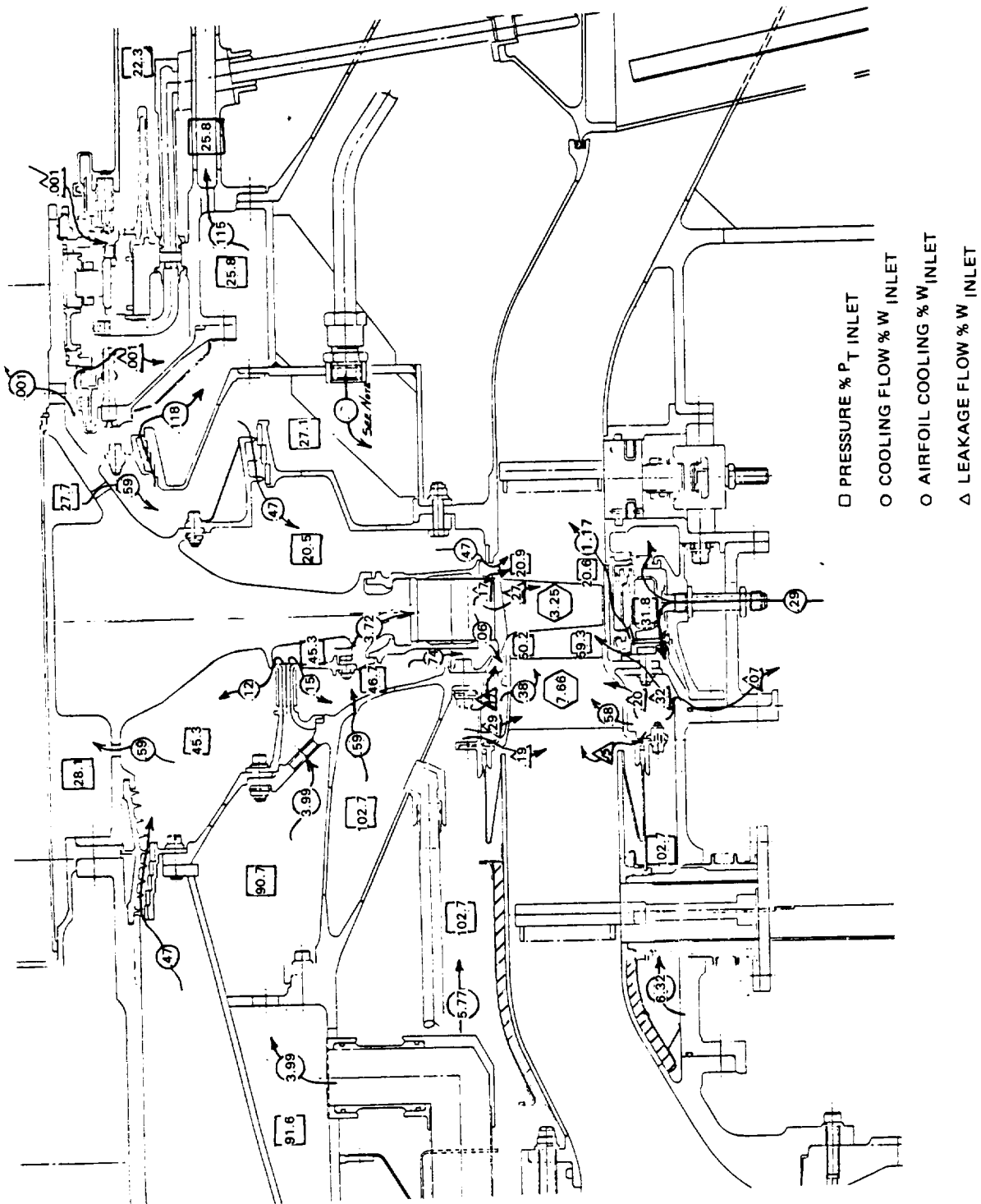


Figure 8.4-1 High-Pressure Turbine Component Test Rig Secondary Flows

TABLE 8.5-I

INSTRUMENTATION SUMMARY

	T_T	P_T	T_{Air}	T_{metal}	P_S	Miscellaneous
Rig Super- visory Control	2	2	10	-	16	-
Inlet	80	40			24	
Vane Surface & Shrouds					153	
Blade Outer Air Seal (OAS) and Active Clearance Control (ACC) System			22	28	22	Laser Prox.
Exit	48	48			24	4 Air Angle
Vane Cooling			16		16	
Tangential On- Board Injector (TOBI)			22		22	
Disk Bore Cooling		12	64		64	
Exit Cavities			8		8	
Bearing Com- partments			10	24	22	10 Vibration 3 speed
Totals	P_T	102				
	T_T	130				
	P_S	371				
	T_{AIR}	152				
	T_{metal}	52				
Laser Proximity	4					
Vibration	10					
Speed	3					
Air Angle	4					

8.5.1 Performance Instrumentation

Performance instrumentation measures inlet and exit flow, and blade tip clearance.

Inlet Instrumentation. Inlet instrumentation consists of 4 total pressure rakes, each with 10 sensors. In addition, there are 12 static pressure taps located on both the inner and outer flowpath. The inlet rakes are properly located circumferentially to prevent any rotor excitation.

Exit Instrumentation. Exit instrumentation consists of 4 total pressure rakes and 4 total temperature rakes each with 12 sensors. In addition, there are 12 static pressure taps located in both the inner and outer flowpath. The rakes are located on a ring that can be traversed circumferentially approximately 30 degrees. These rakes are positioned 90 degrees apart. Coupled with the pressure and temperature rakes, there are 4 air angle probes located at the exit plane. These probes are wedge shaped and have the ability to traverse radially as well as circumferentially. They are used to measure two static pressures and a total pressure, and are also used to calculate exit air angle.

Blade Tip Clearance Measurement. Four equally spaced laser probes will be used to measure and monitor the blade tip clearance. These probes will be attached to the blade outer air seal shoes, extend through the outer cases, and sealed by means of piston rings. Temperature variations in the flow to the active clearance control system will provide tip clearance changes. Probe measurements will then be used to determine any changes in performance resulting from variations in tip clearance.

Compartment Air Temperature. Air temperature measurements taken in various compartments, especially those conducting secondary air flow, will be useful in calculating performance parameters.

8.5.2 Structural Integrity Instrumentation

This instrumentation verifies design assumptions and measures static temperatures, pressures, and bearing temperatures. Probe strain gages and accelerometers are also used.

Static Pressure. Two turbine vanes will be instrumented on the airfoil surface at three spanwise locations. Seventeen airfoil static pressure taps will be positioned at each location, 10 on the suction surface and 7 on the pressure surface. Endwall static pressure taps will be placed at both the inner and outer flowpath platforms. The number of these used will depend on available platform area. Static pressure taps will also be located throughout the rig in order to determine cooling and leakage flows.

Static Temperature. One vane will be instrumented in the airfoil section to determine the effectiveness of the cooling scheme. In addition, instrumentation will be located on the active clearance control system to verify its operation. All cooling flow systems will be instrumented to monitor and maintain control of coolant flow temperatures.

Bearing Temperatures. Thermocouples will be located in the bearing compartments to ensure proper bearing and seal operating temperatures. This instrumentation will be monitored throughout the test program.

Probe Strain Gages. The fixed inlet rakes will be strain gaged at the root of the rake to detect probe vibratory modes that might exist at test conditions.

Accelerometer. Both horizontal and vertical accelerometers will be located on the front and rear bearing supports. These will be monitored throughout the test program.

8.6 FACILITY/RIG ADAPTATION

The facility for testing the high-pressure turbine component rig will provide an open-loop air supply system. Two natural gas burners heat the primary air to approximately 426°C (800°F). The secondary air, supplied by the main-stream air upstream of the combustor, is delivered to the rig at approximately 65°C (150°F), thus maintaining the proper main air temperature and cooling air temperature ratio. Power generated by the turbine is absorbed through two 10,000 horsepower dynamometers. The rig is connected to the power absorption system through a coupling and gearbox. There are provisions for seven independent secondary cooling air systems. Flow for both the primary and secondary air systems is metered through critical flow venturies. An automated data secondary system will be used to process data, and a rig supervisory system will be employed to control all secondary flows.

SECTION 9.0 CONCLUDING REMARKS

The high-pressure turbine design in the Energy Efficient Engine represents a considerable advancement in turbine technology. The design capitalizes on the inherent economic and weight advantages offered with a single stage system by applying technology advancements in the areas of structures, aerodynamics and materials. On the basis of results acquired from design analyses and, more importantly, supporting experimental test programs, turbine performance and durability goals are achievable. The predicted efficiency of 88.8 percent for the flight propulsion system exceeds the goal of 88.2 percent. Durability expectations are commensurate with commercial service operation.

Overall, the technology evolved through the turbine design processes and eventual demonstration during the integrated core/low spool test program will have wide application. Much of this technology, particularly high temperature capability materials, is applicable to any gas-turbine engine of the next generation, including advanced derivative models of current commercial engines.

APPENDIX A

ENERGY EFFICIENT ENGINE HIGH PRESSURE TURBINE
COMPONENT VANE AND BLADE AIRFOIL COORDINATES

PRECEDING PAGE BLANK NOT FILMED

EEE ENGINE VANE COORDINATES

ROOT, RADIUS = (13.880 in.) 35.255 cm

<u>X/BX</u>	<u>X</u>	<u>PRESSURE SIDE Y - TOP</u>	<u>SUCTION SIDE Y - BOTTOM</u>
0.0	-1.67371	3.64059	3.64059
0.010	-1.65670	3.73242	3.54876
0.020	-1.63969	3.76822	3.51296
0.030	-1.62267	3.79410	3.48708
0.040	-1.60566	3.81911	3.46595
0.050	-1.58865	3.83236	3.44833
0.060	-1.57164	3.84859	3.42941
0.070	-1.55462	3.86415	3.40907
0.080	-1.53761	3.87901	3.38754
0.090	-1.52060	3.89318	3.36497
0.100	-1.50359	3.90665	3.34151
0.125	-1.46106	3.93728	3.27951
0.150	-1.41853	3.96354	3.21359
0.175	-1.37600	3.98534	3.14448
0.200	-1.33346	4.00263	3.07267
0.225	-1.29093	4.01530	2.99851
0.250	-1.24840	4.02322	2.92225
0.275	-1.20597	4.02625	2.84413
0.300	-1.16334	4.02420	2.76425
0.325	-1.12081	4.01687	2.68276
0.350	-1.07828	4.00399	2.59974
0.375	-1.03575	3.98527	2.51528
0.400	-0.99322	3.96035	2.42941
0.425	-0.95069	3.92880	2.34220
0.450	-0.90816	3.89008	2.25366
0.475	-0.86563	3.84357	2.16381
0.500	-0.82310	3.78844	2.07268
0.525	-0.78057	3.72369	1.98025
0.550	-0.73804	3.64796	1.88653
0.575	-0.69551	3.55953	1.79147
0.600	-0.65298	3.45580	1.69506
0.625	-0.61044	3.33349	1.59725
0.650	-0.56791	3.19012	1.49800
0.675	-0.52538	3.02581	1.39720
0.700	-0.48285	2.84281	1.29482
0.725	-0.44032	2.64261	1.19066
0.750	-0.39779	2.43150	1.08463
0.775	-0.35526	2.20734	0.97652
0.800	-0.31273	1.97950	0.86604
0.825	-0.27020	1.74354	0.75285
0.850	-0.22767	1.50299	0.63647
0.875	-0.18514	1.25882	0.51613
0.900	-0.14261	1.01178	0.39080
0.910	-0.12559	0.91227	0.33881
0.920	-0.10858	0.81245	0.28551
0.930	-0.09157	0.71236	0.23073
0.940	-0.07456	0.61190	0.17326
0.950	-0.05755	0.51123	0.11320
0.960	-0.04053	0.41033	0.04902
0.970	-0.02352	0.30914	-0.01428
0.980	-0.00651	0.20783	-0.02674
0.990	0.01050	0.10620	-0.02544
1.000	0.02752	0.00221	-0.23526

ORIGINAL PAGE IS
OF POOR QUALITY

EEE ENGINE VANE COORDINATES

MEAN, RADIUS = (15.001 in.) 38.103 cm

<u>X/BX</u>	<u>X</u>	<u>PRESSURE SIDE Y - TOP</u>	<u>SUCTION SIDE Y - BOTTOM</u>
0.0	-1.67335	3.91742	3.91742
0.010	-1.65634	4.00945	3.82538
0.020	-1.63933	4.04534	3.78950
0.030	-1.62232	4.07129	3.76354
0.040	-1.60531	4.09185	3.74302
0.050	-1.52830	4.10909	3.72520
0.060	-1.57130	4.12553	3.70704
0.070	-1.55429	4.14148	3.68795
0.080	-1.53728	4.15691	3.66797
0.090	-1.52027	4.17181	3.64717
0.100	-1.50326	4.18619	3.62561
0.125	-1.46074	4.21973	3.56857
0.150	-1.41822	4.24969	3.50752
0.175	-1.37570	4.27590	3.44289
0.200	-1.33317	4.29813	3.37501
0.225	-1.29065	4.31615	3.30414
0.250	-1.24813	4.32969	3.23049
0.275	-1.20561	4.33843	3.15421
0.300	-1.16309	4.34205	3.07545
0.325	-1.12057	4.34016	2.99432
0.350	-1.07804	4.33231	2.91090
0.375	-1.03552	4.31796	2.82526
0.400	-0.99300	4.29658	2.73744
0.425	-0.95048	4.26742	2.64750
0.450	-0.90796	4.22969	2.55544
0.475	-0.86544	4.18239	2.46128
0.500	-0.82292	4.12431	2.36501
0.525	-0.78039	4.05398	2.26664
0.550	-0.73787	3.96931	2.16610
0.575	-0.69535	3.86790	2.06337
0.600	-0.65283	3.74823	1.95842
0.625	-0.61031	3.60056	1.85113
0.650	-0.56779	3.43406	1.74144
0.675	-0.52526	3.25073	1.62920
0.700	-0.48274	3.05359	1.51428
0.725	-0.44022	2.84441	1.39651
0.750	-0.39770	2.62461	1.27566
0.775	-0.35518	2.39545	1.15140
0.800	-0.31266	2.15772	1.02343
0.825	-0.27014	1.91197	0.89123
0.850	-0.22761	1.65890	0.75421
0.875	-0.18509	1.39875	0.61152
0.900	-0.14257	1.13200	0.46157
0.910	-0.12556	1.02389	0.39922
0.920	-0.10855	0.91452	0.33554
0.930	-0.09155	0.80392	0.26953
0.940	-0.07454	0.69248	0.20168
0.950	-0.05753	0.58006	0.13099
0.960	-0.04052	0.46692	0.05762
0.970	-0.02351	0.35261	-0.01430
0.980	-0.00650	0.23737	-0.02674
0.990	0.01051	0.12109	-0.02543
1.000	0.02752	0.00194	0.24012

ORIGINAL PAGE IS
OF POOR QUALITY

EEE ENGINE VANE COORDINATES

LE. TIP, RADIUS = (16.582 in.) 42.118 cm

<u>X/BX</u>	<u>X</u>	<u>PRESSURE SIDE Y - TOP</u>	<u>SUCTION SIDE Y - BOTTOM</u>
0.0	-1.67284	4.31186	4.31185
0.010	-1.65584	4.40384	4.21987
0.020	-1.63883	4.43971	4.18401
0.030	-1.62183	4.46565	4.15807
0.040	-1.60483	4.48529	4.13756
0.050	-1.58782	4.50353	4.11964
0.060	-1.57082	4.51997	4.10120
0.070	-1.55382	4.53591	4.08156
0.080	-1.53681	4.55135	4.06083
0.090	-1.51981	4.56628	4.03907
0.100	-1.50281	4.58071	4.01636
0.125	-1.46030	4.61452	3.95581
0.150	-1.41779	4.64506	3.89042
0.175	-1.37528	4.67225	3.82078
0.200	-1.33277	4.69600	3.74732
0.225	-1.29026	4.71617	3.67033
0.250	-1.24775	4.73263	3.59012
0.275	-1.20525	4.74524	3.50698
0.300	-1.16274	4.75379	3.42079
0.325	-1.12023	4.75806	3.33197
0.350	-1.07772	4.75778	3.24053
0.375	-1.03521	4.75265	3.14656
0.400	-0.99270	4.74229	3.05012
0.425	-0.95019	4.72625	2.95125
0.450	-0.90768	4.70398	2.84998
0.475	-0.86518	4.67400	2.74635
0.500	-0.82267	4.63785	2.64033
0.525	-0.78016	4.59204	2.53190
0.550	-0.73765	4.53585	2.42106
0.575	-0.69514	4.46716	2.30773
0.600	-0.65263	4.38318	2.19186
0.625	-0.61012	4.27294	2.07336
0.650	-0.56762	4.14600	1.95211
0.675	-0.52511	3.97714	1.82799
0.700	-0.48260	3.77593	1.70083
0.725	-0.44009	3.54845	1.57038
0.750	-0.39758	3.29764	1.43639
0.775	-0.35507	3.02703	1.29852
0.800	-0.31256	2.73928	1.15632
0.825	-0.27006	2.43612	1.00921
0.850	-0.22755	2.11948	0.85638
0.875	-0.18504	1.79083	0.69665
0.900	-0.14253	1.45117	0.52639
0.910	-0.12553	1.31249	0.45812
0.920	-0.10852	1.17244	0.38581
0.930	-0.09152	1.03084	0.31065
0.940	-0.07452	0.88912	0.23384
0.950	-0.05751	0.74394	0.15359
0.960	-0.04051	0.59240	0.06844
0.970	-0.02351	0.45127	-0.01430
0.980	-0.00650	0.30305	-0.02673
0.990	0.01050	0.15392	-0.02543
1.000	0.02751	0.00152	-0.33327

ORIGINAL PAGE IS
OF POOR QUALITY

EEE ENGINE BLADE COORDINATES

ROOT, RADIUS = (13.678 in.) 34.742 cm

<u>X/BX</u>	<u>X</u>	<u>SUCTION SIDE Y - TOP</u>	<u>PRESSURE SIDE Y - BOTTOM</u>
0.0	0.00006	1.08397	1.08397
0.010	0.01352	1.18073	1.04116
0.020	0.02698	1.16034	1.02650
0.030	0.04045	1.10643	1.01756
0.040	0.05391	1.21508	1.01216
0.050	0.06737	1.24155	1.00955
0.060	0.08084	1.23638	1.00941
0.070	0.09430	1.29018	1.01175
0.080	0.10776	1.31302	1.01680
0.090	0.12123	1.33495	1.02512
0.100	0.13469	1.35601	1.03475
0.125	0.16835	1.40513	1.05515
0.150	0.20201	1.44951	1.07394
0.175	0.23567	1.48957	1.08831
0.200	0.26933	1.52554	1.09943
0.225	0.30299	1.55766	1.10747
0.250	0.33665	1.58606	1.11253
0.275	0.37030	1.61003	1.11470
0.300	0.40396	1.63203	1.11406
0.325	0.43762	1.64975	1.11069
0.350	0.47128	1.66390	1.10464
0.375	0.50494	1.67446	1.09592
0.400	0.53860	1.68131	1.08460
0.425	0.57226	1.68435	1.07065
0.450	0.60592	1.68339	1.05409
0.475	0.63958	1.67816	1.03491
0.500	0.67323	1.66835	1.01311
0.525	0.70689	1.65351	0.98863
0.550	0.74055	1.63303	0.96143
0.575	0.77421	1.60610	0.93151
0.600	0.80787	1.57158	0.89873
0.625	0.84153	1.52772	0.86303
0.650	0.87519	1.47161	0.82430
0.675	0.90885	1.39837	0.78241
0.700	0.94251	1.30202	0.73724
0.725	0.97617	1.21310	0.68856
0.750	1.00982	1.11368	0.63620
0.775	1.04348	1.01140	0.57925
0.800	1.07714	0.90717	0.51924
0.825	1.11080	0.80101	0.45397
0.850	1.14446	0.69305	0.38345
0.875	1.17812	0.58330	0.30721
0.900	1.21178	0.47136	0.22434
0.910	1.22524	0.42674	0.18918
0.920	1.23870	0.38123	0.15270
0.930	1.25217	0.33535	0.11456
0.940	1.26563	0.28949	0.07499
0.950	1.27909	0.24275	0.03371
0.960	1.29256	0.19573	-0.00955
0.970	1.30602	0.14835	-0.02621
0.980	1.31943	0.10022	-0.02944
0.990	1.33295	0.05151	-0.02561
1.000	1.34641	-0.00199	-0.00199

ORIGINAL PAGE IS
OF POOR QUALITY

EEE ENGINE BLADE COORDINATES

MEAN, RADIUS = (14.913 in.) 37.879 cm

<u>X/BX</u>	<u>X</u>	<u>SUCTION SIDE Y - TOP</u>	<u>PRESSURE SIDE Y - BOTTOM</u>
0.0	0.11588	1.37101	1.37101
0.010	0.12748	1.41588	1.33092
0.020	0.13907	1.44625	1.31674
0.030	0.15066	1.47411	1.30765
0.040	0.16225	1.49979	1.30162
0.050	0.17384	1.52358	1.29709
0.060	0.18543	1.54570	1.29611
0.070	0.19703	1.56630	1.29615
0.080	0.20862	1.58553	1.29801
0.090	0.22021	1.60351	1.30183
0.100	0.23180	1.62032	1.30797
0.125	0.26078	1.65774	1.32937
0.150	0.28976	1.68527	1.34718
0.175	0.31874	1.71555	1.35856
0.200	0.34772	1.73717	1.36453
0.225	0.37670	1.75429	1.36554
0.250	0.40568	1.76721	1.36193
0.275	0.43466	1.77606	1.35399
0.300	0.46364	1.78091	1.34166
0.325	0.49261	1.78177	1.32803
0.350	0.52159	1.77861	1.30652
0.375	0.55057	1.77129	1.28342
0.400	0.57955	1.75965	1.25696
0.425	0.60853	1.74542	1.22722
0.450	0.63751	1.72822	1.19436
0.475	0.66649	1.69949	1.15044
0.500	0.69547	1.66243	1.11957
0.525	0.72445	1.62107	1.07777
0.550	0.75343	1.57205	1.03215
0.575	0.78241	1.50979	0.98376
0.600	0.81139	1.43295	0.93562
0.625	0.84037	1.35028	0.88277
0.650	0.86935	1.26468	0.82727
0.675	0.89832	1.17735	0.76907
0.700	0.92730	1.09067	0.70928
0.725	0.95628	0.99380	0.64485
0.750	0.98526	0.90208	0.57070
0.775	1.01424	0.81639	0.51007
0.800	1.04322	0.72403	0.43077
0.825	1.07220	0.63081	0.36476
0.850	1.10118	0.53681	0.29310
0.875	1.13016	0.44205	0.20371
0.900	1.15914	0.34643	0.12659
0.910	1.17073	0.30793	0.09297
0.920	1.18232	0.26924	0.05806
0.930	1.19391	0.23035	0.02427
0.940	1.20550	0.19147	-0.01061
0.950	1.21710	0.15220	-0.04626
0.960	1.22869	0.11255	-0.07201
0.970	1.24028	0.07297	-0.07848
0.980	1.25187	0.03329	-0.07909
0.990	1.26346	-0.00666	-0.07435
1.000	1.27505	-0.05190	-0.05190

ORIGINAL PAGE IS
OF POOR QUALITY

EEE ENGINE BLADE COORDINATES

TIP, RADIUS = (16.149 in.) 41.018 cm

<u>X/BX</u>	<u>X</u>	<u>SUCTION SIDE Y - TOP</u>	<u>PRESSURE SIDE Y - BOTTOM</u>
0.0	0.17520	1.95437	1.95437
0.010	0.18522	1.99237	1.91736
0.020	0.19524	2.00598	1.90375
0.030	0.20526	2.01502	1.89471
0.040	0.21528	2.02150	1.88836
0.050	0.22530	2.02714	1.88397
0.060	0.23532	2.03233	1.88118
0.070	0.24534	2.03707	1.87982
0.080	0.25537	2.04136	1.87956
0.090	0.26539	2.04522	1.87915
0.100	0.27541	2.04864	1.87728
0.125	0.30046	2.05528	1.86900
0.150	0.32551	2.05921	1.85291
0.175	0.35057	2.06041	1.83251
0.200	0.37562	2.05983	1.80741
0.225	0.40067	2.05441	1.77009
0.250	0.42572	2.04703	1.74492
0.275	0.45077	2.03453	1.70823
0.300	0.47583	2.02274	1.66843
0.325	0.50088	2.00534	1.62573
0.350	0.52593	1.98400	1.58045
0.375	0.55098	1.95822	1.53267
0.400	0.57604	1.92732	1.48274
0.425	0.60109	1.89029	1.43089
0.450	0.62614	1.84567	1.37713
0.475	0.65119	1.79575	1.32164
0.500	0.67625	1.72245	1.26457
0.525	0.70130	1.64489	1.20598
0.550	0.72635	1.56466	1.14410
0.575	0.75140	1.48326	1.07981
0.600	0.77646	1.40133	1.02244
0.625	0.80151	1.31922	0.95885
0.650	0.82656	1.23690	0.89429
0.675	0.85161	1.15447	0.82059
0.700	0.87667	1.07197	0.76224
0.725	0.90172	0.98941	0.69495
0.750	0.92677	0.90685	0.62677
0.775	0.95182	0.82422	0.55785
0.800	0.97688	0.74160	0.48822
0.825	1.00193	0.65893	0.41785
0.850	1.02698	0.57628	0.34690
0.875	1.05203	0.49359	0.27540
0.900	1.07709	0.41092	0.20323
0.910	1.08711	0.37784	0.17420
0.920	1.09713	0.34477	0.14510
0.930	1.10715	0.31164	0.11590
0.940	1.11717	0.27850	0.08668
0.950	1.12719	0.24552	0.05915
0.950	1.13721	0.21244	0.03032
0.970	1.14723	0.17936	0.04738
0.990	1.15725	0.14630	0.04029
0.990	1.16727	0.11315	0.05352
1.000	1.17729	0.07474	0.07474

APPENDIX B

LIST OF SYMBOLS

A	Annulus area
ACC	Active clearance control
ADP	Aerodynamic design point
amb.	Ambient
Btu	British thermal unit
CET	Combustor exit temperature
C _{pb}	Base pressure coefficient
C _x	Axial flow velocity
D	Diameter
FP	Flow parameter, $W\sqrt{T}/P$
FPS	Flight propulsion system
HPC	High-pressure compressor
HPT	High-pressure turbine
IC/LS	Integrated core/low spool
ID	Inner diameter
LE	Leading edge
LPT	Low-pressure turbine
M, M _n	Mach number
N	Mechanical speed, rpm
N ₂	High-pressure rotor speed, rpm
OAS	Outer airseal
OD	Outer diameter
P	Pressure
PF	Pattern factor
$\Delta P/P, Pr$	Pressure ratio

LIST OF SYMBOLS (Continued)

P_T	Total pressure
R	Rankine
rpm	Revolutions per minute
S	Span
SLTO	Sea level take-off
T	Temperature
TE	Trailing edge
TOBI	Tangential on-board injection
U	Tangential wheel speed
U_{rim}	Rim speed
W_{ae}	Engine airflow
$W_{c/a}$	Total cooling airflow
θ	Angle
α	Angle
Δ	Delta
δ	Deflection
η	Efficiency
σ	Stress

REFERENCES

1. Energy Efficient Engine High-Pressure Turbine Uncooled Rig Technology Program (CR-165149)
2. Energy Efficient Engine High-Pressure Turbine Supersonic Cascade Technology Report (CR-165567)
3. Energy Efficient Engine High-Pressure Turbine Leakage Technology Report (CR-165202)
4. Energy Efficient Engine High-Pressure Turbine Cooling Model Technology Report (CR-165374)

DISTRIBUTION LIST

GOVERNMENT AGENCIES

NASA Headquarters
600 Independence Ave., SW
Washington, D.C. 20546
Attention: RTP-6/R.S. Colladay
RTP-6/C.C. Rosen
RTP-6/L. Harris
RRP-6/J. Facey
Library

NASA-Lewis Research Center
21000 Brookpark Road
Cleveland, OH 44135
Attention: D. L. Nored MS 301-2
C. C. Ciepluch MS 301-4 (20 copies)
J. W. Schaefer MS 301-4
P. G. Batterton MS 301-4
G. K. Sievers MS 301-2
Library MS 60-3 (2 copies)
Report Control Office MS 5-5
Tech Utilization Office MS 3-19
M. A. Beheim MS 3-5
M. J. Hartmann MS 5-3
R. A. Rudey MS 60-4
R. A. Weber MS 500-127
W. C. Strack MS 501-10
T. P. Moffitt MS 77-2
J. E. Rohde MS 77--2
R. L. Dreshfield MS 105-1
A. Long MS 500-305
W. M. Braithwaite MS 500-208
L. Reid MS 5-9
AFSC Liaison Office MS 501-3
Army R&T Propulsion Lab MS 302-2

NASA-Lewis Research Center 21000 Brookpark Road Cleveland, Ohio 44135 Attention: D.L. Nored	MS 301-2	NASA-Lewis Research Center 21000 Brookpark Road Cleveland, Ohio 44135 Attention: R.J. Weber	MS 500-127
NASA-Lewis Research Center 21000 Brookpark Road Cleveland, Ohio 44135 Attention: C.C. Ciepluch	MS 301-4 20 Copies	NASA-Lewis Research Center 21000 Brookpark Road Cleveland, Ohio 44135 Attention: W.C. Strack	MS 501-10
NASA-Lewis Research Center 21000 Brookpark Road Cleveland, Ohio 44135 Attention: J.W. Schaefer	MS 301-4	NASA-Lewis Research Center 21000 Brookpark Road Cleveland, Ohio 44135 Attention: T.P. Moffitt	MS 77-2
NASA Lewis Research Center 21000 Brookpark Road Cleveland, Ohio 44135 Attention: P.G. Batterton	MS 301-4	NASA-Lewis Research Center 21000 Brookpark Road Cleveland, Ohio 44135 Attention: J.E. Rohde	MS 77-2
NASA-Lewis Research Center 21000 Brookpark Road Cleveland, Ohio 44135 Attention: G.M. Sievers	MS 301-2	NASA-Lewis Research Center 21000 Brookpark Road Cleveland, Ohio 44135 Attention: R. L. Dreshfield	MS 105-1
NASA-Lewis Research Center 21000 Brookpark Road Cleveland, Ohio 44135 Attention: Library	MS 60-3 2 Copies	NASA-Lewis Research Center 21000 Brookpark Road Cleveland, Ohio 44135 Attention: A. Long	MS 500-305
NASA-Lewis Research Center 21000 Brookpark Road Cleveland, Ohio 44135 Attention: Report Control Office	MS 5-5	NASA-Lewis Research Center 21000 Brookpark Road Cleveland, Ohio 44135 Attention: W.M. Braithwaite	MS 500-208
NASA-Lewis Research Center 21000 Brookpark Road Cleveland, Ohio 44135 Attention: Tech Utilization Office	MS 3-19	NASA-Lewis Research Center 21000 Brookpark Road Cleveland, Ohio 44135 Attention: L. Reid	MS 5-9
NASA-Lewis Research Center 21000 Brookpark Road Cleveland, Ohio 44135 Attention: M.A. Beheim	MS 3-5	NASA-Lewis Research Center 21000 Brookpark Road Cleveland, Ohio 44135 Attention: AFSC Liaison Office	MS 501-3
NASA-Lewis Research Center 21000 Brookpark Road Cleveland, Ohio 44135 Attention: M.J. Hartmann	MS 3-7	NASA-Lewis Research Center 21000 Brookpark Road Cleveland, Ohio 44135 Attention: Army R&T Propulsion	MS 302-2
NASA-Lewis Research Center 21000 Brookpark Road Cleveland, Ohio 44135 Attention: R.A. Rudey	MS 86-5	NASA Ames Research Center Moffett Field, CA 94035 Attention: 202-7/M. H. Waters Library	

NASA Langley Research Center
Langley Field, VA 23365
Attention: R. Leonard
D. Maiden
L. J. Williams
Library

NASA Dryden Flight Research Center
P.O. Box 273
Edwards, CA 93523
Attention: J. A. Albers
Library

NASA Scientific and Technical Information
Facility
P.O. Box 8757
B.W.I. Airport, MD 21240
Attention: Acquisition Branch (10 copies)

Department of Defense
Washington, D.C. 20301
Attention: R. Standahar 3D1089 Pentagon

Wright-Patterson Air Force Base
Dayton, Ohio 45433
Attention: APL Chief Scientist AFWAL/PS

Wright-Patterson Air Force Base
Dayton, Ohio 45433
Attention: E.E. Abell ASD/YZE

Wright-Patterson Air Force Base
Dayton, Ohio 45433
Attention: H.I. Bush AFWAL/POT

Wright-Patterson Air Force Base
Dayton, Ohio 45433
Attention: E.E. Bailey (NASA Liaison)
AFWAL/NASA

Wright-Patterson Air Force Base
Dayton, Ohio 45433
Attention: R.P. Carmichael ASD/XRHI

Wright-Patterson Air Force Base
Dayton, Ohio 45433
Attention: R. Ellis ASD/YZN

Wright-Patterson Air Force Base
Dayton, Ohio 45433
Attention: W.H. Austin, Jr. ASD/ENF

Eustis Directorate
U.S. Army Air Mobility
R&D Laboratory
Fort Eustis, VA 23604
Attention: J. Lane, SAVDL-EU-Tapp

Navy Department
Naval Air Systems Command
Washington, D. C. 20361
Attention: W. Koven AIR-03E

Navy Department
Naval Air Systems Command
Washington, D. C. 20361
Attention: J.L. Byers AIR-53602

Navy Department
Naval Air Systems Command
Washington, D. C. 20361
Attention: E.A. Lichtman AIR-330E

Navy Department
Naval Air Systems Command
Washington, D. C. 20361
Attention: G. Derderian AIR-5362C

NAVAL AIR Propulsion Test Center
Trenton, NJ 08628
Attention: J. J. Curry
A. A. Martino

U.S. Naval Air Test Center
Code SY-53
Patuxent River, MD 20670
Attention: E. A. Lynch

USAVRAD Command
PO Box 209
St. Louis, MO 63166
Attention: Ropbert M. Titus (ASTIU)

Department of Transportation
NASA/DOT Joint Office of Noise Abatement
Washington, D.C. 20590
Attention: C. Foster

Federal Aviation Administration
Noise Abatement Division
Washington, D.C. 20590
Attention: E. Sellman AEE-120

Environmental Protection Agency
1835 K Street, NW
Washington, D.C. 20460
Attention: J. Schettino
J. Tyler

Environmental Protection Agency
2565 Plymouth Road
Ann Arbor, MI 48105
Attention: R. Munt

Federal Aviation Administration
12 New England Executive Park
Burlington, MA 18083
Attention: Jack A. Sain, ANE-200

Curtiss Wright Corporation
Woodridge, NJ 07075
Attention: S. Lombardo
S. Moskowitz

Detroit Diesel Allison Div. G.M.C.
P.O. Box 894
Indianapolis, IN 46206
Attention: W. L. McIntire

Cummins Engine Co.
Technical Center
500 S. Poplar
Columbus, IN 47201
Attention: J. R. Drake

AVCO/Lycoming
550 S. Main Street
Stratford, CT 06497
Attention: H. Moellmann

Detroit Diesel Allison Div. G.M.C.
333 West First Street
Dayton, Ohio 45402
Attention: F. H. Walters

The Garrett Corporation
AIRResearch Manufacturing Co.
Torrance, CA 90509
Attention: F. E. Faulkner

The Garrett Corporation
AIRResearch Manufacturing Co.
402 S. 36 Street
Phoenix, AZ 85034
Attention: Library

General Electric Co./AEG
One Jimson Road
Evendale, Ohio 45215
Attention: R.W. Bucy (3 copies)
T. F. Donohue

Pratt & Whitney Aircraft Group/UTC
Government Products Division
P.O. Box 2691
West Palm Beach, FL 33402
Attention: B. A. Jones

The Garrett Corporation
AIRResearch Aviation Co.
19201 Susana Road
Compton, CA 90221
Attention: N. J. Palmer

AIRResearch Manufacturing Co.
111 South 34th Street
P.O. Box 5217
Phoenix, AZ 85010
Attention: C. E. Corrigan
(93-120/503-4F)

Williams Research Co.
2280 W. Maple Road
Walled Lake, MI 48088
Attention: R. VanNimwegen
R. Horn

Teledyne CAE, Turbine Engines
1330 Laskey Road
Tolendo, Ohio 43612
Attention: R. H. Gaylord

General Electric Co./AEG
1000 Western Ave.
Lynn, MA 01910
Attention: R. E. Neitzel

Pratt & Whitney Aircraft Group/UTC
Commercial Products Division
East Hartford, Ct 06108
Attention: W. Gardner
I. Mendelson

Boeing Commercial Airplane Co.
P.O. Box 3707
Seattle, WA 98124
Attention: P. E. Johnson MS 9H-46
D. C. Nordstrom MS 73-01

Boeing Aerospace Co.
P.O. Box 3999
Seattle, Wa 98124
Attention: D. S. Miller MS 40-26
H. Higgins

The Boeing Co., Wichita Division
Wichita, KS 67210
Attention: D. Tarkelson

Douglas Aircraft Company
McDonnell Douglas Corp.
3855 Lakewood Boulevard
Long Beach, CA 90846
Attention: R. T. Kawai Code 36-41
M. Klotzsche

Lockheed California Co.
Burbank, CA 91502
Attention: J. F. Stroud, Dept. 75-42
R. Tullis, Dept. 75-21
J. I. Benson

General Dynamics Convair
P. O. Box 80847
San Diego, CA 92138
Attention: S. Campbell, MZ 632-00

Rockwell International
International Airport
Los Angeles Division
Los Angeles, CA 90009
Attention: A. W. Martin

Gates Learjet Corp.
P. O. Box 7707
Wichita, KS 67277
Attention: E. Schiller

McDonnell Aircraft Co.
McDonnell Douglas Corp.
P. O. Box 516
St. Louis, MO 63166
Attention: F. C. Claser Dept. 243

Lockheed Georgia Co.
Marietta, GA 30060
Attention: H. S. Sweet

Grumman Aerospace Corp.
South Oyster Bay Road
Bethpage, New York 11714
Attention: C. Hoeltzer

American Airlines
Maint. & Engr. Center
Tulsa, OK 74151
Attention: W. R. Neeley

Eastern Airlines
International Airport
Miami, FL 33148
Attention: A. E. Fishbein

Delta Airlines, Inc.
Hartsfield-Atlanta International Airport
Atlanta, GA 30320
Attention: C. C. Davis

TransWorld Airlines
605 Third Avenue
New York, NY 10016
Attention: A. E. Carrol

Pan American World Airways, Inc.
JFK International Airport
Jamica, NY 11430
Attention: J. G. Borger
A. MacLarty

United Airlines
San Francisco International Airport
Maint. Operations Center
San Francisco, CA 94128
Attention: J. J. Overton

Hamilton Standard
Bradley Field
Windsor Locks, CT 06096
Attention: P. J. Dumais, MS 1A-3-1
A. T. Reiff, MS 1-2-2

FluiDyne Engineering Corp.
5900 Olson Memorial Highway
Minneapolis, MN 55422
Attention: J. S. Holdhusen

Rohr Corporation
P.O. Box 878
Foot & H Street
Chula Vista, CA 92012
Attention: Library

Solar Division
International Harvester
2200 Pacific Highway
San Diego, CA 92112
Attention: Library

Gas Dynamics Laboratories
Aerospace Engineering Building
University of Michigan
Ann Arbor, MI 48109
Attention: Dr. C. W. Kaufmann

Massachusetts Inst. of Technology
Dept. of Astronautics & Aeronautics
Cambridge, MA 02139
Attention: Jack Kerrebrock

Massachusetts Inst. of Technology
Dept. of Structural Mechanics
Cambridge, MA 02139
Attention: James Mar

Westinghouse Electric Corp.
P.O. Box 5837
Beulah Road
Pittsburgh, PA 15236
Attention: Library

University of Tennessee
Space Institute
Tullahoma, TN 37388
Attention: Dr. V. Smith

TRW Equipment Group
TRW Inc.
23555 Euclid Ave.
Cleveland, OH 44117
Attention: I. Toth

Aerospace Corporation
R & D Center
Los Angeles, CA 90045
Attention: Library

George Shevlin
P.O. Box 1925
Washington, D.C. 20013

Brunswick Corporation
2000 Brunswick Lane
Deland, FL 32720
Attention: A. Erickson

Pennsylvania State University
Department of Aerospace Engineering
233 Hammond Building
University Park, Pennsylvania 16802
Attention: Dr. B. Lakshminarayana

Iowa State University
Department of Mechanical Engineering
Ames, Iowa 50011
Attention: Dr. Patrick Kavanagh

Detroit Diesel Allison
P.O. Box 894
Indianapolis, Indiana 46206
Attention: Mr. Robert Delanie
Speed Code U29A
Mr. H. L. Stocker
Speed Code U21A

KVB Inc*
18006 Skypark Blvd.
P.O. Box 19518
Irvine CA 92714
Attention: A. M. Mellor

